Fábio Alexandre Teixeira Ferreira Carlos
Licenciado em Biologia

Development and Validation of Gold Nanoprobes for Human SNP Detection Towards Commercial Application

Dissertação para obtenção do Grau de Doutor em
Biotecnologia

Orientador: Doutor Pedro Viana Baptista, Professor Associado com Agregação, Faculdade de Ciências e Tecnologia da Universidade Nova de Lisboa.
Orientador Empresarial: Orfeu Flores, CEO, STAB VIDA, Investigação e Serviços em Ciências Biológicas, Lda.
Co-orientador: Doutor Gonçalo Doria, Project Mannager, STAB VIDA, Investigação e Serviços em Ciências Biológicas, Lda.

FACULDADE DE CIÊNCIAS E TECNOLOGIA
UNIVERSIDADE NOVA DE LISBOA

November 2015

COPYRIGHT

Autorizo os direitos de copyright da minha tese de doutoramento, com o título:
"Development and validation of gold nanoprobes for human SNP detection towards commercial application".

ACKNOWLEDGEMENTS

This incredible journey was not possible to be accomplished without the tireless and endless help of several people. Forget to mention someone will be almost inevitable and my sincere apologize for that. Expressing gratitude only in words may not fully represent the extension of thankfulness that I have for you all, but I will do my best.

First I would like to thank, my PhD supervisors:

- Prof. Pedro Viana Baptista. The example of what every supervisor should be. I will never find the right words to demonstrate how grateful I am to you. The support and guidance that you gave me throughout these years were absolutely crucial, if not determinant, for the success of the work presented here. My scientific and personal growth was only possible due the innumerous, insightful and inspirational discussions had in your office, in the laboratory, in the student's office, in the stairs, everywhere. You were always available to shown me the right way to go and never limited my horizons, but always demand the best out of me. The passion and pleasure that you put in every scientific discussion is contagious and I feel fortunate to still can be part of them. Most important, you taught me how to be in science, that is far more important to teach how to do science. You started has my Professor, Supervisor and Group Leader and today I can say that you are a very good Friend that taught me how to be a better man, father, husband and friend…and this was one of the best results of my PhD. Thank you very much for these years Pedro!

- Gonçalo Doria. I was very fortunate to have you as my co-supervisor, you were always there when I most needed. Thank you for all the help that you gave me since the first day of this journey, literally. You were always available for discussing each step of the work contributing with all the support and guidance needed to make most of the ideas come to fruition. All the suggestions, commentaries and improvements that you have shared for this dissertation were extremely important and crucial. I hope that the growing relation stablished in these past years can continue for a long time.

- Orfeu Flores. I was very privileged to be handpicked in 2008 between the hundreds of candidates that are egger to work in STAB VIDA. In my job interview you told me that when you felt that I was ready, a PhD proposition would be waiting for me. The promises are to be kept and you kept yours and for that I will be forever grateful. Thank you for providing in STAB VIDA the necessary means for the completion of my work, with prompted discussions and suggestions. Most important thank you for aroused the bug of entrepreneurship in me, I believe that I've learned with the best!

I also have to thank **Dr. José Silva-Nunes**, **Prof. Miguel Brito** and **Prof. Luísa Veiga** from Escola Superior de Tecnologia da Saúde de Lisboa (ESTeSL), for providing the biological samples and the relevant data most needed for the association study. Thank you for all the insightful discussion regarding statistical analysis and necessary comments and suggestions during manuscript writing.

I also have to thank the fruitful collaboration stablished with all the people in **CENIMAT/I3N** during the development of the bio-microfluidic platform. Specially, Iwona Bernacka-Wojcik, Prof. Hugo Águas, Prof. Elvira Fortunato and Prof. Rodrigo Martins for letting enter in the world of microfluidic fabrication, giving all the supervision and support needed for a layman in the subject like me. The little I know it is thanks to you all.

An endless thank you for all **STAB VIDA members**. Thank you for putting up with me all of these years. THANK YOU for the friendship, THANK YOU for the companionship and THANK YOU for being a family that I will always cherishes. All of you, each in their own way, have paved and thought something that I always carry with me. A special thank you to Daniela Leão and Carla Clemente, Liliana Castro (aka A Máquina), Rui Crespo (aka Maestro), Hugo Pereira (aka O Maior), Pedro Penedo (aka O Puto), Nanci Lopes and Vitaliy Sobchuck for all the moments and friendship. Once STABiano always a STABiano!!

To all my friends and colleagues of **Lab. 315.** Never in a million years, I ever thought that I will feel so at home like I felt in that laboratory. What a PERFECT group of people! What a pleasure was waking up every day to go to work, learn and laugh with all of you! You were outstanding colleagues and professionals and flawless friends! A big thank you to Large, Rosa, Mílton, Rita, Pedrosa, Mafalda, Raquel, Letícia, Joana, Ana Sofia (aka Catraia), Bárbara, Daniela, Catarina, Marisa and Rafaela for always being present and never let me give up. A special thank you to **Bruno Veigas**, I hope that one day I can be half of the scientist that you are today. I guess I never thanked you enough for everything you taught me over the years, often neglecting your work in detriment of my. For the friendship and presence in all up and downs in these last years a special thank you. A true brother in arms! Thank you, fofinho!! To **Sara Figueiredo**, my mom and sister in the Laboratory. We have started with the wrong foot (don't you ever steal my office seat again!!), but end with a homerun friendship. I could thank you for always being available to look at my results and discussed them until the death with me or thank you for all the corrections, suggestions and comments made at every manuscript that I wrote (including this one), or even thank you for all the wonderful Augustus's months spent in the laboratory generating huge amount of results and going complete insane with them but I prefer to thank you for your friendship that is priceless and that I hope last for many years!! A special thank you to **Prof. Alexandra Fernandes** (aka A Loira), I had the pleasure to meet you at an advanced stage of my work, but it was definitely in the right time…The time that I most needed…The time when wise words were needed to keep up the way (I will never forget that talk in your office!!). Thank you for your kindness, amiability and friendship..and NanoMONGOS all the way!!!

To the **Department of Life Sciences**, for hosting the doctoral program in Biotechnology and providing all the necessary means for the development of research during this years. Thank you to all the members for all the help, support and availability for discussing a broad range of subjects that most contribute to my scientific growth.

To **Fundação para a Ciência e Tecnologia/MEC** and **STAB VIDA** for the financial support; without it this work would not have been possible (SFRH/BDE/51103/2010).

Aos meus amigos, que não são muitos, mas que muito estimo e que sempre procuraram de uma forma ou outra manter a minha sanidade mental durante estes anos: Rita Calado, João, Daniela, Carlos, Mt, Tânia, Andreia, Pedro, Filipa, Rita Gomes, Bruno, Carina e Ivan. Um dia o meu avó, disse-me que se chegasse ao final da vida e conseguisse reunir 12 bons amigos a uma mesa de jantar é porque algo de bom eu tinha feito na vida. Ainda não tenho os 12, mas vocês - João Pedro, Ramiro, Rodrigo e Pedro Daniel vão estar nessa mesa de certeza. Obrigado pela vossa amizade incondicional e companheirismo constante.

À minha família. Um grande obrigado aos meus **Tios (Padrinhos)**, às minhas primas **Xanda**, **Cris** e **Ritinha** e ao meu primo **Paulo** pelo carinho, amizade, apoio incondicional e pelas jantaradas de festas de anos a ter discussões animadas de temas recorrentes nesses dias: futebol, política e laços familiares ☺ Aos meus queridos **sogros**, vocês são uns segundos pais para mim. Sem o vosso constante apoio, compreensão e ajuda esta tese não existiria. Este trabalho também é vosso. Aos meus cunhados, **Sérgio** e **Tiago,** os meus novos irmãos! À minha **irmã Sandra**, o meu ídolo e exemplo. Sei que não sabes isto, mas foi em ti que muita vezes fui buscar as forças para continuar, o teu espírito guerreiro e batalhador é inspirador. Sei que por vezes é difícl perceberes a minha profissão, mas nunca deixaste de apoiar-me e guiar-me para que chegasse a bom porto. Adoro-te!! Aos meus **Pais** (**Mainhã** e **Piapai**), a quem devo tudo o que sou!! Obrigado por tudo o que passaram e ainda passam por mim. Desde o dia que vos disse que queria ir "estudar os animais", sempre me apoiaram cega e incondicionalmente, sempre dando todas as ferramentas necessárias para o fazer. Se estou hoje aqui a escrever estas palavras é por vossa causa, amo-vos do fundo do meu coração! Obrigado por tudo, famelga!!

Raquel, minha amiga, companheira e mulher! Agradecer-te é pouco, muito pouco. És pequena de tamanho, mas grande de espírito ☺ A força, coragem e determinação que deste-me ao longo desta caminhada foram decisivos e determinantes para que a palavra "desistir" nunca me passasse pela cabeça. Os sacrifícios que tiveste que passar e enfrentar para que eu pudesse dedicar-me de corpo e alma ao trabalho são impagáveis (mas Prometo que vou tentar pagar). Obrigado por nunca teres disistido de mim

quando era mais do que justo que assim o fizesses. Obrigado por seres o meu porto de abrigo. Obrigado por estares aqui agora, hoje e sempre! Á minha **filha Leonor**, a minha pitú, que tanta alegria e cor trouxe à minha vida. Um sorriso, abraço ou beijo teu, dão sentido à minha vida. Tu e a tua mãe são a minha razão, os meus amores.

I can no other answer make but thanks, and thanks, and ever thanks…

RESUMO

As técnicas de biologia molecular convencionais para a detecção e caracterização de sequências de ácidos nucléicos (p.e. DNA) são actualmente, dispendiosas, demoradas e de portabilidade reduzida. O principal objetivo desta dissertação consistiu na optimização e validação de uma metodologia nanotecnologica colorimetrica, para a detecção de polimorfismos de nucleotídeo único (SNPs). Tal foi feito considerando SNPs associados à obesidade, que eram de interesse comercial para a empresa STAB VIDA, e posterior avaliação de outros alvos clinicamente relevantes. Além disso, foi alcançada a integração desta metodologia numa plataforma microfluídica que contempla a portabilidade do método e aplicação em pontos de interesse (POC).

Para garantir o sucesso na prossecução destes objectivos, o trabalho experimental foi dividido em quatro seções: i) associação de genes/SNPs relacionados com a obesidade para a população Portuguesa; ii) optimização e validação da abordagem *non-cross-linking* para caracterização genotipica completa dos SNPs relacionados com a obesidade; iii) incorporação do método numa plataforma de microfluídica e iv) a tradução para outros alvos reevantes com interesse comercial.

Os portadores do *FTO* dbSNP rs #: 9939609 apresentam um maior índice de massa corporal (IMC), a massa de gordura corporal total, perímetro da cintura e um risco 2.5 vezes acrescido para a obesidade. As *AuNPs* funcionalizadas com oligonucleotídeos tiolados (Au-nanossondas) foram utilizadas para validar o método de *non-cross-linking* como uma abordagem de diagnóstico contra a técnica padrão de ouro – sequenciação de Sanger - com elevada sensibilidade (87,50%) e especificidade (91,67%). Um sistema POC de prova de conceito em microfluidica foi desenvolvido para incorporação da estratégia de detecção molecular validada.

Em conclusão foi desenvolvido e validado com sucesso um sistema para a detecção de SNPs com interesse comercial para STAB VIDA, no sentido da sua tradução futura para um dispositivo POC autónomo.

Termos chave: obesidade, estudo de associação, nanopartículas, nanopartículas de ouro, nanossondas de ouro, microfluídica

ABSTRACT

Conventional molecular techniques for detection and characterization of relevant nucleic acid (i.e. DNA) sequences are, nowadays, cumbersome, expensive and with reduced portability. The main objective of this dissertation consisted in the optimization and validation of a fast and low-cost colorimetric nanodiagnostic methodology for the detection of single nucleotide polymorphisms (SNPs). This was done considering SNPs associated to obesity of commercial interest for STAB VIDA, and subsequent evaluation of other clinically relevant targets. Also, integration of this methodology into a microfluidic platform envisaging portability and application on points-of-care (POC) was achieved.

To warrant success in pursuing these objectives, the experimental work was divided in four sections: i) genetic association of SNPs to obesity in the Portuguese population; ii) optimization and validation of the non-cross-linking approach for complete genotype characterization of these SNPs; iii) incorporation into a microfluidic platform; and iv) translation to other relevant commercial targets.

FTO dbSNP rs#:9939609 carriers had higher body mass index (BMI), total body fat mass, waist perimeter and 2.5 times higher risk to obesity. AuNPs functionalized with thiolated oligonucleotides (Au-nanoprobes) were used via the non-cross-linking to validate a diagnostics approach against the gold standard technique - Sanger Sequencing - with high levels of sensitivity (87.50%) and specificity (91.67%). A proof-of-concept POC microfluidic device was assembled towards incorporation of the molecular detection strategy.

In conclusion a successful framework was developed and validated for the detection of SNPs with commercial interest for STAB VIDA, towards future translation into a POC device.

Keywords: obesity, association study, nanoparticle, gold nanoparticles, gold nanoprobes and microfluidic.

LIST OF ABBREVIATIONS

Ala: alanine

APOA5: apolipoprotein A-V

Arg: arginine

ARMS: amplification-refractory mutation system

AS-LAMP: allele-specific loop-mediated isothermal amplification

AuNP: gold nanoparticle

BMI: body mass index

CAGR: compound annual growth rate

CHARGE: Cohorts for Heart and Aging Research in Genomic Epidemiology

CHO: carbohydrates

CI: confidence interval

dbSNP: database single nucleotide polymorphism

DLS: dynamic light scaterring

dNTP: deoxynucleotide triphosphate

FAO: Food and Agriculture Organization

FDA: Food and Drug Administration

FTO: fat mass and obesity-associated

GIANT: Genetic Investigation of Anthropometric Traits

GWAS: genome wide association studies

HDA: helicase dependent amplification

HTR: heterozygous

HWE: Hardy-Weinberg equilibrium

INE: Instituto Nacional de Estatística

JFET: junction gate field-effect transistor

LAMP: loop-mediated isothermal amplification

LEPR: leptin receptor

LNA: locked nucleic acid

LOD: limit of detection

LSPR: localized surface plasmon resonance

MC4R: melanocortin 4 receptor

MCM6: minichromosome maintenance complex component 6

MS: metabolic syndrome

MTBC: *Mycobacterium tuberculosis* complex

MUT: mutated

NASBA: nucleic acid sequence-based amplification (NASBA)

NHLBI: National heart, Lung and Blood Institute

NP: nanoparticle

One-way ANOVA: One-way analysis of variance

op amp: operational amplifier

OPL: optical path length

OR: odd ratio

P/S ratio: ratio of polyunsaturated to saturated fatty acids

p: p-value

PCR: polymerase chain reaction

PDMS: polydimethylsiloxane

PEG: polyethylene glycol

PKU: phenylketonuria

PNA: protein nucleic acid

POC: point-of-care

PPARs: peroxisome proliferator–activated receptors

PPARγ: peroxisome proliferator-activated receptor gamma

Pro: proline

r(Abs): ratio of absorbance

RCA: rolling circle amplification

Rs: detection response

SERS: surface-enhanced Raman scattering

SMD LED: surface-mount-device light-emitting diode

SNP: single nucleotide polymorphism

SU8: epoxy photoresist

T2DM: type II diabetes mellitus

TB: tuberculosis

TEM: transmission electron microscopy

TM: melting temperature

TG: triglycerides

Trp: tryptophan

UVO: UV ozone cleaner

UV-Vis: ultraviolet–visible

WC: waist circumference

WHO: World Health Organization

WHR: waist hip ratio

WTCCC: Welcome Trust Case Control Consortium

ζ-potential: zeta-potential

TABLE OF CONTENTS

ACKNOWLEDGEMENTS ..... **V**

RESUMO ..... **IX**

ABSTRACT ..... **XI**

LIST OF ABBREVIATIONS ..... **XIII**

TABLE OF CONTENTS ..... **XVII**

FIGURE INDEX ..... **XIX**

TABLE INDEX ..... **XXI**

***CHAPTER 1* - INTRODUCTION** **1**

THESIS SCOPE **3**

1.1 OBESITY **4**

1.1.1 Causes to Obesity *5*

1.1.2 Prevalence and Economic Burden of Obesity *7*

1.1.3 Diagnosis and Management *10*

1.1.4 Nutrigenetics/Nutrigenomics *12*

1.2 SINGLE NUCLEOTIDE POLYMORPHISM (SNP) IN HUMAN DISEASES **13**

1.2.1 SNPs and their value in disease risk prediction – Obesity *15*

1.3 NANOTECHNOLOGY **19**

1.3.1 Noble Metal Nanoparticles *20*

1.3.2 Nanodiagnostics *24*

***CHAPTER 2* - MATERIALS AND METHODS** **35**

2.1 MATERIALS **37**

2.1.1 Equipment *37*

2.1.2 Consumables *38*

2.1.3 Reagents *38*

2.1.4 Solutions *39*

2.1.5 Biological Material *40*

2.2 METHODS **44**

2.2.1 Molecular Biology *44*

2.2.2 Nanotechnology *50*

2.2.3 Microfluidic fabrication *53*

2.2.4 Statistical analysis *55*

***CHAPTER 3* - ASSOCIATION OF FTO, PPARG AND APOA5 POLYMORPHISMS WITH OBESITY IN PORTUGUESE POPULATION** **57**

3.1 INTRODUCTION **59**

3.2 RESULTS AND DISCUSSION **59**

3.2.1 Genetic population characterization *59*

3.2.2 Association of SNP obesity-related (FTO rs9939609 / PPARG rs1801282/ APOA5 rs662799) and anthropometric traits *64*

3.3 CONCLUDING REMARKS **67**

***CHAPTER 4* - GOLD NANOPROBES AND THE NON-CROSS-LINKING METHOD FOR THE DETECTION OF SINGLE NUCLEOTIDE POLYMORPHISMS** **71**

4.1 INTRODUCTION **73**
4.2 RESULTS AND DISCUSSION **76**
4.2.1 Optimization and characterization *76*
4.2.2 SNP/mutation detection: proof-of-concept for FTO Au-nanoprobes *82*
4.2.3 Non-cross-linking method validation with biological sample for the obesity-related SNP in the FTO gene *89*
4.2.4 Extending the method to other the other targets scoped as obesity-related (PPARG dsSNP rs#: 1801282 and APOA5 dsSNP rs#: 662799) *93*
4.3 CONCLUDING REMARKS **96**

***CHAPTER 5* - MICROFLUIDIC PLATFORM FOR OBESITY-RELATED SNP DETECTION MEDIATED BY GOLD NANOPROBES** **99**

5.1 INTRODUCTION **101**
5.2 RESULTS AND DISCUSSION **102**
5.2.1 Set-up optimization *102*
5.2.2 Microlenses design and fabrication *104*
5.2.3. Effect of microlenses on colorimetric AuNPs analysis *107*
5.2.4 SNP detection using the optimized system *108*
5.3 CONCLUDING REMARKS **111**

***CHAPTER 6* - APPLICATION OF GOLD NANOPROBE-BASED ASSAY IN INDUSTRY SETTING – TECHNOLOGY TRANSFER TO STAB VIDA** **115**

6.1 INTRODUCTION **117**
6.1.1 Effective translation of Au-nanoprobe assay to STAB VIDA context *119*
6.2 RESULTS AND DISCUSSION **120**
6.2.1 Loop-mediated isothermal amplification (LAMP) of commercial relevant target/SNP for STABVIDA and detection mediated by Au-nanoprobes using the non-cross-linking approach . *120*
6.2.2 Allele-specific loop-mediated isothermal amplification (AS-LAMP) of commercial relevant target/SNP for STABVIDA and detection mediated by Au-nanoprobe using the non-cross-linking approach *124*
6.3 CONCLUDING REMARKS **128**
6.3.1 Development and characterization of gold nanoprobes for SNP/mutation detection *128*

***CHAPTER 7* - FINAL CONSIDERATIONS AND FUTURE PERSPECTIVES** **131**

REFERENCES **139**

APPENDICES **169**

APPENDIX I – AUNPS METHODS FOR DNA/RNA SENSING **169**
APPENDIX II – SNP GENOTYPES AND RELATED FLANKING SEQUENCES **175**
APPENDIX III – NANOFABRICATION CHARACTERIZATION **181**
APPENDIX IV – LIST OF PUBLICATIONS **185**

FIGURE INDEX

Figure 1.1 – Body Mass Index classification. 4
Figure 1.2 – Adult obesity prevalence by gender and worldwide 7
Figure 1.3 – Adult prevalence of overweight and obesity in Portugal in the adult population by gender. 8
Figure 1.4 – Fluctuation rates of overweight and obesity in Portugal and World. Comparison between overweight and obesity rates in Portugal and World in a similar period of time. 9
Figure 1.5 – Recommendation for obesity treatment. 11
Figure 1.6 – Example of a single nucleotide polymorphism. 14
Figure 1.7 – Illustration of how DNA variations (SNPs), depending the gene region which are located, can alter protein expression 14
Figure 1.8 - Schematic representation of metal nanoparticles LSPR. 20
Figure 1.9 – Effect of inter-particle distance of AuNPs on LSPR. 21
Figure 1.10 – Schematic representation of an AuNP loaded with a plethora of molecules. 23
Figure 1.11 - Microarray DNA detection via AuNPs. 26
Figure 1.12 - Gold nanoparticle based colorimetric assays. 28
Figure 1.13 - Au-nanoprobe strategy for the detection of MTBC members. Schematic representation of detection of M. tuberculosis using Au-nanoprobes and a paper platform. 31
Figure 2.1 – Illustrated example of one of the targets detection and characterization mediated by thiol-modified oligonucleotide probes. 43
Figure 3.1 – Genotype and allele frequencies data for *FTO* (dbSNP rs#: rs9939609), *PPARG* (dbSNP rs#: rs1801282) and *APOA5* (dbSNP rs#: rs662799). 60
Figure 3.2 – SNP analyses of 23 European sub-populations. 61
Figure 3.3 – Allele frequencies available from National Center for Biotechnology Information (NCBI) based on the 1000 Genome Project to the SNPs in study 63
Figure 4.1 – Sato's Non-cross-linking approach for SNP recognition 74
Figure 4.2 – Schematic representation of Baptista's non-cross-linking method 75
Figure 4.3 – Characterization of the synthesized gold nanoparticles 77
Figure 4.4 – Au-nanoprobes analytical characterization by DLS, ζ-potential and UV-Vis peak 79
Figure 4.5 – Schematic representation of differences in Au-nanoprobes hydrodynamic radius due oligonucleotide size 80
Figure 4.6 – Au-nanoprobes stability by increasing $MgCl_2$ concentration 81
Figure 4.7 – Determination of stability range against salt-induced ($MgCl_2$) aggregation for all Au-nanoprobes synthesized 82
Figure 4.8 – FTO Au-nanoprobes salt-induced aggregation profiles 83
Figure 4.9 – Hybridization assay test performed with ssDNA oligonucleotides for FTOwt20 and FTOmut20 Au-nanoprobes 84
Figure 4.10 – pH effect on FTOwt20 Au-nanoprobe hybridization event 85
Figure 4.11 – Hybridization assay results with PCR-generated targets for FTOwt20 and FTOmut20 Au-nanoprobes 86
Figure 4.12 – UV-Vis spectroscopy data from detection and discrimination of FTO (dbSNP rs#: 9939609) mediated by Au-nanoprobes 87
Figure 4.13 – FTO (dbSNP rs#: 9939609) detection mediated by the non-cross-linking method 88
Figure 4.14 – Limit of detection (LOD) profile for FTOwt20 Au-nanoprobe. 89
Figure 4.15 – Non-cross-linking SNP genotyping validation mediated by a set of two Au-nanoprobes 90
Figure 4.16 – Procedure and validation of FTOwt20 Au-nanoprobe genotyping method with biological samples 91

Figure 4.17 – Hybridization assay results with ssDNA oligonucleotides for PPARG and APOA5 Au-nanoprobes 94
Figure 4.18 – Hybridization assay results with PCR-generated targets for PPARG and APOA5 Au-nanoprobes 95
Figure 4.19 – Non-cross-linking method for SNP detection 97
Figure 5.1 - Emission spectra of SMD LEDs used for the colorimetric analysis 103
Figure 5.2 – Circuit diagram used for optical-to-electrical signal conversion and amplification 104
Figure 5.3 – LED guidance in the microfluidic channel 105
Figure 5.4 – 2D schematics of light propagation in PDMS chip of 2 mm long optical path. 106
Figure 5.5 – Microfluidic platform response for AuNP detection 108
Figure 5.6 – FTOwt20 Au-nanoprobe detection pattern in the microfluidic chip 109
Figure 5.7 - Microscopic images of air microlenses chip with FTOwt20 Au-nanoprobe for dbSNPrs#: 9939609 detection 111
Figure 6.1 – Example of POC commercial products employing isothermal DNA amplification 118
Figure 6.2 – Schematic representation of loop-mediated isothermal amplification (LAMP) 119
Figure 6.3 – Agarose gel electrophoresis of LAMP product of *MCM6* (dbSNP rs#: 4988235) optimization and biological sample amplification 121
Figure 6.4 – Biological sample characterization of *MCM6* gene (dbSNP rs:# 4988235) by comparison between via-direct sequencing and Au-nanoprobe genotyping methods 123
Figure 6.5 – AS-LAMP SNP detection by Badolo and co-workers 124
Figure 6.6 – Different approaches for the AS-LAMP method 125
Figure 6.7 – AS-LAMP temperature gradient analyses for wild type and mutated F3 primers in a 2% agarose gel electrophoresis 126
Figure 6.8 – Proof-of-concept of AS-LAMP proposed 126
Figure 6.9 – Detection of AS-LAMP products mediated by the non-cross-linking approach 127
Figure 6.10 – Prototype design for future development for targeting relevant SNP based on AS-LAMP and the non-cross linking approach 129
Figure AII.1 – Genotype characterization of each SNP studied 175
Figure AIII.1 - Confocal microscope images of fabricated 2D microlenses: 181
Figure AIII.2 - Scanning electron micrographs of the PDMS chip: 182
Figure AIII.3 - Absorption spectra of the dispersed and aggregated AuNPs. 182
Figure AIII.4 - Transmission spectra of green and red LEDs. 183
Figure AIII.5 - Microscopic images of chip with air microlenses 183

TABLE INDEX

Table 1.1 - Classification of Overweight and Obesity by BMI, waist circumference and associated disease risk……5
Table 1.2 - The four levels of obesity susceptibility according to the environment surroundings……...7
Table 1.3 - Obesity risk status determination in adults……..….11
Table 1.4 - Gene vs. nutritional intake interactions on obesity/adiposity markers…….....13
Table 1.5 - Common covalent immobilization strategies for AuNP functionalization…….24
Table 3.1 - Allele frequencies for the SNPs in study in European sub-populations…….....63
Table 3.2 - Anthropometric data of all subjects subdivided byphenotype……..…64
Table 3.3 - Anthropometric measures in function of each genotype of each SNP……..…65
Table 3.4 - OR values between control-case and case-case groups……66
Table 4.1 - Comparison between genotyping methods for the SNP rs9939609 present in the FTO gene……92
Table 4.2 - Au-nanoprobe characteristization used for genotyping SNPs from PPARG (dsSNP rs#: 1801282) and APOA5 (dsSNP rs#: 662799)……..93
Table 6.1 - LAMP primer design for MCM6 SNP (dbSNP rs#: 4988235)……..121
Table 6.2 - Comparison between genotyping methods for the SNP rs4988235 present in the MCM6 gene ……..123
Table AI.1 - AuNPs methods for DNA/RNA sensing……..169
Table AIII.1 - Main characteristics of the operational amplifiers used in various system optimization stages…….....181
Table AIII.2 - The curvatures (R), distances (d) and the characteristics of the resulting light beam (y and θ) for the input bi-concave air microlens and the input bi-convex PDMS microlens……..181
Table AIII.3 - The curvatures (R), distances (d) and the characteristics of the resulting light beam (y and θ) for the output bi-concave and bi-convex air microlens……181

To my parents, sister, wife and daughter

If we knew what it was we were doing, it would not be called research, would it?

Albert Einestein

CHAPTER 1 - INTRODUCTION

Disclaimer: Part of the literature review presented in this chapter has been published, whole or in fraction, elsewhere:

Franco R, Pedrosa P, **Carlos FF**, Veigas B, Baptista PV. 2016. Gold Nanoparticles for DNA/RNA based diagnostics – Handbook of Gold Nanoparticle Research. Springer (accepted).

Larguinho M, Figueiredo S, Cordeiro A, **Carlos FF**, Cordeiro M, Pedrosa P, Baptista PV. 2015. Nanoparticles for diagnostics and imaging. Frontiers in Nanomedicine Vol.1. pp 3-46. Bentham Science Publishers.

Vinhas R, Cordeiro M, **Carlos FF**, Mendo S, Fernandes AR, Figueiredo S, Baptista PV. 2015 Gold nanoparticle-based theranostics: disease diagnostic and treatment using a single nanomaterial. Nanobiosensors in Disease Diagnosis. 4:11-23.

Thesis Scope

To fully understand the motivation behind the dissertation here presented, it is necessary to address some aspects. This PhD was co-funded and accepted by a Portuguese biotech company, STAB VIDA. STAB VIDA is a DNA-based-laboratory specialized in genetics and is focused in the development of user-friendly applications in diagnostics, personalized medicine, and genetics self-knowledge. The company started its activities in 2001 and in 2008 initiated the development of genetic tests related to food intolerance. Hence, risk assessment is part of the R&D and portfolio outlines. In 2008, I was accepted in STAB VIDA and had the opportunity to work in the R&D department of the Human Genetic Laboratory. During this period, one of the main goals consisted in the development and validation of genetic tests, including the genetic test for obesity risk assessment. This test was successfully developed, with the final outcome of a national patent. In parallel, the R&D outline in nanotechnology-based schemes was already in progress, as result of a successful collaboration between STAB VIDA and Universidade Nova de Lisboa. This concerted partnership resulted in the development of an innovative approach for single nucleotide polymorphism (SNP) genotyping mediated by nobel metal nanoparticles (Gold Nanoparticles). Hence, taking advantage of this background, a new collaboration between both entities was proposed, and the end result is the PhD here presented. In summary, this second collaboration is focused in the validation of the nano-scheme with biological samples for risk assessment of obesity-related SNPs. Another goal consisted in the optimization of the assay for future implementation in a point-of-care (POC) platform. Moreover, after validation, the aim is to translate the knowledge generated to STAB VIDA laboratory routine and span this method to other relevant SNPs with commercial interest for the company.

In conclusion, the main objective of the PhD project is to optimize and validate a nanodiagnostic scheme for the detection of genetic variations associated with obesity and spanning the methodology to other relevant targets with commercial interest. In order to attain this milestone the project proposed intends to:

Task 1 - Identify the most relevant genetic variations associated with obesity in the Portuguese population;

Task 2 - Optimize and validate a nanotechnology-based approach, developed by the company STAB VIDA in collaboration with Universidade Nova de Lisboa at Nanomedicine@FCT group, for SNPs detection based on noble metal nanoparticles;

Task 3 - Integrate the validated test into a microfluidics platform aiming its portability and application on point-of-care (POC);

Task 4 - Translate the nanoscheme for full SNP genotype characterization to STAB VIDA's laboratory routine – to be performed after optimization and validation against gold standard techniques for SNP genotyping (Sanger Sequencing). Extension to other potential targets with commercial interest for STAB VIDA shall be considered.

1.1 Obesity

The World Health Organization (WHO) defines obesity and overweight as a medical condition that may increase health problems and decreased life expectancy driven by abnormal or excessive fat mass accumulation (WHO 2000). Indeed, several chronic diseases are correlated with obesity and overweight, parameters that are considered a risk factor to hypertension and cardiovascular diseases (Clark et al. 2014), type 2 diabetes (Kahn et al. 2006, Freemantel et al. 2008)) and cancer (Renehan et al. 2008, Park et al. 2014).

Obesity can be related to the total fat mass of an individual and preferably measured by direct fat-measuring methods (imaging techniques). Nevertheless, is usually estimated by surrogate measurements such as the Body Mass Index (BMI) or waist circumference (WC), due to practical and economic reasons. To evaluate the patient personal risk towards obesity, several anthropometric measurements have to be considered, namely weight, height, waist and hip circumference and fat mass. The standard and most robust method to classify obesity in the population was firstly created by Adolphe Quetelet in 1830-1850 and is entitled the Body Mass BMI or Quetelet Index (Eknoyan et al. 2008). BMI allows to determine how much of a person body weight is deviated from what is consider normal or expected for total weight and is resolute by the weight (in kilograms) of a subject divided by the square of his height (in meters) and is age and gender independent in adults (Prentice et al. 2001) (Figure 1.1).

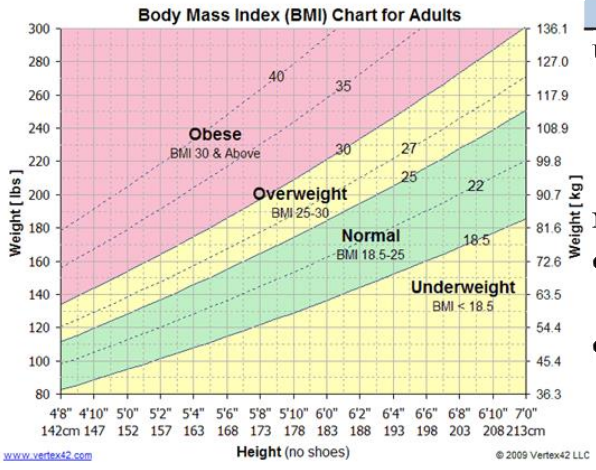

Classification	BMI (Kg/m^2)
Underweight	< 18.00
Severe thinness	<16.00
Moderate thinness	16.00-16.99
Mild thinness	17.00-18.49
Normal Range	18.50-24.99
Overweight	≥ 25.00
Pre-Obese	25.00-29.99
Obese	≥ 30.00
Obese Class I	30.00-34.99
Obese Class II	35.00-39.99
Obese Class III	≥ 40.00

Figure 1.1 – Body Mass Index classification. The standard method to determine and classify obesity in the adult population (WHO, 2000).

Moreover, it is important to mention that WC can be considered when evaluating the risk to obesity in patients who are categorized as normal or overweight by itself, but not in those who are already obese (BMI ≥ 30 Kg/m^2) since it adds little to the predictive power of the disease risk classification of BMI. There is a restrict correlation between waist circumference and BMI as a predictive risk assessment to type 2 diabetes (T2D), hypertension and cardiovascular disease.

Taking in account the BMI, men are at relative high risk to obesity if the waist circumference is greater than 102 cm and women if greater than 88 cm. Moreover, waist circumference can be used as a powerful tool for monitoring increment or decrement abdominal fat even in the absence of BMI alterations. The degree of risk it summarized in Table 1.1 (WHO 2000).

Table 1.1 - Classification of Overweight and Obesity by BMI, waist circumference and associated disease risk (WHO 2000).

		Disease Risk (Relative to Waist Circumference)	
	BMI (Kg/m^2)	**Men ≤ 102 cm Woman ≤ 88 cm**	**Men > 102 cm Woman > 88 cm**
Underweight	< 18.50	-	-
Normal Range	18.50-24.99	-	-
Overweight	25.00-29.99	Increased	High
Obese	≥ 30.00	-	-
Class I	30.00-34.99	High	Very High
Class II	35.00-39.99	Very High	Very High
Class III	>40.00	Extremely High	Extremely High

1.1.1 Causes to Obesity

It is common knowledge that for centuries the human race fought against food scarceness, diseases and extreme hostile environments and in the last decades of 19th century, it was determined that poverty, malnutrition and health problems were indicators of low industrial productivity. It was then considered that it was essential to suppress health and nutrition problems of the working class, in order to extend life expectancy, but also to improve economic productivity (Fogel et al. 1997). The improvement of the BMI (from underweight to the normal range) was attained by John Boyd Orr, the founding director of the Food and Agriculture Organization (FAO), that achieve this goal with the addition of sugars and comestible fats to the common diet (Orr, 1936). This social economical decision led, in the following decades, to major increment in accessibility of dietary energy as was never seen before. FAO estimates that in 2002 global food production reached the historical 2600 kcal per capita and is rising (Bruinsma, 2003). Finally it is important to mention that in 20th century developed countries suffer a deviation in the height/weight progressive growth. This was mainly registered due better-off countries started to gain more weight than height, and BMI suffered deviations from normal to overweight and obese ranges. During the course of human evolution cultural variations have occurred far more rapidly than genetic adaptation and obesity finds its genesis in this discrepancy (Eaton et al. 1998).

The excessive accumulation of fat mass in the body that is correlated to obesity cannot be characterized only by the ingestion of large amounts of food (calories) and low physical activity. Several factors play a leading role in the manifestation of this disease and distinguish them can be a key instrument in obesity management. The main elements considered by epidemiological studies are:

- *Sociocultural*

  In developed countries, the prevalence of obesity is higher in those that present low educational level and/or income (Visscher et al. 2002, Seppänen-Nuijten et al. 2009, Marques-Vidal et al. 2010). Also, it is stated that marital status seems to have influence in obesity prevalence after marriage (Tzotzas et al. 2010).

- *Demographic*

  Obesity status tends to increase with age, men and women equally increase their weight at least up until 50-60 years (Moody 2014) (Age); women show generally higher obesity rates when compared to men (Kanter and Caballero, 2012) (Gender); ethnicity cannot be used as factor of obesity association.

- *Behavioral*

  By the laws of thermodynamics, when the system input exceeds the output, a positive balance is achieved. This consideration can be translated to what happens in the human body – when the dietary energy intake exceeds the normal dosage and is not suppress with convenient energy output, it is converted in body weight accumulation. The topic dietary energy intake and expenditure is believed to be one of the most important. However, it still is a controversial subject as a proper study in controlled conditions is considered irksome job. Moreover, the methodologies used are flawless and limited since are based on self-reported dietary intake and physical activity (Sazonov and Schuckers, 2010).

  The effect of some risk behaviors such as smoking (Molarius et al. 1997, Dare et al. 2015) and alcohol consumption (Suter 2005, Traversy and Chaput 2015) are associated with body weight increment but in both of them vary considerably among populations. The cessation of smoking and moderate alcohol consumption are related with weight gain.

- *Genetic*

  Genes may play an important role in obesity development. Several twin, adoption and family studies were conducted and determine that obesity represents 40-70% level of obesity heritability (Stunkard et al. 1990, Sørensen et al. 1992). Reports on monogenic forms of obesity represent only a small fraction of all obesity cases (Farooqi and O'Rahilly 2005, Walley et al. 2006) and most of them result from interactions between genes (polygenic) and environment (obesogenic environment) - Susceptibility for obesity – See Table 1.2. To date 52 genetic *loci* were identified to be associated to obesity–traits by Genome Wide Association Studies (GWAS) (Loos 2012, Apalasamy and Mohamed 2015).

Table 1.2 – **The four levels of obesity susceptibility according to the environment surroundings** (Loos and Bouchard 2003).

Level of genetic susceptibility	Body size in a non-obesogenic environment	Body size in an obesogenic environment
Genetic Obesity	Massively Obese	Massively Obese
Strong Predisposition	Overweight	Obese
Slight Predisposition	Normal Weight / Overweight	Overweight / Obese
Genetically Resistant	Normal Weight	Normal Weight

1.1.2 Prevalence and Economic Burden of Obesity

Defining overweight and obesity prevalence rates has become an important tool commonly used for public and political statements to point out how obesity is becoming an epidemic disease (Caballero 2007). Nevertheless, defining these rates has become an irksome quest due the rapidly fluctuating rates seen in the last decades that are translated in constant out of date data. The classification of a population by weight and the awareness of its determining factors are essential elements and cannot be overemphasized in order to i) obtain significant comparisons of weight status within and between populations; ii) clearly identify individuals at increased risk of morbidity or mortality and its economic consequences; iii) undertake health planning programs and health promotion projects (Bariohay et al. 2011). The last senses made in 2008 estimates that the prevalence of overweight worldwide in the adult population (20 years and older), already surpass the barrier of 1 billion, being estimated that 1.5 billion are overweight of which 200 million men and 300 million women are obese (WHO 2000). In a practical way this mean that 1 in every 3 adults in the world is overweight and 1 in every 9 is obese (Figure 1.2).

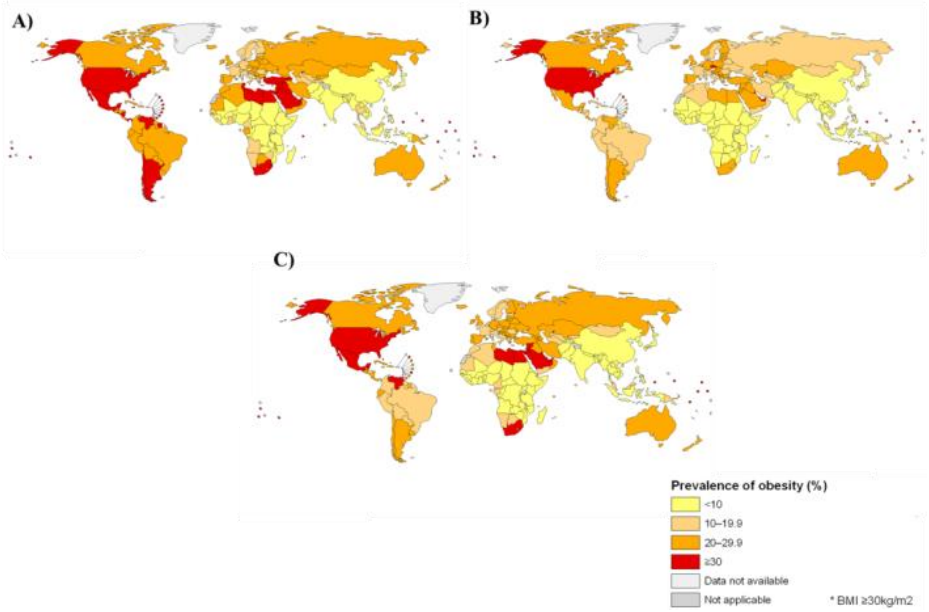

Figure 1.2 – Adult obesity prevalence by gender and worldwide. **A)** Adult (>20 years old) female obesity prevalance, **B)** Adult (>20 years old) male obesity prevalance and **C)** Global adult obesity prevalance.

Also, 1 in 5 women are obese in 117 counties while 1 in 5 men are obese in 73 counties (Figure 1.2). In the last three decades (1980-2008), in absolute values obesity rates almost doubled, from 6.4% in 1980 to 12% in 2008, being half of this growth (2.8%) felt between 2000 and 2008 (WHO 2000).Formally recognized as a pandemic disease in 1997 by the WHO, obesity was first associated with high socioeconomic status present in developed regions, such as North America (USA) and Europe. Nevertheless, new data suggest a significant shift in this theory where the most dramatic increase is occurring in countries such as Mexico, India, China, New Zeeland and Thailand (Popkin and Gordon-Larsen 2004, Popkin and Slining 2013.). Also, through global longitudinal and cross-sectional data available it is postulated that obesity is no longer a disease exclusively from developed countries since it is estimated that obesity rates of intermediate development countries increased between 30 and 100% in the last 10 years (Popkin 2004a).

Portugal, like most of developed countries (Prentice 2006), faces a serious health problem related to overweight and obesity. Data from 1995 showed that 49.6% of the adult Portuguese population was overweight (35.2%) or obese (14.4%) (Carreira et al. 2012). More recently, in the last survey performed the Portuguese population already overdoes the 50% barrier - overweight (39.4%) and obesity (14.2%) (do Carmo et al. 2008). (Figure 1.3). Comparing the overall rates of overweight and obesity of the Portuguese population with the worldwide it is possible to see that both are increasing. Although Portugal presents higher rates when compared to the world rates, the fluctuation felt was not as marked as the mean of the world, where the obesity rates, for example, almost doubled (Figure 1.4).

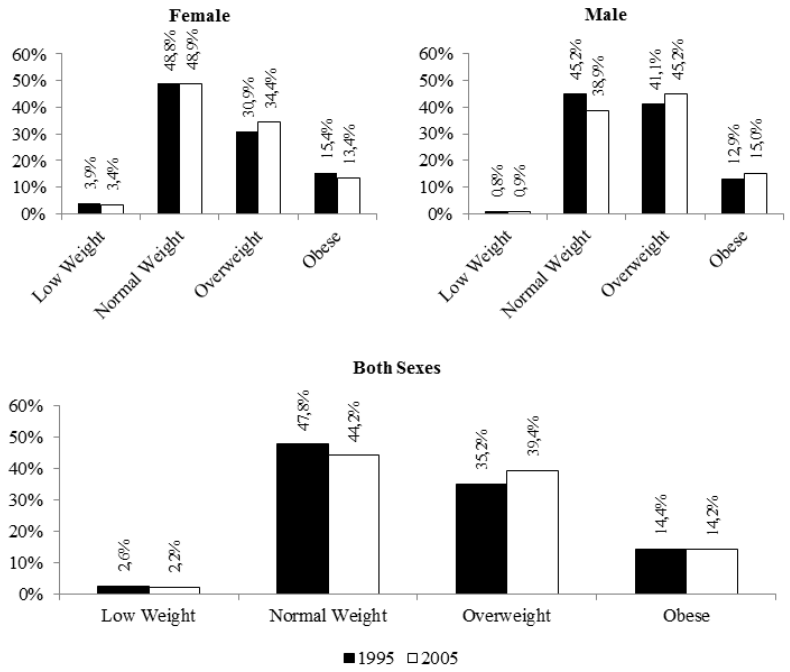

Figure 1.3 – Adult prevalence of overweight and obesity in Portugal in the adult population by gender. Adult Portuguese population BMI modifications between 1995-1998 and 2003-2005.

What is important to retain, from Portugal data, is that despite the slight obesity rate decrement, an important growth in overweight was registered, that was driven from the decrement of total normal weight. Despite obesity has been targeted as a serious public health problem in Portugal, more than one decade ago, from these data it is possible to assume that actions made in order to reduce obesity rates in Portugal seam not being effective. In conclusion it is possible to infer that the prevalence of overweight/obese adults is rising in the Portuguese population and that populations risk groups are: i) middle age; ii) 7-9 years old; iii) low socioeconomic level and iv) low-education level (Carreira et al. 2012).

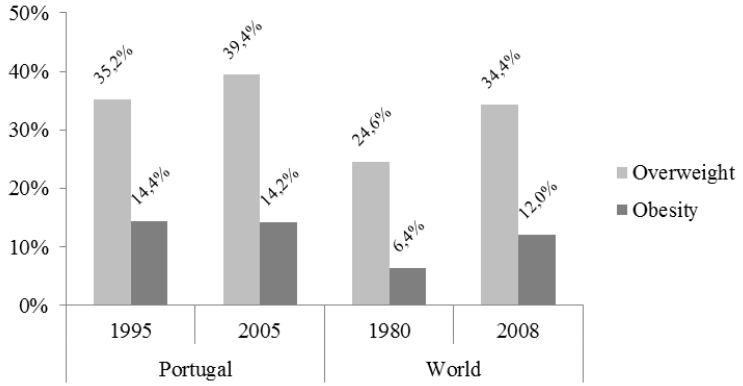

Figure 1.4 – Fluctuation rates of overweight and obesity in Portugal and World. Comparison between overweight and obesity rates in Portugal and World in a similar period of time.

The treatment and medical monitoring of a patient with obesity and associated diseases, such as hypertension, stroke, heart failure and diabetes naturally has remarkable economic consequences for health care services. Furthermore, the associated diseases, conditioned by obesity, involve loss of valuable production through absenteeism and premature mortality.

In 1967, Dorothy Rice developed a methodology to evaluate the economic burden of an illness (Rice 1967). This methodology allows inferring and differentiates three types of costs: direct, indirect and intangible. Translating this to obesity, the direct costs, the most perceptible and easy to assess, are related to financial consequences of medical resources devoted to treating all obesity-related conditions, such as ambulatory care, hospitalization, pharmacotherapy, radiological or laboratory tests, and long-term care (including nursing home). The indirect costs are related to economic burden driven by the disease, such as work absenteeism or reduced productivity, early retirement and disability pensions, etc. The intangible costs are associated to general impact of the individual well-being (social segregation, loss of mobility, pain, dependence, etc.) that are less straightforward and much challenging to determine from an economic point-of-view.

In a recent systematic review from 2011 (Withrow and Alter 2011) a study was conducted aimed to determine the worldwide direct costs associated to obesity. It was determined that disease account for 0.7% to 2.8% of a country's total healthcare expenditure. The reports available in Portugal from the Instituto Nacional de Estatística (INE), concludes that the direct costs with obesity is 3.5% of all healthcare expenditure. In conclusion, these findings indicate that Portugal spends a total of 500 M€/year with obesity and associated diseases, from which 300 M€ is account in direct costs and 200 M€ are from indirect costs (Pereira and Mateus 2003). A recent report from 2011 states that improving the health of individuals would save about 20% of the overall health care budget, about 15% of social security benefits and enhance labor productivity to the extent of about 1.4% of gross domestic product (McKee 2011).

1.1.3 Diagnosis and Management

In order to reverse the prevalence and trends of worldwide overweight and obesity, collective changes should be made, not only individually, but the overall society, in order to contribute for healthier lifestyle behaviors and factors (Orzano and Scott 2004, Tsigos et al. 2008). Physicians and health care professionals play an important role in addressing preventive actions for weight gain, promoting safe and effective weight loss and weight maintenance programs as well as identify patients at increased risk and target them for an earlier clinical and lifestyle intervention (Bardia et al. 2007, Kushner et al. 2013).

Obesity assessment and diagnosis includes determination of the degree of obesity and overall health status. By the document released in 1998 by the expert panel from National Heart, Lung and Blood Institute (NHLBI) these factors can be determined by measuring regularly BMI patient, which although do not directly measure body fat, nor does it differentiate between fat and muscle, still is a robust measurement to evaluate changes over time. Also, WC should also be measured in order to estimate abdominal adiposity, an independent risk for cardiovascular disease, type 2 diabetes, dyslipidemia, and hypertension. Furthermore, if the patient has a BMI equal or greater than 25 kg/m^2 or presents a WC greater than 88 cm in women and 102 cm in men, blood pressure, lipid levels should be measured and fasting glucose tested. Since overweight and obesity causes are in most of the cases a combination of hereditary predisposition and lifestyle factors, additional evaluation parameters should be taken such as dietary and exercise habits, age at onset of weight gain, previous weight-loss efforts and smoking history (NOEIE Panel 1998). The assessment and evaluation of a patient involves the disease risk status determination (Table 1.3) in order to established an effective and long-term management plan that should comprises 6 steps, that varies from patient: i) definition of realistic and objective goals; ii) dietary strategies to reduce energy intake or manipulate macronutrient distribution; iii) exercise program to increase physical activity; iv) behavior and or psychological therapy; v) pharmacotherapy to increase

thermogenesis or reduce appetite (only after lifestyle therapy has failed) and vi) weight loss surgery (i.e., persons with a BMI ≥40 kg/m^2 or with a BMI ≥35 kg/m^2 with comorbid conditions).

Table 1.3 - Obesity risk status determination in adults (NOEIE Panel 1998).

Obesity risk status determination in adults
Assess degree of overweight based on BMI
Assess presence of abdominal obesity based on waist circumference
Assess presence of underlying diseases and conditions:
Coronary heart disease
Other atherosclerotic diseases:
Peripheral arterial disease
Abdominal aortic aneurysm
Symptomatic carotid artery disease
Type 2 (formerly non–insulin-dependent) diabetes mellitus
Sleep apnea
Gynecologic abnormalities
Osteoarthritis
Stress incontinence
Gallstones and their complications
Assess presence of cardiovascular disease risk factors:
Cigarette smoking
Hypertension
High low-density lipoprotein cholesterol
Low high-density lipoprotein cholesterol
Impaired fasting glucose
Family history of premature coronary heart disease
Age (men ≥ 45 years; women ≥ 55 years or postmenopausal)
Assess other risk factors:
Physical inactivity
Elevated serum triglyceride level
Genetic factors

In conclusion, screening, management and treatment of obesity can be a very intricate issue with several obstacles to overcome. Nonetheless, when effective, will not only help a patient to lose weight but also to guide and teach the importance of weight maintenance. In a long-term basis this is translated in patient status health improvement (Figure 1.5).

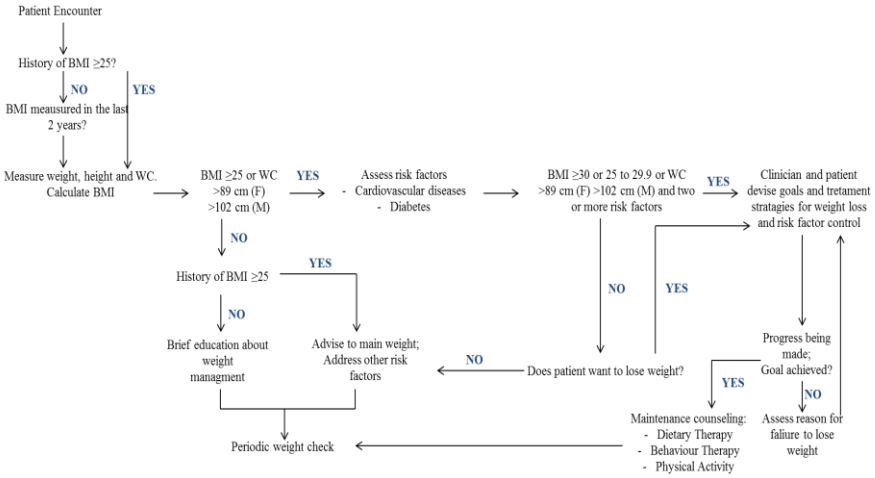

Figure 1.5 – Recommendation for obesity treatment. Obesity treatment references for patients with BMI ≥30 Kg/m^2 regardless of risk factors (NOEIE Panel 1998).

1.1.4 Nutrigenetics/Nutrigenomics

Understanding the multifactorial components that contribute to weight gain of an individual or a population can be an arduous and intricate job. Several factors should be taken in account when talking about overweight and obesity. In the last few years a new area of research has gained strength and it may play a pivotal role in understanding and controlling this disease – Nutrigenetics. Nutrigenetics tries to explain the role of DNA sequence variation in response to nutrients intake, in other words, focused their attention in the biological and behavioral potential responses that several genomic markers have in response to micronutrients, macronutrients and calories intake (Mariman 2006). Nutrigenetics should not be confused with Nutrigenomics, another branch of nutritional genomics –which is also an important field for the study obesity, which attempts to identify how nutrition or diet can influence gene expression and related biological and molecular events (Kussmann and Fay 2008). A classic fitting model where a single nutrient can be used to manage a genetic background is Phenylketonuria (PKU). PKU is characterized by deficiency production of a specific enzyme (phenylalanine hydroxylase) that metabolizes phenylalanine, an essential amino acid found in any common diet (e.g. meat, fish, nuts, etc.), to tyrosine. Reduced levels of this enzyme lead to phenylalanine accumulation and subsequently conversion to phenylpyruvate that is very harmful to the brain. Patients with PKU need to have a restricted or low phenylalanine diet for life to decrease/avoid the symptoms (Giovannini et al. 2012). The importance of Nutrigenetics research for obesity-trait is based on the assumption that individual differences exist in reaction to severe or repeated exposure to a specific and/or combination of nutrients and that the differences rely on specific genomic markers (Qi 2014). This assumption is well documented and is focused on DNA variations related to appetite control, energy and lipid usage and adipocyte metabolism and signaling, where the measured output were obesity risk, BMI, body composition and/or appetite/satiety levels – for more insight please see Table 1.4.

Tagging individual relevant genetic determinants that may affect a specific nutritional intervention with the purpose of preventing excessive weight gain, achieving effective weight loss and successful long-term maintenance can be an important tool for obesity management and therapy. It is noteworthy that already has been proven that subjects presenting specific genetic determinants revealed differences in response to caloric restriction diets (Abete et al. 2012). Nevertheless, to take advantage of this extraordinary opportunity that is to match a specific dietary guideline to the individual biology, it is necessary to bridge some existing issues in order to move forward with Nutrigenetics (Doo and Kim 2015). For instance it is essential to gather all the information brought by high-throughput genotyping and sequencing technologies so that genome-wide explorations of DNA, given by large consortium that analyze variant-nutrient interactions, like GIANT (Lindgren et al. 2009) and CHARGE (Heard-Costa et al. 2009) can generate reliable and accurate information so new mechanisms and pathways of interests can be addressed. Also,

better comprehension of the molecular mechanisms underlying many of these gene-nutrient interactions still remain unclear and are needed to be clarified before individualized recommendations are given (San-Cristobal et al. 2013).

Table 1.4 - Gene vs. nutritional intake interactions on obesity/adiposity markers (Marti et al. 2010).

Genes	Controlled Nutritional Factor	Main Variable	Outcome depending on gene polymorphism	Reference
PPARG	Total fat P/S ratio	BMI	In rs1801282, BMI was greater among Ala allele carriers only when the P/S ratio was low and in Pro homozygotes when this ratio is high.	Luan et al. 2001
	CHO	BMI/ obesity risk	In rs1801282, Pro 12 Ala carriers were associated with increased risk of obesity in those subjects in which > 49% energy came from CHO	Marti et al. 2002
APOA5	Energy and fat intake	BMI	In rs662799, carriers of the Apo5-1131C allele had lower obesity risk only when in the high fat intake group, but higher obesity risk with low fat intake	Corella et al. 2007
ADBR3	Total energy	Obesity risk	Arg 64 allele carriers were associated with higher obesity risk than Trp64Trp homozygotes only in the highest energy consumers	Miyaki et al. 2005
FTO	Macronutrient intake	Appetite/ satiety	Children carrying the A variant allele (rs9939609AT) showed higher calorie and total fat intake	Timpson et al. 2008

P/S ratio: ratio of polyunsaturated to saturated fatty acids; CHO: carbohydrates; Pro: Proline; Ala: Alanine; Arg: Arginine; Trp: Tryptophan

1.2 Single Nucleotide Polymorphism (SNP) in Human Diseases

The chronic condition of obesity has been extensively studied in various areas of health sciences and the interconnections of areas such as endocrinology, psychology, nutrition and genetics allowed determining several factors that contribute to overweight and obesity. Genetics has been an extremely useful tool in understanding this disease and led to the discovery of different *loci* in different genes that allow better understanding of the genetics behind obesity. The genetic component that contributes to obesity is multifactorial, involving several genes and polymorphisms that have been associated with an increased risk of hypertension **(**Rahmouni et al. 2005, DeMarco et al. 2014), type II diabetes (Mokadad et al. 2003, van Greevenbroek et al. 2013), cardiovascular (Cepeda-Valery et al. 2014) and several cancer types **(**Renehan et al. 2008). There are several important genes in the development of obesity and related diseases that are described in numerous association studies that establish the correlation phenotype / genotype (Rankinen et al. 2006, Meyre et al. 2009, Wang et al. 2011, Fall and Ingelsson 2014, Locke et al. 2015, Pers et

al. 2015). The human genome is 99.9% equal between two distinct individuals, the residual 0.1% contains millions of inherited differences in our DNA sequence, contributing to phenotypic variations in an individual, that may influence anthropometric traits, risk to a certain disease or response to environment (Bell 2004, Goldstein 2009). Several types of variations can occur in the DNA sequence and the simplest form of these variations is the substitution of one nucleotide for another, denominated Single Nucleotide Polymorphism (SNP) – See Figure 1.6.

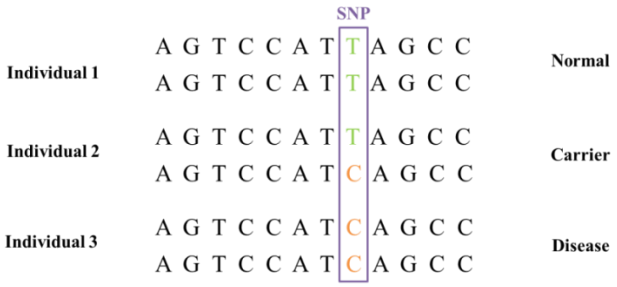

Figure 1.6 – Example of a single nucleotide polymorphism.

SNPs are far more common in our DNA sequence that any other polymorphism accounting a frequency of 1 SNP for 1000 base pairs (bp) (Brookes 1999). The 1.42 million SNP already pinpoint by genetics in our DNA (Sachidanandam et al. 2001) give valuable information that contribute most significantly to population variation in each trait (Suh and Vijg 2005, Norrgard and Schultz, 2008, Albert and Kruglyak, 2015). The direct effect given by a certain SNP in a human trait can be felt dependent the gene region in which is located. A variant may result in an amino acid change or splicing process modification, thus directly modifying the relevant protein, or it may be present in a regulatory region, altering the level of expression or the stability of the mRNA (non-synonymous SNP). Nevertheless, most of the SNPs already tagged are known to be stable and are present in intergenic spacers and are not deleterious to organisms (Shastry 2002, The International HapMap Consortium 2003) – Figure 1.7

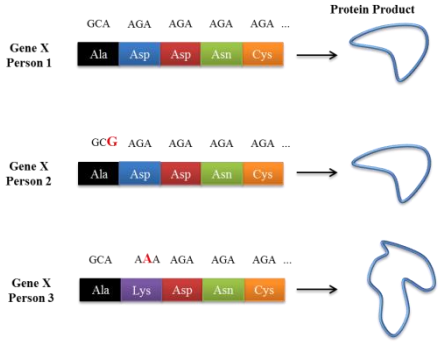

Figure 1.7 – Illustration of how DNA variations (SNPs), depending the gene region which are located, can alter protein expression. The SNP present in Person 2, do not modify the amino acid (synonymous SNP) and no change occurs in protein production. However, in Person 3, the variation is a non-synonymous SNP, and led to the amino acid variation (Asp – Lys) and protein variation can play a direct or indirect role in phenotypic expression.

Most of the genetic variants are shared between populations, thus diseases can or is expected to be influenced by variants that are common in all populations. For this reason, one of the main goals of tagging SNPs that play a direct role in a disease is to understand the mechanism of the disease, in order to figure out therapeutic intervention that can prevent or in the best case scenario cure the disease (Wang and Moult 2001 / Do et al. 2012).

1.2.1 SNPs and their value in disease risk prediction – Obesity

The first studies carried out in 90's that tried to correlate or associate candidate genes to common obesity were heavily relying on their role in the appetite-regulating hormones or their receptors, such as leptin (*LEPR*) (Clément et al. 1998) or melanocortin 4 (*MC4R*) (Vaisse et al. 1998). These genes were subsequently tested in different populations. However, the approach was limited by the small size sample ($n<1000$), heterogeneous genetic background from the candidate genes and difficult in results replication (Rankinen et al. 2006, Wray et al. 2006). Data available from the Human Genome Project (McPherson et al. 2001) published in 2001 and the HapMap Project finished in 2005 allowed to have an alternative methodology to search for obesity susceptibility genes between distinct populations. The massive genetic information given by this two projects and the development of high-throughput genotyping techniques and bioinformatics platforms allowed the identification of several genetic variants relevant for obesity and other traits, through large-scale genome wide association studies (GWAS) (Iles 2008, Welter et al. 2014). Genome-wide outlines of variations across populations give significant information about human evolution (i.e.: migration and adaptation patterns) (Sirén et al. 2011) but also can explain the heritable risk and biological pathways and linkages of complex diseases (Hirschhorn and Daly et al. 2005, Pearson and Manolio 2008). GWAS are the most commonly used method to identify important *loci* associated to a particular trait or phenotype and can be set in two stages: i) the discovery stage – several hundred thousands of SNPs are tested for association with a particular trait in a population, ii) the validation stage – the SNPs that show the highest level of association with the trait of interest in the first stage are now tested for association in a new population (same similar size and design) (McCarthy et al. 2008, Yang et al. 2013). The results given by these two stages are meta-analyzed and the association established between trait and SNPs that hold for these procedures are called ''genome-wide significant'' (Panagiotou et al. 2013). Nowadays, and to ensure that the likelihood of false-positive findings is reduce in a GWAS derived from multiple testing, correction and replication in independent samples is performed and the significant value has to be highly stringent. For this reason, a SNP is only considered genome-wide significant for a certain trait if the association level is $p<5x10^{-8}$ (Panagiotou et al. 2012).

From what concerns obesity GWAS the main goal is to find out candidate gene/SNPs that identify a possible *locus* obesity-related (i.e. BMI, WC, WHR, fat mass or other associated

diseases). Since the GWAS era in 2005, there were 5 big waves of GWAS linked to obesity. The first GWAS that discovered an important *locus* associated with BMI was published in 2007 by the Welcome Trust Case Control Consortium (WTCCC) (Frayling et al. 2007) and until now more than 50 *loci* has been identified and associated with at least one obesity-related trait (Loos 2012, Sandholt et al. 2012, Xia and Grant, 2013).

1.2.1.1 Fat mass and obesity-associated (*FTO*) gene

The first report that associated a common variant with strong statistical significance for BMI was published in 2007 by Frayling and co-workers (Frayling et al. 2007). This work was attained as a by-product of GWAS for type 2 diabetes (T2D), comprising 39,000 subjects. The dbSNP rs#: rs9939609 present in the intron 1 of the *FTO* gene was found to be strongly correlated with BMI increment both in adult and children, regardless of the gender. In this report the authors demonstrate that homozygous carriers for the risk allele had 1.67-fold increased risk to obesity and weighed 3 kg more when compared with those not inheriting a risk allele. Afterwards, others GWAS replicated these results both in child and adult European population and similar robust significance were found for BMI (Scuteri et al. 2007, Dina et al. 2007, Jacobsson et al. 2008, Legry et al. 2009, Hakanen et al. 2009, Rodríguez-López et al. 2010, Zavattari et al. 2011, González et al. 2012, Sentinelli et al. 2012, Aluquerque et al. 2013). These findings were replicated in other studies in groups with non-European ancestry. Large-scale studies in East Asian (Hotta et al. 2008, Liu et al. 2010, Dorajoo et al. 2012, Wen et al. 2012) and African (Grant et al. 2008, Hennig et al. 2009, Deliard et al. 2013) populations identified *FTO* dbSNP rs#: rs9939609 as significantly associated with obesity or BMI. This specific variation in the intron 1 of the *FTO* gene not only confers higher risk to BMI increment in different population and is not gender and age dependent, but also to other anthropometric traits obesity-related such as higher waist circumference and waist-hip circumference.

When the first associations between SNPs present in *FTO* and BMI were initially described, little was known about the function of the *FTO* gene product. However, some murine studies brought a new perspective on the issue. *FTO* was firstly identified as one of the six contiguous genes in a 1.6 Mb chromosomal deletion causing the fused-toe phenotype in mice (Peters et al. 1999). Mice that are homozygous for the deletion died mid-gestation, whereas heterozygous fused-toe mutants presented severe developmental abnormalities, reduced hypothalamic development, (van der Hoven et al. 1994, Anselme et al. 2007) besides fused digits and hyperplasia of the thymus without any metabolic alterations. On the other hand, data from the first FTO knock-out mouse model did not show such severe developmental defects, nevertheless present retarded postnatal growth, a significant reduction in body weight and fat mass due increment of energy expenditure and relative decreased of hyperphagia (Fischer et al.

2009). *FTO* is ubiquitously expressed, with relatively high expression in the brain, particularly in the hypothalamus (Gao et al. 2010). This region is known to be where control of energy homoeostasis is centered and influenced by the nutritional states, hence suggesting that *FTO* increases risk of obesity through a central regulation of food intake (Gerken et al. 2007). In a recent work of Church and co-workers it was demonstrated that overexpression of FTO leads to increased energy intake and body mass increment (Church et al. 2010). In addition to the role of modulating hypothalamic function in energy homeostasis Wu and co-workers suggest that *FTO* may play an important role as transcriptional co-activator in modulating the transcriptional regulation of adipogenesis (Wu et al. 2010).

1.2.1.2 Peroxisome proliferator-activated receptor gamma (*PPARγ*) gene

Peroxisome proliferator–activated receptors (PPARs), belongs to the super family of nuclear receptors and plays an important role in transcription of several genes responsible for adipogenesis and lipid metabolism (Barish et al. 2006). PPARs forms heterodimers with retinoid X receptors and these heterodimers by binding to specific DNA-response elements in the promoter of target genes leads to recruitment of co-activators and chromatin remodeling, that conducts to gene transcription (Smith 1997, Bocher et al. 2002). The ligand-activated transcription factors belonging to PPARs family are involved in the regulation of inflammation and energy homeostasis and represent important targets for obesity, obesity-induced inflammation and metabolic syndrome in general (Lapsys et al. 2000, Ahmadian et al. 2013). One of the three subtypes of PPARs known – PPAR-gamma (*PPARγ*) - is a nuclear receptor, which upon activation with various types of ligands (natural and synthetic) activates the transcription of genes that are mandatory for the growth and differentiation of adipocytes (Kersten et al. 2000). Rare inactivating mutations of the gene encoding *PPARG* are associated with insulin resistance, type-II diabetes, and hypertension, whereas a rare gain of function mutation causes extreme obesity (Stumvoll et al. 2002). Nevertheless, a common polymorphism (Pro12Ala) of the adipose tissue-specific g2 isoform (dbSNP rs#: rs1801282), a missense mutation first described in 1997, a C→G substitution that results in the conversion of proline to alanine at residue 12 of the *PPARγ2* protein (Yen et al. 1997), highly prevalent in the Caucasian population, has been associated with increased insulin sensitivity and obesity (Beamer et al. 1998, Ghoussaini et al. 2005, Tönjes et al. 2006, Morini et al. 2008). Studies carried out *in vitro* and *in vivo* have shown that receptors expressing the 12Ala allele showed lower DNA-binding affinity and impaired transcriptional activity in the target genes (Deeb et al. 1998). For this reason it was expected that the Ala carriers would be protected against adipose tissue mass accumulation due to less efficient stimulation and concomitant of *PPARG* target genes receptors. Nevertheless, studies in human subjects show that 12Ala carriers were associated with increased accumulation of adipose tissue (Masud et al. 2003,

Tok et al. 2006). These findings indicate a central role of *PPARG* and this point mutation in fat cell biology and in the pathophysiology of obesity, diabetes, and insulin resistance.

1.2.1.3 Apolipoprotein A-V (APOA5) gene

The gene apolipoprotein A-V (APO A-V or *APOA5*) was first identified by van der Vliet and co-workers in 2001 (van der Vliet et al. 2001) in a study with the objective of isolating novel genes that were being expressed in early phase of liver regeneration. The protein encoded by this gene is an apolipoprotein highly expressed in the liver and secreted to the plasma (Wang et al. 2008). The protein is known to play a critical role as plasma triglycerides (TG) regulator, and this fact was described in van der Vliet's work, where mice overexpressing this gene showed a reduction of 70% plasma TG when compared to *wild type* mice. On the other hand, APOA5 knockout mice have shown a four-fold increase in TG plasma levels when compared with *wild type* ones. These findings suggest a strong inverse correlation between ApoA5 protein and TG plasma levels and deficient function of ApoA5 can be seen as a risk factor for hypertriglyceridemia (Pennacchio et al. 2001). The exact pathway by which APOA5 influences plasma TG is not properly understood, but it has been suggested that the activation of lipoprotein lipase as a potential APOA5 function (Merkel et al. 2005).

The *APOA5* gene is quite polymorphic, with five common haplotypes composed by seven SNPs, that are associated with high levels of plasma TG, having a possible role in mediating genetic predisposition to hyperlipidemia (Charriere et al. 2008, Ariza et al. 2010, Di Taranto et al. 2015) and metabolic syndrome (MS) (Niculescu et al. 2007, Dallongeville et al. 2008, Vasilopoulos et al. 2011, Zaki et al. 2014), a disorder of energy intake and expenditure, very complex and involving a strong interplay between genetic and environmental factors and diagnosed by the occurrence of three of five medical conditions: abdominal obesity, elevated fasting plasma glucose, high level of serum triglycerides, low levels of high-density cholesterol and elevated blood pressure (Park et al. 2003). The rare polymorphism -1131T/C (dbSNP rs#: rs662799), inserted in the *APOA5**2 haplotype, with low allelic frequency in Caucasian population (Eichenbaum-Voline et al. 2004) but highly correlated with high levels of TG (Dorfmeister et al. 2007, De Caterina et al. 2011) and MS, one of the common forms of obesity (Dallongeville et al. 2008, Zaki et al. 2014). Moreover, it is suggested that the -1131C allele, present in the APOA5*2 haplotype, confer susceptibility to the development of obesity, when in strong linkage disequilibrium with C-482T or T-455C polymorphism of the Apo CIII gene, which is located nearby the *APOA5* gene (Horvatovich et al. 2011, Hsu et al. 2013).

1.3 Nanotechnology

Nanotechnology can be defined as the design, evaluation, manufacture and application of structures, devices and systems by controlling size and shape of the matter at a nanometer scale (1-100 nm) (ASTM Standard E2456 2006, 2012 Bhattacharyya et al. 2009). Nanotechnology gained relevance with Richard Feynman in a well-known talk in 1959 at the American Physical Society meeting – "There's plenty of room at the bottom". For the first time, the possibility of manipulating matter at the nanoscale level was mentioned, using atomic units as foundations at the molecular level (Feynman 1960). Due to the wide-range of applications within this field, the development of new nanomaterials, nanostructures, devices and platforms in several areas, namely medicine, has significantly grown in the 90's (Edwards and Thomas 2007, Morigi et al. 2012). The development of nano-based systems can be performed in two distinct ways: bottom-up and top-down approaches. The first one, the most conventional, relies on the creation of a nanostructure starting from molecular components (e.g. chemical synthesis and self-assembly). On the other hand, the top-down strategy uses several eroding procedures (e.g. laser ablation and lithography) to remove and/or shape portions of larger materials in order to create a nanostructure (Biswas et al. 2012).

Nanotechnology has brought forth new materials suitable for application in biomedicine that greatly boost current methodologies for clinic diagnostics, including gene expression profiling, biomarker quantification and imaging (Baptista et al. 2008, Larguinho et al. 2012, Parveen et al. 2012, Chapman et al. 2013). Such strategies are focused on i) development of nanoscale devices and platforms that can be used for single molecule characterization (nucleic acids or proteins) at an increased rate when compared to conventional systems; and ii) construction of novel contrast agents to improve existing diagnostics *via* tissue/organ imaging (Nune et al. 2009). Most platforms specifically designed for protein detection often include standard assembly concepts using antigens and antibodies for molecular recognition (e.g. sandwich immunoassay), coupled to distinct detection strategies, such as spectroscopy (Quian et al. 2008, Luo et al 2014) or electrochemistry (de la Escosura-Muñiz et al. 2009, Kumar et al. 2015). Similarly, systems designed towards nucleic acid sensing, whether for screening of nucleotide sequences or single base mismatch discrimination (e.g. SNP), are usually based on differential hybridization stringency due to mismatch, causing a conformational shift in the duplex, which is then detected (Thaxton et al. 2006). Identification of specific relevant molecules by using nucleic acid probes or aptamers can also be performed and detection is often carried by means of an intercalating agent or dye (Sarpong and Datta 2012). Currently employed bioassays for detection of known biomarkers or nucleotide sequences, have progressively been integrated into nanoparticle-based systems, increasing sensitivity and lowering costs (Nam et al. 2003, Baptista et al. 2006, Saha et al. 2012, Howes et al. 2014).

1.3.1 Noble Metal Nanoparticles

Over the past couple of decades, noble metal nanoparticles (NPs), due to their optical and physic-chemical properties have been used for the development of biosensing tools for multiple fields such as medicine and molecular diagnostics (Dreaden et al. 2012, Majdalawieh et al. 2014). Among this group of nanomaterials is one of the most studied ones, gold nanoparticles (AuNPs) (Shah et al. 2014). Due to their nanoscale proprieties (e.g. optical, electrochemical, etc.), AuNPs have already proven to be an important tool for several biomedical application, such as drug delivery (Pissuwan et al. 2011), therapy (Llevot and Astruc 2012, Jain et al. 2012), imaging (Hainfeld et al. 2006, Curry et al. 2014) and molecular diagnostics (Baptista et al. 2006, Liu and Ye 2013).

One of the most studied and interesting proprieties of AuNPs is their localized surface plasmon resonance (LSPR) - Figure 1.8. When AuNPs are exposed to the oscillating electromagnetic field of light a collective and coherent oscillation of conduction electrons present in the surface of the NPs undergo forming instantaneous dipoles. This interaction will induce dipole moments that oscillate at the respective frequency of the incident wave consequently dispersing secondary radiation in every direction (Pelton et al. 2008, Ringe et al. 2013).

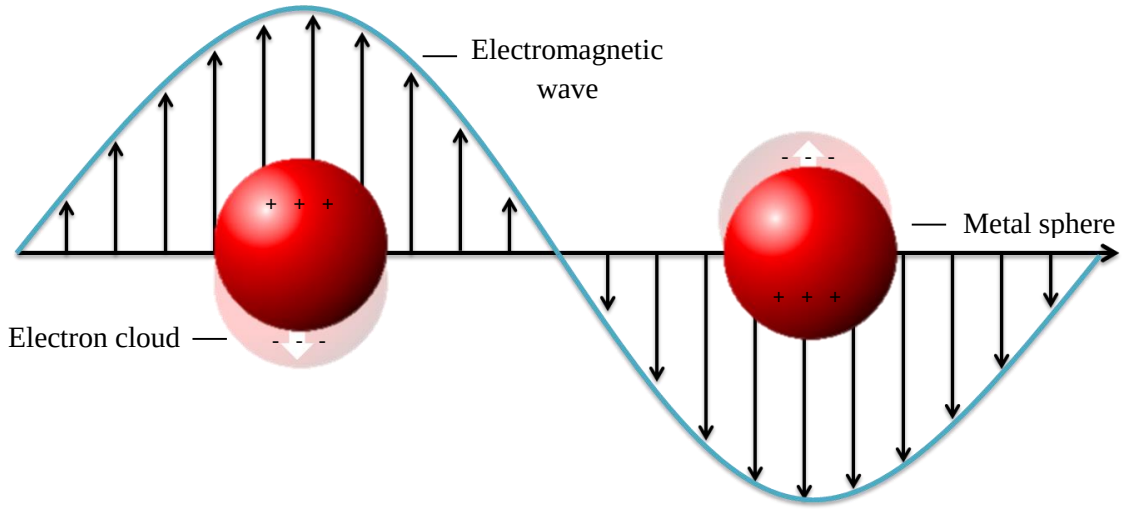

Figure 1.8 - Schematic representation of metal nanoparticles LSPR. Interaction of the electromagnetic waves with the metal NPs surface electrons generates a surface plasmon resonance.

Moreover, in the case of AuNPs, the electric field intensity and the scattering and absorption cross-sections are all strongly enhanced at the LSPR frequency, lying in the visible region of the electromagnetic spectrum. Due to this surface plasmon enhancement, optical cross-sections of metal nanoparticles (10-100 nm) are 5 orders of magnitude or larger than those of dye molecules (Jain et al. 2006). LSPR can also be tuned by changing the nanostructure size, shape, composition, or environment (Jain et al. 2006, 2008). The aggregation phenomena of AuNPs reflect the outstanding properties of these nanoparticles. For example, colloidal 14 nm spherical

AuNPs present a resonance characteristic absorption band at ~520 nm giving the solution a bright red color. When the environment of the AuNPs media suffers a variation, aggregation phenomena can occur with an inherent inter-particle distance decrease, leading to a pronounced change in color from red (520 nm) to blue (600 nm) due to plasmon coupling between nanoparticles (Jain et al. 2007) - Figure 1.9. Moreover, their nano-size scale confer high surface-area-to-volume ratio, with great capability of interaction in the same scale of target biological molecules (Azzazy and Mansour 2009, Conde et al. 2014).

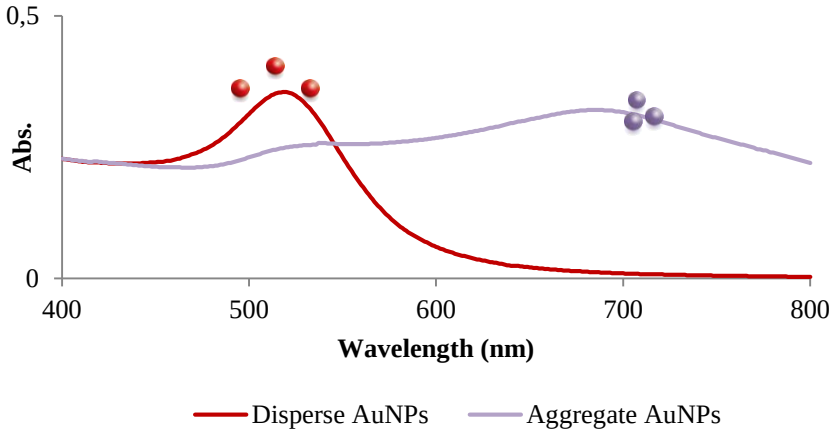

Figure 1.9 – Effect of inter-particle distance of AuNPs on LSPR. A red-shift occurs when the inter-particle distance decreases affecting the LSPR peak.

1.3.1.1 Synthesis of Gold Nanoparticles

The versatility of AuNPs in several biological assays has provided useful materials for a wide range of biomedical applications. This remarkable utility is only possible with the guarantee that the approaches used can generate AuNPs with desired characteristics, such as adequate morphology, size dispersion and surface functionalities (Yeh et al. 2012). Several methodologies and approaches have been developed to generate AuNPs with a good level of homogeneity and provide fine control over size, shape and surface properties, in order to better take advantage of their unique physicochemical properties. Those methods are based on chemical or physical methods, but only few produce particles with uniform size and narrow size distribution (Jana et al. 2001, Majdalawieh et al. 2014). One of the most used approaches is based on the chemical or electrochemical reduction of a precursor with gold III ions, like choloraurate, to metallic gold in the presence of a capping agent that binds to the nanoparticle surface, due their simplicity and high yield. Capping agents are pivotal in the synthesis of AuNPs since control the particle size by blocking their growth and provide colloidal stability by inhibiting particle aggregation phenomena. Several compounds can be used to reduced ionic gold and produced AuNPs (e.g. citric acid, sodium borohydride, or tetrakis (hydroxymethyl) phosphonium chloride) (Frens 1973, Duff et al. 1993, Brust et al. 1994), but the citrate reduction method due to his simplicity has the

advantage to be conducted in aqueous phase and produce fairly stable and quite monodispersed AuNPs with high-yield is one of the most commonly used approach. The citrate method reduction firstly described Turkevich and co-workers in 1951 (Turkevich et al. 1951) and later refined by Frens in 1973 (Frens 1973), is carried out initially with the dissolution of chloroauric acid ($HAuCl_4$) in water. Afterwards, sodium citrate act as a reduction agent, reducing Au^{3+} ions to Au^0, and also as capping agent limiting the size of the particle, preventing them from aggregation by conferring mild stability due to electrostatic repulsion between citrate-capped AuNPs. The size of the AuNPs produced can be easily controlled by varying the concentration of citrate in solution, where higher sodium citrate concentrations promote the formation of smaller nanoparticles and vice-versa (Wilcoxon and Abrams, 2006).

This method was the one employed for AuNPs synthesis in this thesis and has been widely used to generate moderately stable spherical AuNPs with diameters of 10 to 20 nm, though recent modifications allows the production of larger AuNPs (e.g., 100 nm) with fairly good size distribution and size control (Kimling et al. 2006, Ji et al. 2007, Alex and Tiwari 2015).

1.3.1.2 Functionalization of Gold Nanoparticles

Nanoparticles, in particular AuNPs, due to their noteworthy physicochemical proprieties, easiness of synthesis and facile surface chemistry for functionalization with appropriate recognition biomolecules represents an optimal tool to be applied in areas of biotechnology and biomedicine in the development of new biomarker platforms. For this purpose the functionalization of AuNPs surface has to be conjugated with one or more biomolecule, such as nucleic acids (i.e., ssDNA/RNA, dsDNA/RNA), peptides, antibodies, fluorescent dyes, biocompatible polymers, drugs, *etc.* (Sperling and Parak 2010, Conde et al. 2014), in order to specifically interact with the analyte to be targeted Figure 1.10. It is important to mention that the non-functionalization of AuNPs does not prevent them to be used as recognition agents of biomolecular targets (Li et al. 2004, Xia et al. 2010, Shawky et al. 2010).

One of the mostly used conjugation method to mediate the interaction between a biomolecule and AuNPs is through electrostatic interaction, that constitutes a simple approach that is based on electrostatic attraction between oppositely charged AuNPs surface and target biomolecules. However, the method is sensitive to environmental changes (e.g., pH, ionic strength, etc.) (Sperling and Parak 2010). Molecules harboring a thiol moiety, such as thiol-modified ssDNA oligonucleotides, can be conjugate with an AuNP citrate-capped due to the extraordinary affinity of thiol groups towards gold surfaces (Love et al. 2005, Conde et al. 2014). This outstanding approach was first applied in Mirkin's group in 1996 (Mirkin et al 1996), where the modification of a nucleic acid at 5' or 3' position with a one or more thiol group allowed a fine-tune of DNA assembly into AuNPs surface, adjusting several analytical variations, such as

nanoparticle size, ratio NP/Oligo, *etc*. and establishing what is known as Au-nanoprobe (Li et al. 2002, Hurst et al. 2006).

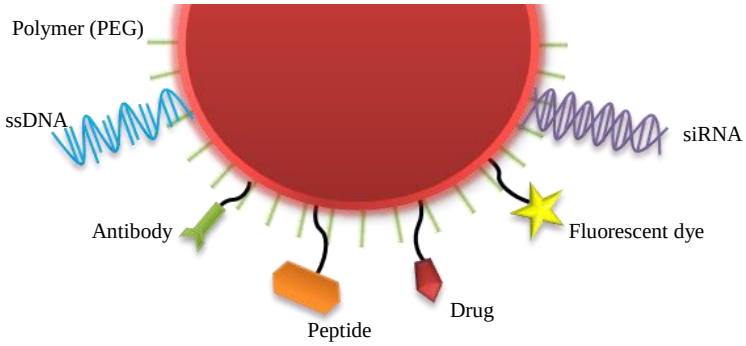

Figure 1.10 – Schematic representation of an AuNP loaded with a plethora of molecules. These moieties allow AuNPs to act as molecular sensors for disease diagnosis as well as therapeutic agents.

An improvement to this approach is the "salt aging" method, in which salt concentration is gradually increased to reduce the repulsions between nanoparticles and oligonucleotides (both negatively charged). This supports the interaction between the AuNP surface and the thiol group and significantly increments the probe density on the AuNP surface (Hurst et al. 2006). Moreover, the use of anionic surfactants such as SDS or Tween-20 prior to salt aging stabilizes the process of functionalization by reducing non-specific binding and also confers method reproducibility since surfactants agents can protects AuNPs from aggregate and coalesce, particularly at high salt concentrations (Stoeva et al. 2006). With this approach a new form of targeting relevant DNA sequences was achieved. Conjugating the strong affinity, sensitivity and selectivity given by the DNA base paring stacking and by the unique optical proprieties of AuNPs, can be translated to the development of new platforms or devices to be used at point-of-need (Cao et al. 2005). Bi-functional PEGs with a thiol group in one extremity and a different functional group on the other extremity (amine, carboxylic, biotin, azide) has also been used to allow further functionalization with other biomolecules – see Table 1.5. For example, the crosslinking agent EDC (1-Ethyl-3-(3-dimethylaminopropyl)-carbodiimide) is efficiently used for the coupling carboxyl or phosphate groups to primary amines. The surface of an AuNP can also be modified simply using ionic coupling methods, where the ligand exhibits an opposite charge of the AuNP or of the capping agent (Thobhani et al 2010, Conde et al. 2012). Although the ionic coupling procedures are faster and do not require pre-activation of molecules, these approaches lead to more unstable constructs and the control over the biomolecule orientation is hindered (DeLong et al. 2010). The widely known biotin-streptavidin interaction can also be used for the surface modification of AuNPs. Although non covalent, the functionalization of the AuNP with avidin or with biotin usually requires a covalent immobilization of these molecules (either by direct functionalization using a thiolated molecules or through EDC coupling). Hydrophobic interactions, while not being

covalent interaction, usually require a covalent attachment using a thiol coupling (Kim et al. 2009).

Table 1.5 – Common covalent immobilization strategies for AuNP functionalization (Vinhas et al. 2015)

Coupling Reaction	Functional group at AuNP surface	Functional group on ligand	Linker/Spacer	Examples of biomolecules coupled
Thiol	Direct coupling	Thiol	-	Thiolated DNA (Conde et al. 2013) Thiolated PEG (Manson et al. 2011) Thiolated fluorophores (Cordeiro et al. 2013)
EDC/NHS	Carboxylic/phosphate or amine	Amine or carboxylic/phosphate	Bifunctional PEG/DNA chain harboring a thiol and a amine/carboxylic group	Proteins (Sanz et al. 2012) Antibodies (Conde et al. 2014a) Fluorophores (Park et al. 2012)
Maleimide	Thiol/ Maleimide	Maleimide/Thiol	Homo-Bi-functional thiolated PEG or Hetero-bifuntional PEG harboring a maleimide	Peptides (Ravi et al. 2012) DNA (Lee 2011) Chemotherapeutic agents (Hwu et al. 2009)

Abbreviations: AuNP, gold nanoparticle; eDC, 1-ethyl-3-(3-dimethylaminopropyl)carbodiimide; NHS, N-hydroxysuccinimide; PeG, polyethylene glycol.

1.3.2 Nanodiagnostics

The interconnection between nanotechnology and biotechnology contributed to a new field of research – nanobiotechnology, that is defined as the engineering of biological systems (e.g. cells, nucleic acids and proteins, etc.) to develop functional nanostructures comprised organic or inorganic compounds in order to understand and study fundamental biological processes and structures. Due the unique proprieties that nanomaterials can provide, new methods and approaches that most benefit medicine and molecular diagnosis areas are now being exploited (de Morais et al. 2014). Nanodiagnostic, a branch of nanobiotechnology, was created with the intention to fulfill the demands of clinical diagnostics and push forward the conventional diagnostics methods for sensitivity and sensibility increment and earlier disease detection. (Jain 2003). Bioassays for detection of known biomarkers or nucleotide sequences are progressively being integrated into nanoparticle-based systems, increasing sensitivity and lowering costs (Azzazy et al. 2009, Agasti et al. 2010, Doria et al. 2012). These clear advantages have been presented in several detection methods, such as colorimetric sensing (Lee et al. 2010), fluorescence modulation (Guirgis et al. 2012), Raman scattering (Vendrell et al. 2013) and

electrochemical (Afonso et al. 2013). Imaging methodologies for *in vivo* diagnostics have also greatly benefited from the development of nanotechnology, particularly the incorporation of nanoparticles or NPs-conjugates into imaging techniques as novel or improved contrast agents (Cai and Xen 2007, Bae et al. 2011). NPs possess elevated surface area and relative ease-of-derivatization, which present advantageous for increased interaction and site-specific delivery, which in turn may amplify the signal and boost the diagnostic sensitivity (Subbiah et al. 2010).

1.3.2.1 Gold Nanoparticles for DNA Sensing

Despite the wide range of nanoscale systems being used for biomolecular assays in general, AuNP based systems have been the most widely used due to their unique physicochemical properties, and are becoming a critical component in the development of nanotechnology-based for nucleic acid detection (Goluch et al. 2006). Several methods for detection of DNA hybridization are described in the literature, taking advantage of AuNPs plasticity of detection, (i.e. optical, fluorescence, Raman scattering, electrochemical), a list in more detail can be find in Appendix I – Table AI.1. Among the several AuNPs-based methods for DNA detection, the colorimetric approach has been the most explored and, due to their simplicity and portability, are among the most promising for future diagnostics methods at point-of-care (POC). These methods rely on the colorimetric changes of the colloidal solution upon aggregation either mediated by a change to the dielectric medium or by recognition of a specific target. As mentioned earlier, colloidal solutions of spherical AuNPs present a LSPR band strongly dependent on inter-particle distance. The design of these systems is centered in the ability of complementary targets to balance and control inter-particle attractive and repulsive forces, which determine whether AuNPs are in a dispersed or aggregated state (Mirkin et al. 1996, Sato et al. 2003, Li and Rothberg 2004a).

Other approaches based on colorimetric sensing have been applied using the AuNPs reporter. Microarrays, streptavidin-biotin stripes, and lateral flow cytometer systems are usually based on this method (Gubala et al. 2012). Although each varies in its building block, all share the same principle: a DNA probe is fixed on a support, in the form of stripes or spots, and then the sample DNA is hybridized to the fixed probe (Cao et al. 2006, Zhao et al. 2010, Rastogi et al. 2012, Li et al. 2013). The second probe, consisting of AuNPs functionalized with 5' thiol modified oligonucleotides, is then hybridized to a second region of the target sample DNA. Total complementarity with both probes prevents the Au-nanoprobes from being washed and yields the result (Figure 1.11).

Sandwich-based assays are being developed in a lateral flow strip scheme with increased sensitivity, and are today a suitable alternative for detection of PCR amplicons (Kozwich et al. 2000, Baeumner et al. 2003, Suzuki et al. 2006, Mao et al. 2014). Advantages of lateral flow

platforms include ease-of-use, disposable, rapid to perform and relatively low cost (Kumanan et al. 2009, Zeng et al. 2013). Integration of such approaches with gold labels introduce several advantages in lateral flow designs, since they are stable in liquid and dried forms and signal intensity do not fade after staining on membranes (Chun 2009). The most successful case of a nanotechnology-based platform for diagnostic purposes was developed by Mirkin's group and is being commercialized by Nanosphere™. Two products approved by the Food and Drug Administration (FDA), one aimed at identifying typical mutations in coagulation factors FV (1691G>A), FII (20210G>A) and MTHFR (677C>T) without the need for nucleic acid amplification; another used to genotype polymorphisms associated with warfarin metabolism (CYP2C9*2, CYP2C9*3, VKORC1) (Maurice et al. 2010, Lefferts et al. 2010). In both cases the samples are processed through a cartridge where the sample analyzed via an automated processor and reader.

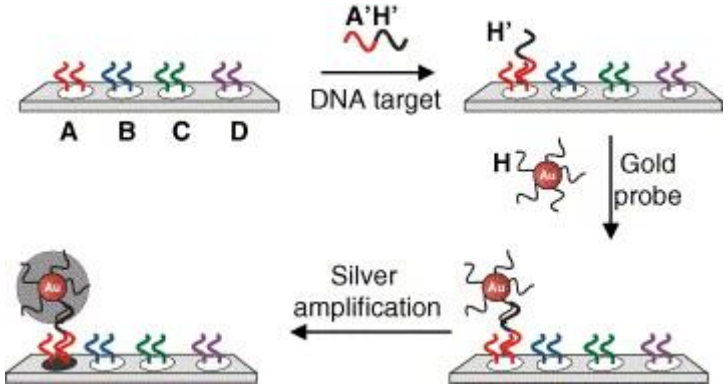

Figure 1.11 - Microarray DNA detection via AuNPs. DNA hybridization to microarrays and detection using silver amplified gold nanoparticle probes. Following target hybridization to a capture probe immobilized on the array surface, a secondary Au-nanoprobe is used for detection. DNA target and Au-nanoprobe hybridization can be performed in a single step. An additional signal amplification step may be introduced *via* silver deposition (Storhoff et al. 2004).

1.3.2.2 Colorimetric Sensing

1.3.2.2.1 Non-functionalized AuNPs

Unmodified AuNPs have also been used for detection of DNA/RNA biomarkers. These systems are based on unspecific adsorption of biomolecules to non-functionalized AuNPs and take advantage of the differential propensity of ssDNA and dsDNA adsorption to their surface to develop a biosensor for DNA detection (Li and Rothberg 2004). Free ssDNA bases interact electrostatically with the negatively charged surface of gold NPs harboring a citrate capping, conferring then enhanced stability to the NPs upon increasing ionic strength. On the other hand, dsDNA molecules present lower tendency to adsorb to the NPs' surface and do not provide stability to increasing ionic strength, hence resulting in aggregation of the NPs (Figure 1.12 A).

Griffin and co-workers used unmodified AuNPs for the detection and quantification of Hepatitis C Virus RNA. Their approach consisted on the adsorption of a synthetic ssDNA probe complementary to the target (Griffin et al. 2009). Whenever the target is present, the ssDNA probes and target hybridize and consequently become unavailable to adsorb to the AuNPs surface and confers them with increased stability to salt induced aggregation. This way, a positive result (i.e., presence of target) yields a colorimetric change from red to blue upon salt addition, while in a negative result the color remains unchanged. Despite a clear colorimetric visual detection, the use of hyper-Rayleigh scattering measurement allows an increase in sensitivity of two orders of magnitude. Shawky and co-workers used the same method in clinical samples to detect the presence of HCV RNA (Shawky et al. 2010). The isolated RNA was added to a solution containing the complementary oligonucleotide probe, and after a denaturing and annealing cycle, unmodified AuNPs were added. This extremely simple and inexpensive assay, which does not include an RT-PCR step, presented a detection limit of 50 copies/reaction and exhibited a sensitivity of 92% and a specificity of 89%. A similar approach using an S1 nuclease to discriminate single mismatches in DNA with unmodified AuNPs was proposed, where dNMPs adsorb to AuNPs stabilizing them even more than ssDNA (Liu et al. 2011). In presence of a mismatch between the synthetic oligonucleotide and DNA sample, the S1 nuclease degrades ssDNA-ssRNA hybrid to its monomers (dNMPs), which increase the stability of AuNPs in solution. Also, using an enzyme mediated process (Xie et al. 2011) it was possible to detect colorimetric the activity of ribonuclease H (RNase H) by HIV-1 reverse transcriptase. In the presence of RNase H activity RNA-DNA hybrids are formed, otherwise ssRNA remains in solution adsorbing to the AuNPs. Deng and co-workers took advantage of asymmetric PCR to generate long ssDNA amplicons that stabilize AuNPs in solution after salt addition. However, if no amplification occurs, no long ssDNA amplicons, AuNPs aggregate due to the increasing ionic strength (Deng et al. 2013).

1.3.2.2.2 Functionalized AuNPs

1.3.2.2.2.1 Cross-linking approach

Functionalization of AuNPs with thiol-modified oligonucleotides led to the first application of AuNPs in nucleic acid detection. In their approach, Mirkin and co-workers functionalized AuNPs with oligonucleotides modified with a thiol group at their 3'- and 5'-ends, whose sequences were contiguous and complementary to a target in a tail-to-tail (or head-to-tail) conformation, and used these probes to identify the target DNA sequence. The hybridization of the two Au-nanoprobes with the target resulted in the formation of a polymeric network (cross-linking mechanism), which brought gold nanoparticles close enough to result in a red to blue color

change, that can readily be detected visually, by UV-Vis spectroscopy or dynamic light scattering (Figure 1.12 B) (Mirkin et al. 1996).

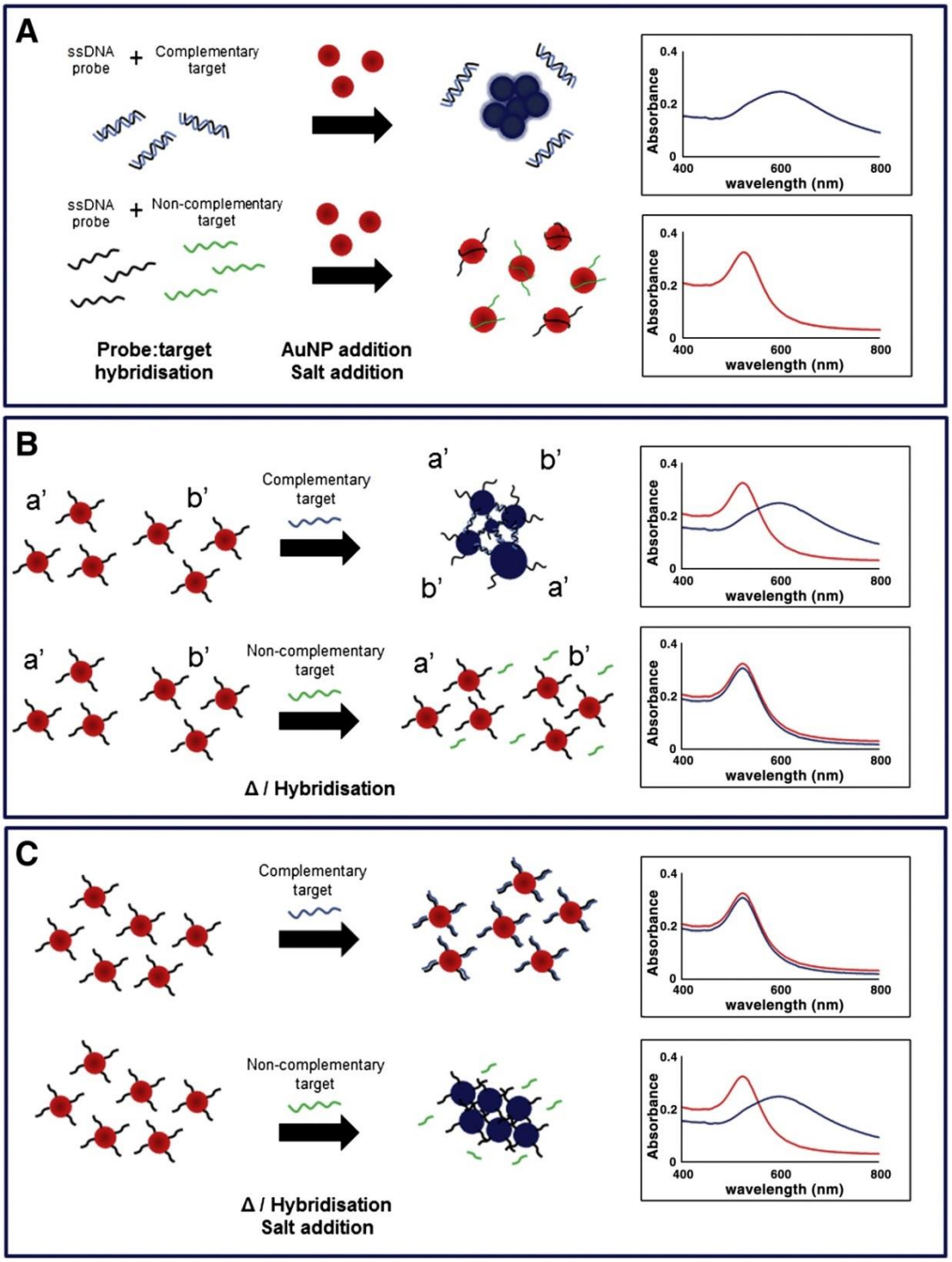

Figure 1.12 - Gold nanoparticle based colorimetric assays. A) Colorimetric assay based on naked AuNPs; **B)** Cross-linking hybridization assay; **C)** Non-cross-linking hybridization assay. (Larguinho and Baptista 2012)

Storhoff and co-workers described the first application of the cross-linking approach, in which a 'spot-and-read' colorimetric detection method for identification of DNA sequences was developed. DNA-modified gold probes, which undergo a color change, were detected when the

solutions were spotted onto an illuminated glass waveguide. This scatter-based method enabled the detection of zeptomole quantities of nucleic acid targets without, signal or target amplification. In comparison to the absorbance-based methods, this approach increased the detection sensitivity by over four orders of magnitude. They were able to detect *mecA* in methicillin-resistant *Staphylococcus aureus* directly from genomic DNA samples. The system showed high sensitivity with a limit of detection (LOD) of 66 ng.μL^{-1} of DNA (Storhoff et al. 2004). Following the same approach several groups were able to develop methods to detect others important biological targets (e.g. *Cryptosporidium parvum*) (Javier et al. 2009) with direct detection capabilities, allowing to circumvent expensive enzymatic DNA amplification reactions. Recently, Weigum and co-workers developed an amplification-free molecular assay for detection of *Cryptosporidium parvum* oocysts. The assay targeted the *C. parvum* 18s rRNA, with a LOD of 4 x 10^5 copies of RNA per µL per reaction mix. The ability to detect the *C. parvum* oocysts without the need for complex amplification is of utmost relevance in resource-limited settings where protozoan detection is needed the most (Weigum et al. 2013).

The development of a system that does not need expensive equipment for the detection and characterization of pathogen´s RNA, Gill and co-workers integrated a nucleic acid sequence-based amplification (NASBA) and AuNP probes for the specific detection of *Mycobacterium tuberculosis.* Primers targeting the 16S rRNA were used for amplification of mycobacterial RNA via isothermal NASBA, and then hybridized with specific probes. This method showed a LOD of 10 CFU ml^{-1} with a sensitivity and specificity of 94.7% and 96%, respectively (Gill et al. 2008). Following the same detection approach, Soo and co-workers designed a set of Au-nanoprobes to specifically recognize *M. tuberculosis* complex (MTBC) strains DNA and the detection limit set at 0.5 pmol of DNA target within two hours. The assay comprises two main steps: target DNA amplification by single or nested PCR, followed by Au-nanoprobe detection (Soo et al. 2009).

Over time, several advances have been made reducing the gap between light scattering imaging and naked eye sensitivity. Earlier methods used enzymatic amplification techniques, such as PCR, asymmetric PCR and NASBA (Chen et al. 2009, Parab et al. 2010, Jung et al. 2010, Wang et al. 2012, Kalidasan et al. 2013, Mancuso et al. 2013). More recently, Zagorovsky and Chan reported on the integration of a multi-component DNA-responsive DNAzyme with colorimetric detection using AuNPs, allowing for non-enzymatic signal amplification. This approach provides a simple and fast colorimetric method for detection of genetic targets of bacterial, viral, and parasitic origins with an LOD of 50 pM, without the need for purification and separation steps, capable of detection of multiple sequences in parallel. The color-based readout does not require any complex equipment and uses stable and cost-effective reagents, making this approach particularly suitable for POC testing (Zagorovsky and Chan.2013).

1.3.2.2.2.2 Non-cross-linking approach

Baptista and co-workers developed a low-cost approach for the colorimetric detection of DNA sequences (Baptista et al. 2006). This method uses just one Au-nanoprobe, instead of the two required for cross-linking. In this scheme, the detection is achieved by color comparison upon salt addition between solutions containing the Au-nanoprobe and either a complementary or a non-complementary/mismatched target sequence. The presence of a complementary target prevents Au-nanoprobe aggregation and the solution remains red, while non-complementary/mismatched targets or their absence do not prevent Au-nanoprobe aggregation, resulting in a visible change of color from red to blue.

The first clinical application of this strategy was presented as a rapid and sensitive detection of *Mycobacterium tuberculosis* (Figure 1.12 C). Au-nanoprobes were functionalized with thiol-modified oligonucleotides harboring a sequence derived from *M. tuberculosis* RNA polymerase β-subunit gene sequence suitable for mycobacteria identification. The methodology was tested in clinical samples demonstrating high efficiency when combined with an initial round of PCR for target amplification (Baptista et al. 2006). This strategy was applied to the detection of MTBC members and simultaneous characterization of mutations associated with rifampicin resistance (Veigas et al. 2010). This low-complexity assay enabled the detection of mutations from MTBC clinical specimens with remarkable sensitivity in just a few hours. LOD was set at 75 nM, however, for robust single base mismatch determination, 117 nM of DNA target was used per assay. Optimization of the above strategy allowed detection and identification of members of the MTBC at the species level. Using a set of three Au-nanoprobes based on the gyrB *locus* was possible to specifically identify MTBC, *M. bovis* and *M. tuberculosis* (Costa et al. 2010). Towards a point-of-care application, Baptista and co-workers further integrated the non-cross-linking Au-nanoprobe-based method in an innovative optoelectronic platform that allows an analytical measurement of the colorimetric changes, hence to detect a target without the need of experienced personnel. The device integrates an amorphous/nanocrystalline biosensor and a light emission source with the non-cross-linking method for specific DNA detection. This low cost, fast and simple optoelectronic platform was optimized for the specific identification of MTBC members and the consequent improvement of the laboratorial diagnostics algorithms of tuberculosis (TB) and integration into a PDMS microfluidic platform allowing the detection of *Mycobacterium tuberculosis* with a 10-fold reduction of reagents (Bernacka-Wojcik et al. 2010, Silva et al. 2011, Bernacka-Wojcik et al. 2013). Recently, in an effort to increase sensitivity and ease of use, this detection strategy was integrated onto a paper-based platform. Differential color scrutiny is captured and analyzed with a generic “Smartphone” device to digitalize the intensity of color associated with each colorimetric assay, perform RGB analysis and transfer relevant information to an off-site lab. Integration of GPS location metadata of every test image may add a new

dimension of information, allowing for real-time epidemiologic data on MTBC identification (Veigas et al. 2012) (Figure 1.13).

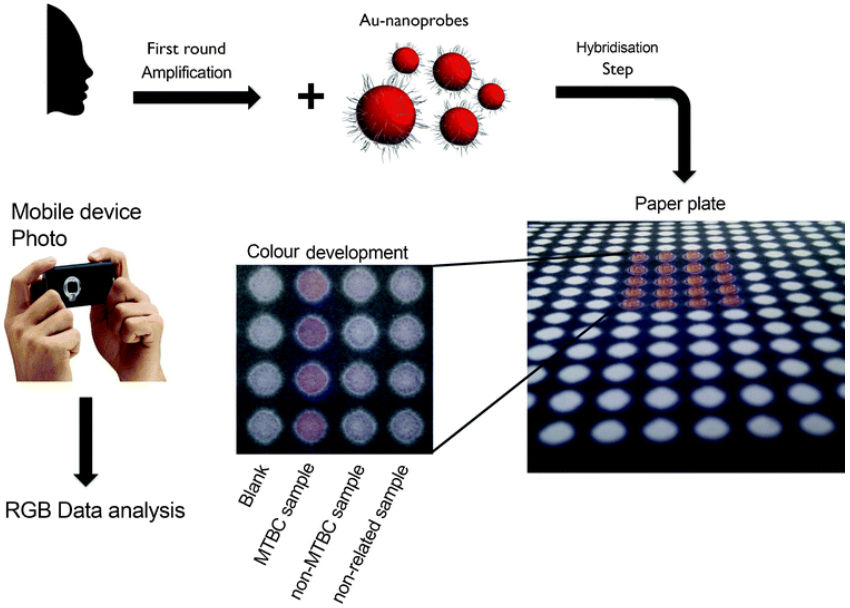

Figure 1.13 - Au-nanoprobe strategy for the detection of MTBC members. Schematic representation of detection of M. tuberculosis using Au-nanoprobes and a paper platform. The colorimetric assay consists of visual comparisons of test solutions after salt induced Au-nanoprobe aggregation on a [$MgCl_2$] impregnated paper plate: MTBC Au-nanoprobe alone - Blank; MTBC Au-nanoprobe in the presence of MTBC sample - M. tuberculosis; MTBC Au-nanoprobe in the presence of a non-MTBC sample; and MTBC Au-nanoprobe in the presence of a non-complementary sample - non-related. After color development a photo of the paper plate is captured and RGB image analysis is performed (Veigas et al. 2012).

Liandris and co-workers optimized the non-cross-linking approach described above to the detection of TB without the need of target amplification. The detection is based on the fact that double and single-stranded oligonucleotides have different electrostatic properties. After hybridization, single-stranded DNA becomes double-stranded DNA. As a result, the double-stranded DNA cannot uncoil sufficiently like the single-stranded DNA to expose its bases toward the Au-nanoprobe. Therefore, the Au-nanoprobe undergoes aggregation in an acidic environment (Liandris et al. 2009). Recently, the same authors improved their technique by introducing an isothermal DNA amplification system – LAMP (Loop-mediated isothermal amplification). Hence, the need of an increasing demand for simple, fast and cheap methods for molecular identification of MTBC and detection of molecular tags associated to drug resistance, suitable for use at point-of-need can be responded. Thus, providing a specific and accurate method Au-nanoprobe based that, if so, do not need sophisticated equipment to be operated (Veigas et al. 2013). Thus, a step forward was taken, and it was also possible to identify specifically the MTBC complex and the most important SNPs that confer antibiotic resistance. More recently, Padmavathy and co-workers reported on the visual direct detection of *Escherichia coli* without the need for any nucleic acid amplification. This approach is able to detect ~54 ng for unamplified genomic DNA, while reducing the overall time for the detection to less than 30 minutes (Padmavathy et al. 2012).

The non-cross-linking method was further applied in the identification and quantitation of RNA associated with human disease (Conde et al. 2010). This system was successfully used in the detection of BCR-ABL fusion gene mRNA, a hallmark for Chronic Myeloid Leukemia. It was possible to detect less than 100 fmol/μl of the specific RNA target, with the possibility of discriminating between a positive and negative from as little as 10 ng/μl of total RNA (Conde et al. 2012a). Also, the non-cross-linking approach allows distinguishing SNPs within the β-globin gene. The authors could detect with only one Au-nanoprobe, three different individual mutations (Doria et al. 2007).

1.3.2.3 Gold nanoparticle at point-of-care

Among the commercially available for biomolecular detection, colorimetric systems are the most common due to their simplicity and portability (Doria et al. 2012). AuNPs and silver nanoparticles (AgNPs) are frequently used in colorimetric systems due to their high scattering in the visible region of the spectra, easiness of synthesis and functionalization with biomolecules. NPs stay in solution in the form of colloids, and present a LSPR band that is dependent of the distance between particles. This fundamental concept has been utilized in two landmark applications – cross-linking and non-cross-linking mechanisms, each having the intrinsic potential of application to diagnostics demonstrated by a plethora of conditions (Larguinho and Baptista 2012 and references therein).

Nanosphere™ presented what might probably be considered the most successful case of an AuNP-based method for DNA detection. This USA Company has several FDA approved diagnostic products that use AuNPs as probes. Its Verigene® line of products is based on cartridges that allow the detection of a palette of pathogens and genetic disorders. The technology is based on the approach described by Storhoff and co-workers without need for nucleic acids amplification (Storhoff et al. 2004). Like was already mentioned earlier in this chapter this system depends on automated machinery that processes samples and a reader that analyzes the results. The available products include clinical microbiology tests (respiratory virus, gram-positive blood culture, *C. difficile*) and cardiac tests (F5, F2, MTHFR, Warfarin metabolism, CYP2C19) (http://www.nanosphere.us/products). A LOD of 50 fM of DNA was reported for SNP discrimination (Bao et al. 2005); sensitivity and specificity vary from product to product but are generally above 90% when compared with gold standard methods.

CHAPTER 2 - MATERIALS AND METHODS

2.1 Materials

2.1.1 Equipment

- ABI 3730XL DNA Analyser (Applied Biosystems, USA)

- Balance Sartorius BP 610 (DWS, USA)

- Confocal scanning microscopy – LSM700 (Carl Zeiss, Germany)

- FTA® Micro Indicating Card (Whatman, USA)

- Gel Doc XR+ Molecular Imager system (Bio-Rad, USA)

- Gel Logic 100 Imaging system (Kodak, USA)

- Harris Micro Punch (Whatman, USA)

- MA6 Mask Aligner (SUSS MicroTec, Germany)

- Microplate reader Infinite M200 with Absorbance module (Tecan, Switzerland)

- Pentax K100D Digital SLR Camera (Pentax, Japan)

- pH meter Basic 20 with combined glass electrode 5209 (Crison, Spain).

- Pigtailed Si Photodiode, GI MM Fiber, Ø62.5 µm Core, 320 - 1000 nm, No Connector (Thorlabs, Germany)

- Platinum DRAGON, red, 3.4 Watt LED, 1000 mA max. current ((Osram, Germany)

- Platinum DRAGON, true green, 4.6 Watt LED, 1000 mA max. current (Osram, Germany)

- Refrigerated SIGMA 3-16K Centrifuge (SciQuip, UK)

- Scanning electron microscopy – SEM-FIB (Zeiss Auriga, Germany)

- Sigma 1-14 Microfuge (SciQuip, UK)

- Stereo Microscope Leica Zoom 2000 (Leica, Germany)

- Tabletop Workstation Fastrans (Analytik Jena AG, Germany)

- Thermal Cycler MyCycler (Bio-Rad, USA)

- Thermal Cycler Tgradient (Biometra, Germany)

- Ultrasonic bath Elmasonic S10H (Elma, Germany)

- UV-Vis Spectrophotometer Cary 50 (Varian, USA)

- UV-Vis Spectrophotometer Nanodrop ND-1000 (Nanodrop Technologies, USA)

- UV-Vis Spectrophotometer UV Mini-1240 (Shimadzu, Germany)

- UVO-Cleaner (Jelight, USA)

- Vertical laminar flow cabinet SPACE120 (Pbibrand, Italy)

- Vortex MS 3 Digital (IKA, Germany)

- Wide Mini-Sub Cell GT electrophoresis cell with PowerPac Basic power supply (Bio-Rad, USA)

2.1.2 Consumables

- 384 well small volume, LoBase Polystyrene microplates, black (Greiner Bio-One, Germany)

- FTA™ Indicated Micro Card (Whatman, UK)

- NAP-5 columns (GE Healthcare, Sweden)

- Quartz absorption cells – 105.202-QS (Hellma, Germany).

2.1.3 Reagents

Reagent	CAS Number	Distributor
Agarose	9012-36-6	VWR
Betaine	107-43-7	Sigma-Aldrich
Bromphenol Blue	115-39-9	Merck
Boric Acid	10043-35-3	Merck
DL-Dithiothreitol (DTT)	3483-12-3	Sigma-Aldrich
Ethylenediaminetetraacetic acid (EDTA)	25102-12-9	Merck
FTA® purification reagent	-	Whatman
Glycerol	56-81-5	Sigma-Aldrich
Gold(III) chloride trihydrate	16961-25-4	Sigma-Aldrich
Hydrochloric acid	7647-01-0	Sigma-Aldrich
Magnesium chloride hexahydrate	7791-18-6	Merck
Nitric acid	7697-37-2	Sigma-Aldrich
Sodium Chloride	7647-14-5	Merck
Sodium phosphate dibasic	10028-24-7	Sigma-Aldrich
Sodium phosphate monobasic monohydrate	10049-21-5	Sigma-Aldrich
Trisodium Citrate	03-04-6132	Merck

2.1.4 Solutions

TBE buffer (5x)

446 mM Tris base

445 mM boric acid

10 mM EDTA (pH8)

Store at room temperature.

TAE buffer (50x)

2 M Tris-Acetate

0.05 M EDTA

Store at room temperature.

TE pH 7.4

10 mM Tris base (pH 7.4)

1 mM EDTA (pH8)

Sterilize by autoclaving and filtration (0.22 μm). Store at room temperature.

Phosphate buffer (10 mM)

pH	Na_2HPO_4 (mM)	NaH_2PO_4 (mM)
7	5.77	4.23
7.5	8.15	1.85
8	9.32	0.68

Sterilize by autoclaving and filtration (0.22 μm). Store at 4ºC.

Buffer Synthesis I

Phosphate Buffer 10 mM (pH8)

2% (w/v) SDS

Sterilize by filtration (0.22 μm). Store at 4 ºC and warm up to 37 °C before use.

Buffer Synthesis II

Phosphate Buffer 10 mM (pH8)

0.01% (w/v) SDS

1.5 M NaCl

Sterilize by filtration (0.22 μm).

Store at 4 ºC and warm up to 37 °C before use.

2.1.5 Biological Material

2.1.5.1 DNA size markers

- GeneRuler™ DNA Ladder Mix, ready-to-use (Fermentas, Canada)

2.1.5.2 Enzymes

- Surf Hot Taq (10U/μl) (STABVIDA, Portugal)

- *SpeI* restriction enzyme (NEB, UK)

2.1.5.3 Molecular Biology Kits

- BigDye® Terminator v3.1 Cycle Sequencing Kit (ABI, USA)

- DNA Extraction Kit prepGEM Blood (ZyGEM, New Zealand)

2.1.5.4 Oligonucleotides

2.1.5.4.1 Unmodified oligonucleotides

Primers

Name	Sequence (5' – 3')	Tm (°C)	Genebank Acc.No.
APOA5Fwd	CCAACCACATCCCTCTTTATG	52	NG_015894.1
APOA5Rev	TTGTGAACGTGTGTATGAGTACTGT	54	
FTOFwd_440nt	GCAAAATGGCAACACACACT	50	NG_012969.1
FTORev_440nt	AACACCATCCTTGGGCTG	50	
FTOFwd_225nt	TTCAAAACTGGCTCTTGAATG	49	
FTORev_225nt	CAGTCAGAAATGGAGTGGGAG	54	
AS-LAMPMCM6_B3	Confidential	-	NG_008958.1
AS-LAMPMCM6_F3wt	Confidential	-	
AS-LAMPMCM6_F3mut	Confidential	-	
AS-LAMPMCM6_FIP	Confidential	-	
AS-LAMPMCM6_BIP	Confidential	-	
LAMPMCM6_B3	Confidential	-	
LAMPMCM6_F3	Confidential	-	
LAMPMCM6_FIP	Confidential	-	
LAMPMCM6_BIP	Confidential	-	
MCM6Fwd	Confidential	-	
MCM6Rev	Confidential	-	
PPARGFwd	CAATTCAAGCCCAGTCCTTT	50	NG_011749.1
PPARGRev	TTATCTCTGTGCATGGCTCC	52	

Synthetic ssDNA targets

Name	Sequence (5' – 3')	Genebank Acc.No.
APOA5_Antisense_ssDNAwt	CAGGAACTGGAGCGAAAGTAAGATTT GCCCCATGAGGAAA	NG_015894.1
APOA5_Antisense_ssDNAmut	CAGGAACTGGAGCGAAAGTGAGATTT GCCCCATGAGGAAA	
APOA5_Sense_ssDNAwt	AGCTTTCCTCATGGGGCAAATCTTACT TTCGCTCCAGTTC	
APOA5_Sense_ssDNAmut	AGCTTTCCTCATGGGGCAAATCTCACT TTCGCTCCAGTTC	
FTO_Antisense_ssDNAwt	CTTGCGACTGCTGTGAATTTTGTGATG CACTTGGATAGTC	NG_012969.1
FTO_Antisense_ssDNAmut	CTTGCGACTGCTGTGAATTTAGTGATG CACTTGGATAGTC	
FTO_Sense_ssDNAwt	TATCCTTCCAAGAGCTTCACAAAATTC ACAGCAGTCGCAA	
FTO_Sense_ssDNAmut	TATCCTTCCAAGAGCTTCACTAAATTC ACAGCAGTCGCAA	
MCM6_Antisense_ssDNAwt	Confidential	NG_008958.1
MCM6_Antisense_ssDNAmut	Confidential	
PPARG_Antisense_ssDNAwt	TGGGAGATTCTCCTATTGACCCAGAAA GCGATTCCTTCAC	NG_011749.1
PPARG_Antisense_ssDNAmut	TGGGAGATTCTCCTATTGACGCAGAAA GCGATTCCTTCAC	
PPARG_Sense_ssDNAwt	CAGTGAAGGAATGCTTTCTGGGTCAAT AGGAGAATCTCCC	
PPARG_Sense_ssDNAmut	CAGTGAAGGAATGCTTTCTGCGTCAAT AGGAGAATCTCCC	

2.1.5.4.2 Modified oligonucleotides

FTO / PPARG / APOA5 / MCM6 Au-nanoprobes design

In order to provide a full characterization and detection of the polymorphism encoded in the FTO (dbSNP rs#: rs9939609), PPARG (dbSNP rs#: rs1821082), APAO5 (dbSNP rs#: rs66279) and MCM6 (dbSNP rs#: rs4988235) genes, a set of two oligonucleotide probes were always designed for each gene, one responsible to fully detect the wild type allele and the other one to tag the expected SNP. The discrimination between alleles is given by the last base in the 3'-end of the thiol-modified oligonucleotide. An illustrated example is shown in Figure 2.1.

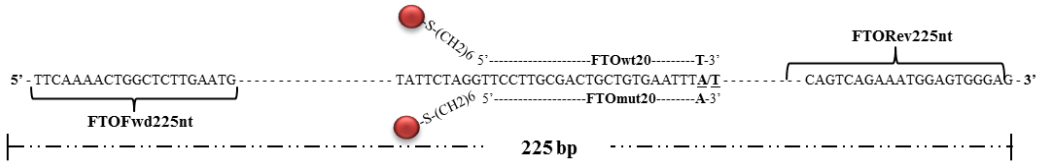

Figure 2.1 – Illustrated example of one of the targets detection and characterization mediated by thiol-modified oligonucleotide probes. Detection of dbSNP rs#:9939609 present in the *FTO* gene, mediated by two thiol-modified oligonucleotide probes.

Thiol modified (probes)

Name	Sequence (5' – 3')	Genebank Acc.No.
AntisenseAPOA5wt20	TTCCTCATGGGGCAAATCTT	NG_015894.1
AntisenseAPOA5mut20	TTCCTCATGGGGCAAATCTC	
APOA5mut17	GAACTGGAGCGAAAGTG	
APOA5wt17	GAACTGGAGCGAAAGTA	
APOA5mut20	CAGGAACTGGAGCGAAAGTG	
APOA5wt20	CAGGAACTGGAGCGAAAGTA	
AntisenseFTOwt17	TATCCAAGTGCATCACA	NG_012969.1
AntisenseFTOmut17	TATCCAAGTGCATCACT	
AntisenseFTOwt20_3NT	GACTATCCAAGTGCATCGCA	
AntisenseFTOmut20_3NT	GACTATCCAAGTGCATCGCT	
AntisenseFTOwt20_6NT	TCCAAGTGCATCACAAAATT	
AntisenseFTOmut20_6NT	TCCAAGTGCATCACTAAATT	
FTOwt17	CGACTGCTGTGAATTTT	
FTOmut17	CGACTGCTGTGAATTTA	
FTOwt20	TTGCGACTGCTGTGAATTTT	
FTOmut20	TTGCGACTGCTGTGAATTTA	
ASLAMP_MCM6	Confidential	NG_008958.1
LAMPwt_MCM6	Confidential	
LAMPmut_MCM6	Confidential	

AntisensePPARGmut20	GTGAAGGAATCGCTTTCTGC	NG_011749.1
AntisensePPARGwt20	GTGAAGGAATCGCTTTCTGG	
PPARGwt17	AGATTCTCCTATTGACC	
PPARGmut17	AGATTCTCCTATTGACG	
PPARGwt20	GGGAGATTCTCCTATTGACC	
PPARGmut20	GGGAGATTCTCCTATTGACG	

Note: All the oligonucleotides here described are 5'-thiol-$(CH_2)_6$ modified.
Oligonucleotides were resuspended in 100 µl of 1 M DTT for 1 hour at room temperature. Subsequently, 900 µl of sterile H_2O DNAse/RNAse Free Water was added to achieve a final concentration 0.1M DTT. All oligonucleotides were immediately used after DTT treatment.

2.1.5.5 Biological Samples

- Blood samples (n=194) for FTO, PPARG and APOA5 studies were kindly provided by José Silva-Nunes M.D. from Endocrinology Department, Curry Cabral Hospital, Lisbon, Portugal.

- Bood samples (n=18) for MCM6 studies were kindly provided by STABVIDA, Investigação e Serviços em Ciências Biológicas, Lda., Caparica, Portugal.

All subjects participating in the studies were duly informed about the study and signed an informed consent. The identification of each subject is confidential and was kept anonymous.

2.2 Methods

2.2.1 Molecular Biology

2.2.1.1 DNA Extraction of dried blood from FTA® Micro Indicating Card

1 – A 0.2 mm punch was made in the FTA® Micro Indicating Card with the help of Harris Micro Punch;

2 – The punch was transferred to a sterile 0.2 ml microtube;

3 – 150 µl FTA purification reagent was transferred to the 0.2 ml microtube containing the punch. After 5 minutes of incubation the FTA purification reagent was discarded;

4 – The step 3 was repeated 3 times;

5 – 150 µl DNAse/RNAse Free Water was transferred to the 0.2 ml microtube containing the punch. After 5 minutes of incubation the DNAse/RNAse Free Water was discarded;

6 – The step 5 was repeated 3 times;

7 – Samples were briefly vortexed to discard the excess of liquid in the 0.2 ml microtube;

8 – The 0.2 ml microtube containing the washed FTA punch was put in the thermocycler for 10 minutes at 56 ºC to completely dry the FTA punch;

9 – The tubes containing the FTA punch were stored at a dry place and protected from light until use.

2.2.1.2 DNA Extraction of dried blood from FTA® Micro Indicating Card with prepGEM Blood Kit

1 – A 0.2 mm punch was made in the FTA® Micro Indicating Card with the help of Harris Micro Punch;

2 – The punch was transferred to a sterile 0.2 ml microtube;

3 – 100 µl DNAse/RNAse Free Water was transferred to the 0.2 ml microtube containing the punch. After 5 minutes of incubation the DNAse/RNAse Free Water was discarded;

4 – The step 3 was repeated 3 times;

5 – A brief vortex was made to discard the excess of liquid in the 0.2 ml microtube;

6 – A mixture containing 57.2 µl DNAse/ RNAse Water, 6.5 µl de 10X Buffer Sky Blue and 1.3 µl de prepGEM™ was added to the 0.2 ml microtube containing the washed FTA punch;

7 – The mixture was incubated in the thermocycler for 15 minutes at 75 ºC, followed by 5 minutes at 95 ºC;

8 – All reaction volume was transferred to a new sterile 0.2 ml microtube and stored at 4 ºC until use.

2.2.1.3 Target amplification by Polymerase Chain Reaction (PCR)

1 – All reagents aliquots were allowed to defrost;

2 – A reaction mix was prepared according to sub-section 2.2.1.7.1 – Standard PCR of this chapter;

3 – Reaction mix was briefly mixed and vortexed;

4 – The reaction mix was distributed to 0.2 ml microtube already containing the micro punch (See sub-section 2.2.1.1 of this chapter);

5 – 0.1 µM of the respective primers were added to the mixture;

6 – Reaction was briefly mixed and vortexed and incubated in the thermocycler for amplification reaction.

2.2.1.4 Direct sequencing using BigDye Terminator V1.3 technology

1 – To a 0.2 ml microtube, 3 µL of a mixture containing BigDye terminator V1.3 was added, together with sequencing buffer 5X in a ratio 1:3;

2 – 10 ng of purified PCR product was added to the previous 0.2 mL microtube;

3 – Finally, 1 µM of the respective primer was added to the mixture and the volume was fulfilled with Type-I H_2O to a final volume of 10 µL;

4 – After amplification reaction, the unincorporated dye terminators were removed by Sephadex G50 before being applied in sequencer ABI3730XL.

2.2.1.5 Target amplification by Loop-mediated isothermal amplification (LAMP)

1 – All reagents aliquots were allowed to defrost;

2 – A reaction mix was prepared according to sub-section 2.2.1.7.1 – LAMP of this chapter;

3 – Reaction mix was briefly mixed and vortexed;

4 – The reaction mix was distributed to 0.2 ml microtube;

5 – 10 ng of template previously extracted (See sub-section 2.2.1.2 of this chapter) was added to 0.2 ml microtube;

7 – Reaction was briefly mixed and vortexed and incubated in the thermocycler at 95 °C for 5 min for denaturation and immediately transferred to ice for 1 minute.

9 – *Bst* DNA polymerase was added and the reaction was briefly mixed and vortexed and incubated in the thermocycler for amplification reaction.

2.2.1.6 Digestion with restriction enzyme

1 – 1 Unit of *SpeI* was mixed 1X CutSmart™ Buffer and 100 ng of Loop-mediated isothermal amplification product and fulfilled with Type-I H_2O to a final volume of 50 µL.

2 – Mixture was incubated for 1 hour at 37 ºC. Digestion was confirmed by electrophoretic analysis in 2% agarose gel.

2.2.1.7 Enzyme mediated amplification

2.2.1.7.1 Reaction Mixtures

Standard PCR		**Sequencing PCR**	
1 x	Surf HOT Taq Buffer	1ng/10bp	PCR template
2.5 mM	$MgCl_2$	1 x	Sequencing Buffer 5X
0.4 µM	Fwd Primer	3% (v/v)	Big Dye Terminator v3.1
0.4 µM	Rev Primer	1 µM	Primer (Fwd or Rev)
0.2 mM	dNTPs		
0.1 U	Surf HOT Taq polymerase		

LAMP and Allele-Specific LAMP		**Digestion**	
2.5 x	Bst Polymerase Buffer	1ng/10bp	PCR template
0.8 µM	FIP primer	1 x	Sequencing Buffer 5X
0.8 µM	BIP primer	3% (v/v)	Big Dye Terminator v3.1
0.2 µM	F3 primer	1 µM	Primer (Fwd or Rev)
0.2 µM	B3 primer		
0.2 mM	dNTPs		
1.6 M	Betaine		
4 mM	$MgCl_2$		
0.3 U	Bst Polymerase		
10 ng	Template		

2.2.1.7.2 Reaction Programs

Standard PCR				**Sequencing PCR**			
1.	15 min	95 ºC	1×	1.	1 min	96 ºC	1×
2.	1 min	94 ºC		2.	10 sec	96 ºC	
3.	30 sec	60 ºC	35×	3.	6 sec	50 ºC	26×
4.	30 sec	72 ºC		4.	4 min	60 ºC	
5.	6 min	72 ºC	1×	5.	Hold	4 ºC	∞
6.	Hold	4 ºC	∞				

LAMP				Allele-Specific LAMP			
1.	60 min	65 ºC	1×	1.	75 min	62 ºC	1×
2.	10 min	80 ºC	1×	2.	10 min	80 ºC	1×
3.	Hold	4 ºC	∞	3.	Hold	4 ºC	∞

Digestion			
1.	60 min	37 ºC	1×
2.	20 min	80 ºC	1×
3.	Hold	4 ºC	∞

2.2.1.8 Target preparation

2.2.1.8.1 *FTO* gene

For dbSNP rs#: 9939609 genotype characterization all 194 biological samples were firstly amplified and subsequently sequenced via direct sequencing with primers FTOFwd_440nt and FTORev_440nt. This genotype characterization allowed determining which biological samples were homozygous for the most common (T) and most rare (A) allele and which were heterozygous (T/A). Later, the association studies with the obesity-related anthropometric data were condcted. For hybridization assays with Au-nanoprobes, 440 bp and 225 amplicons was generated with primers FTOFwd_440nt / FTORev_440nt and FTOFwd_225bp / FTORev_225bp, respectively, to be used as complementary/single-base mismatch targets of FTO Au-nanoprobes.

Additionally, 2 sets of 40 nt oligomers, named FTO_Sense_ssDNAwt and FTO_Sense_ssDNAwt, were ordered to be used as complementary ssDNA targets for FTOwt17 and FTOwt20; and FTOmut17 and FTOmut20 Au-nanoprobes, respectively. The first 20 nt at 3'-end of these ssDNA targets are complementary to these Au-nanoprobes. Other 2 sets, named FTO_Antisense_ssDNAwt and FTO_Antisense_ssDNAmut were ordered, to be used as complementary ssDNA targets for AntisenseFTOwt17 and AntisenseFTOmut17 Au-nanoprobes, respectively. The first 20 nt of these ssDNA targets are complementary to these Au-nanoprobes.

2.2.1.8.2 PPARG gene

A full genotype characterization was determined for all the 194 biological samples: homozygous for the most common (C) and most rare (G) allele and heterozygous (C/G) for the dbSNP rs#: 1801282. A 495 bp amplicon was generated by PCR and subsequently sequenced via

direct sequencing with primers PPARGFwd and PPARGRev. For hybridization assays with the Au-nanoprobes the same PCR products were used as complementary/mismatched targets.

Additionally, 2 sets of 40 nt oligonucleotides were ordered, named PPARG_Sense_ssDNAwt and PPARG_Sense_ssDNAmut, to be used as complementary ssDNA targets for PPARGwt17 and PPARGwt20; and PPARGmut17 and PPARGmut20 Au-nanoprobes, respectively. The first 20 nt at 3'-end of these ssDNA targets are complementary to these Au-nanoprobes. The other 2 sets, named PPARG_Antisense_ssDNAwt and PPARG_Antisense_ssDNAmut were ordered to be used as complementary ssDNA targets for AntisensePPARGwt20 and AntisensePPARGmut20 Au-nanoprobes, respectively. The first 20 nt at 5'-end of these ssDNA targets are complementary to these Au-nanoprobes.

2.2.1.8.3 APOA5 gene

The strategy used for FTO and PPARG genotype characterization was also employed to tag the dbSNP rs#: 662799 present in the APOA5 gene. All the 194 samples were firstly amplified and subsequently sequenced via direct sequencing with primers APOA5Fwd and APAO5Rev. This genotype characterization allowed determining which samples were homozygous for the most common (A) and most rare (G) allele and which were heterozygous (A/G) and allowed to conduct the association studies with the obesity-related anthropometric data. Also, for hybridization assays the PCR products generated by these primers were used as complementary/mismatched targets of APOA5wt17, APOA5mut17, AntisenseAPOA5wt17 and AntisenseAPOA5mut17 Au-nanoprobes.

Moreover, 2 sets of 40 nt oligonucleotides were ordered, named APOA5_Sense_ssDNAwt and APOA5_Sense_ssDNAwt, to be used as complementary ssDNA targets for APOA5wt17 and APOA5mut17 Au-nanoprobes, respectively. The first 20 nt at 3'-end of these ssDNA targets are complementary to these Au-nanoprobes. The other 2 sets, named APOA5_Antisense_ssDNAwt and APOA5_Antisense_ssDNAmut were ordered to be used as complementary ssDNA targets for AntisenseAPOA5wt20 and AntisenseAPOA5wt20 Au-nanoprobes, respectively. The first 20 nt at 5'-end of these ssDNA targets are complementary to these Au-nanoprobes.

2.2.1.8.4 MCM6 gene

The genotype characterization for the dbSNP rs#: rs4988235 was conduct by generating PCR amplicon of 333 bp and subsequently sequenced via direct sequencing with MCM6Fwd and MCM6Rev primers. Also, isothermal amplification (LAMP) of MCM6 gene containing the SNP to be studied was generated by the outer primers MCM6LAMP_F3 and MCM6LAMP_B3 and

the inner primers MCM6LAMP_BIP and MCM6LAMP_BIP. The product generated was used for further genotype identification with LAMPwt_MCM6 and LAMPmut_MCM6 Au-nanoprobes. The allele-specific LAMP products were generated by the outer primers AS-LAMPMCM6_F3wt or AS-LAMPMCM6_F3mut and AS-LAMPMCM6_B3 and by the inner primers AS-LAMPMCM6_BIP and AS-LAMPMCM6_FIP and further identified by ASLAMP_MCM6 Au-nanoprobe.

2.2.2 Nanotechnology

2.2.2.1 Synthesis of Gold Nanoparticles
(Doria 2010b)

Note: All glass materials used for the synthesis of AuNPs were previously immersed overnight in freshly prepared *aqua regia* (1:3, HNO_3:HCl) and later vigorously washed several times with Type-I H_2O (18.2 MΩ.cm at 25 °C). All metal materials used during synthesis were covered with Teflon and Type-I H_2O was used in the preparation of all solutions.

1 – In a 500 mL round bottom flask, 250 mL of 1 mM $HAuCl_4$ was brought to boil while in reflux and vigorously stirring;

2 – Afterwards, 25 mL of 38.8 mM sodium citrate was added and the mixture was kept refluxing for 20 minutes with continuous stirring;

3 – The colloidal solution was left to cool to room temperature while keeping the continuous stirring;

4 – The colloidal solution was then transferred to a 250 mL Erlenmeyer flask, covered with aluminum foil and stored in the dark at room temperature;

5 – AuNPs concentration was determined by the Lambert–Beer law assuming a calculated molar absorptivity for the plasmon resonance band maximum (526 nm) of 2.33×10^8 M^{-1} cm^{-1};

6 – Morphological characterization of the AuNP was performed by Transmission Electron Microscopy (TEM) and Dynamic Light Scattering (DLS).

2.2.2.2 Synthesis of Au-nanoprobes

2.2.2.2.1 Thiol-modified oligonucleotides preparation
1 – One volume of thiol-modified oligonucleotide (See Sub-section 2.1.5.4.2 of this chapter) was extracted with two volumes of ethyl acetate;

2 – The organic phase was discarded after centrifuging for 5 minutes at 14462×g;

3 – Steps 1 and 2 were repeated twice;

4 – The remaining aqueous phase was further purified through a NAP-5 column, accordingly to manufacturer's instructions, using 10 mM phosphate buffer pH 8 as eluent;

5 – The purified thiol-modified oligonucleotide was quantified by UV/Vis spectroscopy with help of NanoDrop, using the extinction coefficient at 260 nm provided by manufacturer.

2.2.2.2.2 AuNPs functionalization

(Doria 2010b)

1 – In a 25 mL polypropylene vial with a conical skirted base, the purified thiol-modified oligonucleotide was mixed with a ~15 nM AuNPs solution in a theoretical ratio of 1:200 (AuNP:oligos);

2 – Synthesis Buffer I was then added to achieve a final concentration of 10 mM phosphate buffer pH 8, 0.01% (w/v) SDS;

3 – Afterwards, the ionic strength of the solution was sequentially increased in 50 mM increments by adding a certain volume of Synthesis Buffer II solution up to a final concentration of 10 mM phosphate buffer pH 8, 0.3 M NaCl, 0.01% (w/v) SDS and let rest at room temperature for an o/n period;

NOTE: After each Synthesis Buffer II addition, the vial was submersed in an ultrasound bath for 10 seconds and let to rest at room temperature for 20 minutes before the next increment.

4 – Functionalized AuNPs were distributed in 2 mL tubes and centrifuged at 14462 ×g for 40 minutes;

5 – The supernatant was discarded and the resulting oily pellet was washed twice with 10 mM phosphate buffer pH 8 and once with 10 mM phosphate buffer pH 8 0.1M NaCl;

6 – The resulting pellets were than mixed and the concentration of functionalized AuNPs was determined by the Lambert–Beer law assuming a calculated molar absorptivity for the SPR peak (526 nm) of 2.33×10^{8} M^{-1} cm^{-1};

7 – The resulting functionalized AuNPs solution (stock solution) was diluted to a final concentration of 15 nM with 10mM phosphate buffer pH 8 0.1M NaCl. The colloidal solution was stored in the dark at 4 ºC.

2.2.2.3 Au-nanoprobes stability assays

1 - A solution containing 15 nM Au-nanoprobe (Au-nanoprobe final concentration of 2.5 nM) and 10 mM phosphate buffer pH 8 alone was prepared by heating for 2 minutes at 95ºC and cool down for 15 minutes at 25 ºC;

2 - The solution was mixed with increasing concentrations of $MgCl_2$ (0-100 mM) solution to fulfil a total volume of 30 µL;

3 - The solutions were transferred to 384-microplate and UV-visible spectroscopic measurements were registered 15, 30 and 45 minutes after salt addition in a microplate reader.

2.2.2.4 Non-cross-linking hybridization assays

1 – Reaction mixtures were performed in 0.2 mL tubes, to a final volume of 30 µL. Assay solutions containing the Au-nanoprobes and target DNA were prepared by mixing the appropriate DNA sample (final concentration varied) with the Au-nanoprobe solution (final concentration 2.5 nM), and by using 10 mM phosphate buffer pH 8. A blank solution was prepared by replacing the DNA for an equivalent volume of 10 mM phosphate buffer pH 8;

2 – Samples were heated for 2 min at 95ºC and then allowed to cool down for 15 minutes at 25 ºC;

3 – Each sample was mixed with the threshold concentration of a concentrated $MgCl_2$ solution. The concentration of $MgCl_2$ to be used was determined beforehand by the stability assays;

4 – Samples were transferred to 384-microplate and UV-visible spectroscopic measurements were registered 15, 30 and 45 minutes after salt addition in a microplate reader.

2.2.2.5 Transmission Electron Microscopy (TEM) analysis

(contracted service)

Samples of AuNPs were sent to Instituto de Ciência e Engenharia de Materiais e Superfícies (ICEMS/IST), Portugal, for TEM analysis. Analysis was performed by depositing 10 µL of the as-prepared colloidal suspensions in carbon copper grids, later washed twice with 10 µL of Type-I water, and air dried. TEM was performed with a HITACHI H-8100 microscope operated at 200 kV.

Particles size and shape were determined by analysis of the TEM pictures using the image software Carnoy 2.0 (performed by candidate).

2.2.2.6 Dynamic Light Scattering (DLS) analysis

The hydrodynamic diameter of AuNPs was determined by DLS. A 100 µL sample of 2.5 nM AuNPs was first stabilized for 15 minutes at 25ºC. Afterwards 60 µL were used to perform 2000 measurements with 3 runs each. DLS analyses were performed at Departamento de Química (FCT-UNL) with a Horiba SZ-100 NanoPARTICA Analyzer.

2.2.2.7 Zeta potential analysis

A total volume of 500 µL at 2 nM of AuNPs and Au-nanoprobes were prepared in 10 mM phosphate buffer pH 8 and equilibrated for 15 minutes at 25ºC and then a total of 5 zeta potential measurements with 250 runs each were registered by using a Horiba SZ-100 NanoPARTICA Analyzer. Zeta potential analyses were performed at Departamento de Química (FCT-UNL)

2.2.3 Microfluidic fabrication

(Work developed under Iwona Bernacka-Wojcik PhD Thesis - Bernacka-Wojcik 2014a)

2.2.3.1 Fabrication of microfluidic chip for Au-nanoprobe based DNA detection

1 – SU-8 2050 were spin-coated to form a ~125 µm thick layer;

2 – Samples were then soft-baked, exposed on a mask aligner with a dose of 309 mJ/cm^2 through an i-line filter and post-baked;

3 – Afterwards, development was performed by submersing in propylene glycol methyl ether acetate, during 18 minutes with magnetic agitation of 500 rpm. The mold was silanized with tridecafluoro-1,1,2,2-tetrahydrooctyl trichlorosilane;

4 – PDMS was prepared by mixing a base and a curing agent in a 10:1 ratio of weight;

5 – Subsequently, the PDMS was poured over the SU-8 mold and cured at 100 ºC on a leveled hot plate for 3 hours, and the PDMS was peeled off from the SU-8 mold;

6 – PDMS structures were placed on top of a Petri dish with the negative relief features up, upon which an epoxy resin was poured to form a ~2 mm thick layer. After ~72 hours degassing in desiccator to remove bubbles, the epoxy glue was cured in an oven at 120 ºC for ~40 minutes;

7 – Cured epoxy was peeled from the PDMS and used as a master mold for PDMS soft lithography using the same procedure as described above;

8 – Chips were irreversibly bonded to glass slides by UVO cleaner;

9 – After the treatment, the PDMS-glass sandwich was baked at 100 ºC for 5 minutes to increase the bond strength;

10 – The microfluidic devices were characterized by confocal scanning microscopy and scanning electron microscopy;

11 – Microscopic images were taken using Stereo Microscope Leica Zoom 2000 and Pentax K100 camera in dark conditions (exposure time 30 seconds; aperture 8).

2.2.3.2 Opto-electronic set-up

The fabricated microfluidic chips were integrated with an optoelectronic set-up.

1 – Firstly, the graded-index multimode optical fibers of 62.5 μm core diameter, 125 μm cladding diameter and NA of 0.275 were stripped, cleaved and inserted into the input and output grooves of the chip with a drop of isopropanol for easier insertion;

2 – The other ends of the fibers were inserted into a bare fiber terminator and mating sleeves. The input fiber was connected with a SMA-ended GIF625 patch cable coupled to green a SMD LED or a red SMD LED;

3 – SMD LEDs were then placed in a box of M530F1 and powered with 400 mA; ii) an output fiber (62.5 μm core multimode fiber) was connected to a pigtailed silicon photodiode. The electrical signal from the photodiode was provided to the input of operation amplifier circuit with a feedback loop resistance of 20 MΩ and supplied by ± 15 V.

2.2.3.3 Microfluidic assays

1 – Microfluidic channel was first rinsed with isopropanol, then 3 μl of each solution to be analyzed was dispensed into the inlet well and injected to the channel by the withdrawing from the outlet using a syringe pump (flow rate: 5 μL/min);

2 – Afterwards, the output voltage was measured for the red LED powered with 400 mA acquiring 150 values every 0.2 seconds, then repeated for the green LED;

3 – Proper $MgCl_2$ concentration was added to solutions in a test tube and then was injected to the microchannel 8 or 26 minutes after salt addition to AuNPs or Au-nanoprobes, respectively;

4 – Measurements were performed after 10 minutes or 30 minutes of salt addition to AuNPs or Au-nanoprobes, respectively, for the color development;

5 – For validation of the prototype, double beam spectrophotometer was used for absorbance measurements of AuNPs solutions and microplate reader for Au-nanoprobes solutions;

6 – The spectra of the solutions in chips were acquired using miniature fiber optic spectrometer;

7 – The reported expanded uncertainties are based on the standard uncertainty multiplied by a coverage factor k = 3, providing a coverage probability of approximately 99.7%. The type A uncertainty evaluation was carried out in accordance with the International Organization for Standardization requirements (Evaluation of measurement data – Guide to the expression of uncertainty in measurement JCGM 100:2008, 2008).

2.2.4 Statistical analysis

All statistics were performed using the GraphPad Prism 5 software from GraphPad, Inc. (California, USA) considering a significance value of 95 % ($\alpha = 0.05$) and 99% ($\alpha = 0.01$), following Zar (1998) and Sheskin (2000).

2.2.4.1 Association between each SNP and obesity-related anthropometric data and odd ratio determination

1 – To determine if any significant differences were found between each genotype group for each studied SNP and the anthropometric measures, a one-way analyses of variance was used (one way-ANOVA) and a *post hoc* Bonferroni test for multiple comparisons;

2 – To determine the risk of each *loci* to obesity, all odd ratio (OR) with 95% confidence interval (CI) were determined through binary logistic regression.

2.4.4.2 Colorimetric assays with Au-nanoprobes

Colorimetric assays involving Au-nanoprobes were analyzed using one away-ANOVA and a *post hoc* Tukey's honest significant difference (HSD) for multiple comparisons.

CHAPTER 3 - ASSOCIATION OF FTO, PPARG AND APOA5 POLYMORPHISMS WITH OBESITY IN PORTUGUESE POPULATION

Disclaimer: Results and data presented in this chapter were published in:

Carlos FF, Silva-Nunes J, Flores O, Brito M, Doria G, Veiga L, Baptista PV. 2013. Association of FTO and PPARG polymorphisms with obesity in Portuguese women. Diabetes, Metabolic Syndrome and Obesity: Targets and Therapy 6 241–245.
Fábio Ferreira Carlos performed all the experimental work, analyzed the data and drafted the manuscript.

- XXXVII Jornadas Portuguesas de Génetica 2012 hosted by Universidade Nova de Lisboa, entitled *"Analysis of FTO (rs9939609) and PPARG (rs1801282) involvement in obesity in the Portuguese population"*. (Poster presentation)
- Seminário Nutrigenómica, Nutrigenética e Epigenética - II Encontro Nacional de Estudantes de Dietética e Nutrição 2014 hosted by Escola Superior de Tecnologia da Saúde de Lisboa, entitled *"Does Genetics Influence our Body Weight? Association of FTO rs9939609 polymorphism and Obesity in Portuguese women"*; (Oral communication)
- XXXVIII Jornadas Portuguesas de Génetica 2013 hosted by Universidade do Porto, entitled *"Association of FTO rs9939609 polymorphism with obesity and type 2 diabetes in Portuguese women"*. (Oral communication)

X Congresso Português de Diabetes hosted by Sociedade Portuguesa Diabetologia, 2012, entitled *"Polimorfismo rs9939609 do gene FTO como determinante do grau de insulinorresistência e de insulinossecreção em mulheres obesas"* (Oral communication)

3.1 Introduction

The XXI century was clearly marked by one of the most important breakthrough in life science – the completion of the human genome sequence in 2003. This major advance was deterministic for the genome architecture understanding and the biological pathways of several traits (Feuk et al. 2006, Hofker et al. 2014). This unparalleled achievement was only possible due to advances in high-throughput genotyping technology that has revealed millions of genetic variants in the human genome and induced the development of GWAS – a major tool that revolutionized the pursuit for genetic risk variants underlying complex diseases (Hindorff et al. 2009). These massive studies have already identified 2000 genetic *loci* with strong association for more than 300 common and complex traits (Welter et al. 2014, http://www.genome.gov/gwastudies), of which 75 were identified as obesity susceptibility *loci* (Day and Loos 2011).

In this section of the thesis the association between 3 obesity-related SNPs, *FTO* (dbSNP rs#: 9939609), *PPARG* (dbSNP rs#: 1801282) and *APOA5* (dbSNP rs#: 662799) and several obesity-related traits will be scrutinized (anthropometric data), namely BMI, total body fat mass, percentage of fat mass, waist perimeter and waist/hip ratio for each genotyped group. Moreover, the odd ratio (OR) risk for each SNP to obesity by comparison of control vs. case group was assessed through several statistical approaches.

The subjects in this study were all Caucasian Portuguese female aged between 18-50 years old and were divided in two groups harboring a total of 194 subjects. As Control group (or Normal), 99 healthy subjects showing a BMI ranged between 18.50 and 24.99 Kg/m^2 were either selected during a routine health check or belonged to the staff of Curry Cabral Hospital. The Case group (or Obese) was composed of 95 subjects showing a BMI $\geq$30.00 Kg/m^2 were all attending the Endocrinology Department of Curry Cabral Hospital. Both groups had a body weight variation inferior to 10% in the last year. The genetic population characterization for the *FTO* (dbSNP rs#: rs9939609), *PPARG* (dbSNP rs#: rs1801282) and *APOA5* (dbSNP rs#: rs662799) was performed by direct sequencing using BigDye terminator V.31 technology in the plus and minus strand. The three possible genotypes of each SNP are illustrated in Appendix II – Figure AII.1

3.2 Results and Discussion

3.2.1 Genetic population characterization

3.2.1.1 Allele and genotype frequencies

It is important to mention that data collected in this study relies only in adult female, not comprising, adult male or infants of both genders. For this reason, the discussion should rely only

on female subjects, nevertheless the literature with this population niche is reduced and for that reason, the discussion will be focused on the population origin, in this case European.

Sequencing showed that genotype frequencies for *FTO* (dbSNP rs#: rs9939609) were 24.74% T/T, 56.70% A/T and 18.56% A/A. When comparing Case and Control groups, no significant deviation from Hardy-Weinberg equilibrium of allele frequencies was observed for this *locus* (p=0.054), with a majority of individual being heterozygous (A/T). Data show that the "T" allele is more frequent in subjects with BMI values between 18.5 and 24.9 Kg/m^2, whereas the "A" allele is preeminent in subjects with BMI ≥30 Kg/m^2. For *PPARG* (dbSNP rs#: rs1801282), the genotype frequencies were 80.93% for homozygous C/C, 18.04% for heterozygous C/G and 1.03% for homozygous G/G. Again, no significant deviation from Hardy-Weinberg equilibrium of allele frequencies was observed for this locus (p=0.975). The alleles in this SNP were equally distributed between the case and control group. For last, in the *APOA5* (dbSNP rs#: rs662799) the genotype frequencies were 88.1% for homozygous A/A, 10.8% for heterozygous A/G and 1.03% for the homozygous.

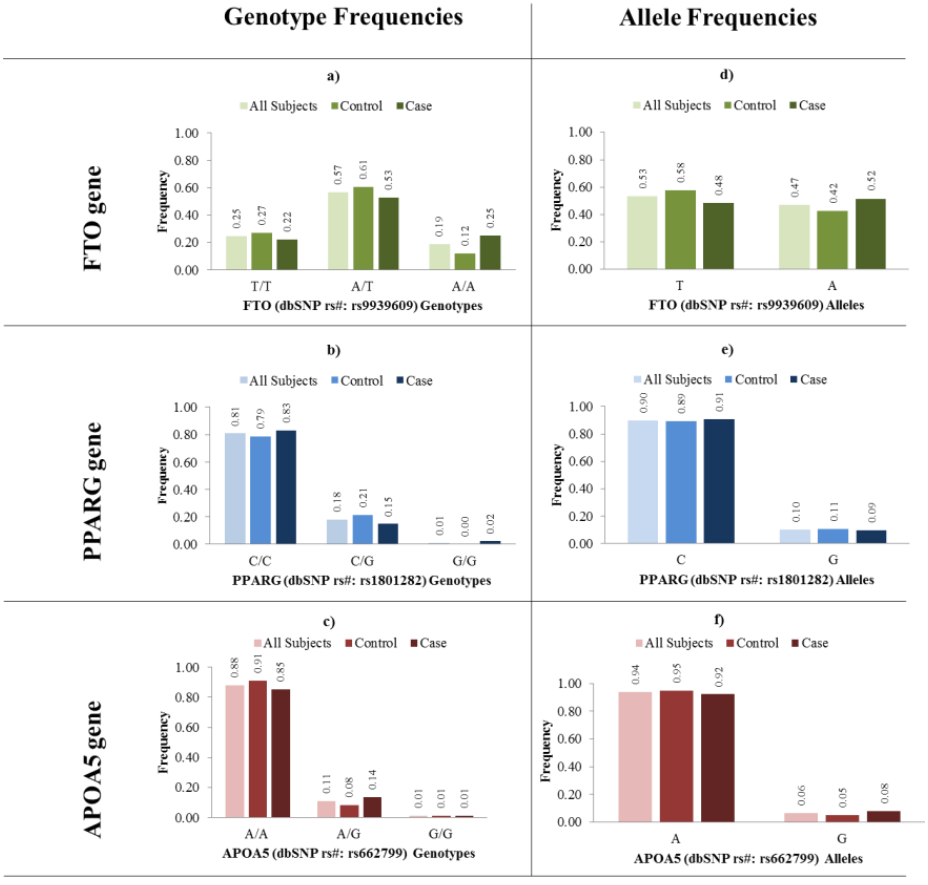

Figure 3.1 – Genotype and allele frequencies data for *FTO* (dbSNP rs#: rs9939609), *PPARG* (dbSNP rs#: rs1801282) and *APOA5* (dbSNP rs#: rs662799). All data was collected from 194 samples by direct sequencing using BidDye terminator V3.1. **a), b)** and **c)** – Genotype frequencies for *FTO* (dbSNP rs#: rs9939609), *PPARG* (dbSNP rs#: rs1801282) and *APOA5* (dbSNP rs#: rs662799), respectively, for all subjects, control and case groups. **d), e)** and **f)** – Allele frequencies for *FTO* (dbSNP rs#: rs9939609), *PPARG* (dbSNP rs#: rs1801282) and *APOA5* (dbSNP rs#: rs662799), respectively, for all subjects, control and case groups.

Hardy-Weinberg equilibrium (HWE) of allele frequencies does not suffer any significant deviation for this SNP (p=0.155) and like *PPARG* (dbSNP rs#: rs1801282) the alleles were equally distributed between the case and control group (see Figure 3.1).

Despite the related genetic background between European populations, demonstrated by Simoni and co-workers,(Simoni et al. 2000) where he reported that the European mitochondrial DNA pool has been found to be quite homogenous, the structure of existing genetic differences are well correlated with geographic distances. This was identified in the work of Lao and co-workers (Lao et al. 2008), where the genetic structure of the European population was assessed by using 309,790 SNPs in 2,457 individuals, ascertained at 23 sampling sites from 20 different European countries. In his work, genetic data was compatible with the European population history, mainly the prehistoric population expansion from southern to northern Europe and that mean heterozygosity was larger in southern than in northern European subpopulations – See Figure 3.2.

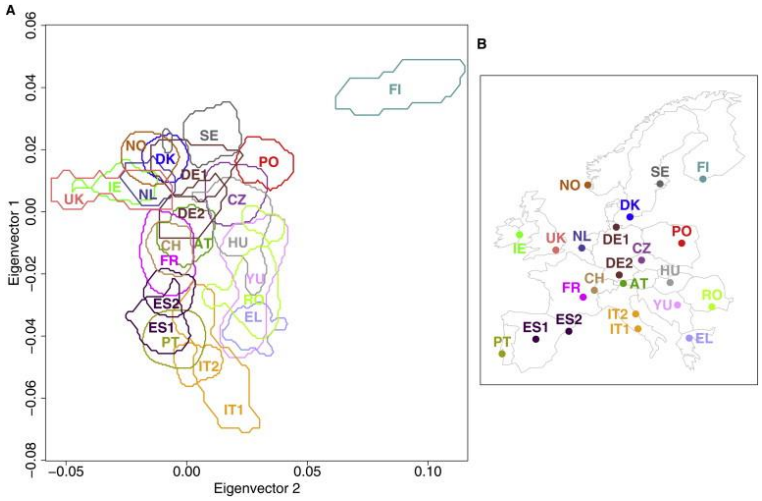

Figure 3.2 – SNP analyses of 23 European sub-populations. A) SNP-based grouping of European sub-populations B) identification of the 23 European sub-populations (Lao et al. 2008).

Several errors can occur while performing association studies (Salanti et al. 2005). HWE is considered an important tool to be used when data analyses are being conducted, since HWE is not simply a theoretical law, as can pinpoint and signal important peculiarities or bias/errors that might occur in the analyzed data set (i.e.: improper sampling approaches and/or population stratification or genotyping inaccuracies). For example, allelic drop-out, where some allele can be poorly amplified and an excess of homozygous status can be observed, boosting the false-negative or false-positive results (Akey et al. 2001, Turner et al. 2011, Johnson et al. 2013). The mathematical HWE equation was developed to underlying population structure by determining the behavior of two alleles at a single genetic *locus* and can be used to calculate the genetic variation of a population at equilibrium. Moreover, HWE theorem states that in a large randomly

breeding population the allelic frequencies will continue constant from one generation to the next assuming the absence of disturbing factors (i.e.: mutation, gene migration, selection or genetic drift (Nussbaum et al. 2007). Nevertheless, the human population does not meet all the HWE assumptions since it evolve from generation to generation resulting in allele frequencies variations. This deviation from the HWE can be determined for genetic association studies to understand whether observed genotyped frequencies are consist with HWE by the chi-squared test ($\chi 2$), where if the squared value is below the 0.05 (5%) significance limit it is possible to conclude that do differ significantly from what we would expect for HWE. The results obtained from the genotyping data for the 3 SNPs in study present no deviation to the HWE since the observed and obtained genotyping frequencies are in accordance ($p>0.05$) and concomitantly a strong indicator that some intrinsic errors related to association studies were avoided. Some authors also indicate that besides HWE checking, a selective and careful comparison analysis between genotype/allele frequencies obtained and the one reported in the existing literature or in reference databases (e.g. dbSNP http://www.ncbi.nlm.nih.gov/SNP/, ALFRED http://alfred.med.yale.edu/) should always be addressed (Yonan et al. 2006, Ziegler et al. 2011, Napolioni 2014). Comparing the allele frequencies obtained for the 3 SNPs for the Portuguese populations with data available in reference databases from the 1000 Genome Project (1000 Genomes Project Consortium et al. 2012), it is possible to conclude that the allele frequencies are in accordance with a European population, presenting slight variations but still accurate. For instance, Figure 3.3 reports on data collected for the SNP rs9939609 of the *FTO* gene, the allele frequency of the most common allele (T) is 53% and 47% for the A allele, that comparing with the data from the reference database is in agreement with a European population (Figure 3.3A), more specifically with the Italian sub-population (Figure 3.3B). The same concordant results were obtained for the PPARG (Figure 3.3C and D) and *APOA5* (Figure 3.3C and D) SNPs, where the similarity with the European allele frequency for these SNPs is higher. The only difference is that for the SNP rs622799 of the *APOA5* gene, the allele frequency is more similar to the Iberian sub-population than to Italian sub-population. Comparing the allele frequencies data obtained for the Portuguese population with that available from other European sub-populations, it is shown that the allele frequencies for the Portuguese population are more similar to the Italian sub-population for the *FTO* (dbSNP rs#: 9939609) and *PPARG* (dbSNP rs#: 1801282), while for the *APOA5* (dbSNP rs#: 662799) the allele frequencies are more similar to the Iberian sub-population (See Table 3.1).

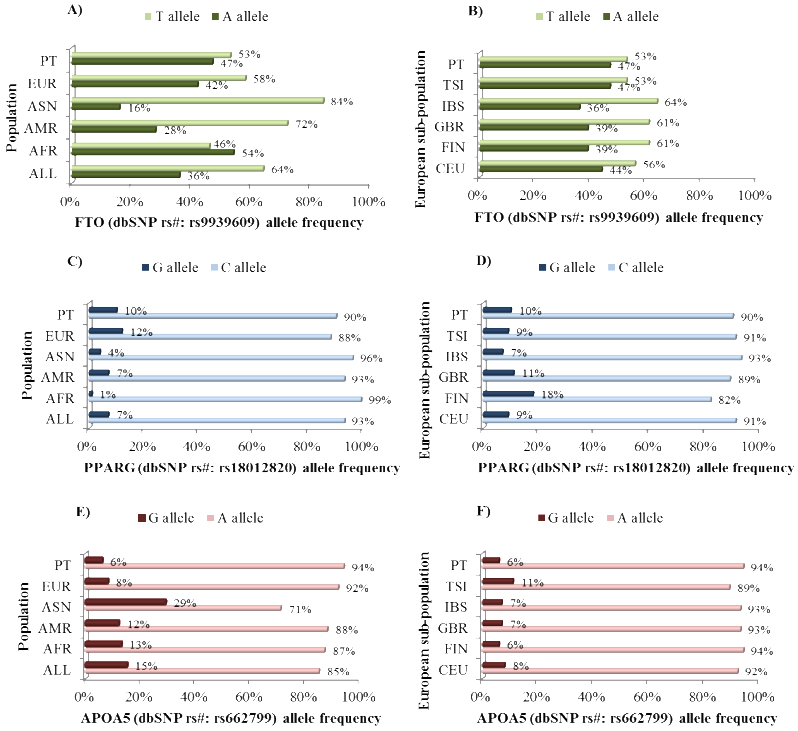

Figure 3.3 – Allele frequencies available from National Center for Biotechnology Information (NCBI) based on the 1000 Genome Project to the SNPs in study. A), C) and **E)** represents the allele frequency of *FTO* (dbSNP rs#: 9939609), *PPARG* (dbSNP rs#: 1801282) and *APOA5* (dbSNP rs#:662799), respectively, for Portuguese (PT), European (EUR), Asian (ASN), and mixed American (AMR), African (AFR) and ALL (EU+ASN+AMR+AFR) populations. **B), D)** and **F)** represents the allele frequency of *FTO* (dbSNP rs#: 9939609), *PPARG* (dbSNP rs#: 1801282) and *APOA5* (dbSNP rs#:662799), respectively, for Portuguese (PT), Toscani in Italia (TSI), Iberian in Spain (IBS), British in England and Scotland (GBR), Finnish in Finland (FIN) and Utah Residents (CEPH) with Northern and Western European ancestry (CEU) sub-populations.

Table 3.1 – **Allele frequencies for the SNPs in study in European Sub-populations.**

European Sub-Populations	***FTO* (dbSNP rs#: 9939609)**			***PPARG* (dbSNP rs#: 1801282)**			***APOA5* (dbSNP rs#: 662799)**			**References**
	Allele frequency (%)		**N**	**Allele frequency (%)**		**N**	**Allele frequency (%)**		**N**	
	T	**A**		**C**	**G**		**A**	**G**		
Portuguese	53.0	47.0	194	90	10	194	94	6	194	Carlos et al. 2013
Italian	53.0	47.0	312	91	9	200	92	8	3728	Mačeková et al. 2013 Buzzetti et al. 2005, De Caterina et al. 2011.
Spanish	60.0	40.0	207	94	7	298	94	6	1825	González-Sánchez et al. 2009, González et al. 2014, Ariza et al. 2010.
UK	60.5	39.5	4862	88	12	2.228	96	4	237	Song et al. 2008, Zeggini et al. 2005, Chandak et al. 2006.
Finish/Swedish	59.0	41.0	18436	84	16	422	-	-	-	Jonsson et al. 2009, Lind et al. 2002.
European overall	61.0	39.0	29596	91	9	375	92	8	47784	Frayling et al. 2007, Sarwar et al. 2010, Vaccaro et al. 2000.

Our data is in agreement with the only two reports available in the literature relating to the allelic distribution of these SNPs in the Portuguese population. Albuquerque and co-workers reported an A-allele frequency of 45% within infant Portuguese population of both genders for the *FTO* (dbSNP rs#: 9939609) gene (Albuquerque et al. 2013). Also, Santos and co-workers reported a G-allele frequency of 5% for the APOA5 (dbSNP rs#: 662799) (Santos et al. 2011). These three comparison methods (HWE, references databases and scientific literature) clearly indicated that the genotyping data obtained for the 3 SNPs in our study were accurate and bias/errors characteristic from genotyping methods were avoided. Moreover, to our knowledge, this is the first report on allele and genotyping frequencies for an adult Portuguese population, which is of fundamental interest to medical, forensic and anthropological sciences, and allows a more comprehensive understanding of European genetic structure and a more appropriate design and interpretation of future genetic epidemiological studies.

3.2.2 Association of SNP obesity-related (*FTO* rs9939609 / *PPARG* rs1801282/ *APOA5* rs662799) and anthropometric traits

The population characterization and the descriptive analysis of the subjects were subdivided by their phenotype group, as shown in Table 3.2. The subjects were divided by their BMI status, and were considered to have a normal phenotype (control group) if their BMI ranged between 18.50 and 24.99 Kg/m^2, while an obese phenotype (case group) was assigned to individuals with a BMI ≥ 30 Kg/m^2. Subjects with overweight (BMI between 25.00 and 29.99 Kg/m^2) were not considered for this study, where the association was only intend to be assessed between normal phenotype and obese phenotype. As it is possible to observe (Table 3.2), all anthropometric measures vary between groups, being the higher values within the obese phenotype.

Table 3.2 - Anthropometric data of all subjects subdivided by phenotype. Obesity status: normal (BMI between 18.50 and 24.99 Kg/m^2), obese (BMI ≥ 30.00 Kg/m^2); all data presented as means ± standard deviation.

Anthropometric Measures	Total	Phenotype	
		Normal	Obese
N	194	99	95
Age (Years)	34.19 (±8.22)	34.24 (±8.30)	34.12 (±8.14)
BMI (Kg/m^2)	32.28 (±12.44)	21.42 (±1.69)	43.60 (±7.83)
Fat Mass (Kg)	33.59 (±22.43)	14.32 (±3.61)	54.00 (±14.88)
Fat Mass (%)	36.22 (±12.25)	25.30 (±4.67)	47.61 (±5.30)
Waist circumference (cm)	94.19 (±25.72)	71.75 (±5.85)	117.57 (±15.49)
Waist/Hip Ratio (cm)	0.80 (±0.09)	0.74 (±0.05)	0.87 (±0.08)

It was scrutinized whether any significant differences were found between each genotype groups for the studied SNP and the anthropometric measures by one-way analyses of variance

(one away-ANOVA) and a *post hoc* Bonferroni test. While the one away-ANOVA determines if there are significant mean differences between groups, the *post hoc* Bonferroni test can determine which means differ from each other. Considering this, the one away-ANOVA analysis revealed significant mean differences for the *FTO loci* to BMI (p-value=0.025), percentage of fat mass (p-value=0.033), total fat mass (p-value= 0.013) and for waist perimeter (p-value= 0.022). For the waits/hip ratio no mean significant differences were found to the *FTO loci*. For the other two *loci* (*PPARG* and *APOA5* gene), no mean significant differences were found to any obesity-related traits or anthropometric measures (p-value>0.05).

The *post hoc* Bonferroni test, which is a more robust test, allowed to corroborate the one away-ANOVA results and further quantify this mean difference. This permitted to observe that significant mean differences were found between the three genotyped groups (A/A, A/T and A/A) to all the anthropometric traits with the exception of percentage of fat mass (Table3.3). Moreover, it was possible to determine that no increment was given per-A allele from the *FTO locus per se*, but in the presence of both A alleles this increment is noticed. Individuals with both A alleles in *FTO* (dbSNP rs#: rs9939609) show 6.37±2.35 Kg/m^2 (P=0.022) higher BMI, 11.99±4.86 Kg (P=0.043) higher body-fat mass and 13.31±4.87 cm (P=0.020) higher waist perimeter compared with both T-alleles carriers.

Table 3.3 – Anthropometric measures in function of each genotype of each SNP.

Data	*FTO* (dbSNP rs#: 9939609)				*PPARG* (dbSNP rs#: 1801282)				*APOA5* (dbSNP rs#: 662799)			
	TT	**AT**	**AA**	**p**	**CC**	**CG**	**GG**	**p**	**AA**	**AG**	**GG**	**p**
N	48	110	36	-	157	35	2	-	171	21	2	-
Age (Years)	33.40 (8.12)	34.35 (8.13)	34.75 (8.79)	0.728	34.32 (8.37)	32.89 (7.15)	45.00 (5.67)	0.307	34.21 (8.02)	34.71 (10.11)	29.00 (8.49)	0.647
BMI (Kg/m^2)	31.42 (13.99)	31.07 (11.49)	37.66 (12.12)	**0.024***	32.72 (12.56)	29.97 (12.00)	38.20 (9.33)	0.487	32.03 (12.51)	35.43 (11.96)	31.85 (9.97)	0.515
Fat Mass (kg)	31.55 (23.98)	31.21 (20.60)	43.55 (23.55)	**0.021***	34.55 (22.61)	28.74 (21.71)	42.48 (13.70)	0.432	33.02 (22.38)	39.51 (22.30)	38.43 (22.30)	0.439
Fat Mass (%)	36.68 (11.88)	35.33 (11.78)	41.04 (13.27)	0.053	36.87 (11.98)	32.74 (13.08)	45.70 (8.63)	0.283	35.90 (12.40)	40.05 (10.25)	37.85 (18.46)	0.337
WC (cm)	92.04 (26.42)	91.61 (24.43)	104.92 (26.59)	**0.030***	94.84 (26.00)	90.51 (24.86)	107.00 (18.38)	0.406	93.42 (25.89)	101.71 (23.69)	105.00 (24.75)	0.314
Waist/Hip ratio (cm)	0.79 (0.08)	0.79 (0.09)	0.84 (0.11)	0.112	0.80 (0.09)	0.79 (0.09)	0.89 (0.06)	0.641	0.80 (0.10)	0.84 (0.08)	0.88 (0.02)	0.065

p=p-value; in parenthesis is represented the standard deviation (±).

Logistic regression models allow estimating the probability of a certain characteristic (obesity) given the values of explanatory variables (genotype). With this data it is possible to determine the odds ratio (OR) of the incidence of that event with a certain confidence interval (CI). Table 3.4 presents the OR values confronting case and control groups for risk to obesity. Analyzing the data from the *FTO* (db SNP rs#: 9939609) it was possible to conclude that significant differences were found in allele frequencies between the control and case groups (p-value<0.05), indicating a 2.5-fold higher risk for obesity for homozygous A/A individuals (OR=2.571, CI 1.048–6.308; p-value=0.039). Comparison between homozygous A/A individuals and T allele carriers (either homozygous T/T or heterozygous A/T) clearly shows a significant association of homozygous A/A with obesity (OR=2.451, CI 1.145–5.243; p-value=0.021). Even

more striking is the allelic expression of A/A homozygosity in subjects with a BMI ≥40.00 Kg/m^2, i.e., class III obesity. Comparing this subgroup of obese women to those with class I and class II obesity, an OR=4.044 (CI 1.099–14.878; p-value=0.035) was found. Analysis of *PPARG* (dbSNP rs#: 1801282) and *APOA5* (dbSNP rs#: 662799) showed no association with obesity (p-value>0.05) within the studied population.

Table 3.4 – OR values between control-case and case-case groups. OR values between case and control groups for risk to obesity for allele A in fat-mass and obesity-associated gene (*FTO*) rs9939609, allele G in peroxisome proliferator-activated receptor gamma (*PPARG*) rs1801282, and allele G in Apolipoprotein A-V (*APOA5*) rs662799 and between BMI ≥30.00–<40.00 Kg/m^2 **(A)** and BMI ≥40.00 Kg/m^2 **(B)**for risk to obesity for allele A in *FTO* rs9939609, allele G in *PPARG* rs1801282 and allele G in *APOA5* rs662799 only in the case group.

	***FTO* (dbSNP rs#: 9939609)**			***PPARG* (dbSNP rs#: 1801282)**			***APOA5* (dbSNP rs#: 662799)**		
		OR[a] (95% IC)	**p**		**OR[a] (95% IC)**	**p**		**OR[a] (95% IC)**	**p**
Case *vs* Control (A)	**T/T[b]**	1 (reference)	-	**C/C[b]**	1 (Reference)	-	**A/A[b]**	1 (Reference)	-
	A/T	1.071 (0.541-2.121)	0.843	**C/G**	0.658 (0.312-1.387)	0.271	**A/G**	1.806 (0.712-4.578)	0.213
	A/A	2.571 (1.048-6.308)	**0.039***	**G/G**	1.013 (0.688-3.213)	0.945	**G/G**	1.111 (0.068-18.054)	0.941
	T/T+A/T[b]	1 (reference)	-	**C/C+G/C[b]**	1 (reference)	-	**A/A+A/G[b]**	1 (Reference)	-
	A/A	2.451 (1.145-5.243)	**0.021***	**G/G**	0.752 (0.366-1.548)	0.439	**G/G**	1.043 (0.064-16.910)	0.977
Case *vs* Case (B)	**T/T+A/T[b]**	1 (reference)	-	**C/C+G/C[b]**	1 (reference)	-	**A/A+A/G[b]**	1 (reference)	-
	AA	4.044 (1.099-14.878)	**0.035***	**G/G**	0.431 (0.026-7.134)	0.556	**GG**	0.298 (0.018-4.917)	0.397

[a]All ORs were calculated by logistic regression; [b]values were considered as reference; *significant difference found. p=p-value. In parenthesis is represented the standard deviation (±).

Moreover, it was possible to determine within the case group if there were mean significant differences between the genotype groups and glycemic status for the *loci* already related to this trait in the literature. (*FTO* dbSNP rs#:9939609 and *PPARG* dbSNP rs#: 1801282). No mean significant differences were found between the genotype groups of the *PPARG loci* and glycemic status. Nevertheless, for the *FTO loci* it was possible to observe significant mean differences between the subjects with or without the T-allele (T/T+A/T vs A/A) (p-value<0.05) and glycemic status. It was also possible to determine that the SNP rs9939609 is a determining factor for the development of intermedia hyperglycemia and diabetes in obese women. Furthermore, the presence of the T-allele is associated to higher insulin sensitivity favoring the maintenance of normoglycemia in women with obesity (Nunes 2013).

Data here presented is in agreement with what has been found for European population and sub-populations for the 3 genotyped SNPs related to obesity. From the 75 obesity susceptibility *loci* identified to date (Rankinen et al. 2006 , Day and Loos 2011), the *FTO locus* is the one that presents the largest effect on BMI and is mostly associated to other obesity-related traits in several ancestries (Lu and Loos 2013). Within the European population, where the minor

allele is present in two thirds of the population, several studies have widely replicated these findings with a variety of obesity-related traits, all obtaining an equal response for this *loci* as an important marker in obesity risk assessment (Frayling et al. 2007, Scuteri et al. 2007, Dina et al. 2007, González-Sánchez et al. 2009, Willer et al. 2009, Zimmermann et al. 2011, Sentinelli et al. 2011, Perry et al. 2012). It is also important to mention that the relation between obesity and type II diabetes mellitus (T2DM) is mostly mediated by *FTO* effect on BMI and other traits, such as insulin levels (Fall et al. 2013). Nevertheless, some studies in European and non-European population suggest that *FTO* might, at least in part, increase the risk of T2DM independently of its effect on BMI which is consistent with previous observations (Hertel et al. 2011, Rees et al. 2011, Li et al. 2012).

The *PPARG* is well established and known to be an important regulator of adipocyte differentiation (Spiegelman 1998) and the dbSNP rs#: 1801282 variation, when first described, was seen as a major contributor to the genetic susceptibility for the multifactorial disorder of obesity (Beamer et al. 1998). Since then, the G-allele risk was identified to be associated to obesity BMI-mediated with some Europeans, sub-populations, such as Finnish, (Deeb et al. 1998) Spanish (González Sánchez et al. 2002) and Italian (Passaro et al. 2011) and other non-Europeans populations (Beamer et al. 1998, Ben Ali et al. 2009, Mirzaei et al. 2009, Yao et al. 2015). Nevertheless, like our findings, this association with obesity fails to be replicated in equal sub-populations (Vaccaro et al. 2000) or others sub-populations with European ancestry (Ghoussaini et al. 2005).

The *APOA5* gene, adjacent to *APOA1*/*APOC3*/*APOA4* gene cluster with known roles in the metabolism of plasma lipids, also controls the risk of obesity in some non-European population studies (Chen et al. 2010, Hsu et al. 2013). Nevertheless, the direct association of *APOA5 loci* with obesity, that has been established with this work, is not clear and it is hypothesized that the mechanism in which these *loci* confer risk to obesity might be attributed with the interaction with other obesity-risk genes, such as *APOA1*, *APOC3* and *APOA4* genes (Fisher et al. 1999).

3.3 Concluding Remarks

Significant differences in BMI between control and case group for *FTO* (dbSNP rs#: 9939609) (p-value<0.05) were found, indicating higher risk for obesity in presence of both risk alleles (A/A): OR=2.571 (1.048-6.308) (p=0.039). Homozygous subjects (A/A) with BMI≥40.00 Kg/m^2 presented 4 times higher risk of obesity: OR=4.044 (1.099-14.878) (p-value=0.035). Moreover, individuals with both "A" alleles in *FTO* (dbSNP rs#: 9939609) shown 6.37±2.35 Kg/m^2 (p-value=0.022) higher BMI, 11.99±4.86 Kg (p-value=0.043) higher body-fat mass and 13.31±4.87 cm (p-value=0.020) higher waist perimeter compared to T-allele carriers. Also,

significant mean differences (p-value<0.05) between the subjects with or without the T-allele and insulin status. No mean significant differences in BMI or any other anthropometric trait, were found between the control and case group for *PPARG* (dbSNP rs#: 1801282) and *APOA5* (dbSNP rs#: 662799 (p>0.05).

For the first time, a study involving an adult Portuguese population shows that individuals harboring both risk alleles in the *FTO* gene *locus* are at higher risk for obesity, which is in agreement to what has been reported for other European populations. Moreover, the presence of both risk alleles (A/A) confers higher BMI, waist perimeter and total fat mass when compared with individuals harboring both T alleles. The risk assessment allowed concluding that *FTO* (dbSNP rs#: 9939609) could be a useful tool for the clinical management and risk assessment of obesity. Identifying individuals at increased risk and target those for clinical intervention could be useful for a structured public health strategy within European Union.

CHAPTER 4 - GOLD NANOPROBES AND THE NON-CROSS-LINKING METHOD FOR THE DETECTION OF SINGLE NUCLEOTIDE POLYMORPHISMS

Disclaimer: Results and data presented in this chapter were published in:

Carlos FF, Flores O, Doria G, Baptista PV. 2014. Characterization of genomic single nucleotide polymorphism via colorimetric detection using a single gold nanoprobe. Analytical Biochemistry 465 1-5.

Fábio Ferreira Carlos performed all the experimental work, analyzed the data and drafted the manuscript.

NanoPortugal International Conference (NanoPT), 2015, held in Porto, Portugal, entitled *"Characterization of genomic sing le nucleotide polymorphism via colorimetric detection using a single gold nanoprobe"* (Poster presentation)

4.1 Introduction

Gold nanoparticles functionalized with thiolated oligonucleotides (Au–nanoprobes), due to their unique optical proprieties, have been used as relevant signal transduction elements in nucleic sequence recognition assays. These innovative tests are prone with high specificity and sensitivity and with reduced costs when compared to conventional methods. Monodisperse Au–nanoprobe solutions present a characteristic SPR band at approximately 525 nm (red color solution) that is red-shifted on salt-induced aggregation (blue color solution) (Sato et al. 2003, Thaxton et al. 2006). This property is explored in the non-cross-linking colorimetric detection of nucleic acids, where hybridization to a specific complementary target leads to Au–nanoprobe stabilization and resistance to salt-induced aggregation (Doria et al. 2007, 2010), whereas mismatch/non-complementary/unrelated targets cannot prevent salt-induced aggregation and the consequent solution color change. Under standard conditions, the use of the non-cross-linking method for full SNP genotyping and characterization (*wild type*, mutant, and heterozygous status) requires a set of two Au–nanoprobes capable of individually identifying each allele variation, since it is limited to a red to blue color change (Baptista et al. 2008).

Sato and co-workers presented one of the first approaches using a non-cross-linking method. Through their methodology, a differential aggregation of the Au-nanoprobe occurs in the presence of fully complementary, mismatched or non-complementary targets by solution ionic strength increase (Sato et al. 2003). This method was developed with synthetic oligonucleotides that have the same length of the Au-nanoprobe. In the presence of a fully complementary target to the Au-nanoprobe and upon ionic strength increment, the blunt-ended heteroduplexes formed were found to be less stable and aggregate, turning the solution from red to blue. On the other hand, if the Au-nanoprobe is in the presence of a mismatch or non-complementary the blunt-end heteroduplexes do not form and the solution remains red at the same ionic strength that led the complex Au-nanoprobe/complementary target to aggregate. This approach has a huge limitation of application in biological samples. Biological targets are usually longer than the sequence of the Au-nanoprobe and the formation of blunt-end heteroduplexes, that is crucial for method application, does not occur, thus committing the method. Considering this limitation, Sato and co-workers later used a PCR amplification followed by a single base extension approach to detect SNPs in biological samples at room temperature (Sato et al. 2005) (See Figure 4.1 for more details).

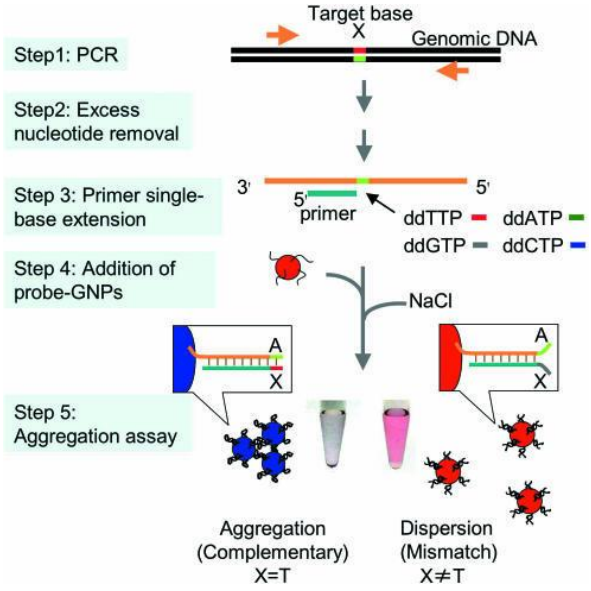

Figure 4.1 – Sato's Non-cross-linking approach for SNP recognition. A single base extension is performed after previous sample amplification with PCR. When target samples allow a successful primer extension, the complex blunt-end heteroduplexes formed between primer/Au-nanoprobe aggregate upon NaCl addition leading to a color change from red to blue. Conversely, non-extended primers (due to target sample mismatch or non-complementarity), will not lead to the formation of blunt-end heteroduplexes and thus, Au-nanoprobe remain disperse upon NaCl addition, preserving its initial red color (Sato et al. 2005).

The non-cross-linking approach developed by Baptista and co-workers, provides a more simplistic methodology and it has proven to be capable of directly identify nucleic acids sequences (DNA/RNA) in biological samples with high levels of sensitivity (Baptista et al. 2005 and 2006, Conde et al. 2010a). Furthermore, it is capable to detect and discriminate between SNPs at room temperature, in particular when considering optimal conditions that allow better mismatch discrimination – mismatch localized at the 3´end of the Au-nanoprobe sequence and oligonucleotide density at the nanoparticle surface should be 24 pmol/cm^2 (≈100 oligos/AuNP) (Doria et al. 2010). The non-cross-linking method, a user-friendly and low-cost approach, claims that in the presence of a fully complementary DNA to the Au-nanoprobe, no red-shift is followed after salt induced aggregation indicating a positive result. On the other hand, in the presence of a non-complementary/mismatch/unrelated target and after increasing of the ionic strength by the addition of a divalent salt, full aggregation pattern undergoes resulting in a visible change of solution color from red to blue (Figure 4.2).

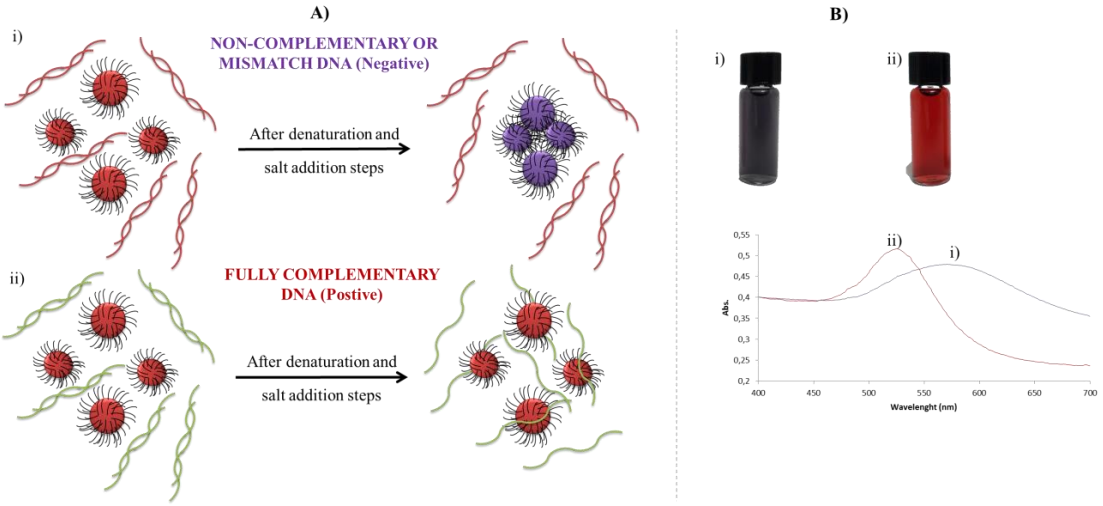

Figure 4.2 – Schematic representation of Baptista's non-cross-linking method. A) Detection system of the non-cross-linking method. **B)** Possible turn around outputs (colorimetric and UV-Vis spectra). **i)** Presence of a mismatch/non-complementary/unrelated target to the Au-nanoprobe and **ii)** Presence of a fully complementary target to the Au-nanoprobe.

The colorimetric and spectrophotometric alteration observed by the increase salt concentration in solution, is derived from the plasmon coupling between Au-nanoprobes as the inter-particle distance decreases, concomitantly leading to Au-nanoprobe aggregation (Jain et al. 2007). This event can be represented by generalist normalization of the ratio between the absorbance of the non-aggregated fraction of Au-nanoprobe (SPR peak at 525 nm) and absorbance from the aggregated fraction of Au-nanoprobe (SPR peak at 600 nm).

$$r(Abs.) = Abs\left(\frac{Non - Aggregated\ fraction}{Aggregated\ fraction}\right)$$

This data interpretation allows to determine that for r(Abs)<1 Au-nanoprobes are mainly aggregated and that the absorbance value of aggregated species is higher than the absorbance value of non-aggregated species, associated with purple-blue colored suspension. The contrary, r(Abs)>1 is mostly associated to a non-aggregated state, in which the absorbance value of the non-aggregated species is higher than the absorbance value of the aggregate species, resulting in a red-pink suspension. Moreover, it is important to mention that the SPR peak of the aggregation fraction can vary around the 600 nm, for lower or higher wavelengths (Veigas et al. 2010, Pedrosa et al. 2014).

An extensive and comprehensive characterization of Au-nanoprobes applied to the non-cross-linking method has been previously performed by a former PhD student of our group, Gonçalo Doria (Doria 2010b). The data generated and available from his thesis allowed determining the most suitable parameters for SNP detection regarding effect of pH, type of salts, effect of reagents commonly used in molecular biology in Au-nanoprobes stability and Au-nanoprobe concentration, to name a few. Hereupon, it was possible to conclude that the divalent

salt, $MgCl_2$, in comparison with monovalent salts, like NaCl, should be used in the non-cross-linking method since lower volumes are required to induce Au-nanoprobe aggregation. Moreover, the Au-nanoprobe stability decreased for pH values below 7.5 (due to decrease of the negative charge of the ssDNA) and in the presence of high concentrations of DMSO or methanol (due the decrease of the repulsive electrostatic forces) and increase in the presence of betaine or formamide (due the adsorption of their amine group on the Au-nanoprobe). For last, since Au-nanoprobe full aggregation remains unchanged above 2 nM, it was determined that 2.5 nM or higher was the optimal Au-nanoprobe concentration to be used. As such, data from SNP detection that will be later presented and discussed in this chapter, were performed with a concentration of Au-nanoprobe of 2.5 nM, at pH between 7 and 8 and using $MgCl_2$ for salt-induced aggregation.

Conclusions of the previous chapter indicate that FTO SNP (dbSNP rs#: 9939609) is strongly correlated to high risk obesity in the Portuguese population. Hence, synthesis and characterization of Au-nanoprobes for detection and discrimination between the homo- or heterozygote condition with high degrees of specificity and sensitivity of this SNP is considered mandatory. Nonetheless, Au-nanoprobes were also synthesized for the other two SNP in study - PPARG (dbSNP rs#: 1801282) and APOA5 (dbSNP rs#: 662799). In order to facilitate the evaluation and discussion of the results, data will be presented as whole in the first section and, in the second section, particular emphasizes will be given to the Au-nanoprobes synthesized for the detection and discrimination of the SNP present in FTO *locus*.

4.2 Results and Discussion

4.2.1 Optimization and characterization

4.2.1.2 Gold nanoparticles physical characterization

Characterization of the synthesized citrate-capped AuNP was assessed by transmission electron microscopy (TEM) imaging, dynamic light scattering measurements (DLS), zeta-potential (ζ-potential) and UV-Vis spectrum. The citrate-capped AuNPs presented average size of 14.6±1.7 nm (TEM measurements), hydrodynamic diameter of 15.8±0.3 nm with polydispersity index of 0.156 (DLS measurements), ζ-potential of -32.1±2.4 mV and a characteristic surface plasmon resonant peak at 518 nm visible in the UV-Vis spectrum (Figure 4.3 – A, C and B, respectively).

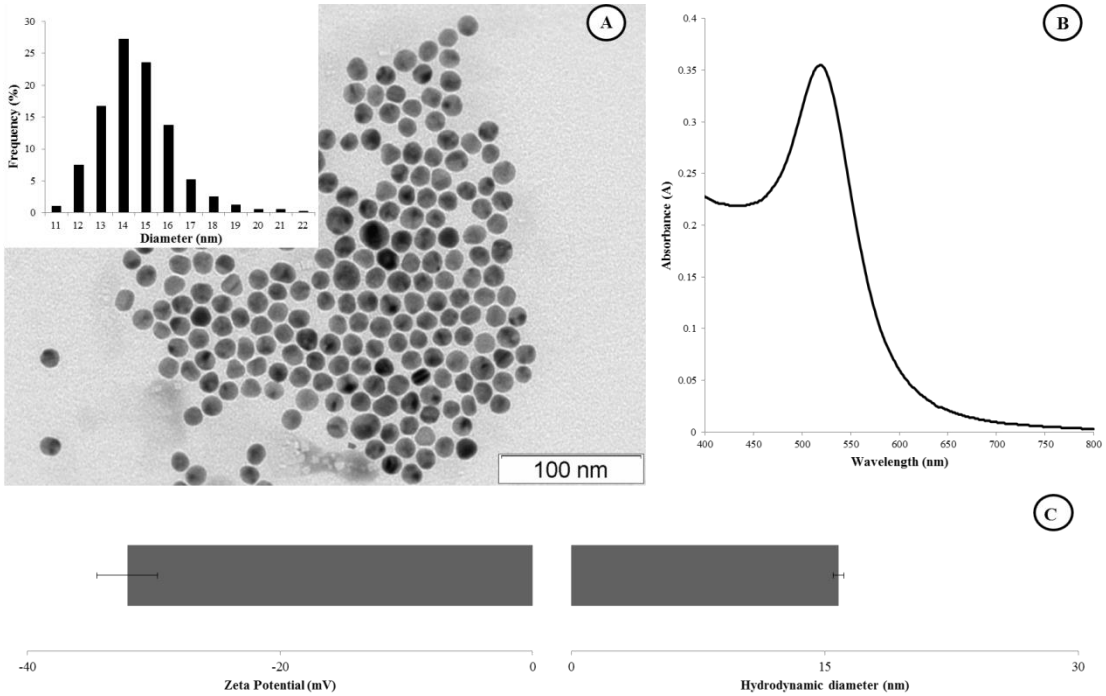

Figure 4.3 – Characterization of the synthesized gold nanoparticles. A) Transmission electron microscopy (TEM) imaging and inset size histogram frequency from ≈ 400 AuNPs counting; **B)** UV-Vis spectrum of spherical AuNPs, with a characteristic maximum absorption peak, **C)** Dynamic light scattering (DLS) measurements to define the hydrodynamic diameter of the AuNPs and zeta-potential (ζ-potential) as AuNP surface charge indicator. For DLS it was performed 3 runs per sample with 2000 measurements each and for ζ-potential a total of 5 runs per sample with 250 measurements.

Collected data allowed the determination of size, distribution, morphology and surface charge of the citrate-capped AuNPs. This information is considered pivotal to standardize the characterization of nanomaterials intended to be used in therapeutics or diagnostics by Nanotechnology Characterization Laboratory, a formal scientific interaction of three US Federal agencies: National Cancer Institute (NCI), FDA and National Institute of Standards and Technology (NIST) of the Department of Commerce.

TEM is considered an essential characterization tool for directly imaging nanomaterials and attains quantitative measures of physical size and morphology and but considers the inorganic core of the nanoparticle for size determination. On the other hand, DLS allows the determination of the overall mean size of the particle, taking in consideration not only the e inorganic core but also the organic coating layer. However, by itself, DLS does not characterize the nanoparticle morphologically. Despite the small differences found in the size of citrate-capped AuNPs given by TEM imaging and DLS measures (Figure 4.3B and C, respectively), those can be explained by the sensitivity of each technique. While TEM imaging is sensitive to the size of primary particles, DLS is easily influenced by the presence of small populations of large particles or groups of smaller particles, which can be translated into a greater overall nanoparticle size (Hinterwirth et al. 2013). The determination of citrate-capped AuNPs size can also be achieved

by the UV-Vis spectrum. Haiss and co-workers demonstrated this possibility with theoretical models that can be translated by calculating the ratio of the absorbance of AuNPs at the surface plasma resonance peak (A_{spr}) to the absorbance at 450 nm (A_{450}). In the referred publication, 14 nm AuNPs should present a (A_{sper}/A_{450}) ratio of 1.61 (Haiss et al. 2007). Prepared citrate-capped AuNPs for this work have a (A_{sper}/A_{450}) ratio of 1.606. Hence, it is possible to infer the excellent agreement between the size average given by TEM imaging and the UV-Vis spectrum. Moreover, all the physical characterization of the citrate-capped AuNPs seems to be in agreement.

4.2.1.3 Au-nanoprobe physical characterization

Citrated-capped AuNP were functionalized with thiol-modified oligonucleotides after physical characterization (See sub-section 2.2.2.2.1 and 2.2.2.2.2 from Chapter 2), aiming at their utilization as Au-nanoprobes for detection of nucleic acids. Loading modified oligonucleotides onto the negatively charged surface of the AuNPs involves several steps: i) gradual increase in salt concentration in solution (salt aging) to minimize secondary interactions between free ssDNA bases (from modified oligonucleotide) with the negative surface of the AuNP (Hurst et al. 2006); ii) employment of surfactant agents (i.e. SDS) prior to salt aging process to decrease AuNPs propensity to aggregate, particularly at high salt concentrations, while reducing non-specific binding and improving reproducibility while maximizing loading of modified oligonucleotide onto AuNP surface (Stoeva et al. 2006) and iii) brief ultrasound pulse on Au-nanoprobes during salt aging, to promote higher loading rates of thiol-modified oligonucleotide on the surface of the AuNP by disrupting non-specific interactions between ssDNA bases and gold-nanoparticles surface, leading to increased DNA loading (Hurst et al. 2006). Synthesis of all Au-nanoprobes used was carried out in agreement with these three fundamental steps, considered to be crucial for an efficient Au-nanoprobe synthesis.

During the development of the non-cross-linking method by Baptista and co-workers, it has been shown that the detection of nucleic acid and complete SNP characterization is dependent on the length and density of thiol-modified oligonucleotide functionalized onto the surface of the citrate-capped AuNP (Veigas 2009). On this basis, different combination parameters were used in the functionalization step in order to attain the finest single base resolution, at room temperature. Two distinct oligonucleotides length (17 and 20 bp) were used and three distinct AuNP:Oligo ratio (1:160, 1:180 and 1:200) were tested for each oligonucleotide length. A total of 43 Au-nanoprobes were synthesized for the discrimination of each SNP in the agenda of this thesis. All were characterized by UV-Vis, DLS and ζ-potential measurements to assess functionalization effectiveness. A summary, represented by mean values of each analytical technique is showed in Figure 4.4.

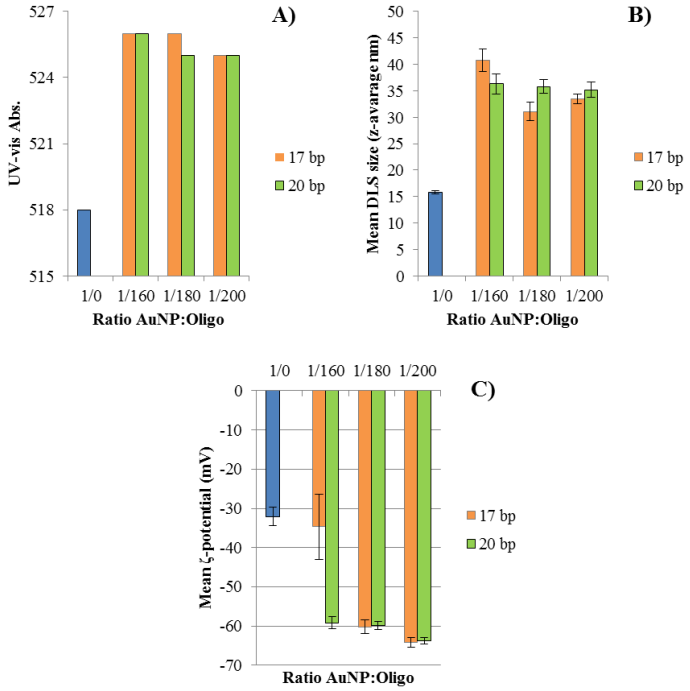

Figure 4.4 – Au-nanoprobes analytical characterization by DLS, ζ-potential and UV-Vis peak. Mean values for UV-Vis peak **(A)**, DLS **(B)** and ζ-potential measures **(C)**, for the Au-nanoprobes functionalized with modified oligonucleotide of 17 and 20 bp long and with ratios AuNP:Oligo varying between 1:160, 1:180 and 1:200.

The physical characterization by DLS, ζ-potential and UV-Vis spectrum allows determining that all Au-nanoprobes were functionalized via thiol-modified oligonucleotide with slight differences: i) Au-nanoprobes presented higher hydrodynamic diameter than citrate-capped AuNPs, indicating that citrate has been substituted by the thiol-modified oligonucleotides. Moreover, it has been observed that Au-nanoprobes functionalized with shorter thiol-modified oligonucleotides (17 bp) presented lower mean hydrodynamic diameter than those with longer (20 bp) for the same ratio AuNP:Oligo. The approximation given by the work of Wilkins and co-workers (Wilkins et al. 1953), considering that each base pair in the DNA double helix extends 3.4 Å (0.34 nm) units approximately, it is possible to roughly infer that, if completely stretched, the Au-nanoprobes here presented confirm this premise (Figure 4.5); ii) the Au-nanoprobes presented higher negative surface potential than citrate-capped AuNP, observation also seen in Au-nanoprobes functionalized with higher density of modified oligonucleotides (1:200) and iii) a characteristic red-shift from 518 to 525/526 nm that clearly indicates an increase in the AuNP diameter, due to bounding of the thiol-modified oligonucleotide to the AuNP surface. Still considering these observations, it is also possible to remark that Au-nanoprobes prepared with low density of short thiol-modified oligonucleotide (17 bp at 1:160) were characterized with an unexpected higher mean hydrodynamic size when compared to Au-nanoprobes with the same oligonucleotide length but higher density (1:180 and 1:200). Moreover, those Au-nanoprobes

presented approximately the same negative charge of the citrate-capped AuNP, indicating a possible phenomenon of interparticle distance decrease and aggregation. The length of thiol-modified oligonucleotides bound to the AuNPs surface has been associated with dramatic Au-nanoprobes stability from 5 to 15 bp and slight increase between 15-20 bp (Storhoff et al. 2002). Nonetheless, bias during salt-aging method cannot be excluded. For instance, insufficient or absence of ultrasound time, combined with lower density of thiol-modified oligonucleotide, is highly correlated with reduced Au-nanoprobe stability (Hurst et al. 2006) and is more prone to non-specific adsorption that can lead to differences in functionalization (Doria 2010b).

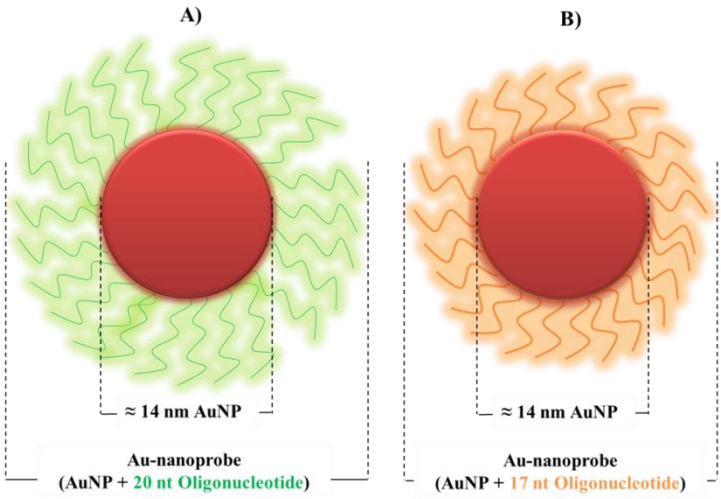

Figure 4.5 – Schematic representation of differences in Au-nanoprobes hydrodynamic radius due oligonucleotide size. The hydrodynamic radius measured by DLS can be higher for Au-nanoprobes functionalized with longer oligonucleotides. **A)** A spherical AuNP with ≈ 14 nm functionalized with a 20 nt thiol-modified oligonucleotide and **B)** A spherical AuNP with ≈ 14 nm functionalized with a 17 nt thiol-modified oligonucleotide.

4.2.1.4 Au-nanoprobes stability assays

The Au-nanoprobes stability assays against salt-induced aggregation were performed to determine the minimal electrolyte concentration needed to induce Au-nanoprobes aggregation and consequent red-shift of the wavelength peak (Figure 4.6). To determine this characteristic, UV-Vis spectrum (400-700 nm) was registered for different $MgCl_2$ concentrations. $MgCl_2$ was used instead of a monovalent salt (i.e. NaCl) given that large volume of NaCl would be needed to determine the minimal electrolyte concentration to induce Au-nanoprobe aggregation, fact incompatible with the assays final volume (30 µL) (Doria 2010b).

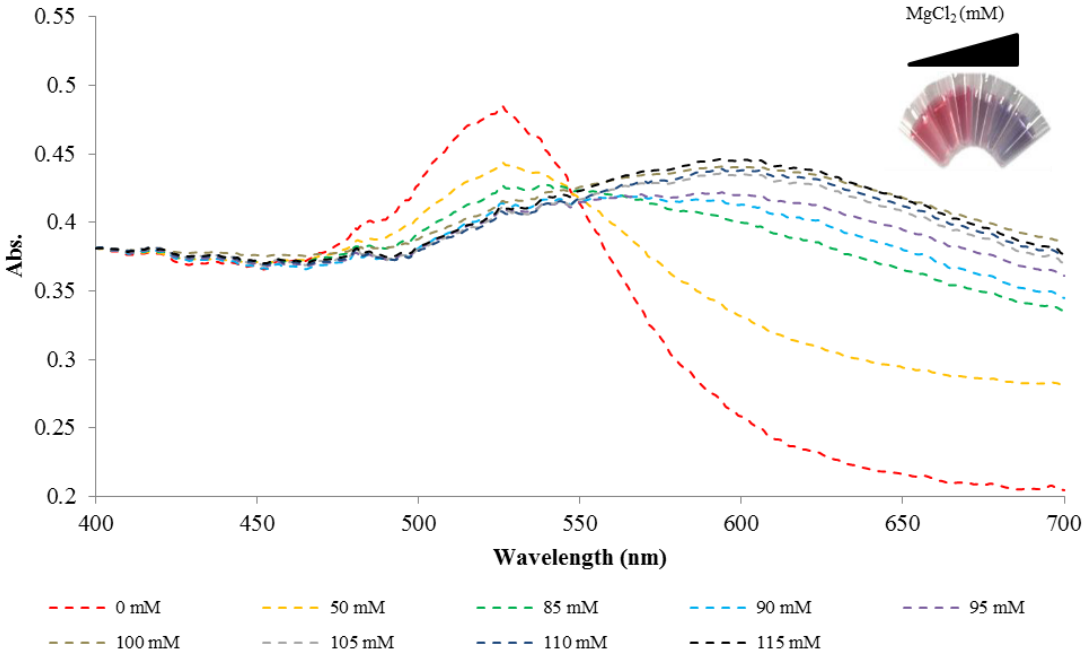

Figure 4.6 – Au-nanoprobes stability by increasing $MgCl_2$ concentration. UV-Vis spectrum registered 30 minutes after salt addition of Au-nanoprobe in phosphate buffer 10mM pH 8, at different $MgCl_2$ concentrations. Inset: Colorimetric changes visible at naked eye by increasing $MgCl_2$ concentration.

Au-nanoprobes presented some stability variations, comprised between 25 and 120 mM of $MgCl_2$. Most of them (n=24), almost 50%, were stable at $MgCl_2$ concentrations between 40-55 mM (Figure 4.7A). Significant differences were observed in stability between the thiol-modified oligonucleotide with 17 bp and 1:160 densities coverage and the ones functionalized with 20 bp thiol-modified oligonucleotide with the same ratio AuNP:oligo (Figure 4.7B). The low stability values of those Au-nanoprobes (17 bp, ratio 1:160) can corroborate the higher mean hydrodynamic size and lower ζ-potential measures found for these Au-nanoprobes, exposed in Figure 4.4 B and C, respectively, corresponding to possible aggregation phenomena due to low thiol-modified oligonucleotide functionalization efficiency. The effectiveness functionalization and higher densities coverage of thiol-modified oligonucleotides are strictly associated with higher degree of Au-nanoprobe stabilization (Hurst et al. 2006, Veigas 2009, Doria 2010b).

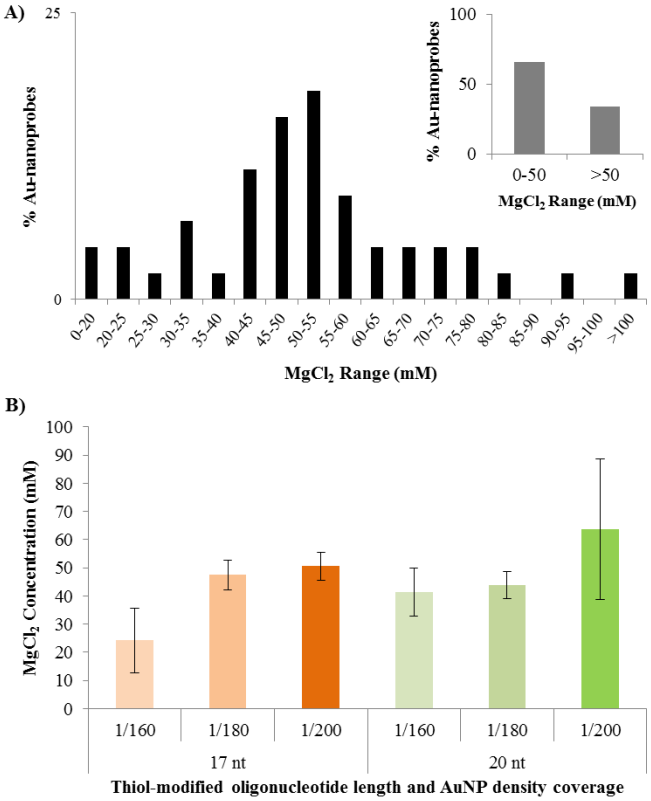

Figure 4.7 – Determination of stability range against salt-induced ($MgCl_2$) aggregation for all Au-nanoprobes synthesized. A) Percentage of Au-nanoprobes that fully aggregate and $MgCl_2$ concentration range which occur. Inset: Percentage of Au-nanoprobes stable at $MgCl_2$ concentrations up to 50mM or higher. **B)** Determination of $MgCl_2$ concentration as function of the thiol-modified oligonucleotide length (17 or 20 bp) and ratio AuNP:Oligo (1:160, 1:180 and 1:200). Error bars represent the standard deviation.

4.2.2 SNP/mutation detection: proof-of-concept for FTO Au-nanoprobes

4.2.2.1 Stability assays

Au-nanoprobes (n=22) overlying the SNP FTO (dsSNP rs#: 9939609), obesity-risk associated, were designed in order to detect and discriminate between homozygote (A/A and T/T) and heterozygote (A/T) conditions via the non-cross-linking method. Au-nanoprobes that showed high viability for this purpose were the FTOwt20 and FTOmut20, responsible for the detection of the wild type allele (T) and the mutated allele (A), respectively. Both were prepared with a 20 bp thiol-modified oligonucleotide at a theoretical ratio AuNP:Oligo of 1:200. The performed stability assays determined that full aggregation was achieved at 95 mM for FTOwt20 Au-nanoprobe and 35 mM of $MgCl_2$ for FTOmut20 Au-nanoprobe (Figure 4.8).

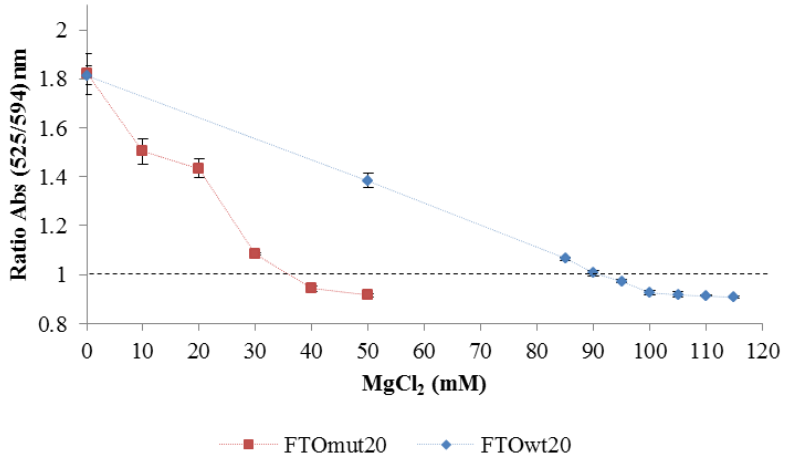

Figure 4.8 – FTO Au-nanoprobes salt-induced aggregation profiles. Determination of FTO Au-nanoprobes stability profile by $MgCl_2$ concentration increase. All data was collected 30 minutes after salt addition. In blue (---♦---) FTOwt20 ionic strength stability profile and in red (---■---) FTOmut20 ionic strength stability profile.

The difference observed between both Au-nanoprobes may be explained due the 3'-end of the FTOwt20 Au-nanoprobe (TTTT-3') that presents a higher thymine content than the FTOmut20 (TTTA-3'). It has already been reported that weaker electrostatic interaction of thymine with the AuNP surface can result in higher surface coverage and consequently enhanced stability (Storhoff et al. 2002, Brown et al. 2008).

4.2.2.1 Au-nanoprobes detection – Synthetic oligonucleotide

In order to assess the promptness of each Au-nanoprobes towards specific hybridization with their fully-complementary targets, a hybridization assay was performed, using ssDNA oligonucleotide (40 bp) as target (Figure 4.9).

For both Au-nanoprobes, in the absence of any target (blank) or in the presence of non-complementary (ssDNA@unrelated) target, Au-nanoprobes aggregate, fact that is associated not only with distinct and expected colorimetric change from red to blue but also a significant quantitative difference in Abs_{525}/Abs_{594} ratio (p-value<0.01). Although, no discrimination was attained between fully complementary and mismatched ssDNA targets for both Au-nanoprobes, it is possible to observe distinct patterns of aggregation for both Au-nanoprobes between fully complementary, single base mismatch and non-complementary targets (p-value<0.01). Clearly, the FTOwt20 Au-nanoprobe, in the presence of fully complementary target (ssDNA@WT) presents a significant higher ratio (p-value<0.05) of absorbance when in the presence of a single base mismatch target (ssDNA@mut). The same observation is attained for the FTOmut20 Au-nanoprobe, where the fully complementary target (ssDNA@mut) presents slightly higher ratios of absorbance when compared with the other target. For both Au-nanoprobes it was expected that

only in the presence of a fully complementary target no red-shift of the SPR red-shift would occur. However, hybridization events seem to have occurred for both Au-nanoprobes in presence of single base mismatched target. It is known that the electrostatic interaction between the negative charges of the exposed phosphate group of nucleic acid backbone ssDNA bases with the negative surface of the AuNP, paly a protective role against salt induced aggregation by non-specifically binding between ssDNA and colloidal gold particles (Storhoff et al. 2002) and flat gold surfaces (Herne et al. 1997). This might explain the smaller effect of aggregation between ssDNA@WT and ssDNA@MUT targets, for both Au-nanoprobes, but not between ssDNA@WT or ssDNA@MUT and ssDNA@Unrelated for both Au-nanoprobes, where increasing ionic strength induces full aggregation in ssDNA@Unrelated target (Figure 4.9). Nevertheless, the viability of FTO Au-nanoprobes only to hybridize with ssDNA oligonucleotide FTO-related was achieved.

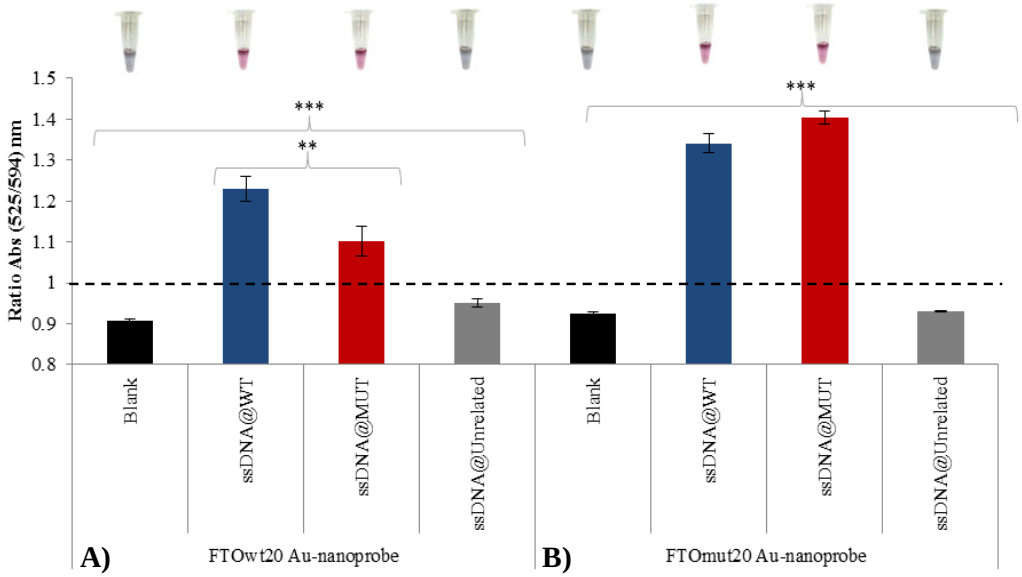

Figure 4.9 – Hybridization assay test performed with ssDNA oligonucleotides for FTOwt20 and FTOmut20 Au-nanoprobes. Au-nanoprobes aggregation was measured by ratio of aggregation (ratio of SPR intensity at 525 and 594 nm) for the assay tests - 2.5 nM Au-nanoprobe, 10 mM phosphate buffer (pH 8), ssDNA targets at a final concentration of 0.3 pmol.μL^{-1}. All spectrophotometric data was collected 30 minutes after salt addition and error bars represent the standard deviation of three independent assays. The horizontal line represents the threshold of 1 considered for discrimination between positive (rAbs≥1) and negative (rAbs<1) result. A representative colorimetric results is showed upon each result bar – red, positive result; blue/purple, negative result. **A)** FTOwt20 Au-nanoprobe hybridization viability. Blank, represents the Au-nanoprobe alone with no target; ssDNA@WT, fully complementary target to the Au-nanoprobe; ssDNA@MUT, single base mismatch target in the 3'end position of the Au-nanoprobe and ssDNA@unrelated, a fully non-complementary target to the Au-nanoprobe. Mean values significantly different between groups with a p-value<0.01 (***) and p-value<0.05 (**) **B)** FTOmut20 Au-nanoprobe hybridization viability. Blank, represents the Au-nanoprobe alone with no target; ssDNA@WT, single base mismatch target in the 3'end position of the Au-nanoprobe; ssDNA@MUT, a fully complementary target to the Au-nanoprobe and ssDNA@unrelated, a fully non-complementary target to the Au-nanoprobe. Mean values are significantly different between groups with a p-value<0.01 (***).

pH effect

Au-nanoprobes are stable between pH 4 and 12 (Sun et al. 2008), being very stable against salt induced aggregation between pH 7.5 and 8 (Doria 2010b). Since the range of pH usually used for DNA recognition techniques is comprised between 6.5 and 8 it was investigated the hybridization efficiency for Au-nanoprobe/ssDNA in this range. The FTOwt20 Au-nanoprobe was washed and re-dispersed in 10 mM phosphate buffer at pH 6.6, 7.1, 7.5 and 8 and differences of recognition event between fully complementary, single-base mismatch and unrelated target and FTOwt20 Au-nanoprobe were assessed. Figure 4.10 shows that, despite higher ratio values for lower pH (6.6 and 7.1), hybridization specificity seems to be low (high standard deviation). Other authors have also showed that (Doria 2010b), for higher pH values (8) the specificity of the system tends to be higher, since fully complementary target (ssDNA@WT) that hybridizes to the Au-nanoprobe (FTOwt20) seems to be higher than a single-base mismatch target (ssDNA@MUT). These findings are in agreement with the work of Zhang and co-workers (Zhang et al. 2012) that have shown that in more acidic environments, electrostatic forces may lead to tensile surface stress, implying the reduced accessibility of the bound ssDNA probe to inefficient and unspecific hybridization. In contrast at higher pH steric interaction between neighboring ssDNA strands is decreased by higher electrostatic repulsive forces allowing a more specific detection.

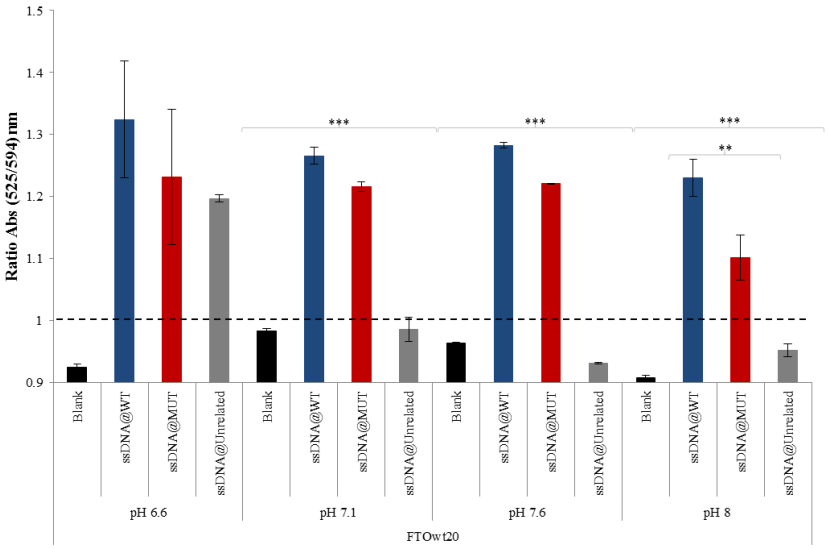

Figure 4.10 – pH effect on FTOwt20 Au-nanoprobe hybridization event. Au-nanoprobes aggregation was measured by ratio of aggregation (ratio of SPR intensity at 525 and 594 nm) for the assay samples - 2.5 nM Au-nanoprobe, 10 mM phosphate buffer (pH 8), ssDNA targets at a final concentration of 0.3 pmol.µL^{-1}. All spectrophotometric data was collected 30 minutes after salt addition and error bars represent the standard deviation of three independent assays. The horizontal line represents the threshold of 1 considered for discrimination between positive (rAbs≥1) and negative (rAbs<1) result. A representative colorimetric results is showed upon each result bar – red, positive result; blue/purple, negative result. FTOwt20 Au-nanoprobe at different pH values where Blank, represents the Au-nanoprobe alone with no target; ssDNA@WT, fully complementary target to the Au-nanoprobe; ssDNA@MUT, single base mismatch target in the 3'end position of the Au-nanoprobe and ssDNA@unrelated, a fully non-complementary target to the Au-nanoprobe. Mean values are significantly different between groups with a p-value<0.01 (***) and p-value<0.05 (**).

4.2.2.2 Au-nanoprobes detection – PCR products samples

After the achievement of the first proof-of-concept for the detection of ssDNA FTO oligonucleotides, the system was calibrated for the detection of biological samples using the parameters previously determined (time of read-out and salt concentrations). To do it so, PCR-generated targets of 445 bp and 225 bp fully complementary and 495 bp and 250 bp non-complementary to the Au-nanoprobes from biological samples were tested to determine if the length of the PCR products could affect the hybridization event. All samples were previously characterized by direct sequencing.

Colorimetric and ratio of absorbance detection and discrimination, between FTO generated PCR products and unrelated target or absence of it, was clearly obtained for both Au-nanoprobes (Figure 4.11). Nevertheless, the discrimination between a fully complementary, a single base mismatch or a heterozygous sample was not attained for both Au-nanoprobes. Nevertheless, significant differences were attained for both Au-nanoprobes for ratio of absorbance between a fully complementary and a single base mismatch target, no colorimetric red-shift was observed (Figure 4.11).

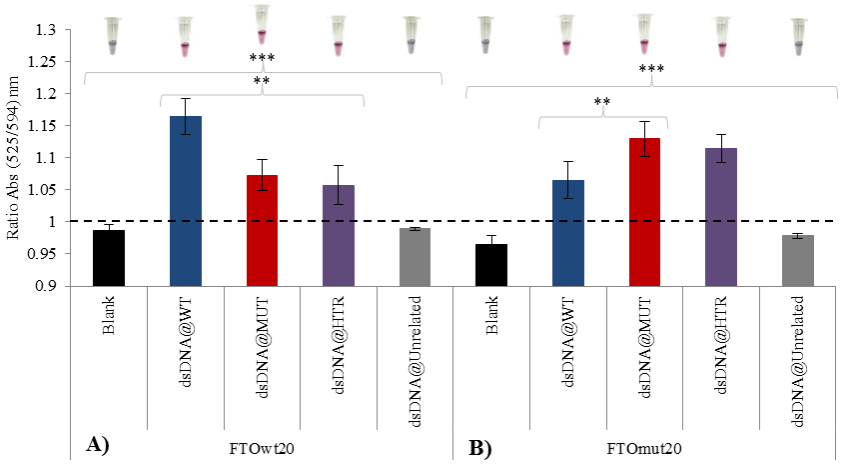

Figure 4.11 – Hybridization assay results with PCR-generated targets for FTOwt20 and FTOmut20 Au-nanoprobes. Au-nanoprobes aggregation was measured by ratio of aggregation (ratio of SPR intensity at 525 and 594 nm) for the assay mixtures - 2.5 nM Au-nanoprobe, 10 mM phosphate buffer (pH 8), purified dsDNA targets (PCR products) at a final concentration of 30 ng.µL^{-1}. All spectrophotometric data was collected 30 minutes after salt addition and error bars represent the standard deviation of three independent assays. The horizontal line represents the threshold of 1 considered for discrimination between positive (rAbs≥1) and negative (rAbs<1) result. A representative colorimetric results is showed upon each result bar – red, positive result; blue/purple, negative result. FTO PCR-generated products (dsDNA@WT, dsDNA@MUT and dsDNA@HTR) were 445 bp long, while unrelated target (dsDNA@unrelated) was 495 bp long. **A)** FTOwt20 Au-nanoprobe hybridization viability. Blank, represents the Au-nanoprobe alone with no target; dsDNA@WT, fully complementary target to the Au-nanoprobe; dsDNA@MUT, single base mismatch target in the 3'end position of the Au-nanoprobe; dsDNA@HTR, heterozygous target and dsDNA@unrelated, fully non-complementary target to the Au-nanoprobe. Mean values are significantly different between groups with a p-value<0.01 (***) and p-value<0.05 (**) **B)** FTOmut20 Au-nanoprobe hybridization viability. Blank, represents the Au-nanoprobe alone with no target; dsDNA@WT, single base mismatch target in the 3'end position of the Au-nanoprobe; dsDNA@MUT, a fully complementary target to the Au-nanoprobe; dsDNA@HTR, heterozygous target and dsDNA@unrelated, a fully non-complementary target to the Au-nanoprobe. Mean values are significantly different between groups with a p-value<0.01 (***) and p-value<0.05 (**).

The "buffer" role played by ssDNA for increasing ionic strength, which is associated with increased stabilization of Au-nanoprobes is not so straightforward for dsDNA, since there are no exposed bases free to interact with the AuNP upon increasing ionic strength (Sandström et al. 2003). As reported by other authors (Doria et al. 2007, Veigas et al. 2010, Pedrosa et al. 2013), both Au-nanoprobes fully aggregate at high ionic strength in presence of dsDNA@Unrelated and that the expected stability for the fully complementary targets with their respective Au-nanoprobes is attained. This can be explained by the fact that the full length of the Au-nanoprobes hybridizes with target. Nevertheless, Sandstrom and co-workers (Sandström et al. 2003) demonstrated that dsDNA and gold nanoparticles can interact, sequence independent, by a dipole induction in the highly polarizable AuNPs from the negative charges, preventing Au-nanoprobes aggregation at high ionic strength. Conversely, the destabilization of the complex Au-nanoprobe/ single-base mismatch target did not occur for both Au-nanoprobes for the 445 bp PCR products.

In parallel, the same hybridization strategy was used for 225 bp FTO PCR-generated targets. In this case, the non-cross-linking strategy for the discrimination between the three possible genotypes, *wild-type* (TT), heterozygous (AT) and mutated (AA) was achieved as is reported in Figure 4.12.

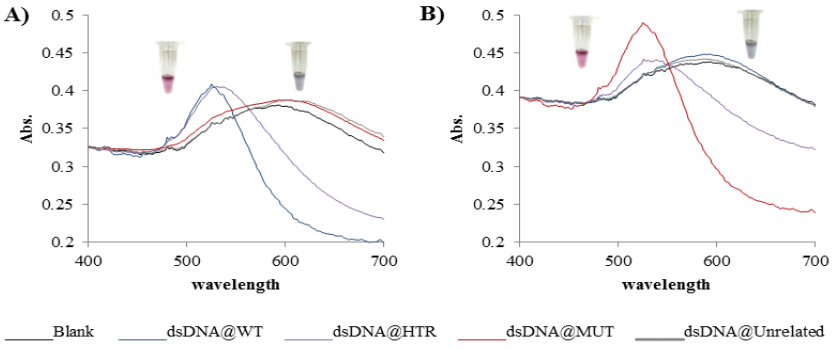

Figure 4.12 – UV-Vis spectroscopy data from detection and discrimination of FTO (dbSNP rs#: 9939609) mediated by Au-nanoprobes. Au-nanoprobes aggregation was measured for the assay mixtures - 2.5 nM Au-nanoprobe, 10 mM phosphate buffer (pH 8), purified dsDNA targets (PCR products) at a final concentration of 30 ng.µL^{-1}. All spectrophotometric data was collected 30 minutes after salt addition. **A)** FTOwt20 Au-nanoprobe in **B)** FTOmut20 Au-nanoprobe**.**

Both Au-nanoprobes when submitted to high ionic strength salt induced could detect FTO related products (dsDNA@WT, dsDNA@MUT and dsDNA@HTR) and discriminate them from the unrelated targets (dsDNA@unrelated) with a clear and distinct SPR red-shift. Furthermore, like it was previously observed by the group, (Baptista et al. 2006, Doria et al. 2007, Veigas et al. 2010) a set of two Au-nanoprobes could give colorimetric and visible spectra discrimination information between *wild-type* (WT) and mutated (MUT) samples. The discrimination between

homozygous (wild-type or mutated) and heterozygous samples was also attained, since bot Au-nanoprobes retained their red color, only with slight alteration, after salt addition in the presence of a heterozygous samples (Figure 4.13).

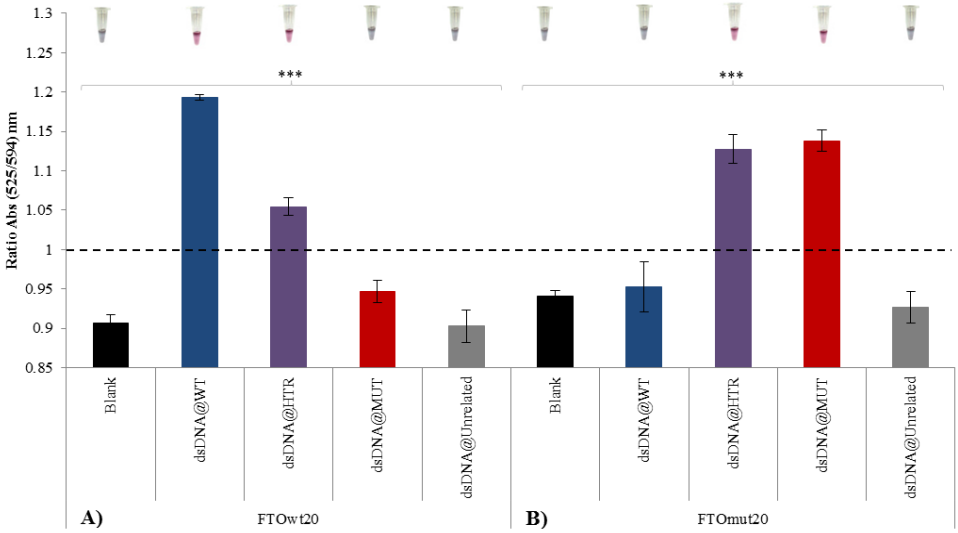

Figure 4.13 – FTO (dbSNP rs#: 9939609) detection mediated by the non-cross-linking method. Au-nanoprobes aggregation as measured by ratio of aggregation (ratio of SPR intensity at 525 and 594 nm) for the assay mixtures - 2.5 nM Au-nanoprobe, 10 mM phosphate buffer (pH 8), purified dsDNA targets (PCR products) at a final concentration of 30 ng.µL^{-1}. All spectrophotometric data was collected 30 minutes after salt addition and error bars represent the standard deviation of three independent assays. The horizontal line represents the threshold of 1 considered for discrimination between positive (rAbs≥1) and negative (rAbs<1) result. A representative colorimetric results is showed upon each result bar – red, positive result; blue/purple, negative result. FTO PCR-generated products (dsDNA@WT, dsDNA@MUT and dsDNA@HTR) were 225 bp long, while unrelated target (dsDNA@unrelated) was 195 bp long. **A)** Blank, represents the Au-nanoprobe alone with no target; dsDNA@WT, fully complementary target to the Au-nanoprobe; dsDNA@HTR, heterozygous target; dsDNA@MUT, single base mismatch target in the 3'end position of the Au-nanoprobe and dsDNA@unrelated, fully non-complementary target to the Au-nanoprobe. Mean values are significantly different between groups with a p-value<0.01 (***) **B)** Blank, represents the Au-nanoprobe alone with no target; dsDNA@WT, single base mismatch target in the 3'end position of the Au-nanoprobe; dsDNA@HTR, heterozygous target; dsDNA@MUT, a fully complementary target to the Au-nanoprobe and dsDNA@unrelated, a fully non-complementary target to the Au-nanoprobe. Mean values are significantly different between groups with a p-value<0.01 (***).

During the determination of the limit of detection (LOD) of the system for the FTOwt20 Au-nanoprobe it was observed that, for this particular Au-nanoprobe, the ratio of absorbance and the colorimetric variation presented a characteristic pattern that distinguishes the three possible genotypes in the FTO *locus*. As it is possible to see in Figure 4.14 in the presence of dsDNA@WT sample (TT) the Au-nanoprobe aggregation profile present ratios higher than 1.1 (1.203±0.012) (---♦---), for dsDNA@MUT samples (AA) sample lower than 1 (0.9539±0.0096) (---■---) and dsDNA@HTR samples (AT) present values between 1 and 1.1 (1.0561±0.0343) (---▲---).

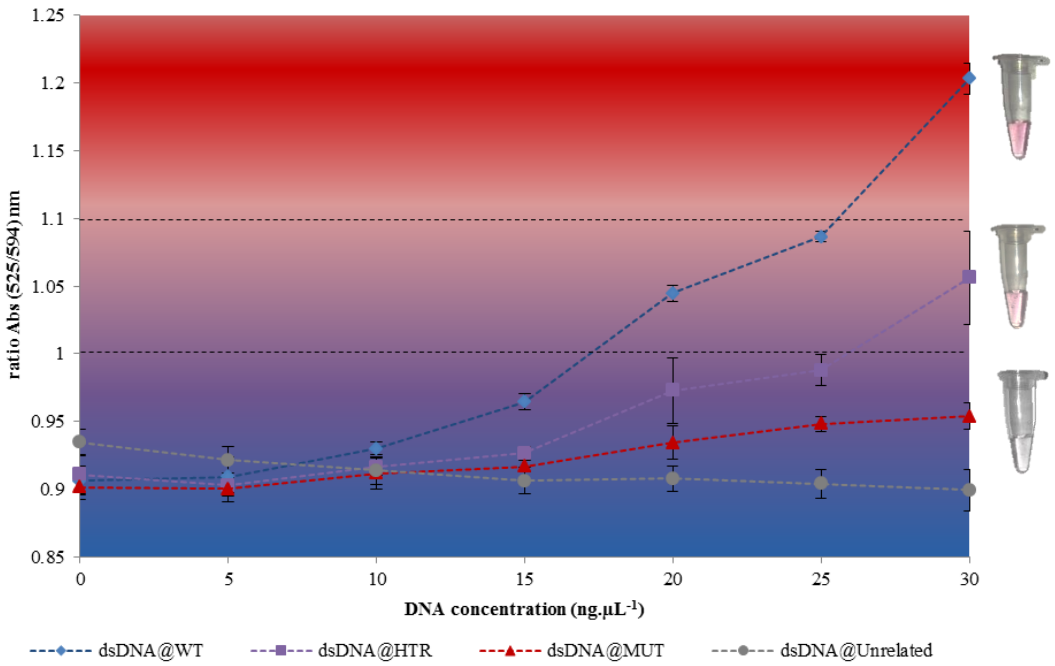

Figure 4.14 – Limit of detection (LOD) profile for FTOwt20 Au-nanoprobe. Ratio of absorbance for FTOwt20 Au-nanoprobe conducted with 2.5 nM of Au-nanoprobe on phosphate buffer 10 mM (pH8) and with purified PCR products of 225 bp of FTO (dbSNP rs#: 9939609). In blue (---♦---), gradient of amplicon fully complementary to Au-nanoprobe (dsDNA@WT); in red (---▲---), gradient of single-base mismatch amplicon (dsDNA@MUT); in purple (---■---), gradient of amplicon heterozygous (dsDNA@HTR) and in grey (---●---) gradient of non-complementary amplicon (dsDNA@unrelated) to Au-nanoprobe. Aggregation induction was carried out by increasing the ionic strength up to 95 mM with the addition of $MgCl_2$. All spectra were taken 30min after salt addition. Dots represent the average of three independent measurements and the error bars indicate standard deviation.

The LOD of the system was determined to be 20 ng.µL^{-1}, for discriminating between a wild type (dsDNA@WT) and the other 2 two possible genotypes (dsDNA@MUT and dsDNA@HTR) of the FTO gene. However, 30 ng.µL^{-1} was required to discriminate between the three genotypes. This is in accordance with other publications using the non-cross-linking method (Baptista et al. 2005, Doria et al. 2012, Pedrosa et al. 2013).

4.2.3 Non-cross-linking method validation with biological sample for the obesity-related SNP in the FTO gene

From the previous results attained for the FTOwt20 and FTOmut20 Au-nanoprobes a validation assay with different biological sample was performed. The goal was to assay the ability of the capability of Au-nanoprobes for genotyping SNP, as well as to test the reproducibility, sensitivity and specificity of the test. The samples were blind tested and only after Au-nanoprobe genotyping the data was compared with Sanger sequencing genotyping method. The results are shown in Figure 4.15.

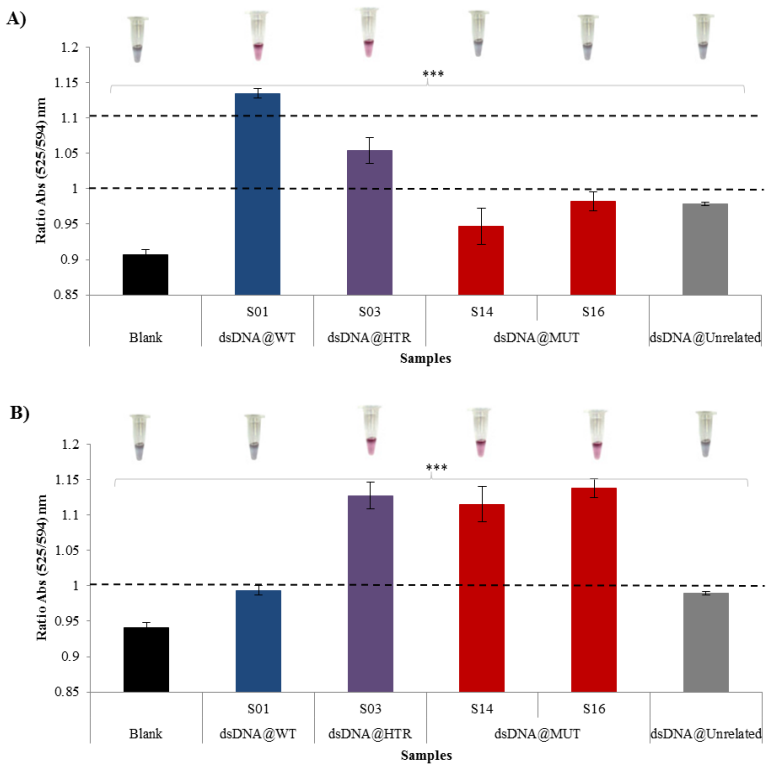

Figure 4.15 – Non-cross-linking SNP genotyping validation mediated by a set of two Au-nanoprobes. Au-nanoprobes aggregation as measured by ratio of aggregation (ratio of SPR intensity at 525 and 594 nm) for the assay mixtures - 2.5 nM Au-nanoprobe, 10 mM phosphate buffer (pH 8), purified dsDNA targets (PCR products) at a final concentration of 30 ng.μL^{-1}. All spectrophotometric data was collected 30 minutes after salt addition and error bars represent the standard deviation of three independent assays. The horizontal line represents the threshold of 1 considered for discrimination between positive (rAbs≥1) and negative (rAbs<1) result. A representative colorimetric results is showed upon each result bar – red, positive result; blue/purple, negative result. FTO PCR-generated products (dsDNA@WT, dsDNA@MUT and dsDNA@HTR) were 225 bp long, while unrelated target (dsDNA@unrelated) was 195 bp long. Mean values are significantly different between groups with a p-value<0.01 (***). In **A)** FTOwt20 Au-nanoprobe genotyping results and in **B)** FTOmut20 Au-nanoprobe genotyping results.

The presented results confirm that it was possible to corroborate the capability of both FTO Au-nanoprobes to detect and discriminate between FTO-related and unrelated targets and discriminate between their genotypes with a high degree of sensitivity and specificity by the non-cross-linking approach. The Au-nanoprobes in the presence of their respective full complementary target and after ionic strength increase remain unaltered by comparison with the blank solution. The presence of single-base mismatch target does not prevent the aggregation event and the solution changed from red to blue, as it occurs with unrelated targets. In the presence of a heterozygous sample, as full complementary target, aggregation is prevented and the shift red-blue does not occur, which is crucial, since identification of this status is only possible with positive results (rAbs>1) in both Au-nanoprobes. Once again, a clear and distinct pattern of aggregation was observed to the FTOwt20 Au-nanoprobe (Figure 4.16A). In the presence of a single-base mismatch (dsDNA@MUT) or an unrelated target (dsDNA@Unrelated) the rAbs(525/594)<1, while for a heterozygous stayed 1.1<rAbs(525/594)≥1 and finally in the

presence of a fully complementary the rAbs(525/594)≥1.1. From this point-of-view it was hypothesized if a single Au-nanoprobe, instead of a set of two, could detect and discriminate the three possible genotypes. Thus, 20 samples were blind tested and Au-nanoprobe genotyping compared with Sanger sequencing genotyping method. The procedure and results are showed in Figure 4.16.

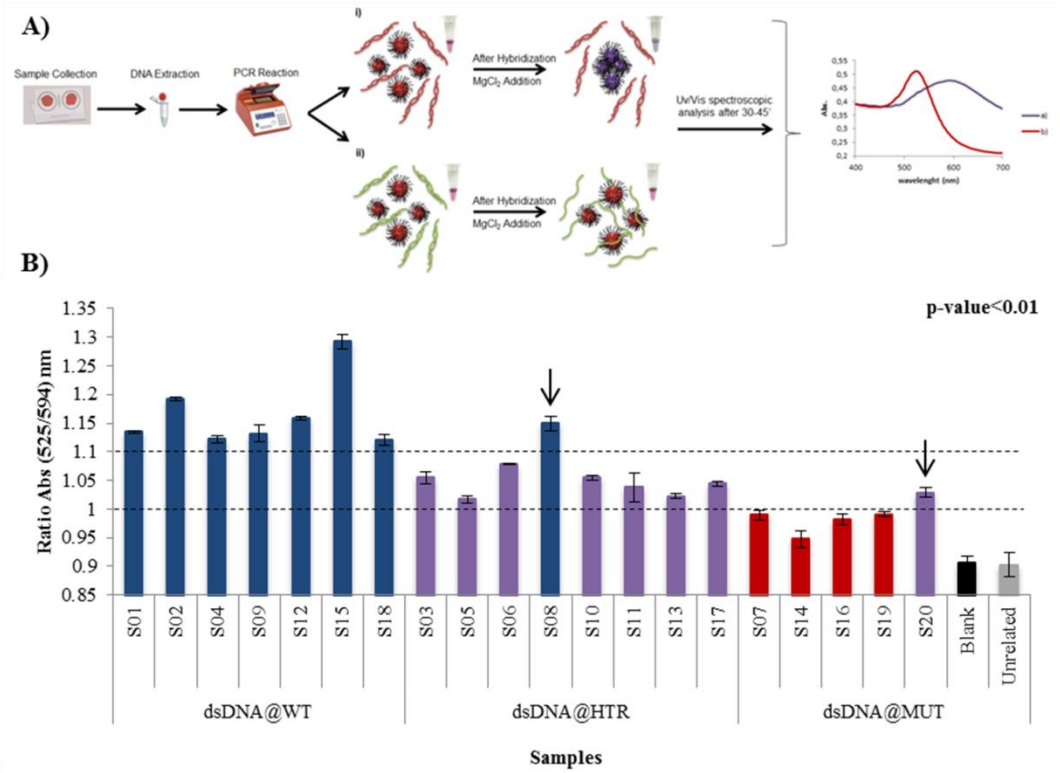

Figure 4.16 – Procedure and validation of FTOwt20 Au-nanoprobe genotyping method with biological samples. Au-nanoprobes aggregation as measured by ratio of aggregation (ratio of SPR intensity at 525 and 594 nm) for the assay mixtures - 2.5 nM Au-nanoprobe, 10 mM phosphate buffer (pH 8), purified dsDNA targets (PCR products) at a final concentration of 30 ng.μL^{-1}. All spectrophotometric data was collected 30 minutes after salt addition and error bars represent the standard deviation of three independent assays. In **A)** Blood sample was collected from finger prick using a lancet and stored in FTA™ Indicated Micro Card. DNA extraction was carried out for subsequently PCR reactions. After PCR reaction, Au-nanoprobe was mixed with PCR products and a hybridization step was carried out **i)** after salt addition in the presence of a single-base mismatch or unrelated PCR product a colorimetric change is visible from red to purple after a certain time, **ii)** after salt addition in the presence of a fully complementary PCR product no colorimetric change is visible and the solution remains red. This color observation can also be observed by UV/Vis spectroscopy in **a)** and **b)**, respectively. In **B)** The first horizontal line (dash line) represents the threshold of 1 considered for discrimination between positive (*wild-type* and heterozygous) and negative (mutated) samples. The second horizontal line (normal line) represents the threshold of 1.1 for the discrimination between a *wild-type* and a heterozygous sample. All the mean values were significantly different between groups with a p-value <0.01, except the ones represented by the black arrow on top of the respective bar.

All 20 samples were genotyped *via* single Au-nanoprobe approach and validated against the gold standard technique – Sanger Sequencing. This data allowed determining sensitivity and specificity (Figure 4.16B). The clear and distinct pattern observed earlier was confirmed. Samples were classified as: *wild-type* (T/T) for a rAbs (525/594 nm) higher or equal than 1.1; heterozygous

(A/T) for rAbs (525/594nm) between 1 and 1.1 and lower than 1 is classified as mutated (A/A) for this probe. Figure 4.16 B shows that from the total of 20 samples genotyped for FTO (dbSNP rs#: 9939609), 9 samples were considered *wild-type* (T/T), 7 samples were heterozygous (T/A) and 4 samples were mutated (A/A). Comparing the genotyping results from Sanger Sequencing and Au-nanoprobe genotyping we can conclude that 2 samples were misclassified by the Au-nanoprobe genotyping method: one as false positive and the other as a false negative (See Table 4.1). In the case of Sample S08, from the sequencing result present a heterozygous genotype (A/T) while the Au-nanoprobe genotyping method classified has a *wild-type* genotype (T/T). The same conclusion can be taken for the sample S20 that was classified as a mutated genotype (A/A) by sequencing while the Au-nanoprobe genotyping method classified this sample as a heterozygous genotype (A/T). From the data here presented it was possible to determine Au-nanoprobe sensitivity to be 87.50% and specificity 91.67%, against Sanger sequencing.

Table 4.1 - Comparison between genotyping methods for the SNP rs9939609 present in the FTO gene. (+/+) *wild type* genotype–T/T; (+/-) heterozygous genotype-A/T; (-/-) mutated genotype-A/A. [a] Samples that differ between genotyping methods marked in red.

Sample Code	Sanger Sequencing Genotyping	Au-nanoprobe Genotyping
S01	+ / +	+ / +
S02	+ / +	+ / +
S03	+ / -	+ / -
S04	+ / +	+ / +
S05	+ / -	+ / -
S06	+ / -	+ / -
S07	- / -	- / -
[a]S08	+ / -	+ / +
S09	+ / +	+ / +
S10	+ / -	+ / -
S11	+ / -	+ / -
S12	+ / +	+ / +
S13	+ / -	+ / -
S14	- / -	- / -
S15	+ / +	+ / +
S16	- / -	- / -
S17	+ / -	+ / -
S18	+ / +	+ / +
S19	- / -	- / -
[a]S20	- / -	+ / -

The one-way ANOVA and *post hoc* Tukey's test determined that significant differences between mean r(Abs) values to all samples of the same genotype groups with a confidence interval (CI) of 99%. The four exceptions were: sample S05 did not show significant differences for all the mutated samples. Sample S08 did not show significant differences for all *wild type* samples (except for samples S02 and S15). Likewise, sample S20 did not present significant differences for all heterozygous samples (except for sample S06). Nevertheless, significant differences

between mean r(Abs) values to all samples of the same genotype groups with a confidence interval (CI) of 95% were observed.

In conclusion, the non-cross-linking method, upon some calibration, was able to detect SNP in nucleic acid sequences from biological samples with high degree of sensitivity and specificity.

4.2.4 Extending the method to other the other targets scoped as obesity-related (PPARG dsSNP rs#: 1801282 and APOA5 dsSNP rs#: 662799)

The full characterization of these two SNPs was also important to validate the reproducibility of the non-cross-linking method in other targets. Nevertheless, it is important to mention that the objective was to developed a set of two Au-nanoprobes that full discriminate between the homo- and heterozygous status of the FTO SNP (previously associated with obesity in the Portuguese population), which has been clearly achieved, with the advantage that genotyping samples mediated by Au-nanoprobes were achieved using a single Au-nanoprobe.

For the detection and discrimination of both SNP, present in the PPARG and APOA5 gene the same strategy was used. Several Au-nanoprobes were functionalized to determine which were more likely to achieve the discrimination between the three possible genotypes for each SNP. In Table 4.2 are represented the set of Au-nanoprobes chosen accordingly to previous knowledge gain from the FTO Au-nanoprobes.

Table 4.2 – **Au-nanoprobe characteristization used for genotyping SNPs from PPARG (dsSNP rs#: 1801282) and APOA5 (dsSNP rs#: 662799).**

Au-nanoprobes	Modified-oligonucleotide length	Ratio AuNP:Oligo	Stability against $MgCl_2$-induced aggregation (mM)	Red-shift peak (nm)	LOD ($ng.\mu L^{-1}$)
PPARGwt20	20	1:200	55	569	≥30
PPARGmut20	20	1:200	50	569	≥60
APOA5wt20_180	20	1:180	70	600	≥20
APOA5mut20_180	20	1:180	45	600	≥20

The decision of using this set of 4 Au-nanoprobes was driven from detection assays done with ssDNA targets. For PPARGwt20, APOA5wt20_180 and APOA5mut20_180 the discriminatory effect that each one should give was achieved. In other words, in the absence or presence of ssDNA upon ionic strength increase, the Au-nanoprobe aggregates. By contrast in the presence of a fully complementary target no colorimetric change was attained. In the presence of a single-base mismatch target, the supposed full aggregation did not occur, like it was described for both Au-nanoprobes of FTO (Figure 4.17). Nevertheless, it is important to note that the rAbs were lower for these cases in comparison with the full complementary target. The Au-nanoprobe

PPARGmut20 presented the characteristic colorimetric and UV-Vis rAbs difference between absence/unrelated and full complementary/single-base mismatch target, nevertheless the difference in rAbs were very low between them (Figure 4.17 B).

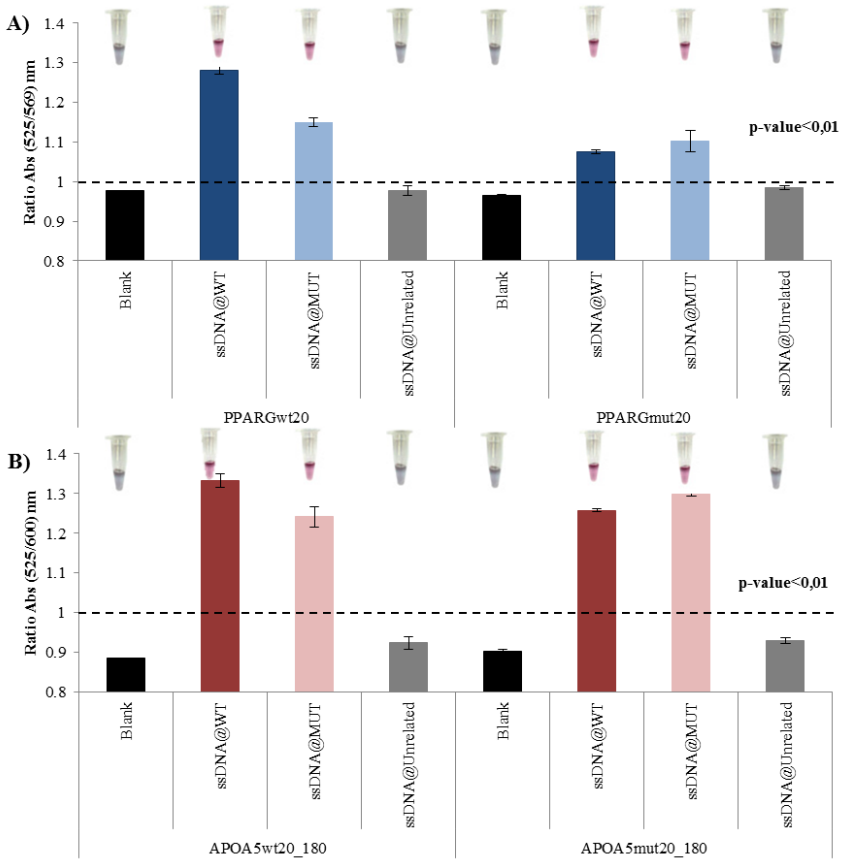

Figure 4.17 – Hybridization assay results with ssDNA oligonucleotides for PPARG and APOA5 Au-nanoprobes. Au-nanoprobes aggregation as measured by ratio of aggregation (ratio of SPR intensity at 525 and 569 nm for PPARG Au-nanoprobes and 525 and 600 nm for APOA5 Au-nanoprobes) for the assay mixtures - 2.5 nM Au-nanoprobe, 10 mM phosphate buffer (pH 8), ssDNA targets at a final concentration of 0.3 pmol.µL^{-1}. All spectrophotometric data was collected 30 minutes after salt addition and error bars represent the standard deviation of three independent assays. The horizontal line represents the threshold of 1 considered for discrimination between positive (rAbs≥1) and negative (rAbs<1) result. A representative colorimetric results is showed upon each result bar – red, positive result; blue/purple, negative result. Mean values are significantly different between groups with a p-value<0.01. In **A)** PPARG Au-nanoprobes hybridization viability and in **B)** APOA5 Au-nanoprobes hybridization viability.

After proven the viability of the Au-nanoprobes to hybridize with their respective targets, the same were tested with PCR-generated targets harboring the SNPs of PPARG and APOA5 genes. While APOA5 PCR-generated products were 195 bp long, the PPARG were 445 bp long. With this approach it was possible also to discriminate if the amplicon size could be an influence in the detection pattern, like it was for the FTO Au-nanoprobes. From the results from Figure 4.18B it is possible to see that better discrimination patterns were obtained for the shorter amplicons (APOA5 PCR-generated products), since both APOA5 Au-nanoprobes could discriminate between fully complementary/single-base mismatch and unrelated targets. The

discrimination between the fully complementary and the single-base mismatch targets it was obtained for both Au-nanoprobes, but the identification of the heterozygous status was not possible since, in APOA5mut20_180 Au-nanoprobe, the rAbs were very near to 1, while the colorimetric results presented a very faint red, meaning that a process of partial aggregation occurred Figure 4.18B. For the PPARG Au-nanoprobes only the PPARGwt20 could detect and discriminate between fully/heterozygous and single-base mismatch/unrelated or absence of target, nonetheless only with 60 ng.µL^{-1}. The PPARGmut20 could not detect the fully complementary or any target, since in all cases, after increasing the ionic strength, this Au-nanoprobe immediately aggregate (Figure 4.18A).

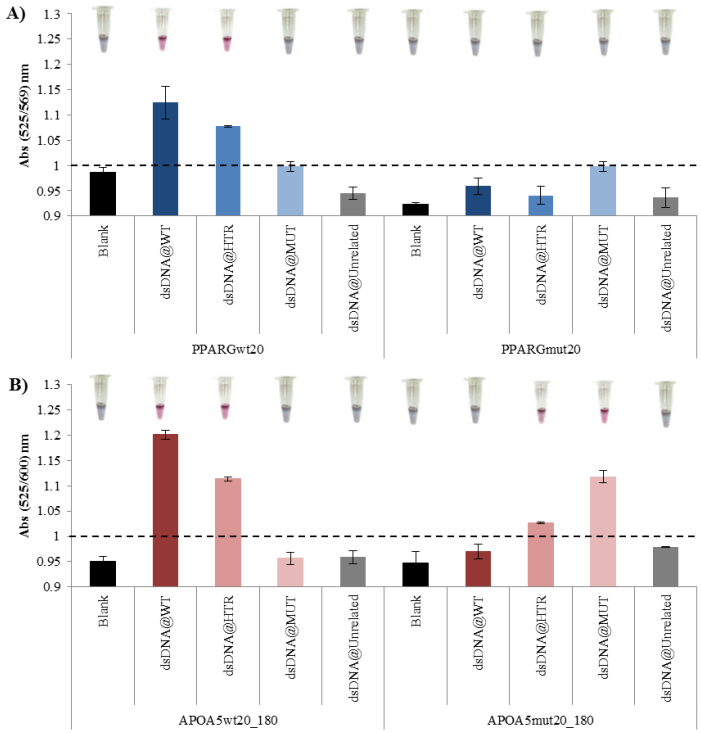

Figure 4.18 – Hybridization assay results with PCR-generated targets for PPARG and APOA5 Au-nanoprobes. Au-nanoprobes aggregation as measured by ratio of aggregation (ratio of SPR intensity at 525 and 569 nm for PPARG Au-nanoprobes and 525 and 600 nm for APOA5 Au-nanoprobes) for the assay mixtures - 2.5 nM Au-nanoprobe, 10 mM phosphate buffer (pH 8), purified dsDNA targets (PCR products) at a final concentration of 60 ng.µL^{-1}for PPARG Au-nanoprobes and 30 ng.µL^{-1} for APOA5 Au-nanoprobes. All spectrophotometric data was collected 30 minutes after salt addition and error bars represent the standard deviation of three independent assays. The horizontal line represents the threshold of 1 considered for discrimination between positive (rAbs≥1) and negative (rAbs<1) result. A representative colorimetric results is showed upon each result bar – red, positive result; blue/purple, negative result. Mean values are significantly different between groups with a p-value<0.01. PPARG PCR-generated products (dsDNA@WT, dsDNA@MUT and dsDNA@HTR) were 495 bp long, while unrelated target (dsDNA@unrelated) was 445 bp long. APOA5 PCR-generated products (dsDNA@WT, dsDNA@MUT and dsDNA@HTR) were 195 bp long, while unrelated target (dsDNA@unrelated) was 225 bp long. In **A)** PPARG Au-nanoprobes SNP detection in **B)** In **A)** PPARG Au-nanoprobes SNP detection.

4.3 Concluding remarks

The main goal of this chapter consisted in the synthesis and characterization of Au-nanoprobes capable of attaining successful discrimination between genotypes for three obesity-related SNPs, with considerable sensitivity and specificity based on the non-cross-linking method. Moreover, it was also envisaged the validation of the non-cross-linking approach against the gold standard technique for SNP genotyping, Sanger sequencing. For this purpose, AuNPs were functionalized with thiol-modified oligonucleotide of either 17 or 20 bp long, with different AuNP:oligo ratio (1:160, 1:180 and 1:200). 6 Au-nanoprobes (two for each *loci* of each SNP) needed to attain the distinction between homo- and heterozygous status were those prepared with longer oligonucleotides (20 nt) and with higher AuNP:Oligo ratio (1:180 and 1:200). From this set of 6 Au-nanoprobes, 5 of them could detect and discriminate between their related target and an unrelated target. Additionally, using a set combination of two Au-nanoprobes the distinction between homo- and heterozygous condition was possible for FTO (rs#:9939609) and APOA5 (rs#:662799) SNPs. In particular, the Au-nanoprobes developed for the detection of the FTO gene harboring the SNP previously associated with obesity in the Portuguese population (Carlos et al. 2013) in this thesis, were submitted to a blind test validation with biological samples. The validation allowed to claim that the non-cross-linking method is able of detect and discriminate between a fully complementary and a single-base mismatch target, with clearly distinction between the two homozygous status, as was already reported in previous reports using the non-cross-linking approach by our group (Doria et al. 007, Baptista et al. 2008, Veigas et al. 2010, Costa et al. 2010). More strikingly, to our knowledge, it has been shown for the first time the capability of a single Au-nanoprobe to distinguish between the three possible genotypes, with high degrees of sensitivity (87.50%) and specificity (91.67%).

The presented results allow concluding that the non-cross-linking method can be used as a SNP genotyping technique with considerable sensitivity and specificity. The blind test validation of the system, performed in comparison to the gold standard Sanger-sequencing with biological samples, proved that this method can be used as a routine technique in conventional laboratory and ultimately be integrated in a miniaturized nano-device to make it available for POC (Veigas et al. 2012, Bernacka-Wojcik et al. 2013). Under some degree of optimization, the non-cross-linking method for detection of SNP can be a reliable tool, but with further developments in molecular biology techniques, that will be addressed further in this thesis, the non-cross-linking here proposed (Figure 4.19) can be potentiated.

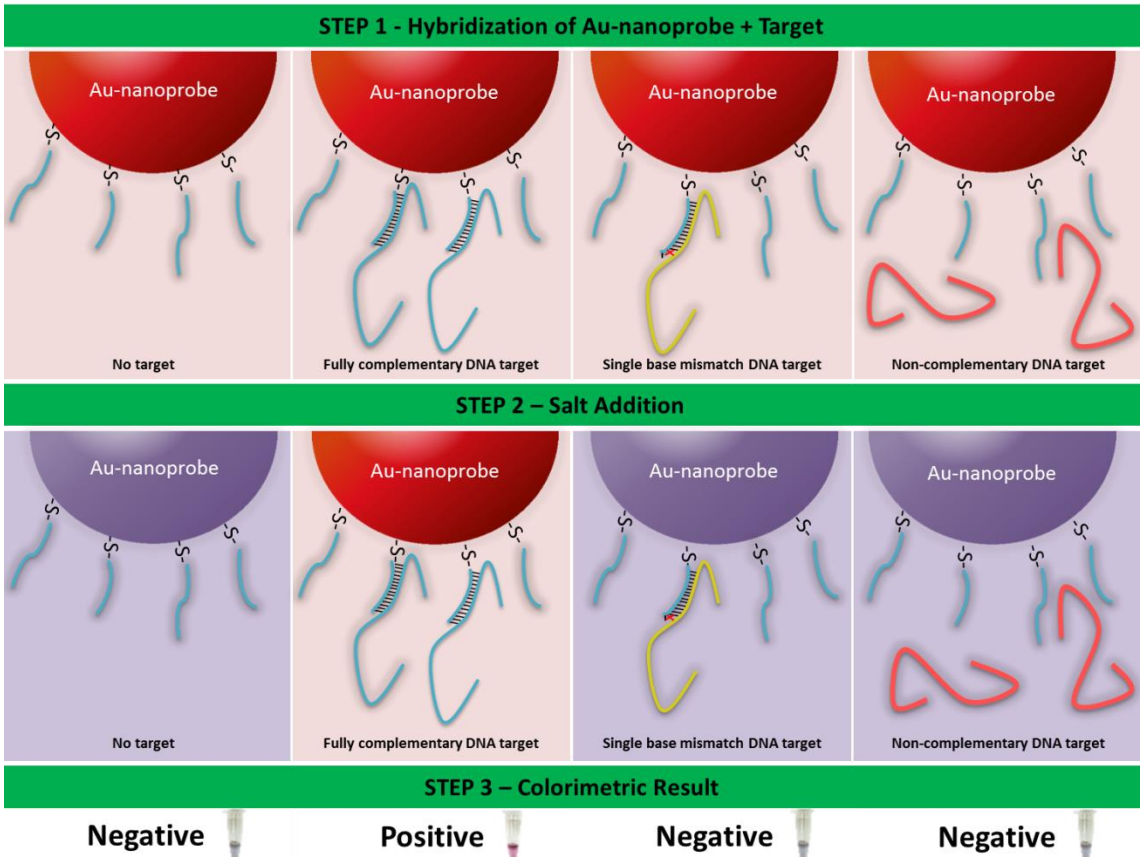

Figure 4.19 – Non-cross-linking method for SNP detection. The first step of the non-cross-linking is to undergo the mixture between the Au-nanoprobe and the DNA targets (fully complementary, single-base mismatch and non-complementary). After all the solutions are heated to denaturize the dsDNA/secondary structures are allowed to cooled down at 25 ºC for 20 minutes so hybridization between Au-nanoprobes and targets can occur. The Au-nanoprobe sequence is only complementary to the fully complementary and single-base mismatch targets and the binding strength between these targets and the Au-nanoprobes is what let hybridization occur. Nevertheless, the destabilization of the duplex in the 3'-end of the Au-nanoprobe in the presence of a single-base mismatch target can decrease this hybridization binding strength, which leads to no target hybridization. In the second step, the increasing of the ionic strength by the addition of a divalent salt will decreases the electrostatic repulsion between Au-nanoprobe conjugates and will lead to Au-nanoprobe aggregation (if in the presence of a non-complementary, single-base mismatch or absence of target), turning the solution red to blue (SPR coupling). Otherwise, the perfect formation of the conjugates duplex Au-nanoprobe/fully complementary target when submitted to increased ionic strength will not be destabilized and the solution remains red.

CHAPTER 5 - MICROFLUIDIC PLATFORM FOR OBESITY-RELATED SNP DETECTION MEDIATED BY GOLD NANOPROBES

Disclaimer: Results and data presented in this chapter were published in:

Bernacka-Wojcik I, Águas H, **Carlos FF**, Lopes P, Wojcik PJ, Costa MN, Veigas B, Igreja R, Fortunato E, Baptista PV and Martins R. 2014. Single nucleotide polymorphism detection using gold nanoprobes and bio-microfluidic platform with embedded microlenses. Biotechnology and Bioengineering DOI: 10.1002/bit.25542

Fábio Ferreira Carlos was only responsible for the biological sample preparation, Au-nanoprobe synthesis and characterization and drafted the manuscript.

5.1 Introduction

Micro-scale dimensions and concomitant high surface-to-volume ratio consists the some of the properties of microfluidic systems, that are prone with numerous advantages including portability, faster sample analysis, higher throughput, potential of automation, high-level integration and reduced reagent use, all of which associated with decreased cost (Mark et al. 2010). These devices can be designed for multi-parallel operations, making the system more reliable as several control assays can be performed simultaneously with multiple samples (Abgrall et al. 2007, Khoshmanesh et al. 2011, Ben-Yoav et al. 2012, Soe et al. 2012). Recently, several microfluidic devices have been developed to tag and characterize specific DNA sequences using for this miniaturized approaches (Zhang et al. 2006) that only need a small amount of analyte (picograms) (Xiang et al. 2012) and often integrate DNA analysis including sample pre-treatment, DNA amplification and detection (Burns et al. 1998, Liu et al. 2004, Oblath et al. 2013). However, a complete lab-on-chip device for DNA analysis has not been successfully commercialized mainly due to high cost of the fabrication and/or manipulation (Choi et al. 2011).

The size-dependent colorimetric properties of AuNPs have been extensively used as a label for DNA and RNA analysis, as was already been mentioned in the previous chapters (Doria et al. 2012, Larguinho et al. 2012). The use of Au-nanoprobes is a very attractive alternative to fluorescence-based assays due to their sensitivity, selectivity and possibility of using simpler instrumentation. In the non-cross-linking nucleic acid (DNA or RNA) detection method developed by Baptista and co-workers, specific sequence detection is achieved by the colorimetric comparison of a solution before and after salt induced Au-nanoprobe aggregation: upon salt addition, the presence of fully complementary nucleic acid sequences prevents aggregation of Au-nanoprobes and the solution remains red; whereas, presence of a non-complementary/single-base mismatch sequences does not convey such protection and the solution turns blue (Doria et al. 2007, Conde et al. 2010, Doria et al. 2010). This molecular detection technique has been integrated into an inexpensive and reliable optoelectronic platform using green and red light sources and a thin p-i-n silicon (Martins et al. 2007, Silva et al. 2007, Silva et al. 2011) or TiO2-based ink-jet printed photodetectors (Bernacka-Wojcik et al. 2010) and more recently with paper-based microfluidics (Veigas et al. 2012).

The use of colorimetric transduction for the Au-nanoprobes based DNA detection offers the advantage of involving only simple equipment such as a light-emitting diode for excitation and a photodiode for detection. However, implementation of colorimetric measurements in microfluidic systems is challenging as reduction of the optical path length (OPL) within the microchannel system can decrease the system sensitivity, particularly when the depth of the channel is used for detection (Viskari et al. 2006). Recently, a bio-microfluidic platform was developed for the colorimetric DNA analysis by extending the OPL by detection along a PDMS microchannel, using optical fibers to transmit the light (Bernacka-Wojcik et al. 2013).

Whenever light is involved, micro-optics may enable to miniaturize a device and to improve its performance increasing the coupling efficiency and reducing the signal to noise ratio (Voelkel 2012). Due to their small dimensions, micro-optical elements can be easily integrated with other optical/microfluidic components and can be mass-produced lowering cost per unit. Microlenses shape the light beam basing on the difference of the refractive indices: the light beam going through materials interface will be deflected, and focused according to the curvature radius of the interface and the incident angle of the light beam. As such, microlenses have attracted a lot of attention in fluorescence-based biological analysis (Camou et al. 2003, Seo et al. 2004, Mohammed et al. 2013, Mohammed et al. 2014), confocal microscopy (Tanaami et al. 2002), optical imaging (Tripathi et al. 2011) and various opto-electronic devices (Voelkel, 2012, Cherng et al. 2014). In microarrays for genome and proteome analysis, microlens arrays allowed detection of numerous samples at the same time, eliminating the need for scanning of the optics/the sample, thereby greatly simplifying the biochip instrumentation and increasing the analysis throughput (Van Overmeire et al. 2005, Roy et al. 2009, Mogi et al. 2011).

The optimization of the bio-microfluidic platform for Au-nanoprobe-based DNA detection (Bernacka-Wojcik et al. 2013) that has resulted in a 160% improvement of colorimetric discrimination by implementation of microlenses and an acquisition system will be described in this chapter. The optimized bio-microfluidic platform with embedded PDMS/air microlenses allowed the detection of a SNP obesity-related to the Portuguese population comprised in FTO gene (dsSNPrs#: 9939609) (Carlos et al. 2013) using the FTOwt20 Au-nanoprobe, previously optimized for SNP detection and allele discrimination in Chapter 4 (Carlos et al. 2014), reducing 10 times lower the solution volume and 5 $ng.\mu L^{-1}$ lower DNA target concentration than required for a conventional microplate reader.

5.2 Results and Discussion

5.2.1 Set-up optimization

Citrate-capped AuNPs were used to optimize the detection protocol and device performance. AuNPs solutions mimic well the optical properties of the colorimetric DNA assay solutions: a dispersed AuNPs solution (red color) spectrum mimics a positive DNA assay, while aggregated AuNPs (blue color) mimic a negative one. The colorimetric discrimination of the AuNP solutions was performed through a developed system that measures an output voltage (U) obtained when the sample is illuminated with red light (from a LED source of dominating wavelength 634 nm) and a green light (from a LED source of dominating wavelength 516 nm; LEDs emission spectra –Figure 5.1). Then, a ratio $U_{634\ nm}/U_{516\ nm}$ is calculated for each sample: the red color solution gives higher ratio than the blue color solution. The detection response (Rs)

is determined by normalization of the sample ratio to the baseline ratio (measured with ultra-pure water for AuNPs or phosphate buffer for Au-nanoprobe) according to equation (1).

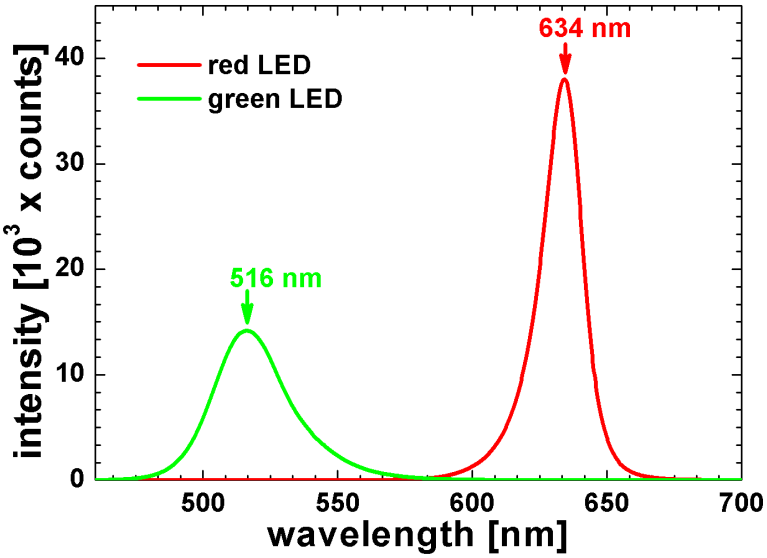

Figure 5.1 - Emission spectra of SMD LEDs used for the colorimetric analysis. The spectra were acquired using miniature fiber optic spectrophotometer integrated with an empty microfluidic chip (integration time: 8 ms; LEDs supplied with 0.4 A).

$$R_s = \frac{U_{sample(634nm)}/U_{sample(516nm)}}{U_{baseline(634nm)}/U_{baseline(516nm)}} \qquad \text{eq. (1)}$$

The colorimetric discrimination (ΔR_s), i.e. the discrimination between red and blue color solutions, is calculated for each set of tests according to equation (2).

$$\Delta R_s = R_s(dispersed\_solution) - R_s(aggregated\_solution) \qquad \text{eq. (2)}$$

As the electrical signal generated by the photodiode is in the nanoampere range, a monitor of such low current should present very low input impedance to respond with negligible voltage across the photodiode. A typical current-to-voltage converter with an op amp can provide almost zero impedance and high-amplifier loop gain, lowering voltage swing from the amplifier input. The electrical circuit for current-voltage conversion presented in the previously published work (Bernacka-Wojcik et al. 2013) was optimized to reduce noise and increase results accuracy (Figure 5.2 and Appendix III Table AIII.1). The op amp 741 (input bias current about 30 nA; input impedance about $2x10^6$ Ω) was replaced by a JFET op amp TL081 that has almost 1000 times lower input bias current (30 pA) and much higher input impedance (10^{12} Ω) leading to an increase in the signal to noise ratio. Furthermore, a three orders of magnitude higher feedback capacitor (1.5 nF) was used to reduce the bandwidth and the noise (by means of the compensation for the photodiode capacitance). To increase the measurements' accuracy, a data acquisition system was implemented: National Instruments USB 6008 data acquisition board with a custom-made LabView programme to register the data. For each measurement, 150 output voltage values are acquired every 0.2 sec, then averaged and standard deviation calculated. With this optimized

setup, the obtained standard deviation was always below 5% per measurement and the AuNPs color discrimination was improved by 96% (previous state-of-the-art detection ratio ΔR_s = 0.128 ± 0.011; the optimized ΔR_s = 0.251 ± 0.012). For the DNA tests, the setup was further optimized by replacing the TL081 with the AD549 op amp with ultralow input bias current of 50 fA and very high input impedance (10^{13} Ω) and input enabling to reduce the standard deviation to values below 2% per measurement.

To reduce the cost of the device, the PDMS chips were sealed to glass using a UV ozone cleaner (UVO) instead of the oxygen plasma system previously utilized. The UVO treatment generates highly active oxygen species that remove the methyl groups from the PDMS surface forming polar silanol groups. When oxidized PDMS surface is brought into contact with UVO treated glass surface, the condensation reaction occurs forming covalent bonds between those surfaces and sealing them irreversibly (Sun et al. 2007). The UVO treatment activates chemically both surfaces (glass and PDMS) making them reactive to physical contact. The irreversible sealing was obtained for the samples that were placed in the cleaner about 5 mm away from the UV lamp and treated during 6 min. After 1 min for the exhaustion of the ozone gas created during exposure, samples were withdrawn from the cleaner and their surface put into contact. To increase the bonding strength, samples were then kept for 20 minutes at 70 ºC in a hot plate and let to rest overnight at room temperature before use. The resulting bonding resisted the manual peel test.

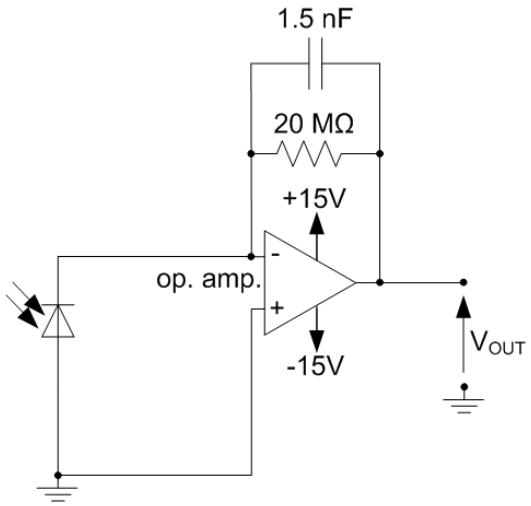

Figure 5.2 – Circuit diagram used for optical-to-electrical signal conversion and amplification. The signal from the photodiode was amplified by an op amp circuit with a feedback resistance of 20 MΩ and supplied by ± 15 V.

5.2.2 Microlenses design and fabrication

To further improve the setup performance, self-aligned planar microlenses were incorporated in the chip to properly collimate light into the detection channel and then to the output fiber core, taking advantage of the refractive index differences between air and PDMS (Camou et al. 2003). These 2D micro-optical components were fabricated by a replica molding

method using a single layer SU-8 mold, so no additional steps were required in the fabrication process.

Various input microlenses configurations were designed using the ray-tracing paraxial approximation. The light emitted by the LEDs was guided to the microfluidic channel by an input optical fiber of 62.5 μm core diameter and the numerical aperture of 0.25 (see Figure 5.3 A and B and Figure 5.4). To focus the light on the channel content (aimed beam width: 100 μm), various input lens configurations were designed and tested: bi-concave air microlens and bi-convex PDMS microlens. The depth of all chip features was around 125 μm allowing optical fibers of 125 μm diameters to be accurately fixed and easily aligned between each other and the channel.

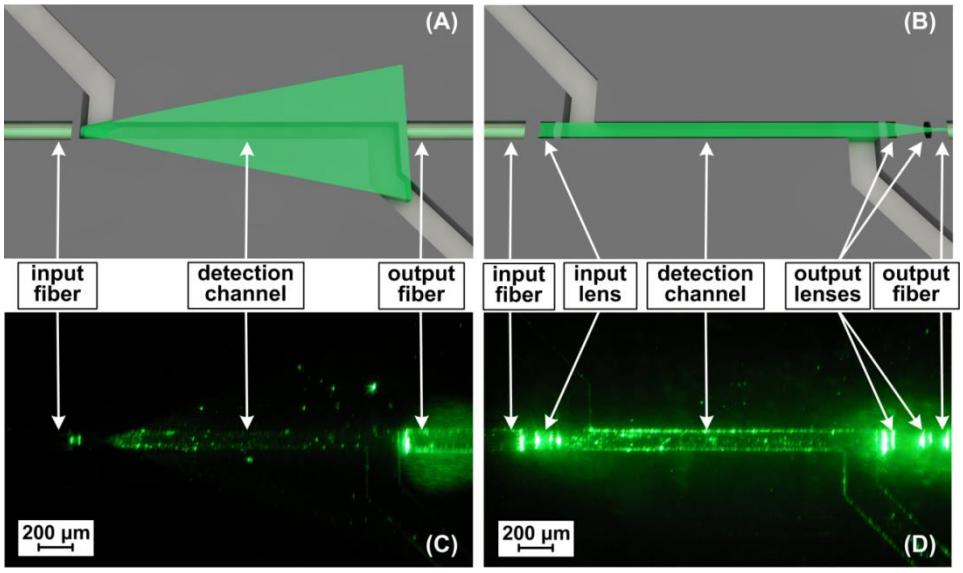

Figure 5.3 – LED guidance in the microfluidic channel. (A) 3D schema of light propagation in chip of 2 mm long optical path without lenses and **(B)** with 2D air microlenses (the schema is drawn to scale; only the light propagation in the plane of the channel is considered as the light in vertical direction remains diverged). **(C)** Top view microscopic images of channel filled with water illuminated by green LED (0.9 A) in chip without lenses and **(D)** with 2D air microlenses.

The microlenses design was done setting the smallest feature width around 50 μm (aspect ratio: 2.5) to prevent fluid leakage or fabrication issues, although an aspect ratio of 10 could be achieved by the used fabrication process (Bernacka-Wojcik et al. 2013). In Table AIII.2 from Appendix III are presented the parameters of the designed input lenses configurations and the characteristics of the resulting beam (y - half of the beam width; θ - the beam propagation maximum angle).

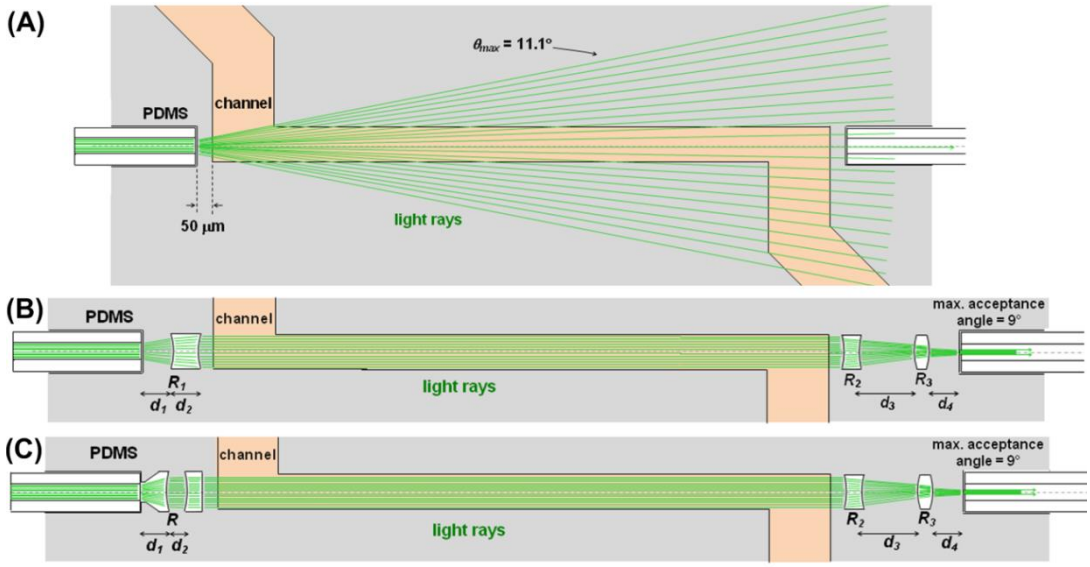

Figure 5.4 – 2D schematics of light propagation in PDMS chip of 2 mm long optical path. (A) uncollimated; **(B)** with input and output air lenses and **(C)** with PDMS input lens and output air lenses (to scale).

After interacting with the fluid to be analyzed, the light should be collected by the output fiber (core diameter: 62.5 µm; NA: 0.25). The output lenses were designed using the thin lenses approximation. To shorten the focusing length taking into account the small acceptance angle, a pair of lenses was used: bi-concave and bi-convex air lenses with the characteristics presented in Table AIII.3 from Appendix III. The chips incorporating the designed lenses were fabricated in PDMS by the replica molding using SU-8 mold and an intermediate epoxy mold (Bernacka-Wojcik et al. 2013). The fabricated lenses were characterized by optical microscopy in dark conditions with long exposure time (30 s; Figure 5.3 C and D), confocal microscopy (Figure AIII.1 from Appendix III) and scanning electron microscopy (Figure AIII.2 from Appendix III). The chip without lenses, the light beam diverges and a big part of the light will not be transmitted into the output fiber core. In this case, only a very small fraction of light will interact with the fluid and an even smaller fraction will be collected by the output fiber core. Furthermore, the light intensity will not be uniform along the channel thus endangering a good interaction. In the case of the chip with air lens, the light beam is well collimated on the channel content and afterwards converged into the output fiber core by the output lenses. It should be noted that those images show scattered light intensity, while for the detection, only the transmitted light is analyzed; however, the propagation of the light beam can be observed, as the scattered light intensity is proportional to the total light intensity.

The incorporation of microlenses increases significantly the number of interfaces on the optical pathway, while on each interface there is light scattering and reflection causing optical losses. Here, these losses were reduced by proper design of the microfabrication process. Firstly, high-resolution chrome mask was used to obtain low roughness features. Secondly, SU-8 was chosen as a mold material for PDMS patterning providing much smoother sidewalls than in the

case of chemically etched molds. Thirdly, SU-8 was UV exposed through i-line filter to prevent formation of T-shape features resulting in nearly vertical sidewalls (87.8 degrees). SEM images (Figure AIII.2 from Appendix III) and confocal microscopy images (Figure AIII.1 from Appendix III) reveal a good definition of the PDMS features and smooth sidewalls. The confocal microscopy images indicated some irregularities on the chip surface that are most probably related with the use of the epoxy mold that is much rougher that the SU-8 mold. However, these irregularities do not cause any leaks and do not interfere with the detection system allowing proper analysis of the colorimetric changes of the AuNPs solutions. The cracks visible on the SEM images are associated with the thin gold layer that was deposited to increase quality of SEM images (the confocal microscopy images of the same samples before the gold deposition show a crack-free surface - see Figure AIII.1 from Appendix III.

5.2.3. Effect of microlenses on colorimetric AuNPs analysis

The performance of the microlenses was tested analyzing the color of AuNPs solution (Figure 5.5A). The discrimination of the color of the AuNPs solution (i.e. the difference between the detection response for the dispersed and the aggregated AuNPs – ΔR_s) was 0.251 ± 0.012 for the chip without lenses, while for the chip with the air lens it was 0.335 ± 0.007 (34% of improvement) and 0.337 ± 0.009 (34% of improvement) for chip with the PDMS lens. Both tested microlens configuration showed the same detection improvement, however from the practical point of view, it is much easier to position the input fiber properly using the air lens configuration instead of the PDMS lens. In the later, the fiber is stopped by the PDMS clips (Figure AIII.1C from Appendix III and Figure 5.4) that due to the PDMS elasticity may not resist the fiber insertion movement. It is more practical to use the air lens where the fiber is stopped by the 50 μm thick PDMS wall. Therefore, in the following experiments only the configuration with air lenses was used. Comparing with the previous state-of-the art ($\Delta R_s = 0.128 \pm 0.011$), the optimized setup with the air lenses provides 160% higher discrimination of the AuNPs color. The incorporated lenses not only increased the light intensity that reaches the output fiber, but also increased the fluid–beam interaction: even setting the signal at the same value for the baseline solution for both configurations, the chip with lenses yields much better discrimination between red and blue color AuNPs solutions.

The two-dimensional (Figure 5.4) and three-dimensional schema of light propagation (Figure 5.3A and B) visualize well this mechanism: in the chip without lenses, the output fiber collects only the irradiation that passed the channel straight from the input fiber core to the output core (max. acceptance angle: 9 deg), therefore only a small portion of the total fluid will interact with propagating light.

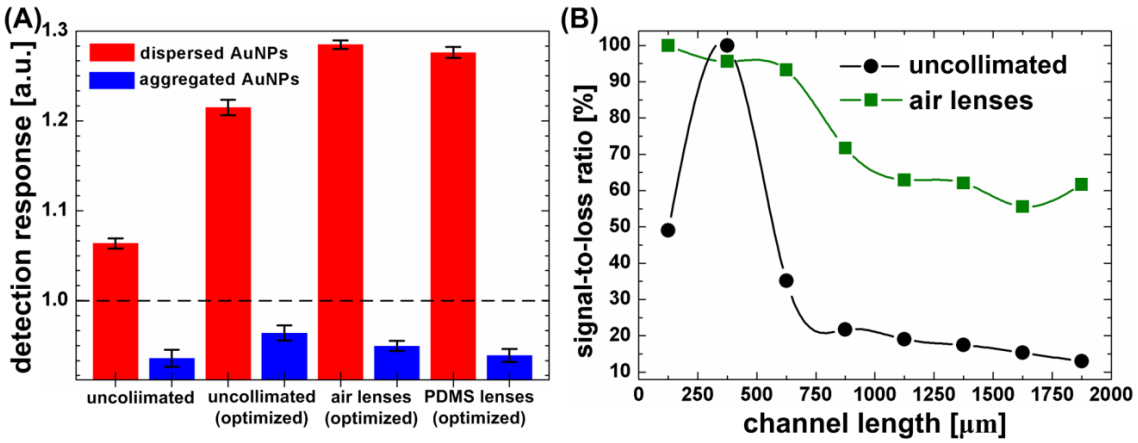

Figure 5.5 – Microfluidic platform response for AuNP detection. (A) The detection response (Rs, eq. (1)) of the microfluidic platform for dispersed (in red) and aggregated (in blue) AuNPs solutions using microfluidics chips without lenses (before and after system optimization described in section 5.1), with air microlenses and with PDMS microlenses (LEDs powered with 0.4 A). The horizontal dashed line represents the threshold of 1 considered for discrimination between red and blue color solutions. **(B)** The propagation of the signal-to-loss ratio along the channel in chip without lenses and chip with the air microlenses based on the analysis of the pixels intensity in Figure 5.3C and D.

The incorporation of the output microlenses allowed the interaction of all the available fluid with propagating light, yielding a much higher discrimination between signals obtained from the solutions of different colors. To quantitatively estimate the propagation of the light signal-to-loss ratio along the channel in the chips with and without air lens, the pixels intensity of the images presented in Figure 5.3 C and D was analyzed by the ImageJ software. The channel was divided into 8 segments of 250 μm length and for each channel segment the integrated density (i.e. the sum of the values of the pixels intensity in the region) was measured. This value was then divided by the region area. The obtained value was defined as the signal, while the integrated density on the regions outside of the channel was defined as loss. Figure 5.5 B presents the propagation of the signal-to-loss ratio along the channel in the chip without lens and chip with air lens as a percentage of the maximum signal-to-loss ratio. In the chip without lens, the highest signal-to-loss ratio is on the channel segment from 250 μm to 500 μm, because on the begging on the channel, the light illuminates only a part of the channel content (see Figure 5.3 A and C and Figure 5.4 A). Then, the signal-to-loss ratio decreases along the channel due to the beam divergence and only about 10% reaches the channel end. In the case of the chip with air lens, the signal-to-loss ratio is more constant along the channel and about 60% is transmitted to the channel end.

5.2.4 SNP detection using the optimized system

The Au-nanoprobe, FTOwt20, previously reported to fully characterized the SNP comprised in FTO gene (dsSNPrs#: 9939609) (Carlos et al. 2014) obesity-related to the Portuguese population (Carlos et al. 2013) was used in microfluidic chip with air lenses. The

FTOwt20 Au-nanoprobe based on the non-cross-linking method using a microplate reader transduction, provided a LOD of 20 ng.µL^{-1} (between fully complementary and single-base mismatch or unrelated targets) with 87.50% of sensitivity and 91.70% of specificity when compared to the gold standard technique for SNP genotyping, i.e. Sanger Sequencing (Carlos et al. 2014). Scanning electron micrographs of the Au-nanoprobe assay for FTO detection (acquired on PDMS surface) show a clear difference in the Au-nanoprobe dispersion in the presence of positive (Figure 5.6A) and negative FTO target (Figure5.6B): as expected, the nanoprobe extensively aggregate in the negative assay.

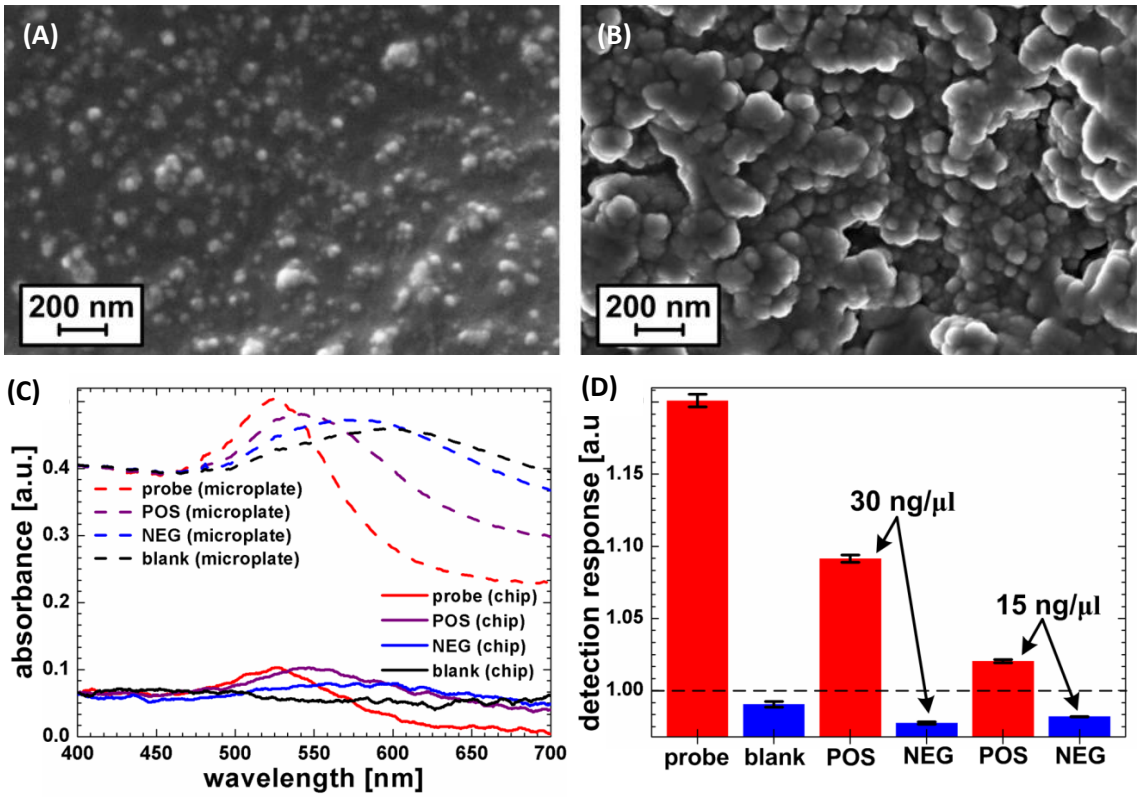

Figure 5.6 – FTOwt20 Au-nanoprobe detection pattern in the microfluidic chip. Scanning electron micrographs of the Au-nanoprobe assay for FTO detection mediated by FTOwt20 Au-nanoprobe: **(A)** positive and **(B)** negative assay. A clear difference in the Au-nanoprobe dispersion is visible. **(C)** Absorption spectra of the FTOwt20 Au-nanoprobe assay for the FTO (dsSNPrs#: 9939609) detection: blank, positive (POS – presence of a fully complementary target) and negative (presence of a single-base mismatch target) assay (30 ng.µL^{-1} target final concentration). The spectra were taken 30 min after salt addition using miniature fibre optic spectrophotometer integrated with a microfluidic chip (3 µl; 2 mm long optical path) and compared to conventional microplate reader (30 µl; 10 mm long optical path). The absorption spectra of blank, POS and NEG were shifted for the same absorbance value at λ = 400 nm as probe, so as to allow better visualization. **(D)** Results of the colorimetric DNA detection (eq. 1) of the FTO (dsSNPrs#: 9939609) using FTOwt20 Au-nanoprobes and the optimized bio-microfluidic platform using 3 µl of solution with 15 and 30 ng.µL^{-1} of target DNA. The horizontal dashed line represents the threshold of 1 considered for discrimination between positive and negative.

Firstly, the microfluidic chip was integrated with a miniature fiber optic spectrometer to analyze the assays' colorimetric changes and their variation with time elapsing after salt addition.

The absorption spectra of blank, POS and NEG were shifted for the same absorbance value at λ = 400 nm as probe, so as to allow better visualization. Comparing the spectra acquired using the fiber optic spectrometer and chip with the spectra acquired by a microplate reader (Figure 5.6 C and also spectra of Figure AIII.3 from Appendix III), a higher noise is attained since the light source in the miniature spectrometer is much weaker and thus the signal-to-noise ratio is low. Absorbance values on chip are about 5 times lower than those from the microplate reader that correlated directly to the difference in optical path length: in chip the optical path is 5 times shorter (2 mm) than in the microplate (10 mm). Nevertheless, the obtained absorption spectra are very similar for these two strategies but the microfluidic chip requires 10 times less volume. The LEDs transmission spectra were acquired using the miniature fiber optic spectrometer integrated with the chip for the channel filled with water, the Au-nanoprobe and blank (8 min; 15 min and 30 min after salt addition - Figure AIII.4 from Appendix III) to see how the transmitted LEDs light is affected by solutions. The obtained spectra were much smoother due to the higher light intensity of the LEDs used when comparing to the halogen lamp. As expected, the red color solution reduces the transmitted intensity of the green LED, while the blue color solutions reduce the red light intensity. A longer time after salt addition (i.e. 15 and 30 min), the transmitted intensity of the LEDs increases because the color of the blank solution becomes weaker with time due to precipitation of the aggregates. The microfluidic platform gave statistically significant discrimination between positive and negative samples using 30 $ng.\mu L^{-1}$ with 10 times less volume than for the microplate reader (Figure 5.6 C). Furthermore, the microfluidic platform could discriminate between samples below the microplate reader's LOD. While the microplate could only give a discriminatory response at concentrations equal or higher than 20 $ng.\mu L^{-1}$, the microfluidic platform begins to discriminate at 15 $ng.\mu L^{-1}$. The use of 15 $ng.\mu l^{-1}$target (final concentration) on the microfluidic platform yields a much weaker response between positive and negative sample, but a statistical analysis using a paired t-test shows these responses are significantly different from each other (p-value < 0.001) with 99.9% confidence interval.

Images of channels using an optical microscope coupled to a digital camera with a long exposure time (30 s) allowed to visualize different scatter intensities of AuNPs within channels. Following salt addition, aggregation may be inferred from the higher intensity scattering punctuation in the channel that increased with time - see Figure 5.7 and Figure AIII.5 from Appendix III. These intensities correlate to expected difference in aggregation between positive (none to small aggregates) and negative samples (larger aggregates).

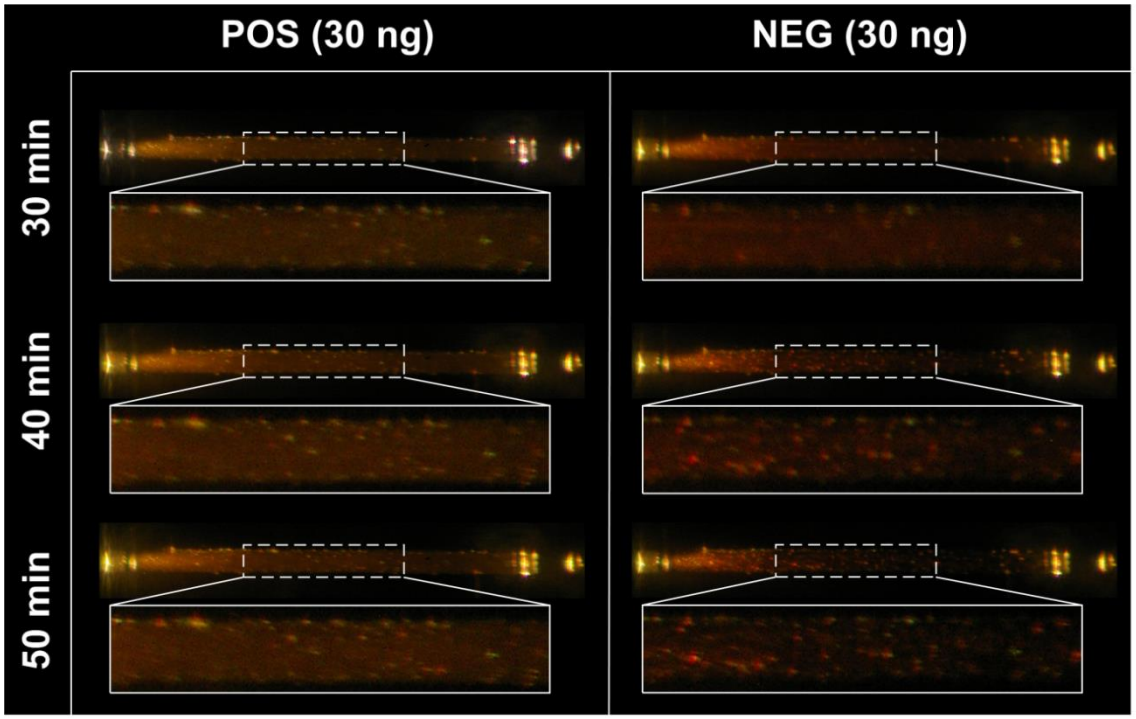

Figure 5.7 - Microscopic images of air microlenses chip with FTOwt20 Au-nanoprobe for dbSNPrs#: 9939609 detection. Illuminated by halogen lamp during the positive and negative colorimetric Au-nanoprobe assays for FTO single-base mismatch detection (target final: 30 ng.μL^{-1}) taken 30; 40 and 50 min after salt addition (the solutions were injected to the channel 26 min after salt addition). The images were taken in dark conditions using a Stereo Microscope and Pentax K100 camera with long exposure time (30 s).

5.3 Concluding remarks

The combination of the unique optical properties of gold nanoprobes with microfluidic platform resulted in a sensitive and accurate sensor for single nucleotide polymorphism detection operating small volumes of solutions, without the need for substrate functionalization or sophisticated instrumentation. The optimized bio-microfluidic platform clearly distinguished between positive and negative samples using 10 times lower solution volume and target DNA concentration below the limit of the detection attained with a conventional microplate reader (i.e. 15 ng.μL^{-1}). The incorporation of planar microlenses increased 6 times the signal-to-losses ratio reaching the output optical fiber and improved by 34% the colorimetric analysis of gold nanoparticles. The thoroughly described optimization of the microfluidic platform (concerning electrical signal processing; design, fabrication and performance of various microlenses) has significantly improved the results of AuNPs colorimetric analysis and can also be applied to other absorbance-based microfluidic devices as a simple and cheap mean to compensate for reduction of optical path length.

Further optimization shall be conducted, where, for example, mixture of reagents could be performed in the microfluidic chip (Bernacka-Wojcik at al. 2014) to reduce risk of sample contamination. Furthermore, waveguides should be incorporated to facilitate chip exchange

towards the point of care use. Moreover, for full integration as an all in one POC device, a sample-processing chamber will be addressed for sample-to-result fully integrated microfluidic chip.

CHAPTER 6 - APPLICATION OF GOLD NANOPROBE-BASED ASSAY IN INDUSTRY SETTING – TECHNOLOGY TRANSFER TO STAB VIDA

6.1 Introduction

STAB VIDA is a Portuguese biotech SME created in 2001, specialized in genetics and genomics, focused in the development of applications for diagnostics and personalized medicine. The company is strategically located on a research and technology park, nearby Unviersidade Nova de Lisboa, one of the most prestigious colleges in Portugal with more than 16 outstanding research centers. In the last few years STAB VIDA invested in the development of new genetic-based technologies for the detection of relevant DNA sequences for human conditions (i.e. Alzheimer, cancer, metabolic disorders, etc.), mainly through participation/coordination on national and European projects as well as doctoral students training. The expertise, technical knowledge and capabilities acquired by this R&D outline, when successfully translated, intend to improve the competiveness of STAB VIDA in the diagnostic POC market.

Taking in account the company's interests, one of the main objectives of the dissertation herein presented consisted in the development of a sustained set of Au-nanoprobes for identification of relevant SNPs related to obesity. These Au-nanoprobes would also require validation using real biological samples retrieved from a clinical setting. This endeavor was aimed at future implementation into a POC platform either for application in commercial setting or in the routine laboratory practice at STAB VIDA as an alternative methodology.

A second stage technology development within the framework of the PhD project was the extension of the non-cross-linking SNP detection method to other targets by means of a suitable POC target amplification technique. Such modification should aim at i) reduce time of amplification; ii) retain the specificity and sensitivity given by PCR-based amplifications and iii) lower the complexity of apparatus needed for target amplification. Ultimately, STAB VIDA goals comprised the extension of this new approach, potentially combining isothermal target amplification with Au-nanoprobes full genotype characterization, to other relevant non-obesity-related SNPs, relevant for clinical diagnostic and, consequently, attaining commercial value for the company.

POC diagnosis is an emerging attractive market to invest, with a market value of 15.5 billion € in 2013 and a compound annual growth rate (CAGR) of 4.5% estimated for 2018 (i.e., 2018's estimated market value of 19.3 billion € (BCC Research Healthcare Report, 2014). Moreover, developments in nanotechnology, specifically newly nanofabrication techniques and nanomaterials, allowed the development of highly sensitive and specific sensors (microfluidic platforms) turning them suitable for the detection of small sequence variations (e.g. Verigene System from Nanosphere Inc.) (Wei et al. 2010). WHO has already put forward some guidelines that POC testing must abide in order to transpose the nanotechnology benefits into a POC detection system – "ASSURED". These guidelines stand for Affordable, Sensitive, Specific, User-friendly, Rapid/Robust, Equipment-free or minimal, and Delivered to the greatest need (Wu et al. 2012). By meeting these standards, POC assays for nucleic acid detection should bring not

only traditional centralized laboratory-based testing (sensitive and specific) closer to both patient and doctor (user-friendly), but also make them suitable to be used in low-income countries where the lack of healthcare facilities is a reality (Delivered to the greatest need).

Several efforts have been made to develop nano-based platforms for nucleic acid detection using PCR-mediated amplification signal due to the advantages of technique, such as reduced power consumption and faster kinetics or heat transfer properties (Zhang et al. 2006, Zhang et al. 2007a, Ahmad et al. 2012). Nevertheless, the thermal cycling necessities (e.g. heaters, temperature sensors, etc.) required by PCR can confer increased platform/device complexity that may not be the most suitable for POC standards. As such, an isothermal amplification of nucleic acids that occurs at a constant temperature may be optimal for integration into microfluidic platforms for POC applications since dramatically reduce the apparatus complexity for target amplification (Craw et al. 2012). Within several isothermal amplification techniques that have been developed so far, loop mediated isothermal amplification (LAMP), nucleic acid sequence-based amplification (NASBA), rolling circle amplification (RCA), and helicase dependent amplification (HDA) are the most popular and serious candidates to be translated into POC systems (Figure 6.1) (Asiello et al. 2011, Chang et al. 2012).

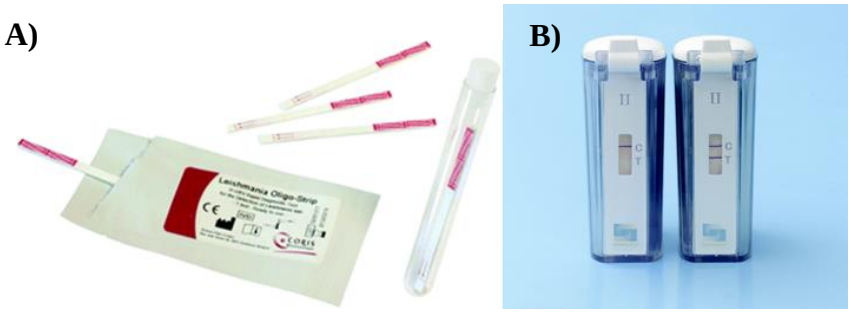

Figure 6.1 – Example of POC commercial products employing isothermal DNA amplification. A) Leishmania OligoC-Test from Coris BioConcept. A NASBA-based, point-of-care amplification reaction and dipstick oligo chromatographic detection test for Leishmania species, **B)** BESt^{TM} Cassette - Type II (BioHelix, Beverly USA). Allows portable detection of amplicons from HDA or PCR reactions in a vertical flow testing format.

LAMP, developed by Notomi and co-workers (Notomi et al. 2000), is one of the most suitable approaches to POC applications for DNA amplification, characterized with high specificity, efficiency and is relatively fast (< 1 hour) under isothermal conditions. It relies on application of a single polymerase characterized with strand displacement activity (*Bst* DNA polymerase), while other isothermal approaches use more than one polymerase. LAMP method uses four specific primers: two outers (F3 and B3 primers) and two inners (FIP and BIP primers) that recognize a total of six distinct sequences on the target DNA. The primers produces stem–loop DNAs with dumbbell structure that enters the exponential amplification cycle and strands with several inverted repeats of the target DNA that is made by repeated extension and strand displacement – See Figure 6.2.

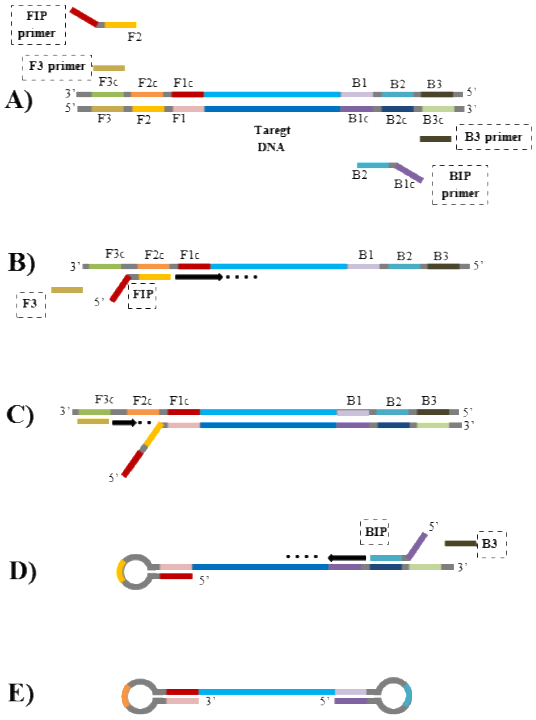

Figure 6.2 – Schematic representation of loop-mediated isothermal amplification (LAMP). A) Primers design for subsequent material formation by LAMP; **B)** DNA synthesis begins with FIP primer and the annealing of the F2 region to the F2c region on the target DNA for elongation; **C)** Primer F3 anneals to F3c region target DNA and strand displacement begins. The DNA strand elongated from FIP primer is further replaced and released; **D)** The released single strand forms a loop structure at the end and DNA amplification proceeds with BIP and B3 primers in a similar manner as FIP and F3 primers, **E)** generation of the loop structure at both ends (dumbbell-like structure) that is the initial material for the subsequent LAMP DNA amplification and elongation steps that lead to many complexes with different distribution of sizes.

6.1.1 Effective translation of Au-nanoprobe assay to STAB VIDA context

6.1.1.1 Lactose intolerance – Business target

STAB VIDA has long pursued the screening and analysis of SNPs associated to human conditions linked to nutrigenomics, such as the obesity SNPs described earlier in this thesis (see Chapter 1 – Section 1.2.1) and the lactose intolerance *loci*. Genetic testing of lactose intolerance is a well-established service in STAB VIDA and was implemented in the market in 2008 throughout distinct distribution channels (e.g. private clinics, Hospitals, etc.). The identification of the SNP that confers genetic intolerance to lactose is a robust routine in STAB VIDA laboratories The SNP, -13910 C/T (dbSNP rs#: 4988235), located in regulatory element of minichromosome maintenance complex component 6 (*MCM6*) gene, play a key role in the expression of the LCT gene, which is responsible for the production of the enzyme lactase that degrades lactose (Enattah et al. 2002, Bersaglieri et al. 2004). The lactase nonpersistance phenotype is considered the ancestral phenotype in humans, being the individuals incapable of digest lactose, suffering for from adverse unspecific abdominal symptoms after consumption of milk or dairy products (Haberkorn et al. 2011). The lactase persistence phenotype is more

prevalent in subjects of the north-western Europe (80–90%), compared to south and east (~50%) (Sahi 1994, Ingram et al. 2009). The -13910 C/T (dbSNP rs#: 4988235) is tightly associated with persistence of the lactase enzyme in the European adulthood population (Enattah et al. 2002). Individuals carrying one or both copy of the T allele (T/T or C/T) have enough enzyme activity in the intestinal cells to digest lactose. Contrariwise, individuals with no copy of the T allele (C/C) are unable to digest lactose and are classified as lactose nonpersistance. The prevalence of this SNP in the European population is heterogeneous, being more prevalent in the northern (70-80%) than in southern (5-10%) European population (Itan et al. 2010). The only report available for the Portuguese population claims, that the allele frequency of the -13910 C/T (dbSNP rs#: 4988235) is estimated at 37% (Coelho et al 2005).

Standard protocol for screening this SNP follows traditional expensive (≥ 25 €) and time-consuming (≈ 10 hours) conventional molecular biology techniques.It goes from sample preparation and DNA extraction, followed by conventional PCR target amplification and SNP identification by direct sequencing. The development of an isothermal strategy for DNA amplification and further genotyping characterization mediated by Au-nanoprobes and non-cross-linking method will be an alternative to the implemented laboratory routine and hereafter be applied to a POC system. As such, a LAMP based amplification protocol followed by Au-nanoprobe sequence identification for this SNP was designed and set up. The procedure and implication shall be discussed.

6.2 Results and Discussion

6.2.1 Loop-mediated isothermal amplification (LAMP) of commercial relevant target/SNP for STAB VIDA and detection mediated by Au-nanoprobes using the non-cross-linking approach

A total of 15 biological samples (A-O) were firstly amplified by conventional PCR and submitted to direct sequencing for SNP (dbSNP rs#:4988235) genotype assessment. The three possible genotypes are illustrated in Appendix II – Figure AII.1. The design of the set of primers for LAMP assays followed the guidelines from Notomi and co-workers (Tomita et al. 2008), always trying to respect the key points for optimal primer design and taking into account the limitations imposed by the specific DNA sequence. Moreover, a set of LAMP primers was designed so that the SNP were comprised between the linear region between F1c and B2.The best set of primers are depicted in Table 6.1.

Table 6.1 – LAMP primer design for *MCM6* SNP (dbSNP rs#: 4988235).

Primer	Site/Domain	Tm (ºC)		Sites/Domain distances (bp)		
		Expected	Obtained		Expected	Obtained
LAMPLacF3	-	(59-61)	58	F2-F1c	40~60	60
LAMPLacB3	-		58	B2-B1c	40~60	55
LAMPLacFIP	F1c	(64-66)	57	F2-B2	<200	193
	F2	(59-61)	58	F3-F2	0~60	0
LAMPLacBIP	B1c	(64-66)	63	B3-B2	0~60	16
	B2	(59-61)	58			

The optimal temperature for the LAMP reaction was 65ºC and only after 1 hour of reaction it was possible to detect by agarose gel electrophoresis the LAMP reaction products. Nevertheless, for greater LAMP products yield, 1.5 hours or moreof reaction was needed (Figure 6.3B). Moreover, using restriction enzyme digestion with a single cut restriction enzyme (*SpeI*), followed by agarose gel electrophoretic analysis, it was possible to confirm amplification of the desired amplicon (Figure 6.3 A). After positively confirming the double strand DNA fragment of ~130 and 160 bp, each specifically achieved by *SpeI* digestion, it was possible conclude that all the 15 samples were successfully amplified *via* LAMP for subsequent identification with a set of two Au-nanoprobes for *MCM6* (dbSNP rs#: 4988235) detection (Figure 6.3 C).

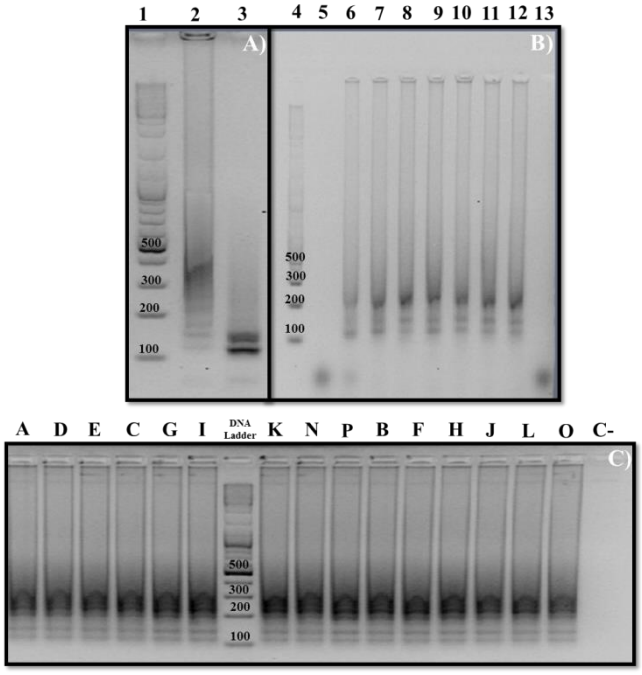

Figure 6.3 – Agarose gel electrophoresis of LAMP product of *MCM6* (dbSNP rs#: 4988235) optimization and biological sample amplification.A) LAMP product at 65 ºC for 1 hour (Lane 2) and digested with *SpeI* (Lane 3). **B)** Reaction time optimization (Lane 5 to 12). First time point was 30 minutes (Lane 5) and subsequent time points were taken every 30 minutes until a total of 4 hours (Lane 12). Lane 13 corresponds to the negative control. **C)** LAMP products of all the 15 biological samples ("A" to "O"). Lane "C-" corresponds to the negative control.

As previously performed for the *FTO*, *PPARG* and *APOA5* SNPs, two set of Au-nanoprobes were design to specifically target the *wild type* allele (T) (LAMPwt_MCM6) and the

mutated allele (C) (LAMPmut_MCM6) of the dsSNP rs#: 4988235. Both Au-nanoprobes were functionalized with 20 bp long modified oligonucleotide and a surface coverage ratio of AuNP:oligo of 1:200. Both Au-nanoprobes presented very similar salt-induced aggregation stability profiles, ranging between 20 and 25 mM $MgCl_2$ (final concentration) for LAMPwt_MCM6 and LAMPmut_MCM6, respectively. For the LAMPmut_MCM6 Au-nanoprobe, the LOD determined was between 25-30 ng.μL^{-1} for colorimetric detection and r(Abs) discrimination between fully complementary and single-base mismatch targets. From all the 15 biological samples successfully amplified via LAMP, 12 hybridize with LAMPmut_MCM6 Au-nanoprobe, retaining the characteristic red/pink color and the rAbs (525/569) nm was higher than 1, which indicates the presence of heterozygous or homozygous for the mutated allele status. The other 3 samples did not hybridize with the LAMPmut_MCM6 Au-nanoprobe and the solution shifted from red to blue in the first minutes after salt addition, aggregation that was confirmed by the rAbs (525/569) nm lower than 1 (Figure 6.4).After comparison between the genotyping results obtained via-direct sequencing and from the LAMPmut_MCM6 Au-nanoprobe genotyping method it was possible to identify a positive correlation for all 15 samples between both methods. The 12 samples positively identified with the LAMPmut_MCM6 Au-nanoprobe, half was heterozygous and the other half was homozygous for the mutated allele via direct sequencing. Moreover, the three samples that fully aggregated in the presence of the LAMPmut_MCM6 Au-nanoprobe were characterized as *wild type* by direct sequencing.

For LAMPwt_MCM6 Au-nanoprobe, even at high concentrations of fully complementary target (e.g. 120 ng. μL^{-1}*wild-type* LAMP product), the solution aggregated, changing color from red to blue in the first minutes (< 3 minutes) after salt addition. Several new Au-nanoprobe functionalization's were performed, but despite all efforts the final results were always equal: a full pattern of aggregation was obtained, not only for the fully complementary target but also for the other targets, in the first minutes upon salt addition. Although the LAMPmut_MCM6 Au-nanoprobe was capable of identifying their respective targets, the results given by the LAMPwt_MCM6 Au-nanoprobe compromised the advantages and value given by a faster, sensitive and more suitable POC amplification method like LAMP. The discrimination between homo- and heterozygous status, possible to be performed in the non-cross-linking method with a set of two Au-nanoprobes was not achieved for the *MCM6* gene (dbSNP rs:# 4988235) (Table 6.2).

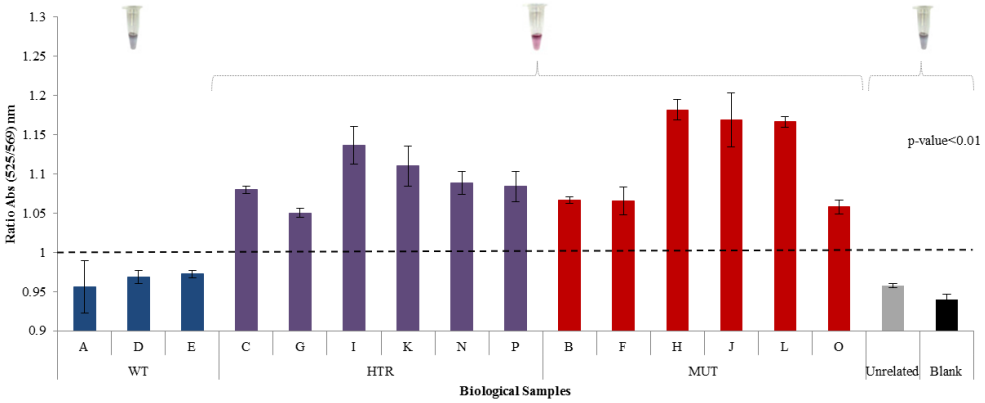

Figure 6.4 – Biological sample characterization of *MCM6* gene (dbSNP rs:# 4988235) by comparison between via-direct sequencing and Au-nanoprobe genotyping methods. Au-nanoprobesaggregation as measured by ratio of aggregation (ratio of SPR intensity at 525 and 569 nm) for the assay mixtures – 2.5 nM Au-nanoprobe (LAMPmut_MCM6), 10 mM phosphate buffer (pH 8), purified dsDNA targets (LAMP products) at a final concentration of 25 ng.µL^{-1}. All spectrophotometric data was collected 30 minutes after salt addition and error bars represent the standard deviation of three independent assays. The horizontal line represents the threshold of 1 considered for discrimination between positive (rAbs≥1) and negative (rAbs<1) result. A representative colorimetric results is showed upon each result bar – red, positive result; blue/purple, negative result. The direct sequencing results indicate the presence of three *wild-type* samples (A/D/E), 8 heterozygous (C/G/I/K/N/P) and 6 homozygous for the mutated allele (B/F/H/J/L/O). The Au-nanoprobe genotyping method positively (solution remains red) identified the heterozygous and homozygous status for the mutated allele and no hybridization was attained in the presence of a wild-type or unrelated sample (red-shift from red to blue – aggregation).

With this in mind, a new LAMP approach was attempted taking advantage of the high sensitivity of LAMP method and the benefits of allele specific (AS) or Amplification-refractory mutation system (ARMS) to allow, *a priori*, discrimination between the homo- andheterozygous status, using then Au-nanoprobes as a reviling agent as an "on-off" mechanism. This new approach, that will be discussed in the next topic of the thesis, was also addressed for the *MCM6* gene SNP (dbSNP rs:# 4988235).

Table 6.2- Comparison between genotyping methods for the SNP rs4988235 present in the *MCM6* gene. (+/+) *wild type* genotype–T/T; (+/-) heterozygous genotype-C/T; (-/-) mutated genotype-C/C; n/a-not available. [a] Samples that differ between genotyping methods marked in red.

Sample Code	Sanger Sequencing Genotyping	Au-nanoprobe Genotyping	
		LAMPwt_MCM6	LAMPmut_MCM6
A	+ / +	n/a	+/+
B	- / -	n/a	- / -
[a]C	+ / -	n/a	- / -
D	+ / +	n/a	+/+
E	+ / +	n/a	+/+
F	- / -	n/a	- / -
[a]G	+ / -	n/a	- / -
H	- / -	n/a	- / -
[a]I	+ / -	n/a	- / -
J	- / -	n/a	- / -
[a]K	+ / -	n/a	- / -
L	- / -	n/a	- / -
[a]N	+ / -	n/a	- / -
O	- / -	n/a	- / -
[a]P	+ / -	n/a	- / -

6.2.2 Allele-specific loop-mediated isothermal amplification (AS-LAMP) of commercial relevant target/SNP for STAB VIDA and detection mediated by Au-nanoprobe using the non-cross-linking approach

The conventional allele-specific PCR usually used for SNP genotyping (Gaudet et al. 2009) is based on the standard that the desired allele is readily amplified by the presence of specific matched primer set, but not amplified in the presence of a mismatched primer set, especially if the mismatch is located at the 3´-terminal base of the primer (Sommer et al. 1992). This system can be translated to an isothermal amplification, like LAMP, with slight variations. In conventional allele-specific PCR the primers can be design to present products of different lengths, which can be further separated and easily visualized by agarose gel electrophoresis. Moreover, the different products lengths allow that the amplification reaction occurs in a single tube, since each allele will have their specific and known size (Liu et al. 2012). Both of these premises are impossible for the AS-LAMP approach. LAMP products, as it was seen in the previous topic of this chapter (See Chapter 6, section 6.2.1 Figure 6.3 C), have a broad range of different product sizes, which make impossible for specific primer design to attained the discrimination between alleles by product size, furthermore and for this reason, each allele amplification has to occur in separate tubes, otherwise it will be impossible to understand which allele was amplified. The first and only approach used for AS-LAMP was published by Badolo and co-workers (Badolo et al. 2012), were is described the detection of a specific SNP (West African-type kdr mutation) trough specifically designing two BIP primers specific to each allele (*wild-type* and mutated), with the mutation on the 3'end of the B2 primer (5' end of the BIP primer) and an additional mismatched nucleotide in the penultimate position (Figure 6.5).

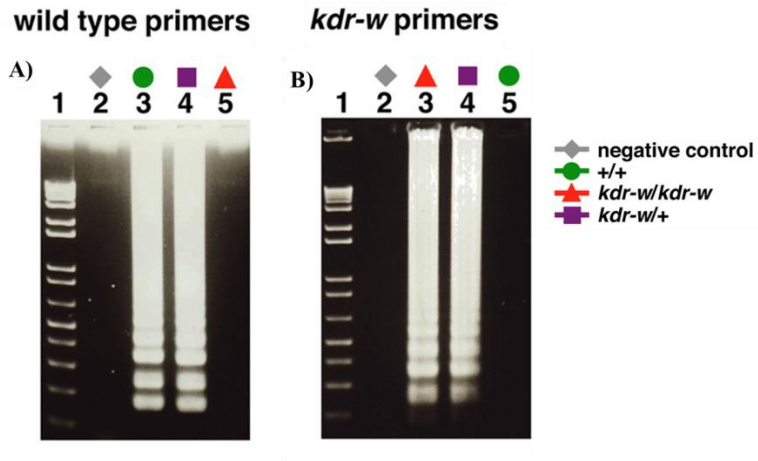

Figure 6.5 – AS-LAMP SNP detection by Badolo and co-workers. SNP detection by AS-LAMP mediated by agarose gel electrophoretic analysisof **A)***wild type* primers BIP primer only amplify wild-type (+/+) or heterozygous (kdr-w/+) samples, **B)** mutated primer only amplify heterozygous (kdr-w/+) or mutated (kdr-w/kdr-w) samples.

The same strategy used for Badolo and co-workers was applied to the MCM6 (dbSNP rs#: 4988235) SNP detection with a slight variation – the allele-specific primer was designed to be at the F3 primer instead of the BIP (B2 domain) primer. Since LAMP amplification depends on the formation of the loop structure at both ends (dumbbell-like structure), that is the initial material for the subsequent LAMP DNA amplification and elongation steps, it was speculated if the discrimination between alleles could be achieved before the formation of the first loop and subsequent released of the single stranded DNA formed, to ensure that no material was available for further amplification (Figure 6.6).

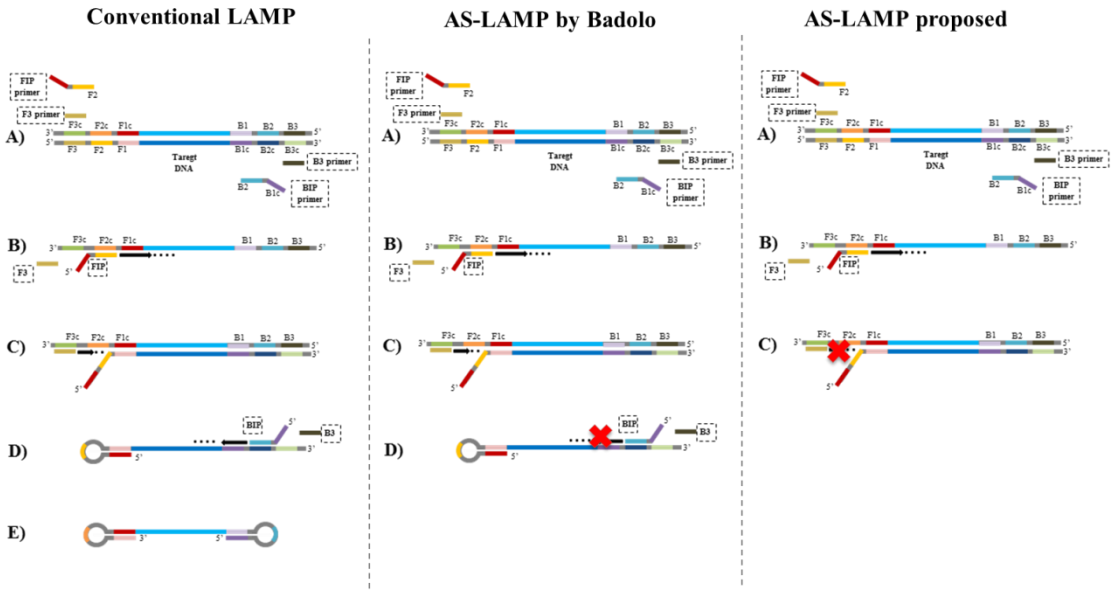

Figure 6.6 – Different approaches for the AS-LAMP method. A) Schematic representation of conventional loop-mediated isothermal amplification (LAMP) **B)** AS-LAMP approach from Badolo and co-workers (Badolo et al. 2012). Discrimination between wild-type and mutated allele is given by the BIP primer (domain B2) **C)** AS-LAMP approach proposed in this thesis. Discrimination could be attained by the F3 primer.

Optimization was addressed for the proposed AS-LAMP. Firstly, it was observed that for the primer that perfectly matched the mutated allele, an additional mismatched nucleotide (adenine) in the penultimate position need to be inserted, since the primer/template mismatch strength was considered weak (T/G) (Zhu et al. 1996). The addition of the mismatched nucleotide was done accordingly to the terminal mismatch and penultimate nucleotide in the primer (Little, 2001). A temperature gradient reaction (Figure 6.7) was performed for the F3 primers and it was possible to determine that both primers presented optimal function at higher temperatures (66 ºC), probably functioning as a stringency condition. For the F3 *wildtype* primer at 66 ºC after 75 minutes of reaction, only *wild type* and heterozygous samples were amplified (Figure 6.7A), the opposite was observed for the F3 mutated primer, amplification only occurs with heterozygous and mutated samples (Figure 6.7B).

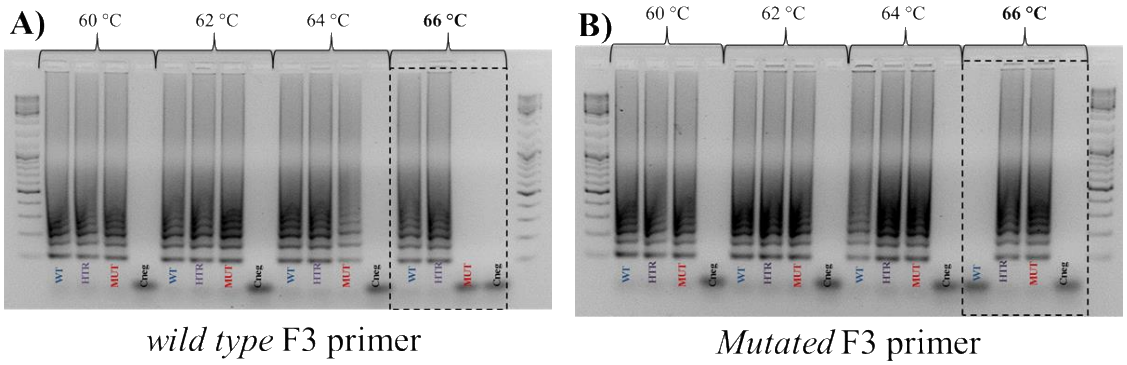

Figure 6.7 – AS-LAMP temperature gradient analyses for wild type and mutated F3 primers in a 2% agarose gel electrophoresis.A) AS-LAMP temperature gradient with F3*wild type* primer **B)** AS-LAMP temperature gradient with F3mutated primer.

The proof-of-concept of the proposed isothermal method of amplification was achieved using 2 biological samples of each genotype, previously genotyped for the *MCM6* (dbSNP rs#: 4988235) either by direct sequencing or by non-cross-linking approach (LAMPmut_MCM6). As it is possible to see in Figure 6.8, from agarose gel electrophoresis analysis, when the amplification reaction was performed with the F3 *wild type* primer, it was only possible to obtain the characteristic LAMP amplification pattern with *wild type* (A and D) and heterozygous (C and G) samples, while no amplification was achieved for fully mutated (F and M) or absence (Cneg) samples. The opposite result was attained with the F3 mutated primer, only in the presence of heterozygous (C and G) or mutated (F and M) samples amplification was successfully visualized in electrophoresis analysis, while in the presence of a *wild type* (A and D) or absence (Cneg) of samples no amplification occurred. The assay was performed in triplicate.

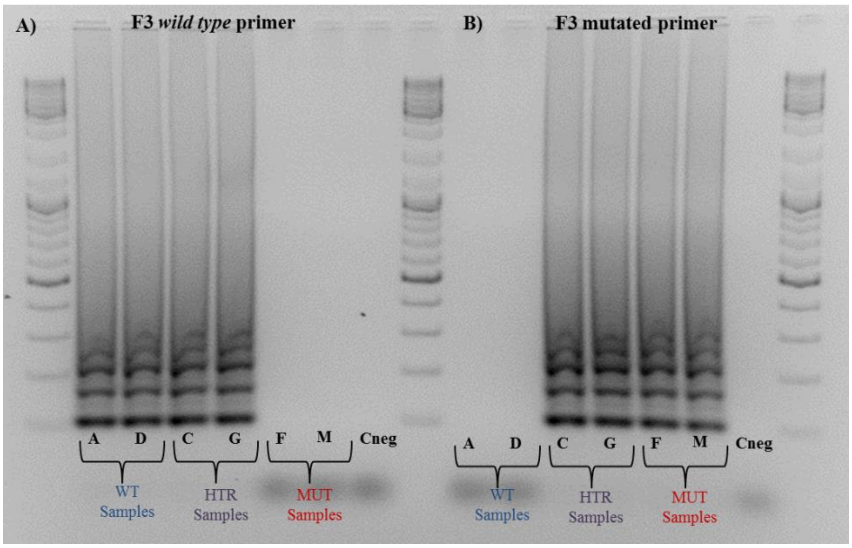

Figure 6.8 – Proof-of-concept of AS-LAMP proposed. Electrophoretic analysis in 2% agarose gel of AS-LAMP products from 6 biological samples. **A)** AS-LAMP with F3*wild type* primer amplification. Amplification only attained for *wild type* (A and D) heterozygous (C and G) samples. **B)** AS-LAMP with F3*wild type* primer amplification. Amplification only attained for heterozygous (C and G) and mutated (F and M) samples.

After validation of the proposed isothermal amplification method with biological samples, a Au-nanoprobe was synthesized with a specific sequence of amplification product. Unlike it was previously done for each SNP detection using the non-cross-linking method, where a set of two Au-nanoprobes were synthesized for the detection of each allele and strictly needed for determining sample genotype status, the allele descrimination for the *MCM6* (dbSNP rs#: 4988235) was obtained by the AS-LAMP and a single Au-nanoprobe could be used to detect the presence or absence of the AS-LAMP product. In other words, like a fluorescent probe is used for probe-target hybridization detection (Kreil et al. 2006), the Au-nanoprobe here would be used as an inexpensive, realibe, fast and equipment free revealingagent of the duplex Au-nanoprobe/taregt formed in comparison with the traditional, expensive, time-consuming and power supply dependent agarose gel electrophoresis. Consequently, an Au-nanoprobe, named ASLAMP_MCM6, was synthesized with 20 bp long modified oligonucleotide and a surface coverage ratio of AuNP:Oligo of 1:200.

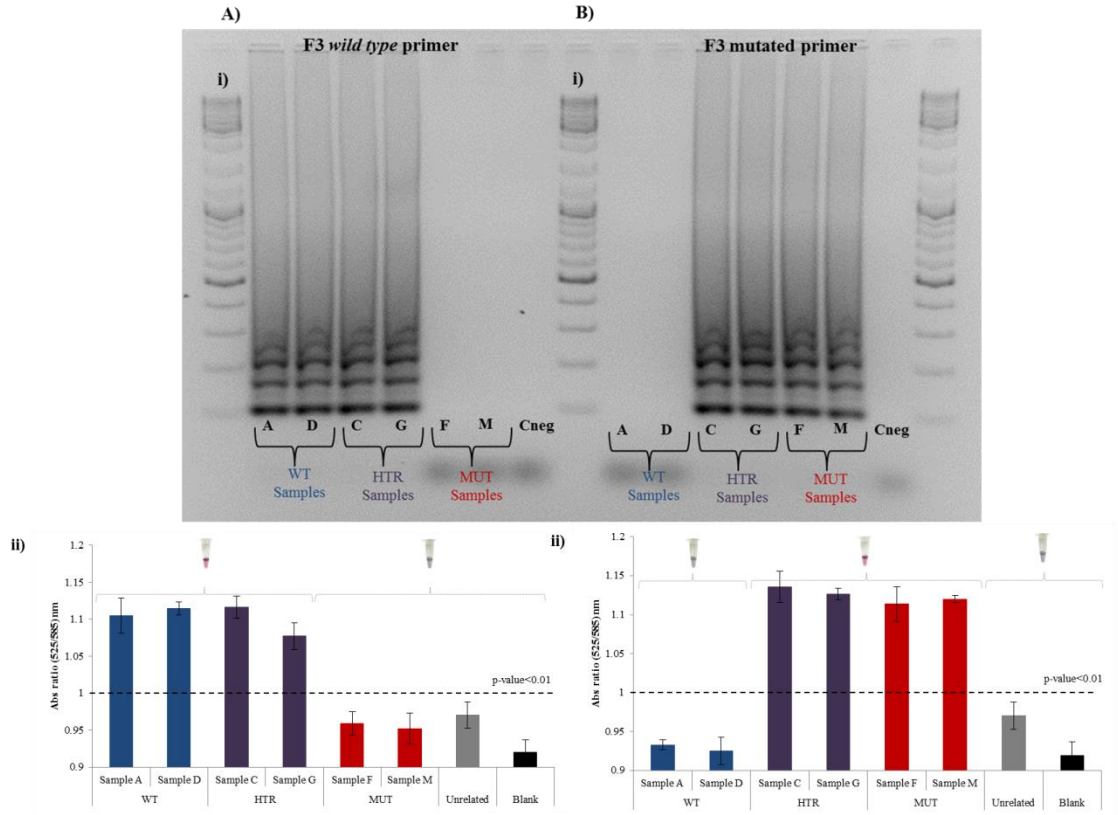

Figure 6.9 – Detection of AS-LAMP products mediated by the non-cross-linking approach. Au-nanoprobe aggregation as measured by ratio of aggregation (ratio of SPR intensity at 525 and 585 nm) for the assay mixtures - 2.5 nM Au-nanoprobe (ASLAMP_MCM6), 10 mM phosphate buffer (pH 8), purified dsDNA targets (LAMP products) at a final concentration of 20 ng.µL^{-1}. All spectrophotometric data was collected 30 minutes after salt addition and error bars represent the standard deviation of three independent assays. The horizontal line represents the threshold of 1 considered for discrimination between positive (rAbs≥1) and negative (rAbs<1) result. A representative colorimetric results is showed upon each result bar – red, positive result; blue/purple, negative result. **A) i)** AS-LAMP amplification carried out with F3 wild type primer and **ii)** previous detection by the non-cross-linking method with ASLAMP_MCM6 Au-nanoprobre; **B)i)** AS-LAMP amplification carried out with F3 mutated primer and **ii)** previous detection by the non-cross-linking method with ASLAMP_MCM6 Au-nanoprobe.

The salt-induced aggregation stability profile of ASLAMP_MCM6 Au-nanoprobe was reached at 20 mM of $MgCl_2$. Each final AS-LAMP amplification products of both F3 primers previously obtained were set for Au-nanoprobe hybridization assay. The Au-nanoprobe was capable of identify the presence of AS-LAMP products from both F3 primers reaction, since in the presence of target the Au-nanoprobe solution remain unaltered, while in the absence of AS-LAMP or in the presence of a unrelated target, no hybridization occurred and the solution changed color from red to blue. All the color changes were corroborated by visible spectra and the rAbs (525/585) (Figure 6.9).

6.3 Concluding Remarks

6.3.1 Development and characterization of gold nanoprobes for SNP/mutation detection

It was demonstrated in this Chapter and in Chapter 4, the strengths and weakness of the non-cross-linking method for the detection of single-base substitutions. It is a very flexible approach since it is possible to apply the technique in different biological targets, always generating results with high degree of sensitivity and specificity (Veigas et al 2010, Doria et al. 2010b, Rosa et al. 2012, Carlos et al. 2014). Moreover, this approach only requires mixing solutions and heat/cooling the samples may be considered a user-friendly method. Also, in 30 minutes or less, full genotype characterization of a biological sample can be attained with an overall cost €0.05/test for one mismatch analysis that already is prone to be integrated in portable application (Veigas et al. 2012). Nevertheless, some drawbacks can also be point out for the non-cross-linking method. The need of a set of two functional Au-nanoprobes for SNP full genotype characterization, as it was shown in Chapter 4 (Please see section 4.2.4), capable of identify their respective targets and discriminates between fully complementary and single-base mismatch targets, is not always possible to achieve. Moreover, the reduced flexibility in Au-nanoprobe design is an obstacle, since it is crucial that the SNP islocated at the 3'-end of the Au-nanoprobe for better discrimination (Doria et al. 2010). Finally, for further implementation in POC systems, a PCR-based approach, normally used for target amplification, for further detection with Au-nanoprobe requires thermal cycling apparatus that is undesirable for a POC instrument (Zhang et al. 2007). In summary, making use of the advantages and improving the limitations of the non-cross-linking method, like it was demonstrated in this chapter, SNP detection and full genotype characterization can be achieved with a single Au-nanoprobe instead of a set of two in allele-specific isothermal conditions, ideal to be integrated into future microfluidic devices. Moreover, since AS-LAMP turns SNP detection into a presence or absence of target discrimination, lower limit of detection can be achieved. Also, the need of only one Au-nanoprobe that is used as a targeting and revealing agent, instead of two, turns the system cheaper. Based on these

considerations, a prototype design for future development based on AS-LAMP and the non-cross linking approach for targeting relevant SNP with commercial interest for STAB VIDA can be seen in Figure 6.10.

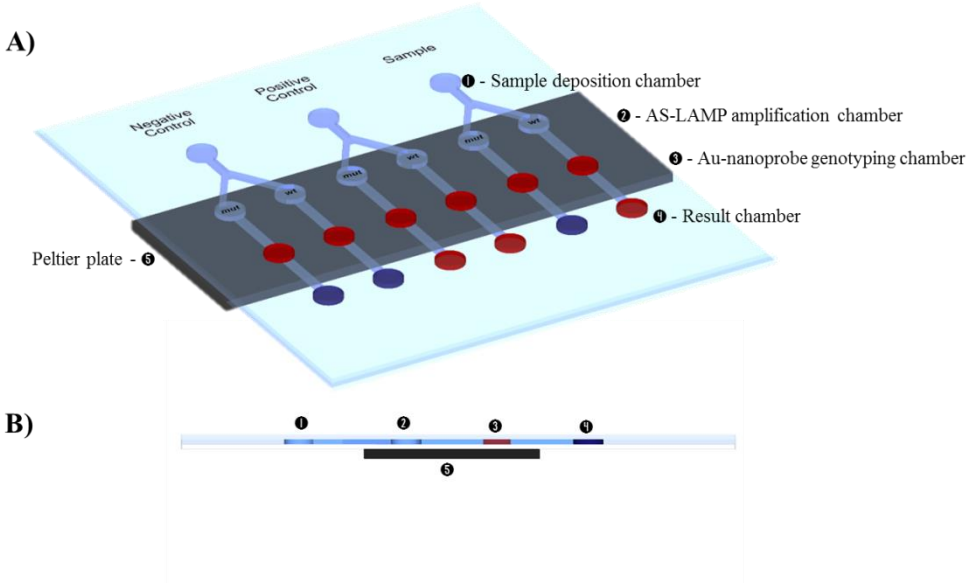

Figure 6.10 – Prototype design for future development for targeting relevant SNP based on AS-LAMP and the non-cross linking approach. The first chamber (1) is intended to biological material deposition (e.g. saliva) and further purification by capillary force implemented by sample migration to the second chambers developed for template amplification mediated by allele–specific isothermal conditions (2). The third section (3), developed for Au-nanoprobe/target hybridization assay for full genotype characterization that will be read-out in the final result chamber (4) containing a salt solution. No color changing can be visible in the result chamber designated for the positive control and the contrary, shift from red to purple, has to been achieved for the negative control in order to guarantee a validate test. (5) A peltier plate responsible for generating temperature to the amplification and genotyping chambers.

CHAPTER 7 - FINAL CONSIDERATIONS AND FUTURE PERSPECTIVES

The completion of the Human Genome Project (Venter et al. 2001) contributed with powerful tools that allowed understanding genetic factors that may significantly modulate the development of particular conditions. In parallel, the advent of novel genetic screening methods considerably increased the amount of information to be used for comprehensive evaluation of these traits. Amongst numerous efforts, results acquired in large epidemiological studies, namely GWAS, have identified millions of single SNPs and tagged SNPs linked to susceptibility to complex traits and that can be consider has potential biomarkers for predicative risk assessment (Shastry et al. 2002). These paved the way for the development of a new era in the healthcare area, where personalized medicine can be used to improve the chances of early detection of onset and/or used as surveillance tool to a more precise guide for medical management (Abul-Husn et al. 2014).

The available information, together with the awareness between the population of the importance of genetic factors for disease/condition onset and progression, has prompted for high demand of DNA testing. Throughout the last decade, the developed world has seen the expansion of genetic testing, gradually moving from the high technical ground of intensive medicine towards the average healthcare user. The demand for DNA testing at point-of-care or point-of-need, capable of rapidly sensing with high degree accuracy and sensitivity biomarkers of susceptibility to for human diseases has been on the rise (Jani and Peter 2013). This sector of biosensing is a growing and sustained market that is expected to be worth $US19.3 billion 2018 and a CAGR of 4% (Scientia Advisors 2013).

The development of POC systems for nucleic acid detection is one of growing R&D lines of STABVIDA. STABVIDA, a Portuguese biotech company leader in the Iberian Peninsula in providing genomics services (e.g. Sanger Sequencing, Next Generation Sequencing, oligonucleotides synthesis, etc.), has expand its portfolio in 2008 with a variety of human genetic testing (obesity screening, celiac disease, lactose intolerance, parental testing, etc.) in collaboration with healthcare institutions (e.g.: Hospital, private clinics, etc.). The main approach has been performed through physician counseling and supervision using a POC collection kit for biological sample (saliva/blood), which is later processed and analyzed by specialized and qualified personnel at STABVIDA's laboratory using direct sequencing. The main purpose for STABVIDA to co-finance this thesis (through a shared entrepreneurship grant with FCT) was to develop and validate a nanotechnology approach for acid nucleic detection and improve laboratory routine with faster, less cumbersome and expensive methods, while paving the way for the development of new nanotechnology-based POC instrumentation for acid nucleic acid detection.

Nanodiagnostics methodologies have the ability to make molecular biological tests quicker, more sensitive and flexible at reduced costs (Jain 2003, Azzazy et al. 2006). Despite the wide range of nanoscale systems being used for biomolecular assays in general, AuNP-based

systems have been the most widely used due to their unique physicochemical properties, and are becoming a critical component in the development of nanotechnology-based detection systems (Goluch et al. 2006, Baptista et al. 2008, Zanoli et al. 2012).

The first objective of this thesis consisted in the assessment and evaluation of the association risk of obesity in the Portuguese population for three obesity-related single-nucleotide gene polymorphisms with commercial interest for STABVIDA: fat-mass and obesity-associated – *FTO* (dbSNP rs#: rs9939609); peroxisome proliferator-activated receptor gamma – *PPARG* (dbSNP rs#: rs1801282); and apolipoprotein A-V – *APOA5* (dbSNP rs#: rs662799). This association study presented in **Chapter 3** and the data therein discussed were considered a pre-requisite for the final assay development – fully characterize a population in a condition of interest within the portfolio of genetic screenings provided by STABVIDA. All the genotyped data generated by direct sequencing (~1200 sequencing data files) and its statistical analysis allowed to find significant differences in allelic expression of *FTO* (dbSNP rs#: rs9939609) ($p<0.05$) between control and case groups, indicating a 2.5-higher risk for obesity in the presence of both risk alleles when comparing the control group with the obese group. A fourfold-higher risk was found for subjects with class III obesity compared to those with classes I and II. Moreover, significant mean differences for the *FTO loci* to BMI (p-value=0.025), percentage of fat mass (p-value=0.033), total fat mass (p-value= 0.013) and for waist perimeter (p-value=0.022) were also found. No significant differences in BMI or any other anthropometric trait studied were found between the control and case groups for *PPARG* (dbSNP rs#: rs1801282) and *APOA5* (dbSNP rs#: rs662799) ($P>0.05$). This data is in agreement for what has been found for European population and sub-populations for the 3 genotyped SNPs obesity-related (Wang et al. 2014). From a total of 72 susceptibility *loci* already identified for BMI *via* global GWAS, *FTO* (dbSNP rs#: rs9939609) is the one *loci* that gathers greater consensus as being an important marker in obesity risk assessment within the European population (Tan et al. 2014). Like it has been linked for other populations of European origin, it was found that *FTO* (dbSNP rs#: rs9939609) in obese women is probably a determining factor for the development of intermediate hyperglycemia and diabetes (Kalnina et al. 2013) and the presence of the T-allele is associated to higher insulin sensitivity favoring the maintenance of normoglycemia in women suffering from obesity. Thus, for the first time, a study involving an adult Portuguese population shows that individuals harboring both risk alleles in the *FTO* gene *locus* present high risk for obesity and that *FTO* (dbSNP rs#: 9939609) could be a useful tool for the clinical management and risk assessment of obesity.

Following the characterization of the target population, a set of Au-nanoprobes for the detection and discrimination between the homo- or heterozygote condition for *FTO* (dbSNP rs#: rs9939609) using the non-cross-linking method, with high degrees of sensitivity and specificity, was developed, optimized and validated and the results are shown in **Chapter 4**. The non-cross-

linking method for nucleic acid detection has already been successfully applied in human SNP/mutation detection (Doria et al. 2007), gene expression (Baptista et al. 2005), RNA quantification, (Conde et al. 2012a) pathogen detection in clinical samples (Costa et al. 2010, Andreadou et al. 2014, Chan et al. 2014) or identification of molecular signatures of antibiotic resistance (Veigas et al. 2014). During the characterization and optimization of the Au-nanoprobes the for detection and discrimination between genotype status of the *FTO* SNP using the non-cross-linking approach, it was possible to conclude that Au-nanoprobes with longer thiol-modified oligonucleotide (20 bp) and higher surface coverage ratio AuNP:oligo (1:200) presented better discrimination efficiency (See Chapter 4 Sub-section 4.2.2.2). This was also valid for Au-nanoprobes synthesized to detect other targets, namely, *PPARG* (dbSNP rs#: rs1801282) and *APOA5* (dbSNP rs#: rs662799).

Validation of the non-cross-linking approach against direct DNA sequencing (gold standard technique) for *FTO* (dbSNP rs#: rs9939609) was imperative in order to compare sensitivity and specificity between genotyping techniques. It possible to discriminate between homo- and heterozygous status using a set of two Au-nanoprobes for *FTO* (dbSNP rs#: rs9939609) in blind tests, but also, after optimization, it was possible to simplify detection *via* a single Au–nanoprobe. This Au-nanoprobe is able of genotyping a homo- or heterozygote condition for a single SNP. For the first time, it was shown that the use of a single Au–nanoprobe can detect SNP for each genetic status (wild type, heterozygous, or mutant) with high degrees of sensitivity (87.50%) and specificity (91.67%). The results were attained in less than 4 h, including PCR amplification from collected samples, and the use of a single Au–nanoprobe simplifies integration in a disposable device for use at the point of care (POC). Nevertheless, further optimization toward increased specificity, lower misidentifications and elapsed time and subsequent validation are still required before translation to routine screening in POC. Two reported strategies can be addressed to increase hybridization specificity: i) The use of spacer d(T) sequences between the thiol group and the probe sequence. This can dramatically increase the hybridization efficiency, since d(A)-rich oligonucleotide strands interact in a higher degree with the AuNPs surface than d(T)-rich oligonucleotide strands. For that reason d(T) spacers may extend perpendicular from the AuNP surface, promoting higher surface coverage, while d(A) spacers segments will partially block AuNP sites by lying flat on the particle surface (Demers et al. 2000, Milton et al. 2013). Nevertheless, it was reported that longer modified oligonucleotide (40 bp) may also increase Au-nanoprobes stability against salt induce aggregation which may compromise their use in the non-cross-linking approach (Doria 2010b). ii) The use of DNA analogs molecules such as LNA (locked nucleic acid) for nucleic acid detection can also be a strategy for increase hybridization specificity (Owczarzy et al. 2011, Briones and Moreno 2012). McKenzie and co-workers have reported higher hybridization affinity and specificity rates using thiol-modified LNA conjugates to the AuNPs instead of thiol-modified ssDNA for the recognition

of ssDNA and even for dsDNA (McKenzie et al. 2007). Nevertheless, the bottleneck of LNA moieties is their high cost of production, which will significantly increase the price of the non-cross-linking approach. To overcome the need of using expensive moieties or spacers in the Au-nanoprobes to attain high discrimination efficiency with the non-cross-linking method, an alternative method is proposed and discussed in **Chapter 6**. This approach is based in an isothermal amplification method (LAMP) that may be considered more suitable for future integration of the non-cross-linking method into a miniaturized POC system (Craw et al. 2012). The reduced complexity level needed for temperature control (unique temperature) and the generation of DNA amplification product in a shorter period of time (in some cases 1 hour or less), when compared to the conventional PCR (2 hours or more), are considered outstanding improvements. The novel allele-specific isothermal amplification (AS-LAMP) successfully developed in this thesis for the detection of SNP with commercial interest for STABVIDA (**Chapter 6**), brings the specificity and sensibility for allele discrimination to the technique itself, while the Au-nanoprobe due their colorimetric proprieties is used as a revealing agent for the presence or absence of target. This innovative combined approach reduces costs, since only one Au-nanoprobe is needed for full genotype characterization, and also reduces the required time for genotype identification. Most importantly, the method allows a more sensitive and specific hybridization event between Au-nanoprobe/target. Contrary to what happens in the SNP identification using a set of two Au-nanoprobes, no hybridization event will occur between Au-nanoprobe and a single-base mismatch target that may lead to Au-nanoprobe stabilization and undesirable color maintenance. Finally, the restriction imposed by the SNP location for Au-nanoprobe design, is easily overcome by leaving more regions for improved Au-nanoprobe design.

The integration of the non-cross-linking approach into a microfluidic platform was also achieved, as described in **Chapter 5**. The bio-microfluidic platform presented consists in a sensitive and accurate sensor for single nucleotide polymorphism detection based on Au-nanoprobes. In order to become a platform with sample-in-answer-out capability, further optimization should still be addressed. Still, the integration of the colorimetric proprieties of Au-nanoprobes in a microfluidic device is a worthy point to move towards the commercial interest of STABVIDA with this PhD thesis - line-out of a POC system for the detection of relevant DNA sequences and with commercial interest. The knowledge generated with this work has been and will be further transferred to STABVIDA – a full training plan will be performed in order to ensure a complete assimilation of the technology: training sessions with company laboratory staff (formation), complete tutorial with detailed protocols and manuals to ensure a successful reproduction of the methodologies and hands-on training activities. The technology transfer to STAB VIDA, when successfully achieved, will allow the use of Au-nanoprobes and the non-cross-linking approach to other potential targets. It can be easily applied to other relevant

mutations (i.e. deletions, insertions, chromosomal translocations, etc.) to the company due to the flexibility and high resolution (single base) of the method. Hereafter, the development of an autonomous microfluidic device that integrates a sample collection and preparation, amplification of the desired target isothermally and a read-out detection system will be further assessed by STABVIDA directive board. It is important to mention that the development of microfluidic device intended to be used for *in vitro* diagnostics in human samples, as to be in accordance with specific validation steps required to comply with regulation: IVD directive and CE marking. The development and manufacturing quality under ISO 9001:2008 quality standards can greatly facilitate and speed up this process.

In summary, the main objectives of this thesis were successfully achieved. It was possible to verify the relevance of 3 obesity-related SNPs in the Portuguese population using association study's methodology. A fast and low-cost nanotechnology-based technique was validated, in blind tests, with biological samples against the gold standard technique (Sanger Sequencing) for SNP genotyping, with high degree of sensitivity and specificity. This strategy is suitable to be applied as routine laboratory protocol and future extended to other relevant targets upon slight optimization. Moreover, a novel isothermal amplification method (AS-LAMP), suitable for POC application in a microfluidic platform, was efficiently developed to improve some constrains related to the non-cross-linking approach for full genotype characterization in biological samples. Further validation of this new approach for SNP tagging based on the non-cross-linking method can be addressed in a short term and be spanned to other potential targets with commercial interests in a medium term.

REFERENCES

1000 Genomes Project Consortium, Abecasis GR, Auton A, Brooks LD, DePristo MA, Durbin RM, Handsaker RE, Kang HM, et al. 2012. An integrated map of genetic variation from 1,092 human genomes. Nature. 491(7422):56-65.

Abete I, Navas-Carretero S, Marti A, Martinez JA. 2012. Nutrigenetics and nutrigenomics of caloric restriction. Prog Mol Biol Transl Sci. 108:323-46.

Abgrall P, Gué A-M. 2007. Lab-on-chip technologies: making a microfluidic network and coupling it into a complete microsystem—a review. Journal of Micromechanics and Microengineering. 17(5):0960-1317.

Abul-Husn NS, Owusu Obeng A, Sanderson SC, Gottesman O, Scott SA. 2014. Implementation and utilization of genetic testing in personalized medicine. Pharmgenomics Pers Med. 7:227-40.

Afonso AS, Pérez-López B, Faria RC, Mattoso LH, Hernández-Herrero M, Roig-Sagués AX, Maltez-da Costa M, Merkoçi A. 2013. Electrochemical detection of Salmonella using gold nanoparticles. Biosens Bioelectron. 40(1):121-6.

Agasti SS, Rana S, Park MH, Kim CK, You CC, Rotello VM. 2010. Nanoparticles for detection and diagnosis. Adv Drug Deliv Rev. 62(3):316-28.

Ahmad F, Hashsham SA. 2012. Miniaturized nucleic acid amplification systems for rapid and point-of-care diagnostics: a review. Anal Chim Acta. 733:1-15.

Ahmadian M, Suh JM, Hah N, Liddle C, Atkins AR, Downes M, Evans RM. 2013. PPARγ signaling and metabolism: the good, the bad and the future. Nat Med. 19(5):557-66.

Akey JM, Zhang K, Xiong M, Doris P, Jin L. 2001. The effect that genotyping errors have on the robustness of common linkage-disequilibrium measures. Am J Hum Genet. 68(6):1447-56.

Albert FW, Kruglyak L. 2015. The role of regulatory variation in complex traits and disease. Nat Rev Genet. 16(4):197-212.

Albuquerque D, Nóbrega C, Manco L. 2013. Association of FTO polymorphisms with obesity and obesity-related outcomes in Portuguese children. PLoS One. 8(1):e54370.

Alex S, TiwariA. 2015. Funtionalized Gold Nanoparticles: Synthesis, Properties and Applications – A Review. J Nanosci Nanotechnol. 15(3):1869-1894.

Andreadou M, Liandris E, Gazouli M, Taka S, Antoniou M, Theodoropoulos G, Tachtsidis I, Goutas N, et al. 2014. A novel non-amplification assay for the detection of *Leishmania* spp. in clinical samples using gold nanoparticles. J Microbiol Methods. 96:56-61.

Anselme I, Laclef C, Lanaud M, Rüther U, Schneider-Maunoury S. 2007. Defects in brain patterning and head morphogenesis in the mouse mutant Fused toes. Dev Biol. 304(1):208-20.

Apalasamy YD, Mohamed Z. 2015. Obesity and genomics: role of technology in unraveling the complex genetic architecture of obesity. Hum Genet. 4(4):361-74.

Ariza MJ, Sánchez-Chaparro MA, Barón FJ, Hornos AM, Calvo-Bonacho E, Rioja J, Valdivielso P, Gelpi JA, et al. 2010. Additive effects of LPL, APOA5 and APOE variant combinations on triglyceride levels and hypertriglyceridemia: results of the ICARIA genetic sub-study. BMC Med Genet. 29:11-66.

Asiello PJ, Baeumner AJ. 2011. Miniaturized isothermal nucleic acid amplification, a review. Lab Chip. 11(8):1420-30.

ASTM Standard E2456, 2006. 2012. Standard terminology relating to nanotechnology. ASTM International, West Conshohocken, PA.

Azzazy HM, Mansour MM, Kazmierczak SC. 2006. Nanodiagnostics: a new frontier for clinical laboratory medicine. Clin Chem. 52(7):1238-46.

Azzazy HM, Mansour MM. 2009. In vitro diagnostic prospects of nanoparticles. Clin Chim Acta. 403(1-2):1-8.

Badolo A, Okado K, Guelbeogo WM, Aonuma H, Bando H, Fukumoto S, Sagnon N, Kanuka H. 2012. Development of an allele-specific, loop-mediated, isothermal amplification method (AS-LAMP) to detect the L1014F kdr-w mutation in *Anopheles gambiae* s. l. Malar J. 11:227.

Bae KH, Chung HJ, Park TG. 2011. Nanomaterials for cancer therapy and imaging. Mol Cells. 31(4):295-302.

Baeumner AJ, Cohen RN, Miksic V, Min J. 2003. RNA biosensor for the rapid detection of viable *Escherichia coli* in drinking water. Biosens Bioelectron. 18(4):405-413.

Bao YP, Huber M, Wei TF, Marla SS, Storhoff JJ, Müller UR. 2005. SNP identification in unamplified human genomic DNA with gold nanoparticle probes. Nucleic Acids Res. 33(2):e15.

Baptista P, Doria G, Henriques D, Pereira E, Franco R. 2005. Colorimetric detection of eukaryotic gene expression with DNA-derivatized gold nanoparticles. J Biotechnol. 119(2):111-7.

Baptista P, Pereira E, Eaton P, Doria G, Miranda A, Gomes I, Quaresma P, Franco R. 2008. Gold nanoparticles for the development of clinical diagnosis methods. Anal Bioanal Chem. 391(3):943-50.

Baptista PV, Koziol-Montewka M, Paluch-Oles J, Doria G, Franco R. 2006. Gold-nanoparticle-probe-based assay for rapid and direct detection of *Mycobacterium tuberculosis* DNA in clinical samples. Clin Chem. 52:1433-4.

Bardia A, Holtan SG, Slezak JM, Thompson WG. 2007. Diagnosis of obesity by primary care physicians and impact on obesity management. Mayo Clin Proc. 82(8):927-32.

Bariohay B, Roux JA, Bonnet MS, Dallaporta M, Troadec JD. 2011. An update in the management of obesity: the weight of CNS targets. Recent Pat CNS Drug Discov. 6(3):164-80.

Barish GD, Narkar VA, Evans RM. 2006. PPAR delta: a dagger in the heart of the metabolic syndrome. J Clin Invest. 116(3):590-7.

BCC Research Healthcare Report. 2014. Technical Report Point of Care Diagnostics – Report Overview. BCC Research. Report Code: HLC043D.

Beamer BA, Yen CJ, Andersen RE, Muller D, Elahi D, Cheskin LJ, Andres R, Roth J, et al. 1998. Association of the Pro12Ala variant in the peroxisome proliferator-activated receptor-gamma2 gene with obesity in two Caucasian populations. Diabetes. 47(11):1806-8.

Bell J. 2004. Predicting disease using genomics. Nature. 429:453-456.

Ben Ali S, Ben Yahia F, Sediri Y, Kallel A, Ftouhi B, Feki M, Elasmi M, Haj-Taieb S, et al. 2009. Gender-specific effect of Pro12Ala polymorphism in peroxisome proliferator-activated receptor gamma-2 gene on obesity risk and leptin levels in a Tunisian population. Clin Biochem. 42(16-17):1642-7.

Beni V, Hayes K, Lerga TM, O'Sullivan CK. 2010. Development of a gold nano-particle-based fluorescent molecular beacon for detection of cystic fibrosis associated mutation. Biosens Bioelectron. 26(2):307-313.

Beni V, Zewdu T, Joda H, Katakis I, O'Sullivan CK. 2012. Gold nanoparticle fluorescent molecular beacon for low-resolution DQ2 gene HLA typing. Anal Bioanal Chem. 402(3):1001-1009.

Ben-Yoav H, Dykstra PH, Bentley WE, Ghodssi R. 2012. A microfluidic-based electrochemical biochip for label-free diffusion-restricted DNA hybridization analysis. Biosens Bioelectron. 38(1):114-20.

Bernacka-Wojcik I, Ribeiro S, Wojcik PJ, Alves PU, Busani T, Fortunato E, Baptista PV, Covas JA, et al. 2014. Experimental optimization of a passive planar rhombic micromixer with obstacles for effective mixing in a short channel length. RSC Adv. 4: 56013-56025.

Bernacka-Wojcik I, Lopes P, Catarina Vaz A, Veigas B, Jerzy Wojcik P, Simões P, Barata D, Fortunato E, et al. 2013. Bio-microfluidic platform for nanoprobe based DNA detection-application to *Mycobacterium tuberculosis*. Biosens Bioelectron. 48:87-93

Bernacka-Wojcik I, Senadeera R, Wojcik PJ, Silva LB, Doria G, Baptista P, Aguas H, Fortunato E, et al. 2010. Inkjet printed and "doctor blade" TIO2 photodetectors for DNA biosensors. Biosens Bioelectron. 25(5):1229-34.

Bernacka-Wojcik. 2014a. Design and development of a microfluidic platform for use with colorimetric gold nanoprobe assays [dissertation]. Universidade NOVA de Lisboa. 43-60 p.

Bersaglieri T, Sabeti PC, Patterson N, Vanderploeg T, Schaffner SF, Drake JA, Rhodes M, Reich DE, Hirschhorn JN. 2004. Genetic signatures of strong recent positive selection at the lactase gene. Am J Hum Genet. 74(6):1111-20.

Bhattacharyya D, Singh S, Satnalika N, Khandelwal A, Jeon SH. 2009. Nanotechnology, Big things from a Tiny World: a Review. International Journal of u- and eService, Science and Technology. 2(3):29-37.

Biswas A, Bayer IS, Biris AS, Wang T, Dervishi E, Faupel F. 2012. Advances in top-down and bottom-up surface nanofabrication: techniques, applications & future prospects. Adv Colloid Interface Sci. 170(1-2):2-27.

Bocher V, Pineda-Torra I, Fruchart JC, Staels B. 2002. PPARs: transcription factors controlling lipid and lipoprotein metabolism. Ann N Y Acad Sci. 967:7-18.

Briones C, Moreno M. 2012. Applications of peptide nucleic acids (PNAs) and locked nucleic acids (LNAs) in biosensor development. Anal Bioanal Chem. 402(10):3071-89.

Brookes AJ. 1999. The essence of SNPs. Gene. 234:177-186.

Brown KA, Park S, Hamad-Schifferli K. 2008. N ucleotide−Surface Interactions in DNA-Modified Au−Nanoparticle Conjugates: Sequence Effects on Reactivity and Hybridization. J Phys Chem C. 112(20):7517-7521.

Bruinsma, J. 2003. World agriculture: towards 2015/2030. An FAO perspective.Earthscan Publications.

Brust M, Walker M, Bethell D, Schiffrin DJ, Whyman R. 1994. Synthesis of thiol-derivatised gold nanoparticles in a two-phase liquid-liquid system. J Chem Soc Chem Commun. (7):801-802.

Burns MA, Johnson BN, Brahmasandra SN, Handique K, Webster JR, Krishnan M, Sammarco TS, Man PM, et al. 1998. An integrated nanoliter DNA analysis device. Science. 282(5388):484-7.

Buzzetti R, Petrone A, Caiazzo AM, Alemanno I, Zavarella S, Capizzi M, Mein CA, Osborn JA, et al. 2005. PPAR-gamma2 Pro12Ala variant is associated with greater insulin sensitivity in childhood obesity. Pediatr Res. 57(1):138-40.

Caballero B. 2007. The global epidemic of obesity: an overview. Epidemiol Rev. 29:1-5.

Cai W, Chen X. 2007. Nanoplatforms for targeted molecular imaging in living subjects. Small. 3(11):1840-54.

Camou S, Fujita H, Fujii T. 2003. PDMS 2D optical lens integrated with microfluidic channels: principle and characterization. Lab Chip. 3(1):40-5.

Cao X, Wang YF, Zhang CF, Gao WJ. 2006. Visual DNA microarrays for simultaneous detection of *Ureaplasma urealyticum* and *Chlamydia trachomatis* coupled with multiplex asymmetrical PCR. Biosens Bioelectron. 22(3):393-398.

Cao YC, Jin R, Mirkin CA. 2002. Nanoparticles with Raman spectroscopic fingerprints for DNA and RNA detection. Science. 297(5586):1536-1540.

Cao YC, Jin R, Thaxton CS, Mirkin CA. 2005. A two-color-change, nanoparticle-based method for DNA detection. Talanta. 67(3):449-55.

Carlos FF, Flores O, Doria G, Baptista PV. 2014. Characterization of genomic single nucleotide polymorphism via colorimetric detection using a single gold nanoprobe. Anal Biochem. 465:1-5.

Carlos FF, Silva-Nunes J, Flores O, Brito M, Doria G, Veiga L, Baptista PV. 2013. Association of FTO and PPARG polymorphisms with obesity in Portuguese women. Diabetes Metab Syndr Obes. 6:241-5.

Carreira H, Pereira M, Azevedo A, Lunet N. 2012. Trends of BMI and prevalence of overweight and obesity in Portugal (1995-2005): a systematic review. Public Health Nutr. 15(6):972-81.

Cepeda-Valery B, Chaudhry K, Slipczuk L, Pressman GS, Figueredo VM, Lavie CJ, Morris DL, Romero-Corral A. 2014. Association between obesity and severity of coronary artery disease at the time of acute myocardial infarction: another piece of the puzzle in the "obesity paradox". Int J Cardiol. 176(1):247-9.

Chan WS, Tang BS, Boost MV, Chow C, Leung PH. 2014. Detection of methicillin-resistant Staphylococcus aureus using a gold nanoparticle-based colourimetric polymerase chain reaction assay. Biosens Bioelectron. 53:105-11.

Chandak GR, Ward KJ, Yajnik CS, Pandit AN, Bavdekar A, Joglekar CV, Fall CH, Mohankrishna P, et al. 2006. Triglyceride associated polymorphisms of the APOA5 gene have very different allele frequencies in Pune, India compared to Europeans. BMC Med Genet. 7:76.

Chang CC, Wei SC, Wu TH, Lee CH, Lin CW. 2013. Aptamer-based colorimetric detection of platelet-derived growth factor using unmodified gold nanoparticles. Biosens Bioelectron. 42:119-23.

Chang CC, Chen CC, Wei SC, Lu HH, Liang YH, Lin CW. 2012. Diagnostic devices for isothermal nucleic acid amplification. Sensors (Basel). 12(6):8319-37.

Chapman S, Dobrovolskaia M, Farahani K, Goodwin A, Joshi A, Lee H, Meade T, Pomper M, et al. 2013. Nanoparticles for cancer imaging: The good, the bad, and the promise. Nano Today. 8(5):454-460.

Charriere S, Bernard S, Aqallal M, Merlin M, Billon S, Perrot L, Le Coquil E, Sassolas A, et al. 2008. Association of APOA5 -1131T>C and S19W gene polymorphisms with both mild hypertriglyceridemia and hyperchylomicronemia in type 2 diabetic patients. Clin Chim Acta. 394(1-2):99-103.

Chen ES, Furuya TK, Mazzotti DR, Ota VK, Cendoroglo MS, Ramos LR, Araujo LQ, Burbano RR, et al. 2010. APOA1/A5 variants and haplotypes as a risk factor for obesity and better lipid profiles in a Brazilian Elderly Cohort. Lipids. 45(6):511-7.

Chen SH, Lin KI, Tang CY, Peng SL, Chuang YC, Lin YR, Wang JP, Lin CS. 2009. Optical detection of human papillomavirus type 16 and type 18 by sequence sandwich hybridization with oligonucleotide-functionalized Au nanoparticles. IEEE Trans Nanobioscience. 8(2):120-131.

Chen SH, Wu VC, Chuang YC, Lin CS. 2008. Using oligonucleotide-functionalized Au nanoparticles to rapidly detect foodborne pathogens on a piezoelectric biosensor. J Microbiol Methods. 73(1):7-17.

Cherng YS, Su GDJ. 2014. Fabrication of polydimethylsiloxane microlens array on spherical surface using multi-replication process. J. Micromech Microeng. 24(1):015016.

Choi S, Goryll M, Sin, LYM, Wong PK, Chae J. 2011. Microfluidic-based biosensors toward point-of-care detection of nucleic acids and proteins. Microfluidics and Nanofluidics. 10(2):231-247.

Chua A, Yean CY, Ravichandran M, Lim B, Lalitha P. 2011. A rapid DNA biosensor for the molecular diagnosis of infectious disease. Biosens Bioelectron. 26(9):3825-3831.

Chun P. 2009. Colloidal Gold and Other Labels for Lateral Flow Immunoassays. In: Wong R, Tse H (eds) Lateral Flow Immunoassay. Humana Press. 1-19.

Church C, Moir L, McMurray F, Girard C, Banks GT, Teboul L, Wells S, Brüning JC, et al. 2010. Overexpression of Fto leads to increased food intake and results in obesity. Nat Genet. 42(12):1086-92.

Clark AL, Fonarow GC, Horwich TB. 2014. Obesity and the obesity paradox in heart failure. Prog Cardiovasc Dis. 56(4):409-14.

Clément K, Vaisse C, Lahlou N, Cabrol S, Pelloux V, Cassuto D, Gourmelen M, Dina C, et al. 1998. A mutation in the human leptin receptor gene causes obesity and pituitary dysfunction. Nature. 392(6674):398-401.

Coelho M, Luiselli D, Bertorelle G, Lopes AI, Seixas S, Destro-Bisol G, Rocha J. 2005. Microsatellite variation and evolution of human lactase persistence. Hum Genet. 117(4):329-39.

Conde J, Ambrosone A, Sanz V, Hernandez Y, Marchesano V, Tian F, Child H, Berry CC, et al. 2012. Design of multifunctional gold nanoparticles for in vitro and in vivo gene silencing. ACS Nano. 6(9):8316–8324.

Conde J, Bao C, Cui D, Baptista PV, Tian F. 2014a. Antibody-drug gold nanoantennas with Raman spectroscopic figerprints for in vivo tumour theranostics. J Control Release. 183:87–93.

Conde J, de la Fuente JM, Baptista PV. 2010. RNA quantification using gold nanoprobes-application to cancer diagnostics. J. Nanobiotechnology. 8:5.

Conde J, de la Fuente JM, Baptista PV. 2010a. RNA quantification using gold nanoprobes - application to cancer diagnostics. J Nanobiotechnology. 8:5.

Conde J, Dias JT, Grazú V, Moros M, Baptista PV, de la Fuente JM. 2014. Revisiting 30 years of biofunctionalization and surface chemistry of inorganic nanoparticles for nanomedicine. Front Chem. 2:48.

Conde J, Doria G, de la Fuente JM, Baptista PV. 2012a. RNA quantification using noble metal nanoprobes: simultaneous identification of several different mRNA targets using color multiplexing and application to cancer diagnostics. Methods Mol Biol. 906:71-87.

Conde J, Rosa J, de la Fuente JM, Baptista PV. 2013. Gold-nanobeacons for simultaneous gene specific silencing and intracellular tracking of the silencing events. Biomaterials. 34(10):2516-2523.

Cordeiro M, Giestas L, Lima JC, Baptista P. 2013. Coupling an universal primer to SBE combined spectral codification strategy for single nucleotide polymorphism analysis. J Biotechnol. 168(1):90-4.

Costa P, Amaro A, Botelho A, Inacio J, Baptista PV. 2010. Gold nanoprobe assay for the identification of mycobacteria of the *Mycobacterium tuberculosis* complex. Clin Microbiol Infect. 16(9):1464-1469.

Craw P, Balachandran W.2012. Isothermal nucleic acid amplification technologies for point-of-care diagnostics: a critical review. Lab Chip. 12(14):2469-86.

Curry T, Kopelman R, Shilo M, Popovtzer R. 2014. Multifunctional theranostic gold nanoparticles for targeted CT imaging and photothermal therapy. Contrast Media Mol Imaging. 9(1):53-61.

Dallongeville J, Cottel D, Wagner A, Ducimetière P, Ruidavets JB, Arveiler D, Bingham A, Ferrières J, et al. 2008. The APOA5 Trp19 allele is associated with metabolic syndrome via its association with plasma triglycerides. BMC Med Genet. 9:84.

Darbha GK, Lee E, Anderson YR, Fowler P, Mitchell K, Ray PC. 2008. Miniaturized Sensor for Microbial Pathogens DNA and Chemical Toxins. IEEE Sensors Journal. 8(6):693-700.

Dare S, Mackay DF, Pell JP. 2015. Relationship between Smoking and Obesity: A Cross-Sectional Study of 499,504 Middle-Aged Adults in the UK General Population. PLoS One. 10(4):e0123579.

Day FR, Loos RJ. 2011. Developments in obesity genetics in the era of genome-wide association studies. J Nutrigenet Nutrigenomics. 4(4):222-38.

De Caterina R, Talmud PJ, Merlini PA, Foco L, Pastorino R, Altshuler D, Mauri F, Peyvandi F, et al. 2011. Strong association of the APOA5-1131T>C gene variant and early-onset acute myocardial infarction. Atherosclerosis. 214(2):397-403.

de la Escosura-Muñiz A, Ambrosi A, Alegret S, Merkoçi A. 2009. Electrochemical immunosensing using micro and nanoparticles. Methods Mol Biol. 504:145-55.

de Morais MG, Martins VG, Steffens D, Pranke P, da Costa JA. 2014. Biological applications of nanobiotechnology. J Nanosci Nanotechnol. 14(1):1007-17.

Deeb SS, Fajas L, Nemoto M, Pihlajamäki J, Mykkänen L, Kuusisto J, Laakso M, Fujimoto W, et al. 1998. A Pro12Ala substitution in PPARgamma2 associated with decreased receptor activity, lower body mass index and improved insulin sensitivity. Nat Genet. 20(3):284-7.

Deliard S, Panossian S, Mentch FD, Kim CE, Hou C, Frackelton EC, Bradfield JP, Glessner JT. 2013. The missense variation landscape of FTO, MC4R, and TMEM18 in obese children of African Ancestry. Obesity. 21(1):159-63.

DeLong RK, Reynolds CM, Malcolm Y, Schaeffer A, Severs T, Wanekaya A. 2010. Functionalized gold nanoparticles for the binding, stabilization, and delivery of therapeutic DNA, RNA, and other biological macromolecules. Nanotechnol Sci Appl. 3(1):53–63.

DeMarco VG, Aroor AR, Sowers JR. 2014. The pathophysiology of hypertension in patients with obesity. Nat Rev Endocrinol. 10(6):364-76.

Demers LM, Mirkin CA, Mucic RC, Reynolds RA 3rd, Letsinger RL, Elghanian R, Viswanadham G. 2000. A fluorescence-based method for determining the surface coverage and hybridization efficiency of thiol-capped oligonucleotides bound to gold thin films and nanoparticles. Anal Chem. 72(22):5535-41.

Deng H, Xu Y, Liu Y, Che Z, Guo H, Shan S, Sun Y, Liu X, et al. 2012. Gold nanoparticles with asymmetric polymerase chain reaction for colorimetric detection of DNA sequence. Anal Chem. 84(3):1253-8.

Deng H, Zhang X, Kumar A, Zou G, Zhang X, Liang XJ. 2013. Long genomic DNA amplicons adsorption onto unmodified gold nanoparticles for colorimetric detection of *Bacillus anthracis*. Chem Commun (Camb). 49(1):51-53.

Di Taranto MD, Staiano A, D'Agostino MN, D'Angelo A, Bloise E, Morgante A, Marotta G, Gentile M, et al. 2015. Association of USF1 and APOA5 polymorphisms with familial combined hyperlipidemia in an Italian population. Mol Cell Probes. 29(1):19-24.

Dina C, Meyre D, Gallina S, Durand E, Körner A, Jacobson P, Carlsson LM, Kiess W, et al. 2007. Variation in FTO contributes to childhood obesity and severe adult obesity. Nat Genet. 39(6):724-6.

do Carmo I, Dos Santos O, Camolas J, Vieira J, Carreira M, Medina L, Reis L, Myatt J, et al. 2008. Overweight and obesity in Portugal: national prevalence in 2003-2005. Obes Rev. 9(1):11-9.

Do CB, Hinds DA, Francke U, Eriksson N. 2012. Comparison of family history and SNPs for predicting risk of complex disease. PLoS Genet. 8(10):e1002973.

Doo M, Kim Y. 2015. Obesity: interactions of genome and nutrients intake. Prev Nutr Food Sci. 20(1):1-7.

Dorajoo R, Blakemore AI, Sim X, Ong RT, Ng DP, Seielstad M, Wong TY, Saw SM, et al. 2012. Replication of 13 obesity loci among Singaporean Chinese, Malay and Asian-Indian populations. Int J Obes (Lond). 36(1):159-63.

Dorfmeister B, Cooper JA, Stephens JW, Ireland H, Hurel SJ, Humphries SE, Talmud PJ. 2007. The effect of APOA5 and APOC3 variants on lipid parameters in European Whites, Indian Asians and Afro-Caribbeans with type 2 diabetes. Biochim Biophys Acta. 1772(3):355-63.

Doria G, Baumgartner DG, Franco R, Baptista PV. 2010. Optimizing Au-nanoprobes for specific sequence discrimination. Colloids Surf B. Biointerfaces. 77(1):122-4.

Doria G, Dias JT, Larguinho M, Pereira E, Franco R, Baptista P. 2010a. AuAg-alloy-nanoprobes for Specific Nucleic Acid Detection. NSTI-Nanotech 2010 Proceedings. 3:62-65.

Doria G, Franco R, Baptista P. 2007. Nanodiagnostics: fast colorimetric method for single nucleotide polymorphism/mutation detection. IET Nanobiotechnol. 1(4): 53-7.

Doria G, Conde J, Veigas B, Giestas L, Almeida C, Assunção M, Rosa J, Baptista PV. 2012. Noble metal nanoparticles for biosensing applications. Sensors (Basel). 12(2):1657-87.

Doria G. 2010b. DNA nanoprobes for molecular detection [dissertation]. Universidade NOVA de Lisboa. 47-49 p.

Dreaden EC, Alkilany AM, Huang X, Murphy CJ, El-Sayed MA. 2012. The golden age: gold nanoparticles for biomedicine. Chem Soc Rev. 41(7):2740-79.

Duff DG, Baiker A, Edwards PP. 1993. A new hydrosol of gold clusters. 1. Formation and particle size variation. Langmuir. 9(9):2301-2309.

Eaton SB, Eaton SB, Sinclair AJ, Cordain L, Mann NJ. 1998. Dietary intake of long chain polyunsaturated fatty acids during the Paleolithic. World Rev NutrDietet. 83:12-23.

Edwards PP, Thomas JM. 2007. Gold in a metallic divided state--from Faraday to present-day nanoscience. Angew Chem Int Ed Engl. 46(29):5480-6.

Eichenbaum-Voline S, Olivier M, Jones EL, Naoumova RP, Jones B, Gau B, Patel HN, Seed M, et al. 2004. Linkage and association between distinct variants of the APOA1/C3/A4/A5 gene cluster and familial combined hyperlipidemia. Arterioscler Thromb Vasc Biol. 24(1):167-74.

Eknoyan G. 2008. Adolphe Quetelet (1796-1874) - the average man and indices of obesity. Nephrol Dial Transplant. 23(1):47-51.

Enattah NS, Sahi T, Savilahti E, Terwilliger JD, Peltonen L, Järvelä I. 2002. Identification of a variant associated with adult-type hypolactasia. Nat Genet. 30(2):233-7

Evaluation of measurement data – Guide to the expression of uncertainty in measurement JCGM 100:2008 (GUM 1995 with minor corrections). 2008. Paris: BIPM Joint Committee for Guides in Metrology.

Fall T, Hägg S, Mägi R, Ploner A, Fischer K, Horikoshi M, Sarin AP, Thorleifsson G, et al. 2013. The role of adiposity in cardiometabolic traits: a Mendelian randomization analysis. PLoS Med. 10(6):e1001474.

Fall T, Ingelsson E. 2014. Genome-wide association studies of obesity and metabolic syndrome. Mol Cell Endocrinol. 382(1):740-57.

Farooqi IS, O'Rahilly S. 2005. Monogenic obesity in humans. Annu Rev Med. 56:443-58.

Feuk L, Carson AR, Scherer SW. 2006. Structural variation in the human genome. Nat Rev Genet. 7(2):85-97.

Feynman RP. 1960. There's plenty of room at the bottom. Engineering and Science. 23:22-36.

Fischer J, Koch L, Emmerling C, Vierkotten J, Peters T, Brüning JC, Rüther U. 2009. Inactivation of the Fto gene protects from obesity. Nature. 458(7240):894-8.

Fisher RM, Burke H, Nicaud V, Ehnholm C, Humphries SE. 1999. Effect of variation in the apo A-IV gene on body mass index and fasting and postprandial lipids in the European Atherosclerosis Research Study II. EARS Group. 40(2):287-94.

Fogel RW, Costa DL. 1997. A theory of technophysio evolution, with some implications for forecasting population, health care costs, and pension costs. Demography. 34(1):49-66.

Frayling TM, Timpson NJ, Weedon MN, Zeggini E, Freathy RM, Lindgren CM, Perry JR, Elliott KS, et al. 2007. A common variant in the FTO gene is associated with body mass index and predisposes to childhood and adult obesity. Science. 316(5826):889-94.

Freemantle N, Holmes J, Hockey A, Kumar S. 2008.How strong is the association between abdominal obesity and the incidence of type 2 diabetes? Int J ClinPract. 62(9):1391-1396.

Frens G. 1973. Controlled Nucleation for the Regulation of the Particle Size in Monodisperse Gold Suspensions. Nature Phys. Scie. 241:20-22.

Gao X, Shin YH, Li M, Wang F, Tong Q, Zhang P. 2010. The fat mass and obesity associated gene FTO functions in the brain to regulate postnatal growth in mice. PLoS One. 5(11):e14005.

Gaudet M, Fara AG, Beritognolo I, Sabatti M. 2009. Allele-specific PCR in SNP genotyping. Methods Mol Biol. 578:415-24.

Gerken T, Girard CA, Tung YC, Webby CJ, Saudek V, Hewitson KS, Yeo GS, McDonough MA, et al. 2007. Science. 318(5855):1469-72.

Ghoussaini M, Meyre D, Lobbens S, Charpentier G, Clément K, Charles MA, Tauber M, Weill J, et al. 2005. Implication of the Pro12Ala polymorphism of the PPAR-gamma 2 gene in type 2 diabetes and obesity in the French population. BMC Med Genet. 22:6-11.

Gill P, Ghalami M, Ghaemi A, Mosavari N, Abdul-Tehrani H, Sadeghizadeh M. 2008. Nanodiagnostic Method for Colorimetric Detection of *Mycobacterium tuberculosis* 16S rRNA. NanoBiotechnol. 4(1-4):28-35.

Giovannini M, Verduci E, Salvatici E, Paci S, Riva E. 2012. Phenylketonuria: nutritional advances and challenges. Nutr Metab (Lond). 9(1):7.

Goldstein DB. 2009. Common genetic variation and human traits. N Engl J Med. 360(17):1696-8.

Goluch ED, Nam JM, Georganopoulou DG, Chiesl TN, Shaikh KA, Ryu KS, Barron AE, Mirkin CA, et al. 2006. A bio-barcode assay for on-chip attomolar-sensitivity protein detection. Lab Chip. 6(10):1293-9.

González JPM, Borrella CC, Mayoral R, Gudino LC. 2014. PPAR gamma pro12Ala polymorphism and type 2 diabetes: a study in a spanish cohort. Journal of Genetics Study. 2:1.

González JR, González-Carpio M, Hernández-Sáez R, Serrano Vargas V, Torres Hidalgo G, Rubio-Rodrigo M, García-Nogales A, Núñez Estévez M, et al. 2012. FTO risk haplotype among early onset and severe obesity cases in a population of western Spain. Obesity. 20(4):909-15.

González Sánchez JL, Serrano Ríos M, Fernández Perez C, Laakso M, Martínez Larrad MT. 2002. Effect of the Pro12Ala polymorphism of the peroxisome proliferator-activated receptor gamma-2 gene on adiposity, insulin sensitivity and lipid profile in the Spanish population. Eur J Endocrinol. 147(4):495-501.

González-Sánchez JL, Zabena C, Martínez-Larrad MT, Martínez-Calatrava MJ, Pérez-Barba M, Serrano-Ríos M. 2009. Variant rs9939609 in the FTO gene is associated with obesity in an adult population from Spain. Clin Endocrinol (Oxf). 70(3):390-3.

Grant SF, Li M, Bradfield JP, Kim CE, Annaiah K, Santa E, Glessner JT, Casalunovo T, et al. 2008. Association analysis of the FTO gene with obesity in children of Caucasian and African ancestry reveals a common tagging SNP. PLoS One. 3(3):e1746.

Griffin J, Singh AK, Senapati D, Rhodes P, Mitchell K, Robinson B, Yu E, Ray PC. 2009. Size- and distance-dependent nanoparticle surface-energy transfer (NSET) method for selective sensing of hepatitis C virus RNA. Chemistry. 15(2):342-351.

Gubala V, Harris LF, Ricco AJ, Tan MX, Williams DE. 2012. Point of care diagnostics: status and future. Anal Chem. 84(2):487-515

Guirgis BS, Sá e Cunha C, Gomes I, Cavadas M, Silva I, Doria G, Blatch GL, Baptista PV, et al. 2012. Gold nanoparticle-based fluorescence immunoassay for malaria antigen detection. Anal Bioanal Chem. 402(3):1019-27.

Haberkorn BC, Ermens AA, Koeken A, Cobbaert CM, van Guldener C. 2011. Improving diagnosis of adult-type hypolactasia in patients with abdominal complaints. Clin Chem Lab Med. 50(1):119-23.

Hainfeld JF, Slatkin DN, Focella TM, Smilowitz HM. 2006. Gold nanoparticles: a new X-ray contrast agent. Br J Radiol. 79(939):248-53.

Haiss W, Thanh NT, Aveyard J, Fernig DG. 2007. Determination of size and concentration of gold nanoparticles from UV-vis spectra. Anal Chem. 79(11):4215-21.

Hakanen M, Raitakari OT, Lehtimäki T, Peltonen N, Pahkala K, Sillanmäki L, Lagström H, Viikari J, et al. 2009. FTO genotype is associated with body mass index after the age of seven years but not with energy intake or leisure-time physical activity. J Clin Endocrinol Metab. 94(4):1281-7.

Hao RZ, Song HB, Zuo GM, Yang RF, Wei HP, Wang DB, Cui ZQ, Zhang Z, et al. 2011. DNA probe functionalized QCM biosensor based on gold nanoparticle amplification for *Bacillus anthracis* detection. Biosens Bioelectron. 26(8):3398-3404.

He W, Huang CZ, Li YF, Xie JP, Yang RG, Zhou PF, Wang J. 2008. One-step label-free optical genosensing system for sequence-specific DNA related to the human immunodeficiency virus based on the measurements of light scattering signals of gold nanorods. Anal Chem. 80(22):8424-8430.

Heard-Costa NL, Zillikens MC, Monda KL, Johansson A, Harris TB, Fu M, Haritunians T, Feitosa MF, et al. 2009. NRXN3 is a novel locus for waist circumference: a genome-wide association study from the CHARGE Consortium. PLoS Genet. 5(6):e1000539.

Hennig BJ, Fulford AJ, Sirugo G, Rayco-Solon P, Hattersley AT, Frayling TM, Prentice AM. 2009. FTO gene variation and measures of body mass in an African population. BMC Med Genet. 10:21.

Herne TM, Tarlov MJ. 1997. Characterization of DNA Probes Immobilized on Gold Surfaces. J. Am Chem Soc. 119(38):8916-8920.

Hertel JK, Johansson S, Sonestedt E, Jonsson A, Lie RT, Platou CG, Nilsson PM, Rukh G, et al. 2011. FTO, type 2 diabetes, and weight gain throughout adult life: a meta-analysis of 41,504 subjects from the Scandinavian HUNT, MDC, and MPP studies. Diabetes. 60(5):1637-44.

Hindorff LA, Sethupathy P, Junkins HA, Ramos EM, Mehta JP, Collins FS, Manolio TA. 2009. Potential etiologic and functional implications of genome-wide association loci for human diseases and traits. Proc Natl Acad Sci USA. 106(23):9362-7.

Hinterwirth H, Wiedmer SK, Moilanen M, Lehner A, Allmaier G, Waitz T, Lindner W, Lämmerhofer M. 2013. Comparative method evaluation for size and size-distribution analysis of gold nanoparticles. J Sep Sci. 36(17):2952-61.

Hirschhorn JN, Daly MJ. 2005. Genome-wide association studies for common diseases and complex traits. Nat Rev Genet. 6(2):95-108.

Hofker MH, Fu J, Wijmenga C. 2014. The genome revolution and its role in understanding complex diseases. Biochim Biophys Acta. 1842(10):1889-1895.

Horvatovich K, Bokor S, Baráth A, Maász A, Kisfali P, Járomi L, Polgár N, Tóth D et al. 2011. Haplotype analysis of the apolipoprotein A5 gene in obese pediatric patients. Int J Pediatr Obes. 6(2-2):e318-25

Hotta K, Nakata Y, Matsuo T, Kamohara S, Kotani K, Komatsu R, Itoh N, Mineo I et al. 2008. Variations in the FTO gene are associated with severe obesity in the Japanese. J Hum Genet. 53(6):546-53.

Hou SY, Hsiao YL, Lin MS, Yen CC, Chang CS. MicroRNA detection using lateral flow nucleic acid strips with gold nanoparticles. Talanta. 99:375-9.

Howes PD, Chandrawati R, Stevens MM. 2014. Bionanotechnology - Colloidal nanoparticles as advanced biological sensors. Science. 346(6205):1247390.

Hsu MC, Chang CS, Lee KT, Sun HY, Tsai YS, Kuo PH, Young KC, Wu CH. 2013. Central obesity in males affected by a dyslipidemia-associated genetic polymorphism on APOA1/C3/A4/A5 gene cluster. Nutr Diabetes. 3:e61.

Hu J, Zhang CY. 2012. Single base extension reaction-based surface enhanced Raman spectroscopy for DNA methylation assay. Biosens Bioelectron. 31(1):451-7.

Hu J, Zheng PC, Jiang JH, Shen GL, Yu RQ, Liu GK. 2010. Sub-attomolar HIV-1 DNA detection using surface-enhanced Raman spectroscopy. Analyst. 135(5):1084-1089.

Hurst SJ, Lytton-Jean AK, Mirkin CA. 2006. Maximizing DNA loading on a range of gold nanoparticle sizes. Anal Chem. 78(24):8313-8.

Hussain MM, Samir TM, Azzazy HM. 2013. Unmodified gold nanoparticles for direct and rapid detection of Mycobacterium tuberculosis complex. Clin Biochem. 46(7-8):633-7.

Hwu JR, Lin YS, Josephrajan T, et al. Targeted paclitaxel by conjugation to iron oxide and gold nanoparticles. J Am Chem Soc. 131(1):66–68.

Hwu JR, Lin YS, Josephrajan T, Hsu MH, Cheng FY, Yeh CS, Su WC, Shieh DB. 2009. Targeted paclitaxel by conjugation to iron oxide and gold nanoparticles. J Am Chem Soc. 131(1):66-68.

Iles MM. 2008. What can genome-wide association studies tell us about the genetics of common disease? PLoS Genet. 4(2):e33.

Ingram CJ, Mulcare CA, Itan Y, Thomas MG, Swallow DM. 2009. Lactose digestion and the evolutionary genetics of lactase persistence. Hum Genet. 124(6):579-91.

Itan Y, Jones BL, Ingram CJ, Swallow DM, Thomas MG. 2010. A worldwide correlation of lactase persistence phenotype and genotypes. BMC Evol Biol. 10:36.

Jacobsson JA, Danielsson P, Svensson V, Klovins J, Gyllensten U, Marcus C, Schiöth HB, Fredriksson R. 2008. Major gender difference in association of FTO gene variant among severely obese children with obesity and obesity related phenotypes. Biochem Biophys Res Commun. 368(3):476-82.

Jain KK. 2003. Nanodiagnostics: application of nanotechnology in molecular diagnostics. Expert Rev Mol Diagn.3(2):153-61.

Jain PK, Huang W, El-Sayed MA. 2007. On the Universal Scaling Behavior of the Distance Decay of Plasmon Coupling in Metal Nanoparticle Pairs: A Plasmon Ruler Equation. Nano Lett. 7(7): 2080-2088.

Jain PK, Huang X, El-Sayed IH, El-Sayed MA. 2008. Noble metals on the nanoscale: optical and photothermal properties and some applications in imaging, sensing, biology, and medicine. Acc Chem Res. 41(12):1578-86.

Jain PK, Lee KS, El-Sayed IH, El-Sayed MA. 2006. Calculated absorption and scattering properties of gold nanoparticles of different size, shape, and composition: applications in biological imaging and biomedicine. J Phys Chem B. 110(14):7238-48.

Jain S, Hirst DG, O'Sullivan JM. 2012. Gold nanoparticles as novel agents for cancer therapy. Br J Radiol. 85(1010):101-13.

Jana NR, Gearheart L, Murphy CJ. 2001. Seeding Growth for Size Control of 5-40 nm Diameter Gold Nanoparticles. Langmuir. 17(22):6782-6786.

Jani IV, Peter TF. 2013. How point-of-care testing could drive innovation in global health. N Engl J Med. 368(24):2319-24.

Jannetto PJ, Buchan BW, Vaughan KA, Ledford JS, Anderson DK, Henley DC, Quigley NB, Ledeboer NA. 2010. Real-time detection of influenza a, influenza B, and respiratory syncytial virus a and B in respiratory specimens by use of nanoparticle probes. J Clin Microbiol. 48(11):3997-4002.

Javier DJ, Castellanos-Gonzalez A, Weigum SE, White AC, Jr., Richards-Kortum R. 2009. Oligonucleotide-gold nanoparticle networks for detection of *Cryptosporidium parvum* heat shock protein 70 mRNA. J Clin Microbiol. 47(12):4060-4066.

Javier DJ, Castellanos-Gonzalez A, Weigum SE, White Jr AC, Richards-Kortum R. 2009. Oligonucleotide-gold nanoparticle networks for detection of *Cryptosporidium parvum* heat shock protein 70 mRNA. J Clin Microbiol. 47(12):4060-4066.

Ji X, Song X, Li J, Bai Y, Yang W, Peng X. 2007. Size control of gold nanocrystals in citrate reduction: the third role of citrate. J Am Chem Soc. 129(45):13939-48.

Johnson EO, Hancock DB, Levy JL, Gaddis NC, Saccone NL, Bierut LJ, Page GP. 2013. Imputation across genotyping arrays for genome-wide association studies: assessment of bias and a correction strategy. Hum Genet. 132(5):509-22.

Jonsson A, Renström F, Lyssenko V, Brito EC, Isomaa B, Berglund G, Nilsson PM, Groop L, et al. 2009. Assessing the effect of interaction between an FTO variant (rs9939609) and physical activity on obesity in 15,925 Swedish and 2,511 Finnish adults. Diabetologia. 52(7):1334-8.

Jung C, Chung JW, Kim UO, Kim MH, Park HG. 2011. Real-time colorimetric detection of target DNA using isothermal target and signaling probe amplification and gold nanoparticle cross-linking assay. Biosens Bioelectron. 26(5):1953-1958.

Jung YL, Jung C, Parab H, Li T, Park HG. 2010. Direct colorimetric diagnosis of pathogen infections by utilizing thiol-labeled PCR primers and unmodified gold nanoparticles.. Biosens Bioelectron. 25(8):1941-6.

Kahn SE, Hull RL, Utzschneider KM. 2006.Mechanisms linking obesity to insulin resistance and type 2 diabetes. Nature. 444(7121):840-6.

Kalidasan K, Neo JL, Uttamchandani M. 2013. Direct visual detection of Salmonella genomic DNA using gold nanoparticles. Mol Biosyst. 9(4):618-621.

Kalnina I, Zaharenko L, Vaivade I, Rovite V, Nikitina-Zake L, Peculis R, Fridmanis D, Geldnere K, et al. 2014. Polymorphisms in FTO and near TMEM18 associate with type 2 diabetes and predispose to younger age at diagnosis of diabetes. Gene. 527(2):462-8.

Kanter R, Caballero B. 2012. Global gender disparities in obesity: a review. Adv Nutr. 3(4):491-8.

Kersten S, Desvergne B, Wahli W. 2000. Roles of PPARs in health and disease. Nature. 405(6785):421-4.

Khoshmanesh K, Nahavandi S, Baratchi S, Mitchell A, Kalantar-zadeh K. 2011. Dielectrophoretic platforms for bio-microfluidic systems. Biosens Bioelectron. 26(5):1800-14.

Kim CK, Ghosh P, Pagliuca C, Zhu ZJ, Menichetti S, Rotello VM. 2009. Entrapment of hydrophobic drugs in nanoparticle monolayers with efficient release into cancer cells. J Am Chem Soc. 131(4):1360–1361.

Kimling J, Maier M, Okenve B, Kotaidis V, Ballot H, Plech A. 2006. Turkevich method for gold nanoparticle synthesis revisited. J Phys Chem B. 110(32):15700-7.

Kozwich D, Johansen KA, Landau K, Roehl CA, Woronoff S, Roehl PA. 2000. Development of a novel, rapid integrated *Cryptosporidium parvum* detection assay. Appl Environ Microbiol. 66(7):2711-2717.

Kreil DP, Russell RR, Russell S. 2006. Microarray oligonucleotide probes. Methods Enzymol. 410:73-98.

Kumanan V, Nugen SR, Baeumner AJ, Chang YF. 2009. A biosensor assay for the detection of *Mycobacterium avium* subsp. *paratuberculosis* in fecal samples. J Vet Sci. 10(1):35-42.

Kumar S, Ahlawat W, Kumar R, Dilbaghi N. 2015. Graphene, carbon nanotubes, zinc oxide and gold as elite nanomaterials for fabrication of biosensors for healthcare. Biosens Bioelectron. 70:498-503.

Kushner RF, Apovian CM, Fujioka K. 2013. Obesity consults - comprehensive obesity management in 2013: understanding the shifting paradigm. Obesity. 21(2):1-15.

Kussmann M, Fay LB. 2008. Nutrigenomics and personalized nutrition: science and concept. Personalized Medicine. 5(5):447-455.

Lao O, Lu TT, Nothnagel M, Junge O, Freitag-Wolf S, Caliebe A, Balascakova M, Bertranpetit J, et al. 2008. Correlation between genetic and geographic structure in Europe. Curr Biol. 18(16):1241-8.

Lapsys NM, Kriketos AD, Lim-Fraser M, Poynten AM, Lowy A, Furler SM, Chisholm DJ, Cooney GJ. 2000. Expression of genes involved in lipid metabolism correlate with peroxisome proliferator-activated receptor gamma expression in human skeletal muscle. J Clin Endocrinol Metab. 85(11):4293-7.

Larguinho M, Baptista PV. 2012. Gold and silver nanoparticles for clinical diagnostics - From genomics to proteomics. J Proteomics. 75(10): 2811-23.

Larguinho M, Baptista PV. 2012. Gold and silver nanoparticles for clinical diagnostics - From genomics to proteomics. Journal of Proteomics. 75(10):2811-2823.

Lee H, Kang T, Yoon KA, Lee SY, Joo SW, Lee K. 2010. Colorimetric detection of mutations in epidermal growth factor receptor using gold nanoparticle aggregation. Biosens Bioelectron. 25(7):1669-74.

Lee JS. Multiplexed detection of oligonucleotides with biobarcoded gold nanoparticle probes. 2011. Methods Mol Biol. 726:17-31.

Lefferts JA, Schwab MC, Dandamudi UB, Lee HK, Lewis LD, Tsongalis GJ. 2010. Warfarin genotyping using three different platforms. Am J Transl Res. 2(4):441-446.

Legry V, Cottel D, Ferrières J, Arveiler D, Andrieux N, Bingham A, Wagner A, Ruidavets JB, et al. 2009. Effect of an FTO polymorphism on fat mass, obesity, and type 2 diabetes mellitus in the French MONICA Study. Metabolism. 58(7):971-5.

Li H, Kilpeläinen TO, Liu C, Zhu J, Liu Y, Hu C, Yang Z, Zhang W, et al. 2012. Association of genetic variation in FTO with risk of obesity and type 2 diabetes with data from 96,551 East and South Asians. Diabetologia. 55(4):981-95.

Li H, Rothberg L. 2004. Colorimetric detection of DNA sequences based on electrostatic interactions with unmodified gold nanoparticles. Proc Natl Acad Sci USA. 101(39):14036-9.

Li H, Rothberg LJ. 2004a. Label-free colorimetric detection of specific sequences in genomic DNA amplified by the polymerase chain reaction. J Am Chem Soc. 126(35):10958-61.

Li J, Deng T, Chu X, Yang R, Jiang J, Shen G, Yu R. 2010. Rolling circle amplification combined with gold nanoparticle aggregates for highly sensitive identification of single-nucleotide polymorphisms. Anal Chem. 82(7):2811-6.

Li W, Wu P, Zhang H, Cai C. 2012. Catalytic signal amplification of gold nanoparticles combining with conformation-switched hairpin DNA probe for hepatitis C virus quantification. Chem Commun (Camb). 48(63):7877-9.

Li XZ, Kim S, Cho W, Lee SY. 2013. Optical detection of nanoparticle-enhanced human papillomavirus genotyping microarrays. Biomed Opt Express. 4(2):187-192.

Li Z, Jin R, Mirkin CA, Letsinger RL. 2002. Multiple thiol-anchor capped DNA-gold nanoparticle conjugates. Nucleic Acids Res. 30(7):1558-62.

Liandris E, Gazouli M, Andreadou M, Comor M, Abazovic N, Sechi LA, Ikonomopoulos J. 2009. Direct detection of unamplified DNA from pathogenic mycobacteria using DNA-derivatized gold nanoparticles. J Microbiol Methods. 78(3):260-264.

Lindgren CM, Heid IM, Randall JC, Lamina C, Steinthorsdottir V, Qi L, Speliotes EK, GIANT Consortium, et al. 2009. Genome-wide association scan meta-analysis identifies three Loci influencing adiposity and fat distribution. PLoS Genet. 5(6):e1000508.

Lindi VI, Uusitupa MI, Lindström J, Louheranta A, Eriksson JG, Valle TT, Hämäläinen H, Ilanne-Parikka P, et al. 2002. Association of the Pro12Ala polymorphism in the PPAR-gamma2 gene with 3-year incidence of type 2 diabetes and body weight change in the Finnish Diabetes Prevention Study. Diabetes. 51(8):2581-6.

Litos IK, Ioannou PC, Christopoulos TK, Traeger-Synodinos J, Kanavakis E. 2009. Multianalyte, dipstick-type, nanoparticle-based DNA biosensor for visual genotyping of single-nucleotide polymorphisms. Biosens Bioelectron. 24(10):3135-9.

Little S. 2001. Amplification-refractory mutation system (ARMS) analysis of point mutations. Curr Protoc Hum Genet. Chapter 9:Unit 9.8.

Liu A, Ye B. 2013. Application of gold nanoparticles in biomedical researches and diagnosis. Clin Lab. 59(1-2):23-36.

Liu J, Huang S, Sun M, Liu S, Liu Y, Wang W, Zhang X, Wang H, et al. 2012. An improved allele-specific PCR primer design method for SNP marker analysis and its application. Plant Methods. 8(1):34.

Liu M, Yuan M, Lou X, Mao H, Zheng D, Zou R, Zou N, Tang X, et al. 2011. Label-free optical detection of single-base mismatches by the combination of nuclease and gold nanoparticles. Biosens Bioelectron. 26(11):4294-4300.

Liu RH, Yang J, Lenigk R, Bonanno J, Grodzinski P. 2004. Self-contained, fully integrated biochip for sample preparation, polymerase chain reaction amplification, and DNA microarray detection. Anal Chem. 76(7):1824-31.

Liu Y, Liu Z, Song Y, Zhou D, Zhang D, Zhao T, Chen Z, Yu L, et al. 2010. Meta-analysis added power to identify variants in FTO associated with type 2 diabetes and obesity in the Asian population. Obesity. 18(8):1619-24.

Llevot A, Astruc D. 2012. Applications of vectorized gold nanoparticles to the diagnosis and therapy of cancer. Chem Soc Rev. 41(1):242-57.

Locke AE, Kahali B, Berndt SI, Justice AE, Pers TH, Day FR, Powell C, Vedantam S, et al. 2015. Genetic studies of body mass index yield new insights for obesity biology. Nature. 518(7538):197-206.

Loos RJ, Bouchard C. 2003. Obesity--is it a genetic disorder? J Intern Med. 254(5):401-25.

Loos RJ. 2012. Genetic determinants of common obesity and their value in prediction. Best Pract Res Clin Endocrinol Metab. 26(2):211-26.

Love JC, Estroff LA, Kriebel JK, Nuzzo RG, Whitesides GM. 2005. Self-assembled monolayers of thiolates on metals as a form of nanotechnology. Chem Rev. 105(4):1103-69.

Low KF, Karimah A, Yean CY. 2013. A thermostabilized magnetogenosensing assay for DNA sequence-specific detection and quantification of Vibrio cholerae. Biosens Bioelectron. 47:38-44.

Lu Y, Loos RJ. 2013. Obesity genomics: assessing the transferability of susceptibility loci across diverse populations. Genome Med. 5(6):55.

Luo SC, Sivashanmugan K, Liao JD, Yao CK, Peng HC. 2014. Nanofabricated SERS-active substrates for single-molecule to virus detection in vitro: a review. Biosens Bioelectron. 61:232-40.

Mačeková S1, Bernasovský I, Gabriková D, Bôžiková A, Bernasovská J, Boroňová I, Behulová R, Svíčková P, et al. 2012. Association of the FTO rs9939609 polymorphism with obesity in Roma/Gypsy population. Am J Phys Anthropol. 147(1):30-4.

Majdalawieh A, Kanan MC, El-Kadri O, Kanan SM. 2014. Recent advances in gold and silver nanoparticles: synthesis and applications. J Nanosci Nanotechnol. 14(7):4757-80.

Mancuso M, Jiang L, Cesarman E, Erickson D. 2013. Multiplexed colorimetric detection of Kaposi's sarcoma associated herpesvirus and *Bartonella* DNA using gold and silver nanoparticles. Nanoscale. 5(4):1678-1686.

Manson J, Kumar D, Meenan B, Dixon D. 2011. Polyethylene glycol functionalized gold nanoparticles: the influence of capping density on stability in various media. Gold Bull. 44(2):99-105.

Mao X, Gurung A, Xu H, Baloda M, He Y, Liu G. 2014. Simultaneous detection of nucleic acid and protein using gold nanoparticles and lateral flow device. Anal Sci. 30(6):637-42.

Mao X, Ma Y, Zhang A, Zhang L, Zeng L, Liu G. 2009. Disposable nucleic acid biosensors based on gold nanoparticle probes and lateral flow strip. Anal Chem. 81(4):1660-8.

Mariman EC. 2006. Nutrigenomics and nutrigenetics: the 'omics' revolution in nutritional science. Biotechnol Appl Biochem. 44(3):119-28.

Mark D, Haeberle S, Roth G, von Stetten F, Zengerle R. 2010. Microfluidic lab-on-a-chip platforms: requirements, characteristics and applications. Chem Soc Rev. 39(3):1153-82.

Marques-Vidal P, Bovet P, Paccaud F, Chiolero A. 2010. Changes of overweight and obesity in the adult Swiss population according to educational level, from 1992 to 2007.

Marti A, Goyenechea E, Martínez JA. 2010. Nutrigenetics: a tool to provide personalized nutritional therapy to the obese. World Rev Nutr Diet. 101:21-33.

Martínez-Paredes G, González-García MB, Costa-García A. 2012. Electrochemical DNA Biosensors - Chapter 9. Screen-Printed Electrodes for Electrochemical DNA Detection. Mehmet Ozsoz. Pan Stanford Publishing. 291-237.

Martins R, Baptista P, Raniero L, Doria G, Silva L, Franco R, Fortunato E. 2007. Amorphous/nanocrystalline silicon biosensor for the specific identification of unamplified nucleic acid sequences using gold nanoparticle probes. Appl Phys Lett. 90(2): 023903.

Masud S, Ye S, SAS Group. 2003. Effect of the peroxisome proliferator activated receptor-gamma gene Pro12Ala variant on body mass index: a meta-analysis. J Med Genet. 40(10):773-80.

Maurice CB, Barua PK, Simses D, Smith P, Howe JG, Stack G. 2010. Comparison of assay systems for warfarin-related CYP2C9 and VKORC1 genotyping. Clin Chim Acta. 411(13-14):947-954.

McCarthy MI, Abecasis GR, Cardon LR, Goldstein DB, Little J, Ioannidis JP, Hirschhorn JN. 2008. Genome-wide association studies for complex traits: consensus, uncertainty and challenges. Nat Rev Genet. 9(5):356-69.

McKee M. 2011. Responding to the economic crisis: Europe's governments must take account of the cost of health inequalities. J Epidemiol Community Health. 65(5):391.

McKenzie F, Faulds K, Graham D. 2007. Sequence-specific DNA detection using high-affinity LNA-functionalized gold nanoparticles. Small. 3(11):1866-8.

McPherson JD, Marra M, Hillier L, Waterston RH, Chinwalla A, Wallis J, Sekhon M, Wylie K, et al. 2001. A physical map of the human genome. Nature. 409(6822):934-41.

Merkel M, Loeffler B, Kluger M, Fabig N, Geppert G, Pennacchio LA, Laatsch A, Heeren J. 2005. Apolipoprotein AV accelerates plasma hydrolysis of triglyceride-rich lipoproteins by interaction with proteoglycan-bound lipoprotein lipase. J Biol Chem. 280(22):21553-60.

Meyre D, Delplanque J, Chèvre JC, Lecoeur C, Lobbens S, Gallina S, Durand E, Vatin V, et al. 2009. Genome-wide association study for early-onset and morbid adult obesity identifies three new risk loci in European populations. Nat Genet. 41(2):157-9.

Milton JA, Patole S, Yin H, Xiao Q, Brown T, Melvin T. 2013. Efficient self-assembly of DNA-functionalized fluorophores and gold nanoparticles with DNA functionalized silicon surfaces: the effect of oligomer spacers. Nucleic Acids Res. 41(7):e80.

Mirkin CA, Letsinger RL, Mucic RC, Storhoff JJ. 1996. A DNA-based method for rationally assembling nanoparticles into macroscopic materials. Nature. 382(6592):607-9.

Mirzaei H, Akrami SM, Golmohammadi T, Doosti M, Heshmat R, Nakhjavani M, Amiri P. 2009. Polymorphism of Pro12Ala in the peroxisome proliferator-activated receptor gamma2 gene in Iranian diabetic and obese subjects. Metab Syndr Relat Disord. 7(5):453-8.

Mogi T, Hatakeyama K, Taguchi T, Wake H, Tanaami T, Hosokawa M, Tanaka T, Matsunaga T. 2011. Real-time detection of DNA hybridization on microarray using a CCD-based imaging system equipped with arotated microlens array disk. Biosens Bioelectron. 26(5):1942-6.

Mohammed MI, Desmulliez MP. 2013. Planar lens integrated capillary action microfluidic immunoas say device for the optical detection of troponin I. Biomicrofluidics. 7(6):64112.

Mohammed MI, Desmulliez MP. 2014. Autonomous capillary microfluidic system with embedded optics for improved troponin I cardiac biomarker detection. Biosens Bioelectron. 61:478-84.

Mokdad AH, Ford ES, Bowman BA, Dietz WH, Vinicor F, Bales VS, Marks JS. 2003. Prevalence of obesity, diabetes, and obesity-related health risk factors. Jama. 289:76-79.

Molarius A, Seidell JC, Kuulasmaa K, Dobson AJ, Sans S. 1997. Smoking and relative body weight: an international perspective from the WHO MONICA Project. J Epidemiol Community Health. 51(3):252–260.

Mollasalehi H, Yazdanparast R. 2012. Non-crosslinking gold nanoprobes for detection of nucleic acid sequence-based amplification products. Anal Biochem. 425(2):91-95.

Mollasalehi H, Yazdanparast R. 2013. An improved non-crosslinking gold nanoprobe-NASBA based on 16S rRNA for rapid discriminative bio-sensing of major salmonellosis pathogens. Biosens Bioelectron. 47:231-236.

Moody A. 2014. Health Survey England 2013 – Volume 1. Chapter 10: Adult anthropometric measures, overweight and obesity. The Health and Social Care Information Centre.

Morigi V, Tocchio A, Bellavite Pellegrini C, Sakamoto JH, Arnone M, Tasciotti E. 2012. Nanotechnology in medicine: from inception to market domination. J Drug Deliv. 2012:389485.

Morini E, Tassi V, Capponi D, Ludovico O, Dallapiccola B, Trischitta V, Prudente S. 2008. Interaction between PPARgamma2 variants and gender on the modulation of body weight. Obesity. 16(6):1467-70.

Nam JM, Thaxton CS, Mirkin CA. 2003. Nanoparticle-based bio-bar codes for the ultrasensitive detection of proteins. Science. 301:1884-1886.

Napolioni V. 2014. The relevance of checking population allele frequencies and Hardy-Weinberg Equilibrium in genetic association studies: the case of SLC6A4 5-HTTLPR polymorphism in a Chinese Han Irritable Bowel Syndrome association study. Immunol Lett. 162(1 Pt A):276-8.

Niculescu LS, Fruchart-Najib J, Fruchart JC, Sima A. 2007. Apolipoprotein A-V gene polymorphisms in subjects with metabolic syndrome. Clin Chem Lab Med. 45(9):1133-9.

NOEIE Panel. 1998. Clinical guidelines on the identification, evaluation, and treatment of overweight and obesity in adults. Am J Clin Nutr. 68:899-917.

Norrgard K, Schultz J. 2008. Using SNP Data to Examine Human Phenotypic Differences. Using SNP data to examine human phenotypic differences. Nature Education. 1(1):85.

Notomi T, Okayama H, Masubuchi H, Yonekawa T, Watanabe K, Amino N, Hase T. 2000. Loop-mediated isothermal amplification of DNA. Nucleic Acids Res. 28(12):E63.

Nune SK, Gunda P, Thallapally PK, Lin YY, Forrest ML, Berkland CJ. 2009. Nanoparticles for biomedical imaging. Expert Opin Drug Deliv. 6:1175-94.

Nunes JSA. 2013. Contribuição para o estudo da obesidade e implicações sobre o risco cardiovascular e metabólico [dissertation]. Universidade de Coimbra.

Nussbaum R, McInnes R, Willard H. 2007. Thompson & Thompson Genetics in Medicine. 7th Edition. W.B. Saunders.

Oblath EA, Henley WH, Alarie JP, Ramsey JM. 2013. A microfluidic chip integrating DNA extraction and real-time PCR for the detection of bacteria in saliva. Lab Chip. 13(7):1325-32.

Orr JB. 1936. The problems of nutrition. Food, Health and Income. The Labour Monthly. 2(6):447-452.

Orzano AJ, Scott JG. 2004. Diagnosis and treatment of obesity in adults: an applied evidence-based review. J Am Board Fam Pract. 17(5):359-69.

Owczarzy R, You Y, Groth CL, Tataurov AV. 2011. Stability and mismatch discrimination of locked nucleic acid-DNA duplexes. Biochemistry. 50(43):9352-67.

Ozsoz M, Erdem A, Kerman K, Ozkan D, Tugrul B, Topcuoglu N, Ekren H, Taylan M. 2003. Electrochemical genosensor based on colloidal gold nanoparticles for the detection of Factor V Leiden mutation using disposable pencil graphite electrodes. Anal Chem. 75(9):2181-7.

Padmavathy B, Vinoth Kumar R, Jaffar Ali BM. 2012. A direct detection of *Escherichia coli* genomic DNA using gold nanoprobes. J Nanobiotechnology. 10(1):8.

Panagiotou OA, Ioannidis JP; Genome-Wide Significance Project. 2012. What should the genome-wide significance threshold be? Empirical replication of borderline genetic associations. Int J Epidemiol. 41(1):273-86.

Panagiotou OA, Willer CJ, Hirschhorn JN, Ioannidis JP. 2013. The power of meta-analysis in genome-wide association studies. Annu Rev Genomics Hum Genet. 14:441-65.

Parab HJ, Jung C, Lee JH, Park HG. 2010. A gold nanorod-based optical DNA biosensor for the diagnosis of pathogens. Biosens Bioelectron. 26(2):667-673.

Park J, Morley TS, Kim M, Clegg DJ, Scherer PE. 2014. Obesity and cancer--mechanisms underlying tumour progression and recurrence. Nat Rev Endocrinol. 10(8):455-65.

Park SY, Lee SM, Kim GB, Kim Y-P. 2012. Gold nanoparticle-based florescence quenching via metal coordination for assaying protease activity. Gold Bull. 45(4):213-219.

Park YW, Zhu S, Palaniappan L, Heshka S, Carnethon MR, Heymsfield SB. 2003. The metabolic syndrome: prevalence and associated risk factor findings in the US population from the Third National Health and Nutrition Examination Survey, 1988-1994. Arch Intern Med. 163(4):427-36.

Parveen S, Misra R, Sahoo SK. 2012. Nanoparticles: a boon to drug delivery, therapeutics, diagnostics and imaging. Nanomedicine. 8(2):147-66.

Passaro A, Dalla Nora E, Marcello C, Di Vece F, Morieri ML, Sanz JM, Bosi C, Fellin R, et al. 2011. PPARγ Pro12Ala and ACE ID polymorphisms are associated with BMI and fat distribution, but not metabolic syndrome. Cardiovasc Diabetol. 10:112.

Pearson TA, Manolio TA. 2008. How to interpret a genome-wide association study. JAMA. 299(11):1335-44.

Pedrosa P, Veigas B, Machado D, Couto I, Viveiros M, Baptista PV. 2014. Gold nanoprobes for multi loci assessment of multi-drug resistant tuberculosis. Tuberculosis (Edinb). 94(3):332-7.

Pelton M, Aizpurua J, Bryant G. 2008. Metal-nanoparticle plasmonics. Laser & Photonics Reviews. 2(3):136-159.

Pennacchio LA, Olivier M, Hubacek JA, Cohen JC, Cox DR, Fruchart JC, Krauss RM, Rubin EM. 2001. An apolipoprotein influencing triglycerides in humans and mice revealed by comparative sequencing. Science. 294(5540):169-73.

Pereira J, Mateus C. 2003. Custos indirectos associados à obesidade em Portugal. Rev Port Saúde Públ. 3:65-80.

Perry JR, Voight BF, Yengo L, Amin N, Dupuis J, Ganser M, Grallert H, Navarro P, et al. 2012. Stratifying type 2 diabetes cases by BMI identifies genetic risk variants in LAMA1 and enrichment for risk variants in lean compared to obese cases. PLoS Genet. 8(5):e1002741.

Pers TH, Karjalainen JM, Chan Y, Westra HJ, Wood AR, Yang J, Lui JC, Vedantam S, et al. 2015. Biological interpretation of genome-wide association studies using predicted gene functions. Nat Commun. 6:5890.

Peters T, Ausmeier K, Rüther U. 1999. Cloning of Fatso (Fto), a novel gene deleted by the Fused toes (Ft) mouse mutation. Mamm Genome. 10(10):983-6.

Pissuwan D, Niidome T, Cortie MB. 2011. The forthcoming applications of gold nanoparticles in drug and gene delivery systems. J Control Release. 149(1):65-71.

Popkin BM, Gordon-Larsen P. 2004. The nutrition transition: worldwide obesity dynamics and their determinants. 28:2-9.

Popkin BM, Slining MM. 2013. New dynamics in global obesity facing low- and middle-income countries. Obes Rev. 14(2):11-20.

Popkin BM. 2004a. The nutrition transition: an overview of world patterns of change. Nutr Rev. 62(7):140-3.

Prentice AM, Jebb SA. 2011. Beyond body mass index. Obes Rev. 2(3):141-7.

Prentice AM. 2006. The emerging epidemic of obesity in developing countries. Int J Epidemiol. 35(1):93-9.

Qi L. 2014. Personalized nutrition and obesity. Ann of Med. 46(5):247-252.

Qian XM, Nie SM. 2008. Single-molecule and single-nanoparticle SERS: from fundamental mechanisms to biomedical applications. Chem Soc Rev. 37:912-20.

Qin WJ, Yim OS, Lai PS, Yung LY. 2010. Dimeric gold nanoparticle assembly for detection and discrimination of single nucleotide mutation in Duchenne muscular dystrophy. Biosens Bioelectron. 25(9):2021-5.

Qin WJ, Yung LY. 2007. Nanoparticle-based detection and quantification of DNA with single nucleotide polymorphism (SNP) discrimination selectivity. Nucleic Acids Res. 35(17):e111.

Rahmouni K, Correia ML, Haynes WG, Mark AL. 2005. Obesity-associated hypertension: new insights into mechanisms. Hypertension. 45(1):9-14.

Rankinen T, Zuberi A, Chagnon Y, Weisnagel SJ, Argyropoulos G, Walts B, Perusse L, Bouchard C. 2006. The human obesity gene map: the 2005 update. Obesity. 14:529-644.

Rastogi SK, Gibson CM, Branen JR, Aston DE, Branen AL, Hrdlicka PJ. 2012. DNA detection on lateral flow test strips: enhanced signal sensitivity using LNA-conjugated gold nanoparticles. Chem Commun (Camb). 48(62):7714-7716.

Ravi S, Krishnamurthy VR, Caves JM, Haller CA, Chaikof EL. 2012. Maleimide-thiol coupling of a bioactive peptide to an elastin-like protein polymer. Acta Biomater. 8(2):627–635.

Rees SD, Islam M, Hydrie MZ, Chaudhary B, Bellary S, Hashmi S, O'Hare JP, Kumar S, et al. 2011. An FTO variant is associated with Type 2 diabetes in South Asian populations after accounting for body mass index and waist circumference. Diabet Med. 28(6):673-80.

Renehan AG, Tyson M, Egger M, Heller RF, Zwahlen M. 2008. Body-mass index and incidence of cancer: a systematic review and meta-analysis of prospective observational studies. Lancet. 371(9612):569-78.

Rice DP. 1697. Estimating the cost of illness. Am J Public Health Nations Health. 57(3):424-440.

Ringe E, Sharma B, Henry AI, Marks LD, Van Duyne RP. 2013. Single nanoparticle plasmonics. Phys Chem Chem Phys. 15(12):4110-29.

Rodríguez-López R, González-Carpio M, Serrano MV, Torres G, García de Cáceres MT, Herrera T, Román A, Rubio M, et al. 2010. Association of FTO gene polymorphisms and morbid obesity in the population of Extremadura (Spain). Endocrinol Nutr. 57(5):203-9.

Rohrman BA, Leautaud V, Molyneux E, Richards-Kortum RR. 2012. A lateral flow assay for quantitative detection of amplified HIV-1 RNA. PLoS One 7(9):e45611.

Rosa J, Conde J, de la Fuente JM, Lima JC, Baptista PV. 2012. Gold-nanobeacons for real-time monitoring of RNA synthesis. Biosens Bioelectron. 36(1):161-7.

Roy E, Voisin B, Gravel JF, Peytavi R, Boudreau D, Veres T. 2009. Microlens array fabrication by enhanced thermal reflow process: Towards efficient collection of fluorescence light from microarrays. Microelectronic Engineering. 86(11):2255-2261.

Sachidanandam R, Weissman D, Schmidt SC, Kakol JM, Stein LD, Marth G, Sherry S, Mullikin JC, et al. 2001. A map of human genome sequence variation containing 1.42 million single nucleotide polymorphisms. Nature. 409(6822):928-33.

Saha K, Agasti SS, Kim C, Li X, Rotello VM. 2012. Gold nanoparticles in chemical and biological sensing. Chem Rev. 112(5):2739-79.

Sahi T. 1994. Genetics and epidemiology of adult-type hypolactasia. Scand J Gastroenterol Suppl. 202:7-20.

Salanti G, Sanderson S, Higgins JP. 2005. Obstacles and opportunities in meta-analysis of genetic association studies. Genet Med. 7(1):13-20.

San-Cristobal R, Milagro FI, Martínez JA. 2013. Future challenges and present ethical considerations in the use of personalized nutrition based on genetic advice. J Acad Nutr Diet. 113(11):1447-54.

Sandholt CH, Hansen T, Pedersen O. 2012. Beyond the fourth wave of genome-wide obesity association studies. Nutr Diabetes. 2:e37.

Sandström P, Boncheva M, Åkerman B. 2003. Nonspecific and Thiol-Specific Binding of DNA to Gold Nanoparticles. Langmuir. 19(18):7537-7543.

Santos T, Rato Q, Gaspar IM, Bourbon M. 2011. Influence of LPL, APOAIV, APOAV, APOCIII and USF1 polymorphisms in a Portuguese population with clinical diagnosis of Familial Combined Hyperlipidaemia.

Sanz V, Conde J, Hernández Y, Baptista P V, Ibarra MR, De La Fuente JM. 2012. Effect of PEG biofunctional spacers and TAT peptide on dsRNA loading on gold nanoparticles. J Nanoparticle Res. 14(6):917.

Sarpong K, Datta B. 2012. Nucleic-Acid-binding chromophores as efficient indicators of aptamer-target interactions. J Nucleic Acids. 2012:247280.

Sarwar N, Sandhu MS, Ricketts SL, Butterworth AS, Di Angelantonio E, Boekholdt SM, Ouwehand W, Triglyceride Coronary Disease Genetics Consortium and Emerging Risk Factors Collaboration, et al. 2010. Triglyceride-mediated pathways and coronary disease: collaborative analysis of 101 studies. Lancet. 375(9726):1634-9.

Sato K, Hosokawa K, Maeda M. 2003. Rapid aggregation of gold nanoparticles induced by non-cross-linking DNA hybridization. J Am Chem Soc. 125(27):8102-3.

Sato K, Hosokawa K, Maeda M. 2005. Non-cross-linking gold nanoparticle aggregation as a detection method for single-base substitutions. Nucleic Acids Res. 33(1):e4.

Sazonov ES, Schuckers S. 2010. The energetics of obesity: a review: monitoring energy intake and energy expenditure in humans. IEEE Eng Med Biol Mag. (1):31-5.

Scientia Advisors. 2013. The point-of-care diagnostics market. Cambridge, MA, USA.

Scuteri A, Sanna S, Chen WM, Uda M, Albai G, Strait J, Najjar S, Nagaraja R, et al. 2007. Genome-wide association scan shows genetic variants in the FTO gene are associated with obesity-related traits. PLoS Genet. 3(7):e115.

Sentinelli F, Incani M, Coccia F, Capoccia D, Cambuli VM, Romeo S, Cossu E, Cavallo MG, et al. 2012. Association of FTO polymorphisms with early age of obesity in obese Italian subjects. Exp Diabetes Res. 2012:872176.

Seo J, Lee LP. 2004. Disposable integrated microfluidics with self-aligned planar microlenses. Sensors and Actuators B. 99:615-622.

Seppänen-Nuijten E, Lahti-Koski M, Männistö S, Knekt P, Rissanen H, Aromaa A, Heliövaara M. 2009. Fat free mass and obesity in relation to educational level. BMC Public Health.9:448.

Sha MY, Penn S, Freeman G, Doering WE. 2007. Detection of human viral RNA via a combined fluorescence and SERS molecular beacon assay. NanoBiotechnology. 3(1): 23-30.

Shah M, Badwaik VD, Dakshinamurthy R. 2014. Biological applications of gold nanoparticles. J Nanosci Nanotechnol. 14(1):344-62.

Shastry BS. 2002. SNP alleles in human disease and evolution. J Hum Genet. 47(11):561-6.

Shawky SM, Bald D, Azzazy HM. 2010. Direct detection of unamplified hepatitis C virus RNA using unmodified gold nanoparticles. Clin Biochem. 43(13-14):1163-8.

Sheng Q, Wang J, Zheng J, Xu Z, Zhang H. 2010. Ultrasensitive electrical biosensing of syphilis DNA using target-guided formation of polyaniline based on enzyme-catalyzed polymerization. Biosens Bioelectron. 25(9):2071-7.

Sheskin FJ. 2000. Handbook of Parametric and Nonparametric Statistical Procedures, 2nd edition. Boca Raton (USA). Chapman & Hall.

Silva LB, Baptista P, Raniero L, Doria G, Franco R, Martins R, Fortunato E. 2007. Novel Optoelectronic Platform using an Amorphous/Nanocrystalline Silicon Biosensor for the Specific Identification of Unamplified Nucleic Acid Sequences. Solid-State Sensors, Actuators and Microsystems Conference. 935-938.

Silva LB, Veigas B, Doria G, Costa P, Inácio J, Martins R, Fortunato E, Baptista PV. 2011. Portable optoelectronic biosensing platform for identification of mycobacteria from the Mycobacterium tuberculosis complex. Biosens Bioelectron. 26(5):2012-7.

Simoni L, Calafell F, Pettener D, Bertranpetit J, Barbujani G. 2000. Geographic patterns of mtDNA diversity in Europe. Am J Hum Genet. 66(1):262-78.

Sirén J, Marttinen P, Corander J. 2011. Reconstructing population histories from single nucleotide polymorphism data. Mol Biol Evol. 28(1):673-83.

Soe AK, Nahavandi S, Khoshmanesh K. 2012. Neuroscience goes on a chip. Biosens Bioelectron. 35(1):1-13.

Sommer SS, Groszbach AR, Bottema CD. 1992. PCR amplification of specific alleles (PASA) is a general method for rapidly detecting known single-base changes. Biotechniques. 12(1):82-7.

Song Y, You NC, Hsu YH, Howard BV, Langer RD, Manson JE, Nathan L, Niu T, et al. 2008. FTO polymorphisms are associated with obesity but not diabetes risk in postmenopausal women. Obesity. 16(11):2472-80.

Soo PC, Horng YT, Chang KC, Wang JY, Hsueh PR, Chuang CY, Lu CC, Lai HC. 2009. A simple gold nanoparticle probes assay for identification of *Mycobacterium tuberculosis* and *Mycobacterium tuberculosis* complex from clinical specimens. Mol Cell Probes. 23(5):240-246.

Sørensen TI, Holst C, Stunkard AJ. 1992. Childhood body mass index--genetic and familial environmental influences assessed in a longitudinal adoption study. Int J Obes Relat Metab Disord. 16(9):705-14.

Sperling RA, Parak WJ. 2010. Surface modification, functionalization and bioconjugation of colloidal inorganic nanoparticles. Philos Trans A Math Phys Eng Sci. 368(1915):1333-83.

Spiegelman BM. 1998. PPAR-gamma: adipogenic regulator and thiazolidinedione receptor. Diabetes. 47(4):507-14.

Stoeva SI, Lee JS, Thaxton CS, Mirkin CA. 2006. Multiplexed DNA detection with biobarcoded nanoparticle probes. Angew Chem Int Ed Engl. 45(20):3303-6.

Storhoff JJ, Marla SS, Bao P, Hagenow S, Mehta H, Lucas A, Garimella V, Patno T, et al. 2004. Gold nanoparticle-based detection of genomic DNA targets on microarrays using a novel optical detection system. Biosensors and Bioelectronics. 19(8):875-883.

Storhoff JJ, Elghanian R, Mirkin CA, Letsinger RL. 2002. Sequence-Dependent Stability of DNA-Modified Gold Nanoparticles. Langmuir. 18(17): 6666–6670.

Storhoff JJ, Elghanian R, Mucic RC, Mirkin CA, Letsinger RL. 1998. One-Pot Colorimetric Differentiation of Polynucleotides with Single Base Imperfections Using Gold Nanoparticle Probes. J. Am. Chem. Soc. 120(9):1959–1964.

Stumvoll M, Häring H. 2002. The Peroxisome Proliferator–Activated Receptor-γ2 Pro12Ala Polymorphism. Diabetes. 51:2341-2347.

Stunkard AJ, Harris JR, Pedersen NL, McClearn GE. 1990. The body-mass index of twins who have been reared apart. N Engl J Med. 322(21):1483-7.

Subbiah R, Veerapandian M, Yun KS. 2010. Nanoparticles: Functionalization and multifunctional applications in biomedical sciences. Curr Med Chem. 17(36):4559-4577.

Suh Y, Vijg J. 2005. SNP discovery in associating genetic variation with human disease phenotypes. Mutation Research. 573:41-53.

Sun L, Irudayaraj J. 2009. PCR-free quantification of multiple splice variants in a cancer gene by surface-enhanced Raman spectroscopy. J Phys Chem B. 113(42):14021-5.

Sun L, Zhang Z, Wang S, Zhang J, Li H, Ren L, Weng J, Zhang Q. 2008. Effect of pH on the Interaction of Gold Nanoparticles with DNA and Application in the Detection of Human p53 Gene Mutation. Nanoscale Res Lett. 4(3):216-220.

Sun Y, Rogers J. 2007. Structural forms of single crystal semiconductor nanoribbons for high-performance stretchable electronics. J. Mater Chem. 17:832-840.

Suzuki T, Tanaka M, Otani S, Matsuura S, Sakaguchi Y, Nishimura T, Ishizaka A, Hasegawa N. 2006. New rapid detection test with a combination of polymerase chain reaction and immunochromatographic assay for *Mycobacterium tuberculosis* complex. Diagn Microbiol Infect Dis. 56(3):275-280.

Tan LJ, Zhu H, He H, Wu KH, Li J, Chen XD, Zhang JG, Shen H, et al. 2014. Replication of 6 obesity genes in a meta-analysis of genome-wide association studies from diverse ancestries. PLoS One. 9(5):e96149.

Tan YN, Lee KH, Su X. 2011. Study of single-stranded DNA binding protein-nucleic acids interactions using unmodified gold nanoparticles and its application for detection of single nucleotide polymorphisms. Anal Chem. 83(11):4251-7.

Tanaami T, Otsuki S, Tomosada N, Kosugi Y, Shimizu M, Ishida H. 2002. High-speed 1-frame/ms scanning confocal microscope with a microlens and Nipkow disks. Appl Opt. 41(22):4704-8.

Thaxton CS, Georganopoulou DG, Mirkin CA. 2006. Gold nanoparticle probes for the detection of nucleic acid targets. Clin Chim Acta 2006. 363(1-2):120-6.

The International HapMap Consortium. 2003. The International HapMap Project. Nature. 426:789-796.

Thiruppathiraja C, Kamatchiammal S, Adaikkappan P, Santhosh DJ, Alagar M. 2011. Specific detection of *Mycobacterium* sp. genomic DNA using dual labeled gold nanoparticle based electrochemical biosensor. Anal Biochem. 417(1):73-79.

Thobhani S, Attree S, Boyd R, Kumarswami N, Noble J, Szymanski M, Porter RA. 2010. Bioconjugation and characterisation of gold colloid-labelled proteins. J Immunol Methods. 356(1-2):60–69.

Tok EC, Ertunc D, Bilgin O, Erdal EM, Kaplanoglu M, Dilek S. 2006. PPAR-gamma2 Pro12Ala polymorphism is associated with weight gain in women with gestational diabetes mellitus. Eur J Obstet Gynecol Reprod Biol. 129(1):25-30.

Tomita N, Mori Y, Kanda H, Notomi T. 2008. Loop-mediated isothermal amplification (LAMP) of gene sequences and simple visual detection of products. Nat Protoc. 3(5):877-82.

Tönjes A, Scholz M, Loeffler M, Stumvoll M. 2006. Association of Pro12Ala polymorphism in peroxisome proliferator-activated receptor gamma with Pre-diabetic phenotypes: meta-analysis of 57 studies on nondiabetic individuals. Diabetes Care. 29(11):2489-97.

Traversy G, Chaput JP. 2015. Alcohol Consumption and Obesity: An Update. Curr Obes Rep. 4(1):122-130.

Tripathi A, Chronis N. 2011. A doublet microlens array for imaging micron-sized objects. J. Micromech Microeng. 21(10):105024.

Tsigos C, Hainer V, Basdevant A, Finer N, Fried M, Mathus-Vliegen E, Micic D, Maislos M et al. 2008. Management of Obesity in Adults: European Clinical Practice Guidelines. Obes Facts 1(2):106-116.

Turkevich J, Stevenson PC, Hillier J. 1951. A study of the nucleation and growth processes in the synthesis of colloidal gold. Discuss Faraday Soc. 11:55-75.

Turner S, Armstrong LL, Bradford Y, Carlson CS, Crawford DC, Crenshaw AT, de Andrade M, Doheny KF, et al. 2011. Quality control procedures for genome-wide association studies. Curr Protoc Hum Genet. Chapter 1:Unit1.19.

Tzotzas T, Vlahavas G, Papadopoulou SK, Kapantais E, Kaklamanou D, Hassapidou M. 2010. Marital status and educational level associated to obesity in Greek adults: data from the National Epidemiological Survey. BMC Public Health. 10:732.

Vaccaro O, Mancini FP, Ruffa G, Sabatino L, Colantuoni V, Riccardi G. 2000. Pro12Ala mutation in the peroxisome proliferator-activated receptor gamma2 (PPARgamma2) and severe obesity: a case-control study. Int J Obes Relat Metab Disord. 24(9):1195-9.

Vaisse C, Clement K, Guy-Grand B, Froguel P. 1998. A frameshift mutation in human MC4R is associated with a dominant form of obesity. Nat Genet. 20(2):113-4.

van der Hoeven F, Schimmang T, Volkmann A, Mattei MG, Kyewski B, Rüther U. 1994. Programmed cell death is affected in the novel mouse mutant Fused toes (Ft). Development. 120(9):2601-7.

van der Vliet HN, Sammels MG, Leegwater AC, Levels JH, Reitsma PH, Boers W, Chamuleau RA. 2001. Apolipoprotein A-V: a novel apolipoprotein associated with an early phase of liver regeneration. J Biol Chem. 276(48):44512-20.

van Greevenbroek MM, Schalkwijk CG, Stehouwer CD. 2013. Obesity-associated low-grade inflammation in type 2 diabetes mellitus: causes and consequences. Neth J Med. 71(4):174-87.

Van Overmeire S, Volckaerts B, Ottevaere H, Pappaert K, Desmet G, Thienpont H. 2005. Simulation, fabrication and characterization of microlens oriented fluorescence detection systems for DNA microarrays. Proceedings Symposium IEEE/LEOS Benelux Chapter.

Vasilopoulos Y, Sarafidou T, Bagiatis V, Skriapa L, Goutzelas Y, Pervanidou P, Lazopoulou N, Chrousos GP, et al. 2011. Association between polymorphisms in MTHFR and APOA5 and metabolic syndrome in the Greek population. Genet Test Mol Biomarkers. 15(9):613-7.

Veigas B, Fernandes AR, Baptista PV. 2014. AuNPs for identification of molecular signatures of resistance. Front Microbiol. 5:455.

Veigas B, Pedrosa P, Couto I, Viveiros M, Baptista PV. 2013. Isothermal DNA amplification coupled to Au-nanoprobes for detection of mutations associated to Rifampicin resistance in *Mycobacterium tuberculosis*. J Nanobiotechnology. 11:38.

Veigas B, Jacob JM, Costa MN, Santos DS, Viveiros M, Inácio J, Martins R, Barquinha P, et al. 2012. Gold on paper-paper platform for Au-nanoprobe TB detection. Lab Chip. 12(22):4802-8.

Veigas B, Machado D, Perdigão J, Portugal I, Couto I, Viveiros M, Baptista PV. 2010. Au-nanoprobes for detection of SNPs associated with antibiotic resistance in Mycobacterium tuberculosis. Nanotechnology. 21(41):415101.

Veigas B. 2009. Au-Nanossondas Aplicação na detecção de Mycobacterium tuberculosis e Plasmodium berghei [dissertation]. Universidade NOVA de Lisboa.

Vendrell M, Maiti KK, Dhaliwal K, Chang YT. 2013. Surface-enhanced Raman scattering in cancer detection and imaging. Trends Biotechnol. 31(4):249-57.

Venter JC, Adams MD, Myers EW, Li PW, Mural RJ, Sutton GG, Smith HO, Yandell M, et al. 2001. Science. 291(5507):1304-51.

Vetrone SA, Huarng MC, Alocilja EC. 2012. Detection of non-PCR amplified *S. enteritidis* genomic DNA from food matrices using a gold-nanoparticle DNA biosensor: a proof-of-concept study. Sensors (Basel). 12(8):10487-10499.

Vinhas R, Cordeiro M, Carlos FF, Mendo S, Fernandes AR, Figueiredo S, Baptista PV. 2015. Gold nanoparticle-based theranostics: disease diagnostics and treatment using a single nanomaterial. Nanobiosensors in Disease Diagnosis 4:11-23.

Viskari PJ, Landers JP. 2006. Unconventional detection methods for microfluidic devices. Electrophoresis. 27(9):1797-810.

Visscher TL, Kromhout D, Seidell JC. 2002. Long-term and recent time trends in the prevalence of obesity among Dutch men and women. Int J ObesRelatMetabDisord. 26(9):1218-24.

Voelkel R. 2012. Wafer-scale micro-optics fabrication. Adv. Opt. Techn. 1:135-150.

Walley AJ, Blakemore AI, Froguel P. 2006. Genetics of obesity and the prediction of risk for health. Hum Mol Genet. 15(2):124-30.

Wang J, Ban MR, Zou GY, Cao H, Lin T, Kennedy BA, Anand S, Yusuf S, et al. 2008. Polygenic determinants of severe hypertriglyceridemia. Hum Mol Genet. 17(18):2894-9.

Wang K, Li WD, Zhang CK, Wang Z, Glessner JT, Grant SF, Zhao H, Hakonarson H, et al. 2011. A genome-wide association study on obesity and obesity-related traits. PLoS One. 6(4):e18939.

Wang L, Wei Q, Wu C, Hu Z, Ji J, Wang P. 2008. The *Escherichia coli* O157:H7 DNA detection on a gold nanoparticle-enhanced piezoelectric biosensor. Chinese Science Bulletin. 53(8):1175-1184.

Wang T, Jia W, Hu C. 2014. Advancement in genetic variants conferring obesity susceptibility from genome-wide association studies. Front Med. [Epub ahead of print].

Wang X, Li Y, Wang J, Wang Q, Xu L, Du J, Yan S, Zhou Y, et al. 2012. A broad-range method to detect genomic DNA of multiple pathogenic bacteria based on the aggregation strategy of gold nanorods. Analyst. 137(18):4267-4273.

Wang X, Qian X, Beitler JJ, Chen ZG, Khuri FR, Lewis MM, Shin HJ, Nie S, et al. 2011a. Detection of circulating tumor cells in human peripheral blood using surface-enhanced Raman scattering nanoparticles. Cancer Res. 71(5):1526-32.

Wang X, Zou M, Huang H, Ren Y, Li L, Yang X, Li N. 2013. Gold nanoparticle enhanced fluorescence anisotropy for the assay of single nucleotide polymorphisms (SNPs) based on toehold-mediated strand-displacement reaction. Biosens Bioelectron. 41:569-575.

Wang Z, Moult J. 2001. SNPs, protein structure, and disease. Hum Mutat. 17(4):263-70.

Wei F, Lillehoj PB, Ho CM. 2010. DNA diagnostics: nanotechnology-enhanced electrochemical detection of nucleic acids. Pediatr Res. 67(5):458-68.

Weigum SE, Castellanos-Gonzalez A, White C, Richards-Kortum R. 2013. Amplification-free detection of *cryptosporidium* nucleic acids using DNA/RNA-directed gold nanoparticle asssemblies. J Parasitol. 99(5):923-6.

Welter D, MacArthur J, Morales J, Burdett T, Hall P, Junkins H, Klemm A, Flicek P, et al. 2014. The NHGRI GWAS Catalog, a curated resource of SNP-trait associations. Nucleic Acids Res. 42(Database issue):D1001-6.

Wen W, Cho YS, Zheng W, Dorajoo R, Kato N, Qi L, Chen CH, Delahanty RJ, et al. 2012. Meta-analysis identifies common variants associated with body mass index in east Asians. Nat Genet. 44(3):307-11.

Wilcoxon JP, Abrams BL. 2006. Synthesis, structure and properties of metal nanoclusters. Chem Soc Rev. 35(11):1162-94.

Wilkins MH, Stokes AR, Wilson HR. 1953. Molecular structure of deoxypentose nucleic acids. Nature. 171(4356):738-40.

Willer CJ, Speliotes EK, Loos RJ, Li S, Lindgren CM, Heid IM, Berndt SI, Elliott AL, et al. 2009. Six new loci associated with body mass index highlight a neuronal influence on body weight regulation. Nat Genet. 41(1):25-34.

Withrow D, Alter DA. 2011. The economic burden of obesity worldwide: a systematic review of the direct costs of obesity. Obes Rev. 12(2):131-41.

World Health Organization. Obesity: preventing and managing the global epidemic. Report of a WHO Consultation. Geneva, Switzerland: World Health Organization, 2000. WHO technical report series 894.

Wray NR, Yang J, Hayes BJ, Price AL, Goddard ME, Visscher PM. 2006. Pitfalls of predicting complex traits from SNPs. Nat Rev Genet. 14(7):507-15.

Wu G, Zaman MH. 2012. Low-cost tools for diagnosing and monitoring HIV infection in low-resource settings. Bull World Health Organ. 90(12):914-20.

Wu Q, Saunders RA, Szkudlarek-Mikho M, Serna Ide L, Chin KV. 2010. The obesity-associated Fto gene is a transcriptional coactivator. Biochem Biophys Res Commun. 401(3):390-5.

Xi D, Luo X, Ning Q. 2007. Detection of HBV and HCV coinfection by TEM with Au nanoparticle gene probes. J Huazhong Univ Sci Technolog Med Sci. 27(5):532-4.

Xia F, Zuo X, Yang R, Xiao Y, Kang D, Vallée-Bélisle A, Gong X, Yuen JD, et al. 2010. Colorimetric detection of DNA, small molecules, proteins, and ions using unmodified gold nanoparticles and conjugated polyelectrolytes. Proc Natl Acad Sci USA. 107(24):10837-41.

Xia Q, Grant SF. 2013. The genetics of human obesity. Ann N Y Acad Sci. 1281:178-190.

Xiang X, Chen L, Zhuang Q, Ji X, He Z. 2012. Real-time luminescence-based colorimetric determination of double-strand DNA in droplet on demand. Biosens Bioelectron. 32(1):43-9.

Xie X, Xu W, Li T, Liu X. 2011. Colorimetric detection of HIV-1 ribonuclease H activity by gold nanoparticles. Small. 7(10):1393-1396.

Yang B, Gu K, Sun X, Huang H, Ding Y, Wang F, Zhou G, Huang LL. 2010. Simultaneous detection of attomolar pathogen DNAs by Bio-MassCode mass spectrometry. Chem Commun (Camb). 46(43):8288-90.

Yang TH, Kon M, DeLisi C. 2013. Genome-wide association studies. Methods Mol Biol. 939:233-51.

Yao YS, Li J, Jin YL, Chen Y, He LP. 2015. Association between PPAR-γ2 Pro12Ala polymorphism and obesity: a meta-analysis. Mol Biol Rep. 42(6):1029-38.

Yeh YC, Creran B, Rotello VM. 2012. Gold nanoparticles: preparation, properties, and applications in bionanotechnology. Nanoscale. 4(6):1871-80.

Yen CJ, Beamer BA, Negri C, Silver K, Brown KA, Yarnall DP, Burns DK, Roth J, et al. 1997. Molecular scanning of the human peroxisome proliferator activated receptor gamma (hPPAR gamma) gene in diabetic Caucasians: identification of a Pro12Ala PPAR gamma 2 missense mutation. Biochem Biophys Res Commun. 241(2):270-4.

Yonan AL, Palmer AA, Gilliam TC. 2006. Hardy-Weinberg disequilibrium identified genotyping error of the serotonin transporter (SLC6A4) promoter polymorphism. Psychiatr Genet. 16(1):31-4.

Zagorovsky K, Chan WC. 2013. A plasmonic DNAzyme strategy for point-of-care genetic detection of infectious pathogens. Angew Chem Int Ed Engl. 52(11):3168-3171.

Zaki M, Amr K. 2014. Apolipoprotein A5 T-1131C variant and risk for metabolic syndrome in obese adolescents. Gene. 534(1):44-7.

Zanoli LM, D'Agata R, Spoto G. 2012. Functionalized gold nanoparticles for ultrasensitive DNA detection. Anal Bioanal Chem. 402(5):1759-71.

Zar JH. 1998. Biostatistical Analysis, 4th edition. Upper Saddle River (USA). Prentice Hall.

Zavattari P, Loche A, Pilia S, Ibba A, Moi L, Guzzetti C, Casini MR, Loche S. 2011. rs9939609 in the FTO gene is associated with obesity but not with several biochemical parameters in Sardinian obese children. Ann Hum Genet. 75(6):648-54.

Zeggini E, Parkinson JR, Halford S, Owen KR, Walker M, Hitman GA, Levy JC, Sampson MJ, et al. 2005. Examining the relationships between the Pro12Ala variant in PPARG and Type 2 diabetes-related traits in UK samples. Diabet Med. 22(12):1696-700.

Zeng L, Lie P, Fang Z, Xiao Z. 2013. Lateral flow biosensors for the detection of nucleic acid. Methods Mol Biol. 1039:161-7.

Zhang C, Xu J, Ma W, Zheng W. 2006. PCR microfluidic devices for DNA amplification. Biotechnol Adv. 24(3):243-84.

Zhang C, Xing D, Li Y. 2007a. Micropumps, microvalves, and micromixers within PCR microfluidic chips: Advances and trends. Biotechnol Adv. 25(5):483-514.

Zhang C, Xing D. 2007. Miniaturized PCR chips for nucleic acid amplification and analysis: latest advances and future trends. Nucleic Acids Res. 35(13):4223-37.

Zhang C, Xu J, Ma W, Zheng W. 2006. PCR microfluidic devices for DNA amplification. Biotechnol Adv. 24(3):243-84.

Zhang D, Carr DJ, Alocilja EC. 2009. Fluorescent bio-barcode DNA assay for the detection of *Salmonella enterica* serovar Enteritidis. Biosens Bioelectron. 24(5):1377-1381.

Zhang J, Lang HP, Yoshikawa G, Gerber C. 2012. Optimization of DNA hybridization efficiency by pH-driven nanomechanical bending. Langmuir. 28(15):6494-501.

Zhao J, Tang S, Storhoff J, Marla S, Bao YP, Wang X, Wong EY, Ragupathy V, et al. 2010. Multiplexed, rapid detection of H5N1 using a PCR-free nanoparticle-based genomic microarray assay. BMC Biotechnol. 10:74.

Zhu KY, Clark JM. 1996. Addition of a competitive primer can dramatically improve the specificity of PCR amplification of specific alleles. Biotechniques. 21(4):586-590.

Ziegler A, Van Steen K, Wellek S. 2011. Investigating Hardy-Weinberg equilibrium in case-control or cohort studies or meta-analysis. Breast Cancer Res Treat. 128(1):197-201.

Zimmermann E, Skogstrand K, Hougaard DM, Astrup A, Hansen T, Pedersen O, Sørensen TI, Jess T. 2011. Influences of the common FTO rs9939609 variant on inflammatory markers throughout a broad range of body mass index. PLoS One. 6(1):e15958.

APPENDICES

Appendix I – AuNPs methods for DNA/RNA sensing

Table AI.1 – AuNPs detection techniques for DNA/RNA based on their physico-chemical proprieties.

Detection Technique	Nucleic Acid Target	Biological Target	Sample Amplification	Detection Limit	References
Colorimetric (non-cross-linking aggregation)					
Naked eye, UV–vis spectroscopy or optical monitoring system	dsDNA, SNP	*M. tuberculosis* Complex	PCR	0.75 ug total DNA	Baptista et al. 2006; Costa et al. 2010; Veigas et al. 2010; Silva et al. 2011; Veigas et al. 2012; Iwona et al. 2013
	dsDNA	*M. tuberculosis* spp.	Direct detection	18.75 ng of mycobacterial DNA diluted in a sample-volume of 10 µl.	Liandris et al. 2009
	dsDNA	Chlamydia infections	PCR	-	Jung et al. 2010
	RNA	*Salmonella typhimurium*	NASBA	-	Mollasalehi and Yazdanparast 2012
	RNA	*Salmonella enteritidis*; Salmonella typhimurium	NASBA RNA amplification	5 CFUs/reaction tube	Mollasalehi and Yazdanparast 2013
	dsDNA	*Escherichia coli*	Direct Detection	-	Padmavathy et al. 2012
	dsDNA	Human	PCR	200 DNA molecules	Sato et al. 2004
	dsDNA	Human	PCR	0.60 µM	Sato et al. 2005
	dsDNA, SNP	Human	PCR	100fmol	Qin and Yung 2007
	dsDNA, SNP	Human	PCR	18-32 ng/µl	Doria et al. 2010

	ssDNA	Human	AsPCR	10 pg	Deng et al. 2012
	mRNA	Human	Direct Detection	10 ng/mul of total RNA	Conde et al. 2010
Colorimetric (cross-linking aggregation)					
Light scattering imaging	ssDNA, dsDNA, SNP	Methicillin-resistant *Staphylococcus aureus* mecA gene	Direct Detection	50 pM–10 nM, 33 fM (using scattered light)	Storhoff et al. 2004
	ssDNA, dsDNA	Human Immunodeficiency virus type 1 *Mycobacterium tuberculosis* glmS *Bacillus glucanase*	Direct Detection	80 pM	He et al. 2008
	dsDNA, dsRNA	*Cryptosporidium parvum* Heat shock Protein 70	PCR, RT-PCR	10 amol	Javier et al. 2009
	RNA	*Cryptosporidium parvum* 18s rRNA	Direct Detection	1.2 x 10^7 copies/µL	Weigum et al. 2013
	RNA	*M. tuberculosis*	NASBA	10 CPU ml^{-1}	Pooria Gill et al. 2008
	dsDNA	MTBC and MTB strains	PCR	0.5 pmol	Soo et al. 2009
	ssDNA	Human papillomaviruses (HPVs)	Asymmetric polymerase chain reaction	1.4 × 10−4 µM	Chen et al. 2009
	dsDNA	*Chlamydia trachomatis*	PCR	0.25 nM	Parab et al. 2010
Naked eye, UV–vis spectroscopy or optical monitoring system	ssDNA	*Chlamydia trachomatis*	Isothermal target and signaling probe amplification (iTPA)	102 copies of target plasmid	Jung et al. 2011
	dsDNA	*Pseudomonas aeruginosa*, *Staphylococcus aureus*, *Staphylococcus epidermidis*, *Klebsiella pneumonia*, *Serratia marcescens*, and *Bacillus cereus*	PCR	-	Wang et al. 2012

	dsDNA	Kaposi's sarcoma-associated herpes virus	Direct detection	1nM	Mancuso et al. 2013
	dsDNA	*N. gonorrhoeae*; *T. pallidum*; *P. falciparum*; HBV virus	Non-enzimatic (MNAzyme)	1 nM	Zagorovsky and Chan 2013
	dsDNA	Salmonella	Direct Detection	37 fM	Kalidasan et al. 2013
	ssDNA	Human	SBE	-	Storhoff et al. 1998
	DNA SNP	Human	RCA	70fM	Li et al. 2010
	dsDNA	Human	PCR	-	Qin et al. 2010
Colorimetric (Sandwich assay)					
Colorimetric detection using gold label silver stain	ssDNA	*Ureaplasma urealyticum*; *Chlamydia trachomatis*	Multiplex asymmetrical PCR	5 pM	Cao et al. 2006
Naked eye or CCD camera (sandwich hybridization)	dsDNA	Hepatitis B virus (HBV)	PCR	10 mol/L	Xi et al. 2007
	RNA	Avian influenza virus H5N1	Direct detection	100 fM	Zhao et al. 2010
Colorimetric detection using gold label silver stain - Micro array	DNA, SNP	Human	Direct Detection	500 ng total gDNA	Bao et al. 2005
	DNA, SNP	Human	Direct Detection	1000 ng gDNA	Lefferts et al. 2010
Latteral flow test strips	dsDNA	*Vibrio cholerae*	PCR	5 ng	Chua et al. 2011
	ssDNA	*E. coli* O157:H7	Direct Detection	~0.4 nM	Rastogi et al. 2012
	RNA	HIV-1 RNA	NASBA RNA amplification	9.5 $\log_{10}$ RNA copies in 20 mL	Rohrman et al. 2012
	dsDNA, SNP	Human	PCR	50pM	Mao et al. 2009
	dsDNA, SNP	Human	PCR or PEXT	-	Litos et al. 2009
	miRNA	Human	Direct Detection	1fmol and 5amol	Hou et al. 2012
Colorimetric (Unmodified AuNPs)					

Hyper-Rayleigh scattering (HRS)	RNA; Single Base Mismatch	Hepatitis C virus	Synthetic Oligos	80 pM	Griffin et al. 2009
	RNA	Hepatitis C virus	Direct detection	< 100 fM	Shawky et al. 2010
	dNMPs - Nuclease nicking	HBV genomic DNA samples	Direct detection	5 nM	Liu et al. 2011
	RNA-DNA	Human immunodeficiency virus type 1 (HIV-1)	Enzymatic activity (HIV-1 RT)	-	Xie et al. 2011
Naked eye or optical monitoring system	dsDNA; ssDNA	*Bacillus anthracis*	Asymmetric polymerase chain reaction	0.1 pmol	Deng et al. 2013
	dsDNA	MTBC	PCR	1 ng for PCR product	Hussain et al. 2013
	dsDNA, SNP	Human	PCR	10nM	Li et al. 2004
	ssDNA, SNP	Human	Direct Detection	-	Tan et al. 2011
	DNA	Human	Direct Detection	6 nM	Chang et al.2013
Flourecence Spectroscopy					
Fluorescence spectroscopy (quenching by AuNPs)	cDNA	Multiplex - Hepatitis A virus, Hepatitis C virus, West Nile Virus, Human Immune Deficiency virus and Severe Acute Respiratory Syndrome virus (HAV, HCV, HIV, SARS, and WNV)	RT-PCR	n.a.	Sha et al. 2007
	dsDNA	*Salmonella enterica* serovar Enteritidis	PCR	2.15×10^{-16} mol (or 1 ng/mL).	Zhang et al. 2009
	dsDNA, SNPS	Human	Direct Detection	1 nM	Beni et al. 2010

	dsDNA, Haplotype	Human	ARMS	0.5 nM	Beni et al. 2012
	ssDNA	Human	Direct Detection	5-10 nM	Wang et al. 2013
	RNA	Human	RT-PCR	10.3 fmol of RNA	Rosa et al. 2012
Fluorescence spectroscopy Surface-energy transfer (NSET)	ssDNA; SNP	Campylobacter; *C. perfringens*; *S. aureus*	Synthetic oligonucleotides	600 fM	Darbha et al. 2008
	RNA; SNP	Hepatitis C virus (HCV)	Direct detection	300 fM	Griffin et al. 2009
Raman Spectroscopy					
Surface-enhanced Raman scattering (SERS)	DNA/RNA	Hepatitis A virus; Hepatitis B virus; Human immunodeficiency virus; Ebola virus; Variola virus; *Bacillus anthracis*	Direct detection	20 fM	Cao et al. 2002
	dsDNA; single base mismatch discrimination	HIV-1	Direct detection	subattomolar 10^{-19} M	Hu et al. 2010
	RNA	Human	RT-PCR	2.3 pM	Sun and Irudayaraj. 2009
	Cancer cells	Human	Direct Detection	1-720 cells/ml	Wang et al. 2011a
	DNA	Human	SBE	3 pM	Hu and Zhang 2012
Piezoelectric					
	dsDNA	*Escherichia coli* O157:H7	PCR	1.2×10^{2} CFU/ml	Chen et al. 2008

Piezoelectric biosensor / DNA probe functionalized quartz crystal microbalance	ssDNA	*Escherichia coli* O157:H7	asymetric PCR	2.0×10^3 CFU/mL	Wang et al. 2008
	ssDNA	*Bacillus anthracis*	asymetric PCR	3.5×10^2 CFU/ml	Hao et al. 2011
Electrochemical					
Cyclic voltammetry and Electrochemical impedance spectroscopy	dsDNA	*T. Pallidum*	PCR	0.5 pM	Sheng et al. 2010
Square wave anodic stripping voltammetry on screen-printed carbon electrode (SPCE) chips	dsDNA	*Bacillus anthracis*, *Salmonella enteritidis*	PCR	0.5 ng/mL for S. enteritidis; 50 pg/mL for B. anthracis	Zhang et al. 2010
Electrochemical impedance spectroscopy	dsDNA	Mycobacterium spp.	Direct detection	1.25 ng/ml genomic DNA	Thiruppathiraja et al. 2011
Cyclic voltammetry anodic stripping voltammetry (Electrochemical sequence-specific detection using silver-enhanced gold nanoparticles)	ssDNA (synthetic oligo nucleotide)	SARS (severe acute respiratory syndrome) virus	Synthetic Oligos	Sensitivity : 1.76 mA/pmol L-1 LOD: 2.5 pmol/L	Martinez-Paredes et al. 2012
Differential pulse voltammetry	dsDNA	*Salmonella enterica* serovar Enteritidis	Direct detection	100 ng/mL	Vetrone et al. 2012
Electrocatalytic signal amplification of gold nanoparticles (AuNPs)	cDNA	Hepatitis C virus	RT-PCR	n.a.	Li et al. 2012
Differential pulse anodic stripping voltammetry	ssDNA	*Vibrio cholerae*	Asymetric PCR	3.9 nM	Low et al. 2013
	dsDNA, SNP	Human	PCR	-	Ozsoz et al. 2003
Other					
Automated System (Light scattering imaging)	dsDNA	Influenza A virus, influenza B virus; respiratory syncytial virus A and B	PCR	-	Jannetto et al. 2010
Bio-MassCode mass spectrometry	dsDNA	Multiplex - HIV, HBV, HCV, and TP	Direct Detection	10^{-18} M	Yang et al. 2010

Appendix II – SNP genotypes and related flanking sequences

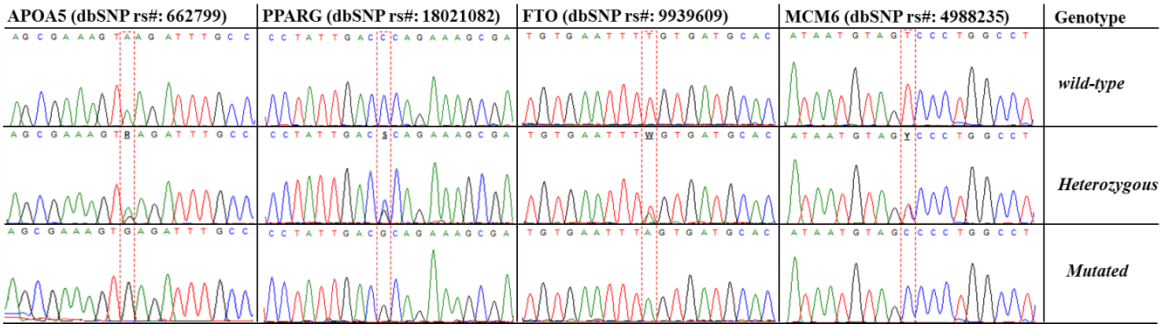

Figure AII.1 – Genotype characterization of each SNP studied. Illustration of chromatogram obtained by Sanger sequencing for the 4 SNPs studied – APOA5 (dsSNP rs#: 662799), PPARG (dsSNP rs#: 1801282), FTO (dsSNP rs#: 9939609) and FTO (dsSNP rs#: 4988235).

Homo sapiens apolipoprotein A-V (APOA5), RefSeqGene on chromosome 11 – Flanking region dsSNP rs#: 662799

TGGGCTGGGGAGCACAGAGCTGTTGGGGCTCAAGAGGACTGACCTAGGTGAGTCA
AGGAGGCTAGGGTGTCTTCCTCAGACATGGGAAGAGGGCGTGCTCTTGCTACCTCA
GTCACATAGCAGGGAGCGTGGTGCTCTAACCCCTTCGCAAAGGTCCCAGACCCCAG
GAACAGTTCTCTAGGCCACTTCTACCACCTCTCCCCTGCCCACCTGTCTCCCTCCCTC
CCATTTCTGGTGGAAAAACTGAGCCATAATGAGGGCGAAGAGGCAACTCTGCCAA
AATGTTCCAAGAGGACGTCTTAGGGGCCACCCCAGGCTCTCCCCTGAGGCCACCTG
CAATGCCCTCCCTTAGGACTGTGACCCCCATCCCTCTGCCCCAGCTGCTCACCTGCT
CACGTCTGGGCACAGAGAGCAGACATTCTGCTTTATACTCCAGGGCCCTGAGCCTC
TGGCACCAATTGCTCTGAGTAAATACCACGTGGAAGTTCAAAAGAAGTTGACCTCA
GCTGCCTCCCAGCACTCACCTCCTGCCCTTTCCCTGGCACCCAGAGGGTTAATGAGT
GCCCTGGTATCAGGGGCTGCCCCAGTAGAGAAGTGCTTCCCAGGAGCTTTACGGGG
GATGGGGCTGAACTCCTCACCCAGTTTCTCCCAAACCCCATGACCTTTAACCTTCCC
ACTGACCTGCTGGCTGGCCCACCAACAGAGAAGAACCTGTTTGTCTGCCAAGGGCC
CCTCTCTTACACAACTACCCAGAGTCACTGTGTCCCAGCCGGCAAGATGGACAGTG
TTCACCTACCAGCCAGAACCCGAGCAGCCCCTGAAAGCTTCACTACAGGTTCCGCA
GGCATCCTCAGCCAGCATTCATAGGGTTAAAGACCAACCACATCCCTCTTTATGAA
ACAATCCTGGAACAAGCAAGGGAAGCCAGGCAGGGTGAAGATGAGATGGCAAGA
GGCATCTGGGCCAGGGACTCTGAGCCCCAGGAACTGGAGCGAAAGTRAGATTTGCC
CCATGAGGAAAAGCTGAACTCCACTCGCAGGGCCTCTGAGGAGAGCAAGCCCAAA
TGCTCAGATCTTCTCTGATGACACACCCACTCCGTCTACAGTACTCATACACACGTT
CACAAGCTCCCGATTCTTGGTCCTAAATGCATCTTGAATCAATCCCCTCTCCTCCAT
TTCCACTACCATCATTGCACCAGTTGTCTGTCACCTTGATTGCATTCATAGCCTCCA
ACAGGTCTTTCTACCACACTCCTGCCCATTTAATTCATCCTCCACTGTGGCTCATCCT
GACTCATTTCCAGTCTCATCTGCTGCCACATAAAACCACGGCATTCCCTGAGCCTTT

ATACAGGCTTCCCTCTGCTTGAAATAGCCTATCCCCTGGTGAATATATATTCATTTT
TTAGAGTTAGTTTGTATTAGTTAGAATTAGACTTGGCTGCAAGGGACATATATATGT
GTGTATATATATACACACACACATGTATATTTTATATTCTTGCATACATATATGTAT
ATATATGTGTGTGTGTATATATACACATATATATATACAAGATACTGCTCTTACCAC
TCATACTGACATCCCATTGGCCACAAGTTAGTCACATGGCTACACTTAGCTGATATA
TATGTGTATATATATATATGCAAGAGAATAGCTTAAACAAAATGGAGTCTTATTTCCTT
CTCATGTAAATGTAGGCCAGCTCGGGCTGCTTTTATCTTGTTGCACTATTATCATCA
ACAAGACGCTCATATCCAAGTTCCAGCTGCTTCACCTCCAGCTACCAAGTTCACCTC
CCAGGGAACAGGAAGGAGGAAAAGGAGAAGGACATGTTCCTTCCTTTTAAAGACA
CATCCCAGATATTGCCATTACCACTTGTACTGACATCCCATTGGCCACAACTTAGTC
ACATGGCTACACTTAGCTGAAAAGGAGGCTGGGAAATATAGTTTTTATTTTGGATG
GCTGTATGCCTAGCTGAAAAAGGACT

Homo sapiens peroxisome proliferator-activated receptor gamma (PPARG), RefSeqGene on chromosome 3 - Flanking region dsSNP rs#: 1801282

AGGCCTTGAGCAAGAAGCCAGCTTTTTCCTGATTACAAAACTGACCACAATTCCTC
GCCAACCTAACAGCGTAAGTCTATTTTTTTCTGGTGGTGTGTTATTCTTCTCATAGA
GAACTCCATTTTTTCATTATGACATAGCACTTATCGTTTAAACATCAATTGATGTTC
AAACATCAGCTGGTGTAACATTGCTGCAGTTGCTATTGATGGATAAGCTGAAGTTTT
TAAGAAAGCAAACCCGATGTATAAAATTGAAACCATATCAAACCCTTCTTCATTCT
CTCAGCTATTTAATTTTACAGAATTTAGATAGCAGTCAGTATCATTTTGGGCTTCAC
AAATCAGTAGAGTAAGTACCTTAGGAATATAACATTTCAGTAGCATGCTGATACCA
ACGTTTAAACTATGGATACATATTTGAATTCCAAATTTTTCTTCAAATAATGTGATT
AGAGATTCAACCAGGAATAGACACCGAAAGAAAACTTTGCCCAAATAAGCTTTCTG
GTATTTCATAAGCAAGAGATTTAAGTTTTCCATTTAAGAAGCAATTGTGAATTTTAC
AACAATAAAAAATGCAAGTGGATATTGAACAGTCTCTGCTCTGATAATTCTAAATA
CAGTACAGTTCACGCCCCTCACAAGACACTGAACATGTGGGTCACCGGCGAGACAG
TGTGGCAATATTTTCCCTGTAATGTACCAAGTCTTGCCAAAGCAGTGAACATTATGA
CACAACTTTTTGTCACAGCTGGCTCCTAATAGGACAGTGCCAGCCAATTCAAGCCC
AGTCCTTTCTGTGTTTATTCCCATCTCTCCCAAATATTTGGAAACTGATGTCTTGACT
CATGGGTGTATTCACAAATTCTGTTACTTCAAGTCTTTTTCTTTTAACGGATTGATCT
TTTGCTAGATAGAGACAAAATATCAGTGTGAATTACAGCAAACCCCTATTCCATGC
TGTTATGGGTGAAACTCTGGGAGATTCTCCTATTGACSCAGAAAGCGATTCCTTCAC
TGATACACTGTCTGCAAACATATCACAAGGTAAAGTTCCTTCCAGATACGGCTATT
GGGGACGTGGGGGCATTTATGTAAGGGTAAAATTGCTCTTGTAGTTTGTCTTCCAG
GTTGTGTTTGTTTTAATACTATCATGTGTACACTCCAGTATTTTAATGCTTAGCTCGT
TGCTATCGCGTTCATTTAAAAACATGTTCAGAACCTTAAAAAAGGAAACCTAACCT

AATCTATTTTATTCTGTGCATGGCTCCCATTTCCTGAATTTTAAGCATTAAAGGTAT
AGTTATATCCAAAAACAATCCTGTTCATTTTTATTTCCTGAGTTTGCATAGATTTCCC
AAGAATACATAAGGGCTTTTTAGACTTGAAGGGTCACTTTTTCCTCTTTTCATCTCA
TATGTTAGAGATCTCTCATAACTGTTTTTATCCCTCTTGCAGCACTTTTATTCCTCTT
GAAGTACTCTCAGCTCTTTTCTGTTCTATTTTGAAATCTAGGTATTGTGTGTGCACTT
CAGCTCTCCCAAAGAATTGTAAATTCCCAGAGTGTAGGACCAAGTGGTGCTCTTTA
TTAGATTTCTTAGGATACTTCCTAGCATAGTGCCTAATGCATTGCAGAATAGATTGT
CGGAACCTTGAAAAATATCTGTTCCAAGCATCACATTTTATGCATAAAGAAAATGA
GGTCCCTAAAACAGTAAATGCCTATTGCAAGTGACTACCTATTAACTTCTCTTCAGA
TGTGTCAGAATCAGATACCTCCTTTTCAATATTTCTTTCTTGGCCATTGCAAAATAT
AAGTTCTCCATTTCTATAGCTCCTTCTACTGGAGTTTCTTAGCACAGCCTTTTCTGTT
TTGTATTGTCTCGTATTGATGTCTATATTTCTATTCATTTTATTTTTCTCTTCTCAGAT
TCTGTGTAAAAATAGATTGTTAGCTAGTGTGATTCATGTTTTATAATATAAGTGCTA
AAGCATTAA

Homo sapiens fat mass and obesity associated (FTO), RefSeqGene on chromosome 16 - Flanking region dsSNP rs#: 9939609

ATGATTAAGAAAGATAGCTGGGCGCGGTGGCTCATGCCTGTAATCCCAGCACTTTG
GGAGGATGAGGCGGGTGGATCATGAGGTCAAGAGATCAAGACCATCCTGACCAAC
ATGGTGAAACCCGGTCTCTACTAAAAATACAAAAATTAGCTGGGCGTGGTGACATG
CGCCTGTAGTCCCAGCTACTCGGGAGGCTGAGGCAGGAGAATTGCTTGAACCCGGG
AGGCGGAGGTTGCAGTTAGCCGAGATTCCGCCGCTGCACTCCAGCCTGGTGACAGA
GCGAGACTCCATCTCAAAAAGAAAAAAAAAAAAAAAAGAAAGTCATGATAAAGA
GTGTGGATTTTATTTTACGCAAAGTGGGAGCTCATTAAGAAGGTAAAAGTTTTTAA
GCAAGGGAATGACATGATTTGACCTACTTTTTAAAGGAGGTTGCTCTGACGGCTGT
AGAGGATAGACCATAGGCAGGGGACAATAGAGAGACCAGGAGGAGGCTGTTGGA
GTGTGTTAGGCGAGATATGGTGAGTGGTTTCAGAGGCTTGTGTGAGAAAGTTGATA
CACTGCCCCTACCCCATGCAAACACACACTTTCTTTTCTTATGATGACCTTTCTTTAA
AAGCATTTGTTGGAATATGAGATTATAGGCCATAAGTGAGAAAACAACTCTTTTTG
AGCTGTGAGGAATACTAGGAGAGGAGAAAGTGAGCTGTGTGTGCTGCCCATGGTG
GTACGCTGCTATGGTTCTACAGTTCCAGTCATTTTTGACAGCATGGATTCAATGCAA
AATGGCAACACACACTCTGTATCTTTTGGCAGATCAGAACATAATGAAAATAAAAT
AAAAAAATTCAAAACTGGCTCTTGAATGAAATAGGATTCAGAAGAGATGATCTCAA
ATCTACTTTATGAGATAATGTCCTTTTTAAAAATAAACACTAACATCAGTTATGCAT
TTAGAATGTCTGAATTATTATTCTAGGTTCCTTGCGACTGCTGTGAATTTWGTGATG
CACTTGGATAGTCTCTGTTACTCTAAAGTTTTAATAGGTAACAGTCAGAAATGGAGT
GGGAGAGCATAAAAGCAAACTGAAATGCAAATAGCTGGTACCCTGAAGCCATTAA

CTTTAAGCTGGTTATTCCTGACCTACTGTTTGGACATAAGATGGTAGAGAGGCTGA
GTGTGACTTGAACATTTGTTCCTTAGAAACACCATCCTTGGGCTGGGCGCAGTGGCT
CACGCCTGTGTTTCCAGGACTTTGGGAGGCTGAGGCGGGCAGATCATGAGGTCAAT
AGATCGAAACTATCCTGGCTAACACGGTGAAATCCCATCTCTACTAAAAATACAAA
AAATTAGCCAGGTGTGGTGGCGGGTGCCTGTAGTCCCAGCTACTCGGGAGGCTGAG
GCAGGAGAATTGCTTGAACCCAGGAGGCAGAGGTTGCAGTGAGCCAAGGTCGCAC
CACTGCACTCTAGCCTGGGCAACAGAGTGAGACTCCTTCTCAAAAAAAAAAAAAA
AAAAAAAAAAAAAAAAAAGAAAAAGAAACACCATCCTTGTAAAGAGAGCGCATA
CACCTTCAATTTCTAGGGCAGCAGCGTTTGCTTTACAACTTCTATGTCTTGGTGGGA
GTAGCACTATCTATCACCTTATGGGCCAAAGGGAAAAAGTCCAGTGAAAATGGCTC
TGATGTTGTTGGAAGTGGGAAAGCAGGTTAATAGGTTCTTCTTAATGGAAAATGCA
GCCAATATTGGCCAACTTACTTTGATTTCGGTAGTCATAACACCACCCTGGAAGGC
ACCCTAGATAGAGGTCACTTGCTACCACTCATTTTACAGATCAGGATACTAAGGAT
TTTCCTGATTTTAAGCATTAAGTATGGATATCCCTGTTGGTTGAAGTTAAATTGGTC
AACTAGAATTTAAAAGCAAAAATTAAAAAAAAATTATTTTGTATTAGGTTTCAAAG
GAATTGTTGTCAGTAGGAGAAGCCTGATTGTTCCTTTTACGCT

Homo sapiens minichromosome maintenance complex component 6 (MCM6), RefSeqGene on chromosome 2 - Flanking region dsSNP rs#: 4988235

CAACTCATTTCAGGAACTATCACAATGAAAAAAAAAGTACAAATGTTAGCATGGTT
TTAGAATGACCTTGTCCCAGGGTATCTTGCCTATCCAAATTCTGCACACCCTTCAGT
GACTGGGTTTAAACGTCGGCACCTCCCTGAGTCCTCCTCCTTCTTTGGTAATAAAGT
AATTCATCTCAGCACTCTGGTTGTGATGCTCTATTCTCCCTCTCGTTTTTTTTTAATTT
CCAACTTATATTTTAGGTTCGGGGGTACACATGCAGGTTTGTTACATAGGTAAACTG
TGTGTCATGGGGATTTAGTATATAGATTATTTCATCACCCACTCTATTTTTTACATGC
TTAATTAAATACATGTCTCGTTCCCACCAGATTAGCAGCAATGGAAGGCAGGGGCT
CTCATTCATTTTTTGTCCCCTACAGGTGTTCCCTAAATATTGGGTGAATCAAAGAAT
ATTAAATAACCTAGTGTGAAAGTACTTCGTCAATAGTAAAGTACCATATCAAAGAA
TTTGAAAATTTAGTGGAAAAAAGCCAAAAAATTAACCTGTGGGATAAAAGTAGTG
ATTGAAGTCGGAACAGTGGTTACTTCAGGGGAAGAGGGCTAAGACTGAAAAGAGG
CAGGGGTTTGGAACTTTCTGAAATTATGGAAATGTTTTGGATCTTGAGCTGGGTATT
CACAAGGATGTATGTGAAAAAACTCACCATGCCATACATTTCCCTTTTTATAAATTA
TACCTCAGTCACACTGTAAAAAAAAGCCAAACCCCCTTTTCAAAGACGACCTTACA
TCAAACCTATTAATAAAACTAGGAAAACGCAGGGCTGCTTTGGTTGAAGCGAAGAT
GGGACGCTTGAATGCCCTTTCGTACTACTCCCCTTTTACCTCGTTAATACCCACTGA
CCTATCCTCGTGGAATGCAGGGCTCAAAGAACAATCTAAAAATCAAACATTATACA
AATGCAACCTAAGGAGGAGAGTTCCTTTGAGGCCAGGGRCTACATTATCTTATCTG

TATTGCCAGCGCAGAGGCCTACTAGTACATTGTAGGGTCTAAGTACATTTTTCCTGA
ATGAAAGGTATTAAATGGTAACTTACGTCTTTATGCACTCTATAAACTATGACGTGA
TCGTCTCCGTCTAACAACTACACTCAAATGCTTACCAAGCTCTTTAAAGGGAAGAA
TTCCATGGTCGTATGAGCATTCAACAGTTACATAAAAATGTATTTGCAGTGAATTCT
AGTATGTCCCATACCAAAGATTAAAAACATGCAACAAATCTGTTTATCTCTGCTCTC
ATCATATCAAAGTGACTCTGATACCTCATCACAGCAGTGCATCCGAGCCATAGCTT
CAGAGAGACGAATCATGCTCTCAAGCTGTCGCACTGTAATCCTCCATGAAGACTTG
GTCACTCCAGAACCATCTCTCTGGCGGAGATGTTTATATTGCTCCACAATGAAGTCC
TCTGACTCTTTGGAAATCTGTTTCAGATCATCACTCAAGTTAGAGAAACATTTCTAT
TTGATGAGAGCTACGGTAAACCTAAGTTTAAGAGCCTTCCAGGTGGAAACATTTAG
GGAACCTGAGAGGGTTGAAACTTTGAGAAGCCAGTGACAATAAATTACTATTGTAA
TGTCTTTCAAAAGAAACTAATATTAAGGAGGCTTGTGAATTCCATGTTACTAATTTT
ATGAACCTGAAAAAAGGCTTAGTATTTAAGCAAATGACCATTTCTAAAAGCTGCTT
AACAAGCTGAAGCAATGGAACAAGATGTAATGTCTTTTACACCTCAGGATGTCAGT
GCTCATTAAATAAATTAATGCTCAGTATTTGAGGCTCAATTAATTAACTCACACTCT
TTGCAGGGAAAAAAAAGCTGTTTCAATAAACTTTATATCTAAAGGATCCTCAGCTT
TTCAGAGCAAGGAATTCACCATATTAAGGAAGCATGCCAAGGTTACAGAGGGATC
AGTATATCAGTATGCAGTAATGGA

Appendix III – Nanofabrication characterization

Table AIII.1 - Main characteristics of the operational amplifiers used in various system optimization stages.

Op. amp.	Input bias current [pA]	Input impedance [Ω]	Used in
741	30000	$2x10^6$	(Bernacka-Wojcik et al. 2013)
TL081	30	10^{12}	AuNPs (present work)
AD549	0.05	10^{13}	Au-nanoprobes (present work)

Table AIII.2 - The curvatures (*R*), distances (*d*) and the characteristics of the resulting light beam (*y* and *θ*) for the input bi-concave air microlens and the input bi-convex PDMS microlens.

	Air lens	PDMS lens
R	-175 μm	250 μm
d_1	100 μm	80 μm
d_2	80 μm	70 μm
y	50.160 μm	50.004 μm
θ	-0.001200°	0.000146°

Table AIII.3 - The curvatures (*R*), distances (*d*) and the characteristics of the resulting light beam (*y* and *θ*) for the output bi-concave and bi-convex air microlens.

	Output air lenses
R2	-210 μm
d3	180 μm
R3	180 μm
d4	50 μm
y	6.044 μm
θ	-0.141970

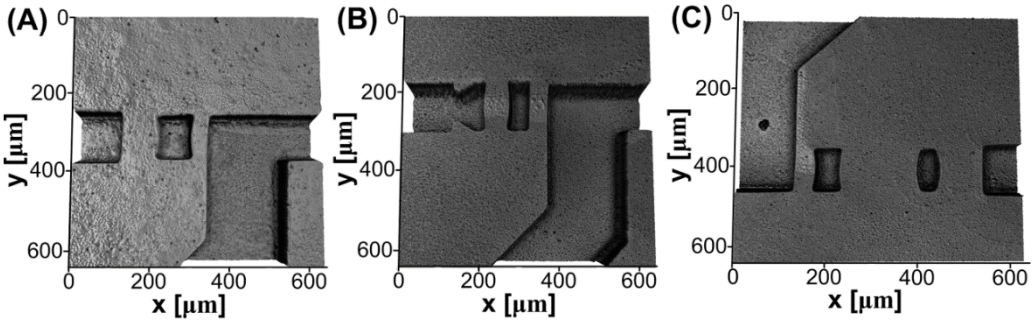

Figure AIII.1 - Confocal microscope images of fabricated 2D microlenses: (**A**) input air lens; (**B**) input PDMS lens and (**C**) output air lenses.

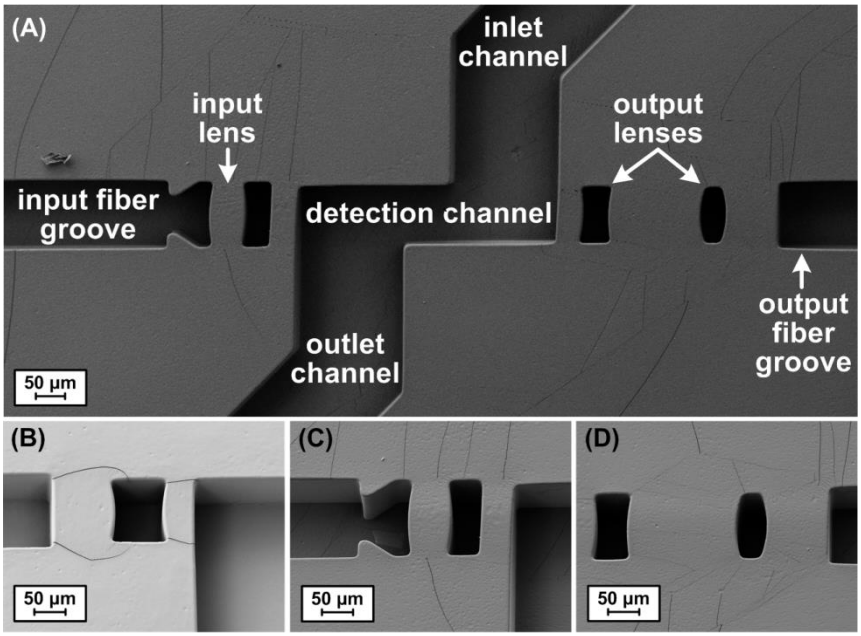

Figure AIII.2 - Scanning electron micrographs of the PDMS chip: (**A**) main chip features; (**B**) input air microlens; (**C**) input PDMS microlens and (**D**) output air lenses. The images B – D were taken with the stage 20 degrees tilted to visualize better the aspect ratio.

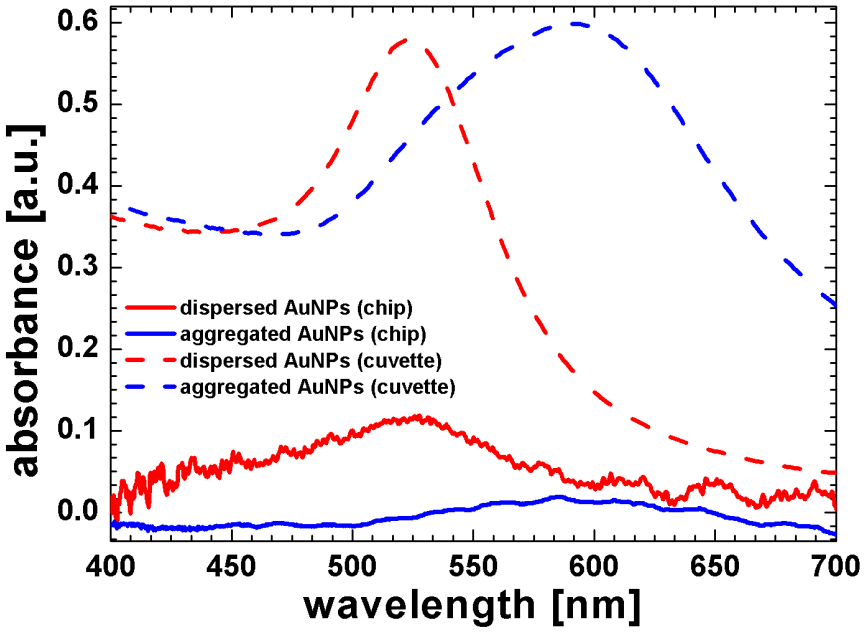

Figure AIII.3 - Absorption spectra of the dispersed and aggregated AuNPs. (3 min after salt addition) acquired using miniature fiber optic spectrophotometer integrated with a microfluidic chip with air lenses ('chip'; 3 µl, integration time: 610 ms, the samples were injected into the channel directly after salt addition) and using Shimadzu spectrophotometer in cuvette ('cuvette'; 60 µl).

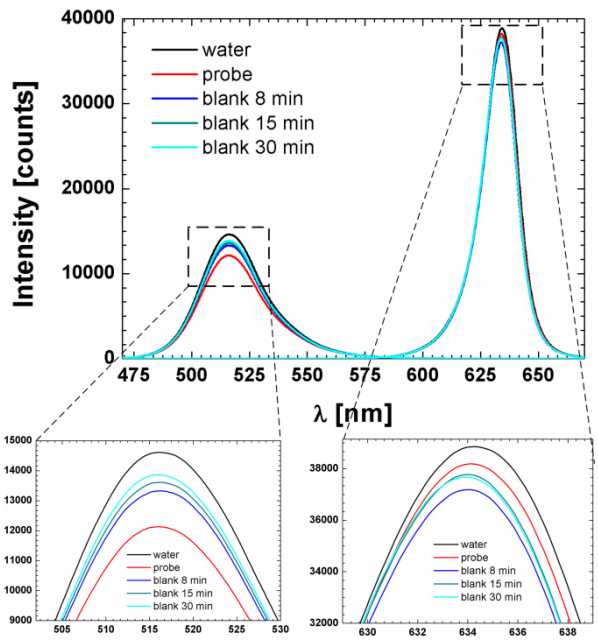

Figure AIII.4 - Transmission spectra of green and red LEDs. Data acquired using miniature fiber optic spectrophotometer integrated with microfluidic chip with air lenses filled with water, the Au-nanoprobe and blank (8 min; 15 min and 30 min after salt addition; the samples were injected into the channel directly after salt addition). LEDs powered with 0.4 A; reference: empty chip; integration time: 8 ms.

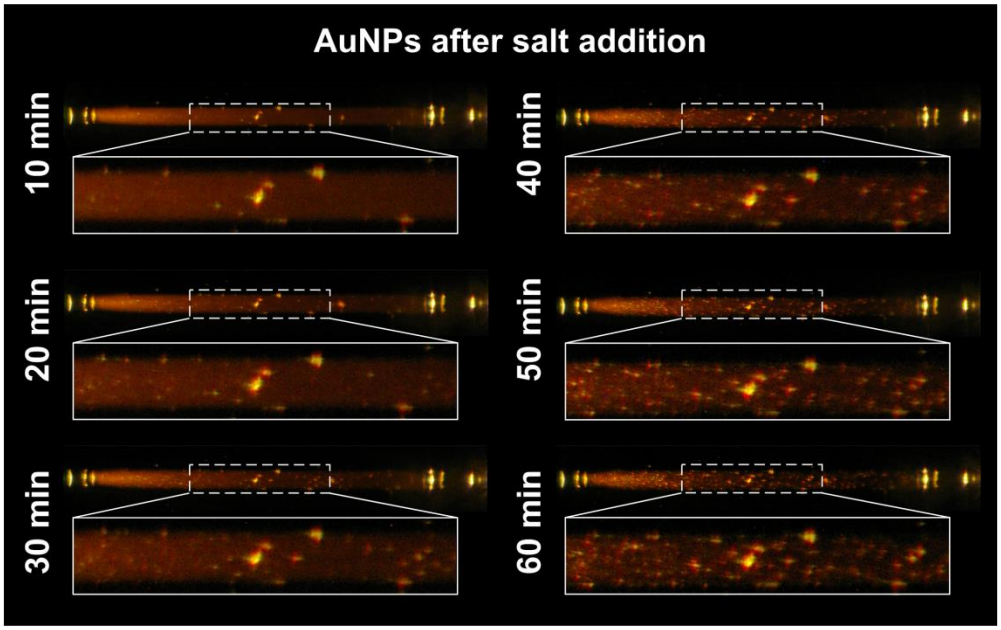

Figure AIII.5 - Microscopic images of chip with air microlenses. Chip illuminated by halogen lamp and filled up with AuNPs 10 to 60 min after salt addition (the samples were injected into the channel directly after salt addition). The images were taken every 10 min in dark conditions using Stereo Microscope and Pentax K100 camera with long exposure time (30 s).

Appendix IV – List of publications

Diabetes, Metabolic Syndrome and Obesity: Targets and Therapy Dovepress
open access to scientific and medical research

Open Access Full Text Article

RAPID COMMUNICATION

Association of *FTO* and *PPARG* polymorphisms with obesity in Portuguese women

Fábio Ferreira Carlos[1,2]
José Silva-Nunes[3,4]
Orfeu Flores[1]
Miguel Brito[3]
Gonçalo Doria[1]
Luísa Veiga[3]
Pedro Viana Baptista[1]

[1]Centro de Investigação em Genética Molecular Humana, Universidade Nova de Lisboa, Caparica, Portugal; [2]Investigação e Serviços em Ciências Biológicas, Stab Vida, Caparica, Portugal; [3]Escola Superior de Tecnologia da Saúde de Lisboa, Lisbon, Portugal; [4]Endocrinology Department, Curry Cabral Hospital, Lisbon, Portugal

Purpose: We evaluated the association between risk of obesity in the Portuguese population and two obesity-related single-nucleotide gene polymorphisms: *fat-mass and obesity-associated* (*FTO*) rs9939609 and *peroxisome proliferator-activated receptor gamma* (*PPARG*) rs1801282.

Patients and methods: A total of 194 Portuguese premenopausal female Caucasians aged between 18 and 50 years (95 with body mass index [BMI] ≥30 g/m^2, 99 controls with BMI 18.5–24.9 kg/m^2) participated in this study. The association of the single-nucleotide polymorphisms with obesity was determined by odds ratio calculation with 95% confidence intervals.

Results: Significant differences in allelic expression of *FTO* rs9939609 ($P<0.05$) were found between control and case groups, indicating a 2.5-higher risk for obesity in the presence of both risk alleles when comparing the control group with the entire obese group. A fourfold-higher risk was found for subjects with class III obesity compared to those with classes I and II. No significant differences in BMI were found between the control and case groups for *PPARG* rs1801282 ($P>0.05$).

Conclusion: For the first time, a study involving an adult Portuguese population shows that individuals harboring both risk alleles in the *FTO* gene locus are at higher risk for obesity, which is in agreement to what has been reported for other European populations.

Keywords: rs9939609, rs1801282, BMI, SNP, odds ratio

Introduction

Obesity prevalence has grown dramatically in recent decades and shows no signs of decline. According to the World Health Organization (WHO), it is estimated that 1.5 billion people are overweight, of which 500 million are obese.[1] Obesity and overweight result from a combination of genetic background, environmental, and lifestyle factors, and are intrinsically associated with increased risk of associated disease, such as hypertension, dyslipidemia, and type 2 diabetes.[2] Several gene-association studies have led to the identification of different loci (single nucleotide polymorphisms [SNPs]) that contribute to obesity and overweight.[3] One of these SNPs, rs9939609, in the *fat-mass and obesity-associated* (*FTO*) gene, has been described as a risk factor to obesity, and strongly associated with body mass index (BMI) increments in European adults.[4] Frayling and colleagues[4] demonstrated that the presence of the risk allele A is cumulative and represent a 20% higher risk for the development of obesity and 13% for the development of overweight. This association was later confirmed by several other studies in different populations.[5–7] Another gene playing an important role in

Correspondence: Pedro Viana Baptista
Centro de Investigação em Genética Molecular Humana, Faculdade de Ciências e Tecnologia, Universidade Nova de Lisboa, Campus de Caparica, Caparica 2829-516, Portugal
Tel/Fax +351 21 294 8530
Email pmvb@fct.unl.pt

submit your manuscript | www.dovepress.com
Dovepress
http://dx.doi.org/10.2147/DMSO.S45779

Analytical Biochemistry 465 (2014) 1–5

Contents lists available at ScienceDirect

Analytical Biochemistry

journal homepage: www.elsevier.com/locate/yabio

Characterization of genomic single nucleotide polymorphism via colorimetric detection using a single gold nanoprobe

Fábio Ferreira Carlos [a,b], Orfeu Flores [b], Gonçalo Doria [a], Pedro Viana Baptista [a,*]

[a] Human Molecular Genetics Research Centre (CIGMH), Department of Life Sciences, Faculdade de Ciências e Tecnologia, Universidade Nova de Lisboa, Campus de Caparica, 2829-516 Caparica, Portugal
[b] STAB VIDA–Investigação e Serviços em Ciências Biológicas, Madan Parque, 2825-182 Caparica, Portugal

ARTICLE INFO

Article history:
Received 28 March 2014
Received in revised form 5 July 2014
Accepted 17 July 2014
Available online 29 July 2014

Keywords:
Gold nanoparticles
Nanodiagnostics
Non-cross-linking method
Point of care
FTO gene
Genotyping

ABSTRACT

Identification of specific nucleic acid sequences mediated by gold nanoparticles derivatized thiol-modified oligonucleotides (Au–nanoprobes) has been proven to be a useful tool in molecular diagnostics. Here, we demonstrate that, on optimization, detection may be simplified via the use of a single Au–nanoprobe to detect a single nucleotide polymorphism (SNP) in homo- or heterozygote condition. We validated this non-cross-linking approach through the analysis of 20 clinical samples using a single specific Au–nanoprobe for an SNP in the FTO (fat mass and obesity-associated) gene against direct DNA sequencing. Sensitivity, specificity, and limit of detection (LOD) were determined, and statistical differences were calculated by one-way analysis of variance (ANOVA) and a post hoc Tukey's test to ascertain whether there were any differences between Au–nanoprobe genotyped groups. For the first time, we show that the use of a single Au–nanoprobe can detect SNP for each genetic status (wild type, heterozygous, or mutant) with high degrees of sensitivity (87.50%) and specificity (91.67%).

Obesity and overweight are a clinical condition developed from the excessive accumulation of fat mass and considered by the World Health Organization as one of the most important diseases of the 21st century [1]. Obesity is a multifactorial disease combining environmental and lifestyle factors onto a genetic background. Therefore, it is relevant to tag and characterize important genetic markers that may allow identification of individuals at increased risk and target them for an earlier clinical and lifestyle intervention. One of the most important single nucleotide polymorphisms (SNPs)[1] associated with increased risk for obesity and body mass index (BMI) increment in several populations is encoded in the FTO (fat mass and obesity-associated) gene (SNPref rs9939609) [2–6]. During the past few decades, SNP genotyping has become increasingly relevant, usually relying on enzyme [7,8] or hybridization-based [9,10] approaches.

Gold nanoparticles functionalized with thiolated oligonucleotides (Au–nanoprobes), due to their unique optical proprieties, have been used as relevant signal transduction elements in nucleic sequence recognition assays with high sensitivity and sensitivity at much lower costs when compared with conventional methods. Monodisperse Au–nanoprobe solutions present a characteristic surface plasmon resonance (SPR) band at approximately 525 nm (red color solution) that is red-shifted on salt-induced aggregation (blue color solution) [11,12]. This is the mechanism of the non-cross-linking colorimetric detection of DNA, where hybridization to a specific complementary target leads to Au–nanoprobe stabilization and resistance to salt-induced aggregation [13–15]. SNP characterization requires that for each locus the three possible genotypes (wild-type, mutant, and heterozygous status) are detected. Under standard conditions, the non-cross-linking method (like most hybridization approaches) requires a set of two Au–nanoprobes capable of individually identifying each allele variation because this method is limited to a red to blue color change. Here, we present the design and optimization of a single Au–nanoprobe that is capable of overcoming this limitation and clearly distinguishes between each genetic status, thereby halving the number of tests per locus. We validate this approach via analysis of SNP (rs9939609) using a sole Au–nanoprobe in clinical samples.

* Corresponding author. Fax: +351 212948530.
E-mail address: pmvb@fct.unl.pt (P.V. Baptista).

[1] *Abbreviations used:* SNP, single nucleotide polymorphism; FTO gene, fat mass and obesity-associated gene; SPR, surface plasmon resonance; Au–nanoprobe, gold nanoparticle functionalized with thiolated oligonucleotide; PCR, polymerase chain reaction; UV, ultraviolet; AuNP, gold nanoparticle; ANOVA, analysis of variance; UV/Vis, UV/visible; LOD, limit of detection; CI, confidence interval.

http://dx.doi.org/10.1016/j.ab.2014.07.019
0003-2697/

ARTICLE

BIOTECHNOLOGY and BIOENGINEERING

Single Nucleotide Polymorphism Detection Using Gold Nanoprobes and Bio-Microfluidic Platform With Embedded Microlenses

Iwona Bernacka-Wojcik,[1] Hugo Águas,[1] Fabio Ferreira Carlos,[2,3] Paulo Lopes,[4] Pawel Jerzy Wojcik,[1] Mafalda Nascimento Costa,[1,2] Bruno Veigas,[1,2] Rui Igreja,[1] Elvira Fortunato,[1] Pedro Viana Baptista,[2] Rodrigo Martins[1]

[1]Departamento de Ciência dos Materiais, Faculdade de Ciências e Tecnologia, Universidade Nova de Lisboa, Campus de Caparica, CENIMAT/I3N, Caparica 2829-516, Portugal; telephone: +351212948562; e-mail: ib@uninova.pt

[2]Departamento de Ciências da Vida, Faculdade de Ciências e Tecnologia, Universidade Nova de Lisboa, Campus de Caparica, CIGMH, Caparica 2829-516, Portugal; telephone: +351212948562; e-mail: pmvb@fct.unl.pt

[3]STABVIDA, Investigação e Serviços em Ciências Biológicas, Lda. Madan Parque, Caparica 2825-182, Portugal

[4]Department of Physics and I3N, Campus Santiago, University of Aveiro, Aveiro 3810-193, Portugal

ABSTRACT: The use of microfluidics platforms combined with the optimal optical properties of gold nanoparticles has found plenty of application in molecular biosensing. This paper describes a bio-microfluidic platform coupled to a non-cross-linking colorimetric gold nanoprobe assay to detect a single nucleotide polymorphism associated with increased risk of obesity fat-mass and obesity-associated (FTO) rs9939609 (Carlos et al., 2014). The system enabled significant discrimination between positive and negative assays using a target DNA concentration of 5 ng/μL below the limit of detection of the conventionally used microplate reader (i.e., 15 ng/μL) with 10 times lower solution volume (i.e., 3 μL). A set of optimization of our previously reported bio-microfluidic platform (Bernacka-Wojcik et al., 2013) resulted in a 160% improvement of colorimetric analysis results. Incorporation of planar microlenses increased 6 times signal-to-loss ratio reaching the output optical fiber improving by 34% the colorimetric analysis of gold nanoparticles, while the implementation of an optoelectronic acquisition system yielded increased accuracy and reduced noise. The microfluidic chip was also integrated with a miniature fiber spectrometer to analyze the assays' colorimetric changes and also the LEDs transmission spectra when illuminating through various solutions. Furthermore, by coupling an optical microscope to a digital camera with a long exposure time (30 s), we could visualise the different scatter intensities of gold nanoparticles within channels following salt addition. These intensities correlate well to the expected difference in aggregation between FTO positive (none to small aggregates) and negative samples (large aggregates).

Biotechnol. Bioeng. 2015;9999: 1–10.

KEYWORDS: microfluidics; DNA; gold nanoparticles; fiber-optics; single nucleotide polymorphism

Correspondence to: I. Bernacka-Wojcik, H. êguas, and P.V. Baptista
Contract grant sponsor: Portuguese Science Foundation (FCT-MEC)
Grant numbers: EXCL/CTM-NAN/0201/2012; PTDC/BBB-IMG/1225/2012; PEst-C/CTM/LA0025/2013-14; PEst-OE/SAU/UI0009/2011
Contract grant sponsor: INVISIBLE
Contract grant number: FP7, ERC Advanced Grant 228144
Contract grant sponsor: A3Ple
Contract grant number: FP7, NMP-2010-SME-4 Grant 262782
Accepted manuscript online xx Month 2015;
Article first published online in Wiley Online Library (wileyonlinelibrary.com).
DOI 10.1002/bit.25542

Introduction

Due to the micro-scale dimensions and the resulting high surface-to-volume ratio, microfluidic systems offer numerous advantages including reduced reagent use, portability, faster sample analysis, higher throughput, potential of automation, and high-level integration, all of which are associated with decreased cost (Mark et al., 2010). These devices can also be designed for multi-parallel operation, making the system more reliable as several control assays can be performed simultaneously with multiple samples (Abgrall, 2007; Ben-Yoav et al., 2012; Khoshmanesh et al., 2011; Soe et al., 2012). Recently, several microfluidic devices have been developed to tag and characterize specific DNA sequences using for this purpose miniaturised approaches (Zhang et al., 2006) that only need a small amount of analyte (pictograms) (Xiang et al., 2012) and even integrated DNA analysis including sample pre-treatment, DNA amplification, and detection (Burns et al., 1998; Liu et al., 2004; Oblath et al., 2013). However, so far a complete lab-on-chip device for DNA analysis has not been successfully commercialized mainly due to high cost of the fabrication and/or manipulation (Choi et al., 2011).

Nanobiosensors in Disease Diagnosis

Dovepress
open access to scientific and medical research

Open Access Full Text Article

REVIEW

Gold nanoparticle-based theranostics: disease diagnostics and treatment using a single nanomaterial

Raquel Vinhas[1,2,*]
Milton Cordeiro[1,3,*]
Fábio Ferreira Carlos[1,4]
Soraia Mendo[1,2]
Alexandra R Fernandes[2]
Sara Figueiredo[1]
Pedro V Baptista[1]

[1]Nanomedicine@FCT, CIGMH (Centro de Investigação em Genética Molecular Humana), UCIBIO, Departamento de Ciências da Vida, Faculdade de Ciências e Tecnologia, Universidade Nova de Lisboa, Campus da Caparica, Caparica, Portugal; [2]UCIBIO (Unidade de Ciências Biomoleculares Aplicadas), Departamento de Ciências da Vida, Faculdade de Ciências e Tecnologia, Universidade Nova de Lisboa, Campus da Caparica, Caparica, Portugal; [3]REQUIMTE, Departamento de Química, Faculdade de Ciências e Tecnologia, Universidade Nova de Lisboa, Campus da Caparica, Caparica, Portugal; [4]STABVIDA, Investigação e Serviços em Ciências Biológicas, Lda, Madan Parque, Caparica, Portugal

*These authors contributed equally to this work

Correspondence: Pedro V Baptista
Nanomedicine@FCT, CIGMH, UCIBIO, Departamento de Ciências da Vida, Faculdade de Ciências e Tecnologia, Universidade Nova de Lisboa, Campus da Caparica, 2829-516 Caparica, Portugal
Tel/Fax +351 212 948 530
Email pmvb@fct.unl.pt

Abstract: Nanotheranostics takes advantage of nanotechnology-based systems in order to diagnose and treat a specific disease. This approach is particularly relevant for personalized medicine, allowing the detection of a disease at an early stage, to direct a suitable therapy toward the target tissue based on the molecular profile of the altered phenotype, subsequently facilitating disease monitoring and following treatment. A tailored strategy also enables to reduce the off-target effects associated with universal treatments and improve the safety profile of a given treatment. The unique optical properties of gold nanoparticles, their ease of surface modification, and high surface-to-volume ratio have made them central players in this area. By combining imaging, targeting, and therapeutic agents in a single vehicle, these nanoconjugates are (ought to be) an important tool in the clinics. In this review, the multifunctionality of gold nanoparticles as theranostics agents will be highlighted, as well as the requirements before the translation of these nanoplatforms into routine clinical practice.

Keywords: nanotheranostics, nanomaterials, gold nanoparticle, theranostics, cancer, nanomedicine

Introduction

Theranostics is aimed toward the development of platforms capable of combining diagnostic and therapeutic agents.[1,2] These innovative systems combined into single platforms should help overcome the troublesome differences in biodistribution and specificity of imaging molecules and therapeutic drugs.[3,4] Theranostic approaches have been proposed for the management of several diseases/disorders, in particular for cancer diagnostics and therapeutics. Cancer therapy greatly relies on chemotherapy and radiotherapy in which most anticancer drugs are essentially taken up by cells with high proliferative rate, a characteristic of cancer cells. However, extensive proliferation is not exclusive for tumor cells, and normal tissue also suffers from chemotherapeutic action, leading to severe side effects.[5–7] The efficacy of conventional therapies is also often limited by the natural tendency of cells to evade therapy through mutational events that lead to multidrug resistance, poor drug penetration into tumor tissues, and serious damage to normal tissues.[8–10]

Conventional therapy toward heterogeneous diseases is rarely targeted directly toward a specific cell type or tissue. In fact, the administration of a specific treatment to a subpopulation of patients in accordance to their molecular profile and risk of adverse effects is believed to be a more effective clinical model for improved patient outcome. By selecting patients for targeted clinical trials, based on biomarker

submit your manuscript | www.dovepress.com
Dovepress
http://dx.doi.org/10.2147/NDD.S60285

CHAPTER 1

Nanoparticles for Diagnostics and Imaging

Miguel Larguinho[1,2], Sara Figueiredo[1], Ana Cordeiro[1], Fábio Ferreira Carlos[1,3], Milton Cordeiro[1,2], Pedro Pedrosa[1] and Pedro V. Baptista[1,*]

[1]CIGMH/DCV, Faculdade de Ciências e Tecnologia/Universidade NOVA de Lisboa, Faculdade de Ciências e Tecnologia, 2829-516 Caparica, Portugal; [2]REQUIMTE/DQ, Faculdade de Ciências e Tecnologia/Universidade NOVA de Lisboa, Faculdade de Ciências e Tecnologia, 2829-516 Caparica, Portugal and [3]STABVIDA, Investigação e Serviços em Ciências Biológicas, Lda. Madan Parque, 2825-182 Caparica, Portugal

Abstract: Nanoparticles possess unique optical and physic-chemical properties that may potentiate applications in biomedicine, in particular in diagnostics, therapy and imaging. Advances on biomolecular diagnostics strategies have greatly focused on single molecule detection and characterization of DNA, RNA or proteins through improved nanoparticle-based platforms. Nanoparticles improve analytical capability when compared to traditional techniques with high resolution and medium-high throughput. Also, particular interest has been directed at SNP detection, gene expression profiles and biomarker characterization through colorimetric, spectrometric or electrochemical strategies.

Molecular imaging has also benefited from the introduction of nanoparticles in standard techniques towards non-invasive imaging procedures that can be used to highlight regions of interest, allowing the characterization of biological processes at the cellular and/or molecular level. Several imaging modalities are associated with low sensitivity, an issue that can be tackled by the use of probes, *e.g.* contrast agents for X-ray and magnetic resonance imaging, radiolabelled molecules for nuclear medicine. Furthermore, nanoparticles can be used as vehicles that deliver specifically these contrast agents, leading to overcome the limitations of conventional modalities.

This chapter will discuss the use of nanoparticles in biomolecular recognition and imaging applications, focusing those already being translated into clinical settings. Current knowledge will be addressed as well as its evolution towards the future of nanoparticle-based biomedical applications.

Keywords: Cancer diagnostics, contrast enhancement, cross-linking assay, DNA detection, gold nanoparticles, gold nanoprobes, liposomes, magnetic nanoparticles, metal enhanced fluorescence, metal nanoparticles, molecular resonance imaging, nanomedicine, nanoparticles, optical imaging, photoacoustic imaging, Positron

***Correspondence author Pedro V. Baptista:** 1CIGMH/DCV, Faculdade de Ciências e Tecnologia/Universidade NOVA de Lisboa. Faculdade de Ciências e Tecnologia, 2829-516 Caparica, Portugal; E-mail: pmvb@fct.unl.pt

Maria Luisa Bondi, Chiara Botto & Erika Amore (Eds)